Assembly of DNA-Inspired Aromatic Oligophosphates into Light-Harvesting Supramolecular Polymers

Inauguraldissertation

der Philosophisch-naturwissenschaftlichen Fakultät

der Universität Bern

vorgelegt von

Caroline D. Bösch

von Grossaffoltern BE

Leiter der Arbeit:

Prof. Dr. Robert Häner

Departement für Chemie und Biochemie der Universität Bern

Assembly of DNA-Inspired Aromatic Oligophosphates into Light-Harvesting Supramolecular Polymers

Inauguraldissertation

der Philosophisch-naturwissenschaftlichen Fakultät

der Universität Bern

vorgelegt von

Caroline D. Bösch

von Grossaffoltern BE

Leiter der Arbeit:

Prof. Dr. Robert Häner

Departement für Chemie und Biochemie der Universität Bern

Von der Philosophisch-naturwissenschaftlichen Fakultät angenommen.

Bern, November 2017   Der Dekan:

                                       Prof. Dr. Gilberto Colangelo

Acknowledgements

It's dangerous to go alone

Table of Contents

Summary

This thesis starts with a general introduction which outlines aspects of supramolecular polymers, the structure and chemical synthesis of DNA and excitation energy transfer in light-harvesting systems. Thereafter follows the actual work which is separated into five chapters. The first chapter presents the self-assembly of short amphiphilic phenanthrene oligomers into tubular objects. These so formed supramolecular polymers can act as light-harvesting antennae in combination with a suitable acceptor. It will be discussed that the energy collection efficiency depends on excitation wavelength.

The second chapter describes the construction of DNA based light-harvesting antennae with light absorbing phenanthrenes and pyrene acceptors. The major topic is the separation of the phenanthrene stack by different numbers of base pairs and investigation of the energy transfer efficiency over those gaps. The mechanism is studied in more detail based on transient absorption spectra.

Principles of the first two chapters will be combined in the third. Supramolecular polymers have the advantage that a large number of chromophores can be assembled in highly organized molecular arrays. The disadvantage is that formation of light-harvesting antennae by co-assembly with an acceptor leads to a presumably random distribution of the latter. Introducing DNA into those systems could control the number and positioning of acceptors due to specific base pairing. A DNA-phenanthrene hybrid will be presented which can form supramolecular polymers via sticky ends. It will be shown that the so arranged phenanthrene units can transfer their excitation energy to doped acceptors. Further investigations regarding the accurate positioning of chromophores in DNA based supramolecular polymers will be discussed.

The fourth and fifth chapter give attention to new chromophores for light-harvesting devices. Such systems work the most efficient if they absorb light in the visible range as the sun emits there more light. Phenanthrene can transfer its excitation energy efficiently to a variety of acceptors, but it only absorbs UV light. Therefore, derivatives based on its scaffold have been synthesized with a view to shift the absorption. Photophysical properties of those derivatives will be presented. Additionally, another type of chromophores, naphthalimides dyes, is presented and tested in supramolecular and DNA based light-harvesting antennae.

General Introduction

Supramolecular Polymers

Supramolecular polymers consist of repeating molecular units which are – in contrast to conventional polymers - linked together by non-covalent interactions.[1] Self-assembly of supramolecular polymers in aqueous medium is based on hydrogen bonds, hydrophobic effects, Coulomb and/or van der Waals interactions.[1e,2] The non-covalent interactions between the monomers ensure a dynamic system, for which reason most supramolecular polymerizations are reversible.[3] Such reversibility brings the advantage that they can heal themselves.[4]

The self-assembly of supramolecular polymers is induced under certain conditions and can be controlled.[5] The synthesis of novel materials and applications are an ongoing field in the material sciences.[6] For example is the arrangement of chromophores in a well-defined order a prerequisite for efficient light-harvesting systems.[7]

The formation of supramolecular polymers can follow three main mechanisms (Figure 1).[1a,b,8] In the isodesmic model the strength of secondary interactions between the polymer and non-aggregated monomer is not affected by the chain length. The increase of thermodynamic stability of the system is proportional to the chain elongation. Therefore, no critical temperature of monomer concentration is required to initiate polymerization. The concentration of individual polymers is increased by increasing the concentration of monomers or the temperature.

The nucleation-elongation (cooperative) model describes the slow formation of small polymer nuclei which then grow rapidly. Monomers which follow this polymerization mechanism have weak non-covalent interactions in the polymer which hinder the formation of longer chains. However, as soon as a stable nucleus is formed, the addition of further monomers becomes favorable and the polymer grows faster. The growth of larger polymers is influenced by the concentration of monomer and the temperature.

The ring-chain mechanism is the third polymerization process for supramolecular polymers, but can also occur in covalent polymers. In this mechanism there is an equilibrium between closed rings of monomers and linear chains. Below a critical monomer concentration, small polymer chains rather react with each other to form a ring than they find another monomer to elongate the chain. Above the critical concentration, the polymers are growing faster.

Supramolecular polymerization can be initiated under iso-thermal or temperature-variable conditions. At constant temperature, the polymerization starts by increasing the monomer concentration, by changing the solvent[1b] or by the addition of an initiator.[9]
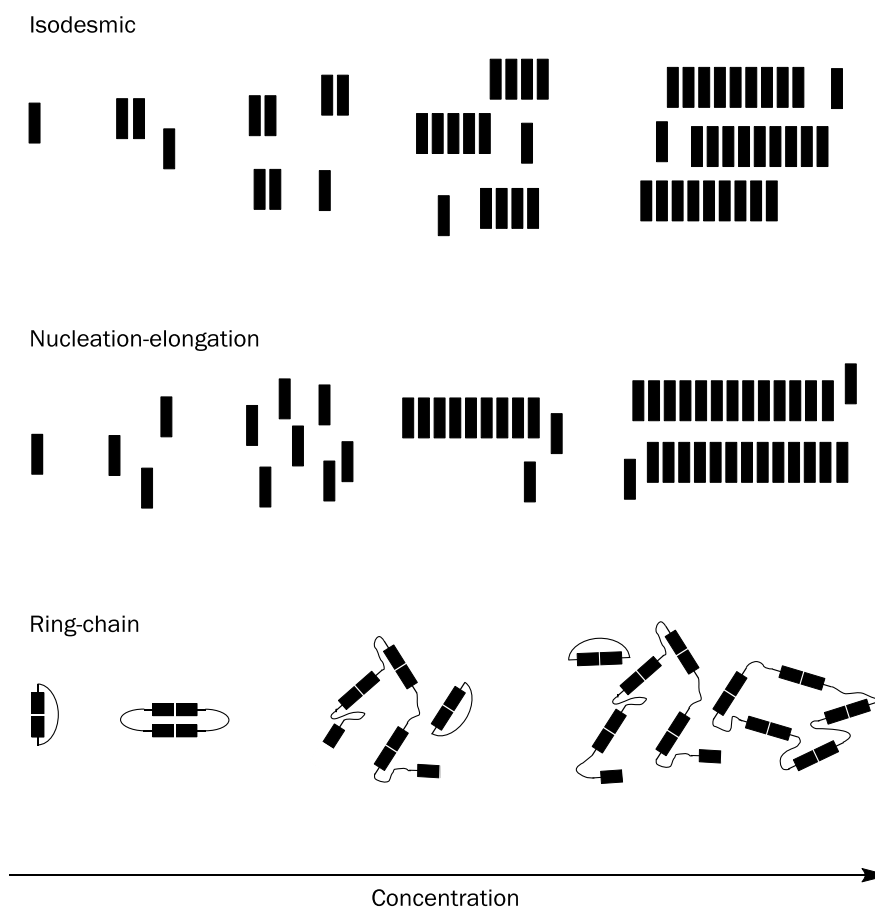
Figure 1: Three different growth mechanisms for supramolecular polymers. Isodesmic: Supramolecular polymers are growing gradually in number and size with increasing monomer concentration. Nucleation-elongation: A nucleus consisting of few assembled monomers is formed at the critical monomer concentration, which then grows rapidly. Ring-chain: Below the critical monomer concentration, short monomer chains react with each other to form rings. By increasing the concentration the polymer chains are rather elongated. Adapted from reference [1a].

DNA

Structural Aspects of DNA

Formation of a DNA duplex is the supramolecular assembly of two single strands. The unique self-recognition properties and chemical accessibility of DNA inspired many scientists to design supramolecular DNA based architectures.[10]

The primary structure of DNA consists of nucleotides built from a sugar (pentose 2-deoxyribose) and a base (adenine, cytosine, guanine or thymine) which are linked by phosphodiester bonds between the 5'-OH of one nucleotide and the 3'-OH of another (Figure 2).[11]
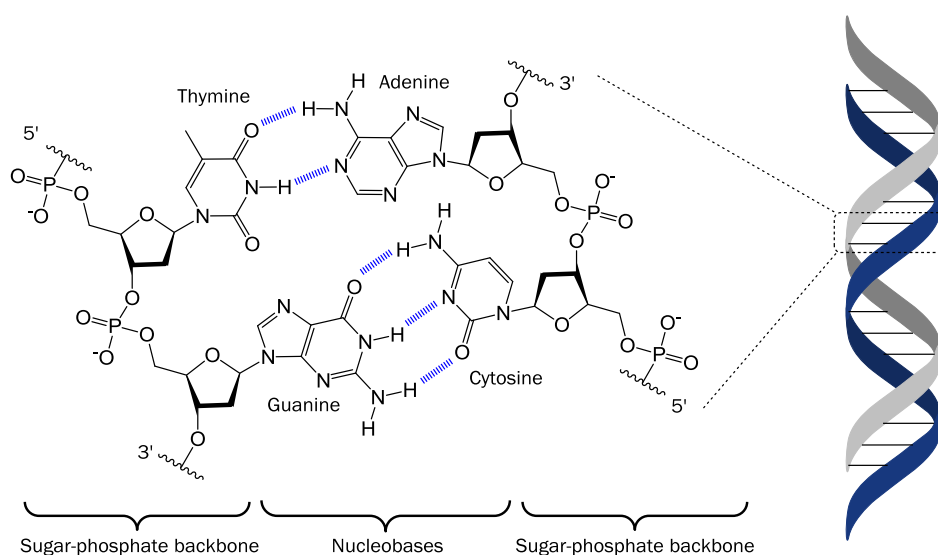
Figure 2: Structure of nucleotides and Watson-Crick base pairs in a DNA duplex. Hydrogen bonds are indicated in blue.

Two complementary strands have the ability to hybridize in an antiparallel fashion. The predominant structure of double stranded DNA at low salt conditions is the right-handed B-DNA double helix.[12] In this conformation the base pairs are localized on the helix axis and are approximately perpendicular to it. The stability of this conformation is due to two main factors: the base pairing between bases via hydrogen bonds on the complementary strands, and base stacking via aromatic π-π stacking interactions.[13] The latter are facilitated by hydrophobic effects, electrostatic interactions, charge transfer and dispersion.[14]

Extended aromatic systems also prefer a stacked conformation.[15] Therefore it is for instance possible to insert flat polycyclic aromatic hydrocarbons (PAHs) between two base pairs when a cavity is formed by unwinding of the helix; this phenomenon is called intercalation.[16] Based on the polarized π-systems the neighboring aromatic rings interact with each other to form an intercalation complex which can be more or less stable depending on the intercalator and its adjacent base pairs.[17]

The well-established solid-phase synthesis of DNA allows incorporation of artificial building blocks in a controlled and efficient way.[18] The DNA scaffold is a useful tool for the assembly of PAHs in various ways.[19]

One possibility among many to modify DNA is the replacement of a nucleobase by a chromophore.[20] Chromophores have also been used to replace nucleosides completely. Either the artificial building blocks are attached with one linker to the DNA backbone[21] or the chromophores are directly incorporated between two phosphate groups.[22] The latter method is the one used in this work. Further methods include the attachement of chromophores to the phosphate[23], or to a nucleobase.[24]
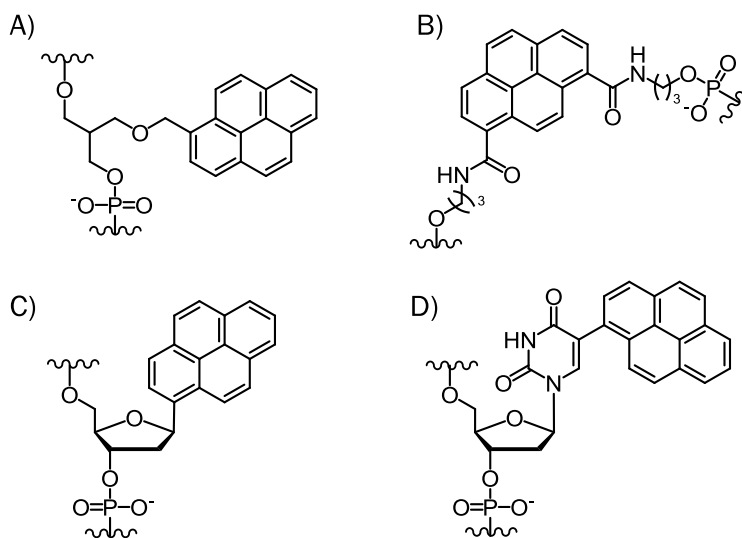
Figure 3: Different possibilities to incorporate chromophores into DNA using the example of pyrene. A) Pyrene is attached to the DNA backbone via a linker.[21c] B) Pyrene is part of the DNA backbone.[22f] C) Pyrene replaces the nucleobase.[20a] D) Pyrene is attached to the nucleobase.[24d]

Phosphoramidite Approach

A very common way to synthesize short sequences of DNA on a solid support is the phosphoramidite approach (Figure 4).[18] Contrary to DNA synthesis in nature, the oligonucleotides are synthesized in the 3' to 5' direction. Essential for a successful synthesis is a solid support which is not soluble in water and organic solvents commonly used in oligonucleotide synthesis. Ideally, the support has a uniform surface, pores which are large enough to contain the oligonucleotide and no surface functionality, so that there are no side reactions with the reagents used in the synthesis.

The covalent linkage on the solid support that binds the oligonucleotide has to be long enough to allow sufficient access for the reagents. Long chain alkylamino linker showed to be suitable for this. Usually a nucleoside-3'-succinate is attached to the linker via an amide bond, so that the solid support already includes the first nucleoside in the sequence.

The nucleosides used in the phosphoramidite approach are protected by an acid labile 4,4'-dimethoxytrityl (DMT) protecting group at the 5'-OH. The 3'-OH is linked to a phosphoramidite. Amines in the nucleobases are protected with base-labile protecting groups forming amides.

The synthesis of oligonucleotides includes four steps for each nucleoside that is added. Before the actual synthesis starts the 5'-OH of the already attached nucleoside on the solid support has to be deprotected. This detritylation is done under acidic condition, for example with 3% trichloroacetic acid in DCM. The formed hydroxyl group can then react with a phosphoramidite.

The first step of the actual synthesis is activation and coupling. A solution of DMT-protected nucleoside phosphoramidite is added to the oligonucleotide chain. A 4,5-dicyanoimidazole solution is added as an activator to protonate the phosphoramidite. An intermediate is formed which can react with the deprotected 5'-OH of the oligonucleotide on the solid support.

In the second step, unreacted 5'-OH groups are capped with an acetyl group to reduce the number of side products in form of shorter oligonucleotides. The capping step requires two solutions which are mixed in situ. The first contains acetic anhydride and 2,6-lutidine as a sterically hindered base. The second contains 1-methylimidazole as a catalyst.

In the third step the phosphorus(III) triester linkage is oxidized to a phosphorus(V) triester. This reaction can be done by using a solution containing iodine, pyridine, H_2O and THF. Iodine is a mild oxidant and H_2O donates the oxygen.

In the last step of the chain elongation the DMT-protected 5'-OH of the added nucleoside is deprotected as described before. Those four steps are repeated until the desired sequence is synthesized. After detritylation of the last nucleoside in the chain, the oligonucleotide has to be cleaved from the solid support, and the bases and the phosphodiester backbone have to be deprotected. Those three reactions are done in one step by adding concentrated NH_4OH and leaving the reaction mixture for several hours at 55°C. The oligonucleotide is then ready for purification by HPLC.
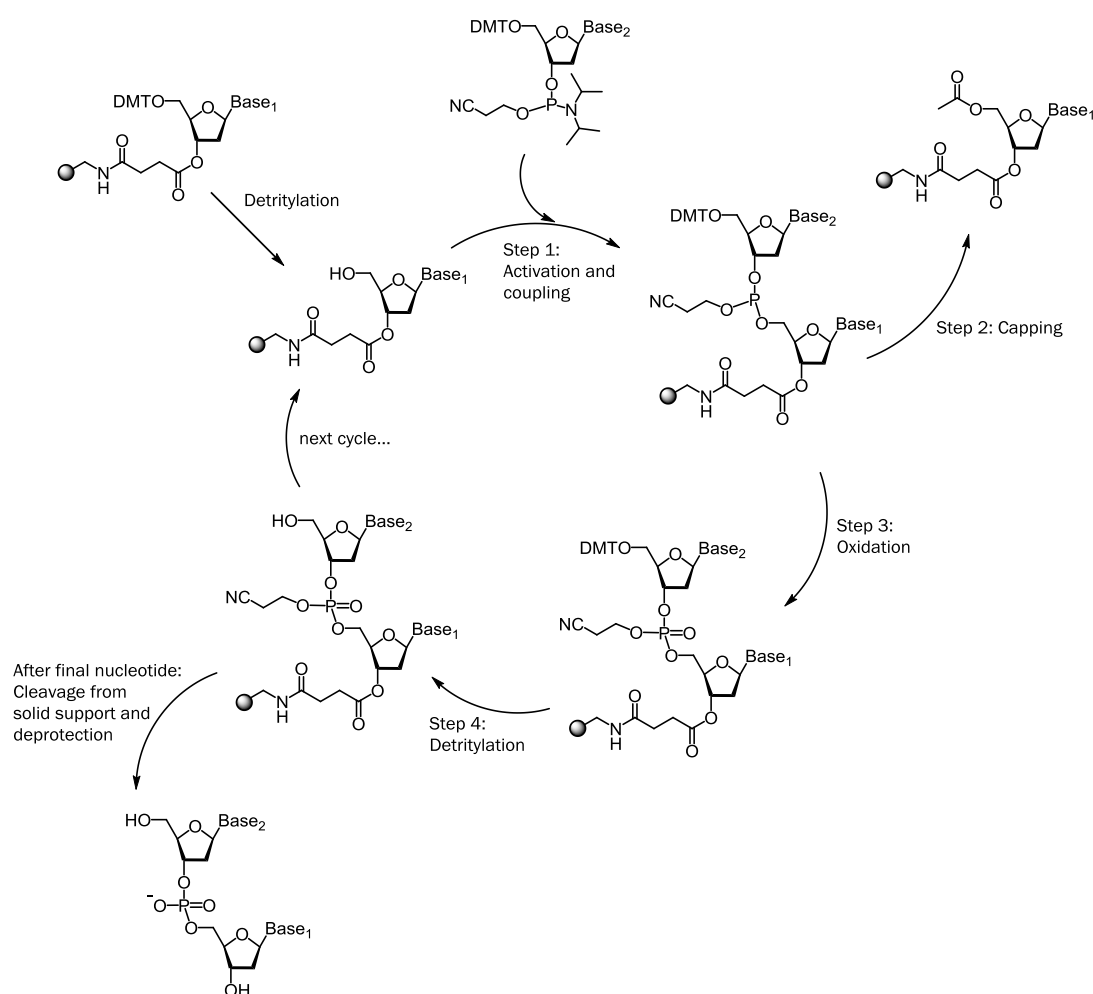
Figure 4: Synthesis of oligonucleotides by the phosphoramidite approach.

Light-Harvesting and Energy Transfer

Photosynthesis is the process which enables life on Earth. Plants, algae and some bacteria possess light-harvesting complexes (LHCs) which produce oxygen and sugar using water, CO_2 and sunlight.[25] LHCs are an accumulation of proteins and chromophores which collect light and transfer the energy to the reaction center. The most important chromophores in LHCs are chlorophylls and carotenoids. Precise arrangement of the light collectors is crucial for efficient energy transfer.[7a]
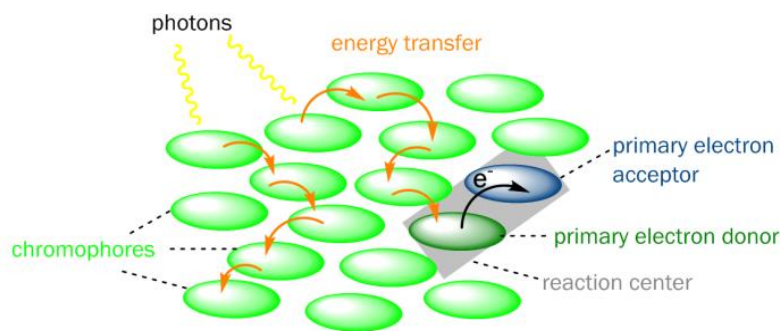
Figure 5: Schematic illustration of a light-harvesting complex. Photons are absorbed by chromophores and the energy is transferred to the primary electron donor in the reaction center. There charge separation takes place as an electron is transferred to the primary electron acceptor, leading to further reactions of photosynthesis.

Excitation energy transfer (EET) describes the process in which the excitation energy is transferred from one chromophore to another. If the electrostatic interactions between the chromophores are weak, the EET can be described by Förster resonance energy transfer (FRET).[26] This model is based on electric dipole-dipole interactions and the excitation hops from the donor to the acceptor. The rate of energy transfer is inversely proportional to the sixth power of the distance between the chromophores. Further, it depends on the orientation of the chromophores and their overlap of energy levels.

The FRET theory is not completely applicable for the EET in photosynthesis. The distances between chrophomores are often less than 10 Å.[25a] Therefore, the interactions between them are much stronger which leads to changes in energy levels and absorption spectra. Newer theories assume additional energy transfer through quantum coherence.[27] In this model the energy migrates through a delocalized excited state (exciton) which is formed by electronically coupled chromophores.
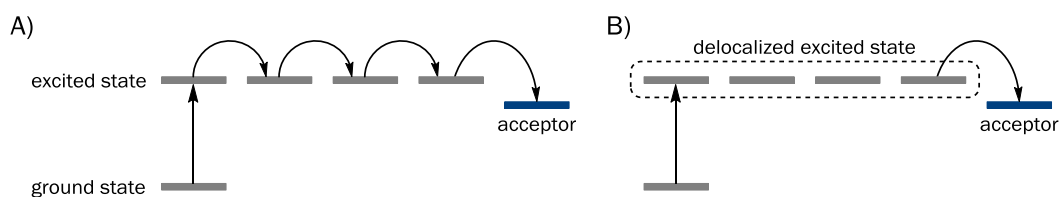
Figure 6: Schematic illustration of different excitation energy transfer mechanisms. A) FRET: The excitation hops from one chromophore to another until it reaches the acceptor. B) Quantum-coherence energy transfer: The excitation is distributed quantum-mechanically over several chromophores and travels wave-like to the acceptor.

Aim of the Thesis

Previous work in our group involved the assembly of chromophores in DNA scaffolds. Chromophores were arranged in DNA duplexes, triplexes, three-way and four-way junctions. It has been shown that DNA is a suitable tool to build up light-harvesting antennae as artificial building blocks can be precisely arranged.

Further progress was done by investigation of the self-assembly behavior of different short oligomers which are composed of phosphate linked chromophores. The formation of different nanostructures has been observed depending on the molecule. Especially the substitution pattern of the linked monomers plays a crucial role on the appearance of the supramolecular polymer.

The aim of this thesis is to investigate other chromophores for their self-assembly behavior. A special attention draws the construction of artificial light-harvesting antennae. Both methods, the incorporation of chromophores into DNA and the self-assembly of short oligomers into supramolecular polymers will be performed. Further, another approach will be investigated which involves the design of a supramolecular DNA assembly. The advantage of DNA based light-harvesting antennae is that the number and positioning of light collectors and acceptors are accurately defined. However, the chemical synthesis of DNA limits the number of monomers per strand due to lower yields for longer sequences. In contrast, self-assembly of short aromatic oligomers leads to the formation of extensive chromophore arrays, but the incorporation of acceptors is presumably random. Therefore, a combination of those two principles will be investigated, where DNA strands form duplexes with aromatic sticky ends which can then self-assemble. The aim is to design a light-harvesting supramolecular polymer with precise arrangement and ratio of different chromophores.

9

References

[1]   (a) A. Harada, *Supramolecular Polymer Chemistry*, Wiley-VCH, Weinheim, 2012.
(b) T. F. A. De Greef, M. M. J. Smulders, M. Wolffs, A. P. H. J. Schenning, R. P. Sijbesma, E. W. Meijer, *Chem. Rev.*, 2009, **109**, 5687-5754.
(c) S.-L. Li, T. Xiao, C. Lin, L. Wang, *Chem. Soc. Rev.*, 2012, **41**, 5950-5968.
(d) F. J. M. Hoeben, P. Jonkheijm, E. W. Meijer, A. P. H. J. Schenning, *Chem. Rev.*, 2005, **105**, 1491-1546.
(e) E. Krieg, M. M. C. Bastings, P. Besenius, B. Rybtchinski, *Chem. Rev.*, 2016, **116**, 2414-2477.
(f) W. Li, Y. Kim, M. Lee, *Nanoscale*, 2013, **5**, 7711-7723.
(g) C. Wang, Z. Wang, X. Zhang, *Acc. Chem. Res.*, 2012, **45**, 608-618.
(h) T. E. Kaiser, H. Wang, V. Stepanenko, F. Würthner, *Angew. Chem. Int. Ed.*, 2007, **46**, 5541-5544.

[2]   (a) L. Brunsveld, J. A. J. M. Vekemans, J. H. K. K. Hirschberg, R. P. Sijbesma, E. W. Meijer, *Proc. Natl. Acad. Sci. U.S.A*, 2002, **99**, 4977-4982.
(b) A. Arnaud, J. Belleney, F. Boué, L. Bouteiller, G. Carrot, V. Wintgens, *Angew. Chem. Int. Ed.*, 2004, **43**, 1718-1721.

[3]   (a) J.-M. Lehn, *Angew. Chem. Int. Ed.*, 2015, **54**, 3276-3289.

[4]   (a) W. H. Binder, *Self-Healing Polymers: From Principles to Applications*, Wiley-VCH, Weinheim, 2013.
(b) L. R. Hart, J. L. Harries, B. W. Greenland, H. M. Colquhoun, W. Hayes, *Polym. Chem.*, 2013, **4**, 4860-4870.

[5]   (a) P. Besenius, *J. Polym. Sci. Pol. Chem.*, 2017, **55**, 34-78.
(b) D. van der Zwaag, T. F. A. de Greef, E. W. Meijer, *Angew. Chem. Int. Ed.*, 2015, **54**, 8334-8336.
(c) S. Ogi, K. Sugiyasu, S. Manna, S. Samitsu, M. Takeuchi, *Nat. Chem.*, 2014, **6**, 188-195.
(d) A. Aliprandi, M. Mauro, L. De Cola, *Nat. Chem.*, 2016, **8**, 10-15.
(e) C. Schaefer, I. K. Voets, A. R. A. Palmans, E. W. Meijer, P. van der Schoot, P. Besenius, *ACS Macro Lett.*, 2012, **1**, 830-833.
(f) M. Endo, T. Fukui, S. H. Jung, S. Yagai, M. Takeuchi, K. Sugiyasu, *J. Am. Chem. Soc.*, 2016, **138**, 14347-14353.

[6]   (a) T. Aida, E. W. Meijer, S. I. Stupp, *Science*, 2012, **335**, 813-817.
(b) O. Ikkala, G. ten Brinke, *Science*, 2002, **295**, 2407-2409.
(c) F. Würthner, T. E. Kaiser, C. R. Saha-Möller, *Angew. Chem. Int. Ed.*, 2011, **50**, 3376-3410.
(d) R. Dong, Y. Zhou, X. Huang, X. Zhu, Y. Lu, J. Shen, *Adv. Mater.*, 2015, **27**, 498-526.
(e) Y. Wang, H. Xu, X. Zhang, *Adv. Mater.*, 2009, **21**, 2849-2864.

[7]   (a) Z. G. Fetisova, A. M. Freiberg, K. E. Timpmann, *Nature*, 1988, **334**, 633-634.
(b) N. Sakai, S. Matile, *Beilstein J. Org. Chem.*, 2012, **8**, 897-904.

[8]   M. M. J. Smulders, M. M. L. Nieuwenhuizen, T. F. A. de Greef, P. van der Schoot, A. P. H. J. Schenning, E. W. Meijer, *Chem. Eur. J.*, 2010, **16**, 362-367.

[9]   J. Kang, D. Miyajima, T. Mori, Y. Inoue, Y. Itoh, T. Aida, Science, 2015, **479**, 1173-1176.

[10]   (a) E. Stulz, G. H. Clever, *DNA in Supramolecular Chemistry and Nanotechnology*, Wiley, Hoboken, NJ, USA, 2015.
(b) F. A. Aldaye, A. L. Palmer, H. F. Sleiman, *Science*, 2008, **321**, 1795-1799.
(c) N. C. Seeman, *Annu. Rev. Biochem.*, 2010, **79**, 65-87.
(d) E. Stulz, *Chem. Eur. J.*, 2012, **18**, 4456-4469.
(e) W. Pfeifer, B. Saccà, *ChemBioChem*, 2016, **17**, 1063-1080.
(f) C. K. McLaughlin, G. D. Hamblin, H. F. Sleiman, *Chem. Soc. Rev.*, 2011, **40**, 5647-5656.
(g) T. J. Bandy, A. Brewer, J. R. Burns, G. Marth, T. Nguyen, E. Stulz, *Chem. Soc. Rev.*, 2011, **40**, 138-148.
(h) A. V. Pinheiro, D. Han, W. M. Shih, H. Yan, *Nat. Nanotechnol.*, 2011, **6**, 763-772.
[11]   (a) J. D. Watson, F. H. C. Crick, *Nature*, 1953, **171**, 737-738.
(b) R. Wing, H. Drew, T. Takano, C. Broka, S. Tanaka, K. Itakura, R. E. Dickerson, *Nature*, 1980, **287**, 755-758.
(c) M. Mandelkern, J. G. Elias, D. Eden, D. M. Crothers, *J. Mol. Biol.*, 1981, **152**, 153-161.
[12]   G. M. Blackburn, M. J. Gait, D. Loakes, D. M. Williams, *Nucleic Acids in Chemistry and Biology*, 3rd edition, RSC Publishing, Cambridge, UK, 2006.
[13]   P. Yakovchuk E. Protozanova, M. D. Frank-Kamenetskii, *Nucleic Acids Res.*, 2006, **34**, 564-574.
[14]   (a) K. M. Guckian, B. A. Schweitzer, R. R.-F. Ren, C. J. Sheils, D. C. Tahmassebi, E. T. Kool, *J. Am. Chem. Soc.*, 2000, **122**, 2213- 2222.
(b) R. Luo, H. S. Gilson, M. J. Potter, M. K. Gilson, *Biophys. J.*, 2001, **80**, 140- 148.
[15]   (a) C. A. Hunter, J. K. M. Sanders, *J. Am. Chem. Soc.*, 1990, **112**, 5525- 5534.
(b) S. Grimme, *Angew. Chem. Int. Ed.*, 2008, **47**, 3430- 3434.
[16]   L. B. Hendry, V. B. Mahesh, E. D. Bransome Jr, D. E. Ewing, *Mutation Research*, 2007, **623**, 53-71.
[17]   (a) C. R. Martinez, B. L. Iverson, *Chem. Sci.*, 2012, **3**, 2191- 2201.
(b) S. Nafisi, A. A. Saboury, N. Keramat, J.-F. Neault, H.-A. Tajmir-Riahi, *J. Mol. Struct.*, 2007, **827**, 35-43.
[18]   (a) M. D. Matteucci, M. H. Caruthers, *J. Am. Chem. Soc.*, 1981, **103**, 3185-3191.
(b) S. L. Beaucage, M. H. Caruthers, *Tetrahedron Lett.*, 1981, **22**, 1859-1862.
[19]   Y. N. Teo, E. T. Kool, *Chem. Rev.*, 2012, **112**, 4221-4245.
[20]   (a) T. Matray, E. T. Kool, *J. Am. Chem. Soc.*, 1998, **120**, 6191-6192.
(b) R. X. F. Ren, N. C. Chaudhuri, P. L. Paris, S. Rumney, E. T. Kool, *J. Am. Chem. Soc.*, 1996, **118**, 7671-7678.
(c) C. Brotschi, A. Häberli, C. J. Leumann, *Angew. Chem. Int. Ed.*, 2001, **40**, 3012-3014.
(d) J. Chiba, S. Takeshima, K. Mishima, H. Maeda, Y. Nanai, K. Mizuno, M. Inouye, *Chem. Eur. J.*, 2007, **13**, 8124-8130.
(e) S. Hainke, O. Seitz, *Angew. Chem. Int. Ed.*, 2009, **48**, 8250-8253.
[21]   (a) H. Kashida, M. Komiyama, H. Asanuma, *Chem. Lett.*, 2006, **35**, 934-935.
(b) C. Wagner, H.-A. Wagenknecht, *Org. Lett.*, 2006, **8**, 4191-4194.
(c) U. B. Christensen, E. B. Pedersen, *Nucleic Acid Res.*, 2002, **30**, 4918-4925.

(d) C. B. Nielsen, M. Pedersen, E. B. Pedersen, P. E. Hansen, U. B. Christensen, *Bioconjug. Chem.*, 2004, **15**, 260-269.

[22]   (a) R. L. Letsinger, T. Wu, *J. Am. Chem. Soc.*, 1994, **116**, 811-812.

(b) F. D. Lewis, X. Liu, S. E. Miller, M. R. Wasielewski, *J. Am Chem. Soc.*, 1999, **121**, 9746-9747.

(c) P. Daublain, K. Siegmund, M. Hariharan, J. Vura-Weis, M. R. Wasielewski, F. D. Lewis, V. Shafirovich, Q. Wang, M. Raytchev, T. Fiebig, *Photochem. Photobio. Sci.*, 2008, **7**, 1501-1508.

(d) W. Wang, W. Wan, H.-H Zhou, S. Niu, A. D. Q. Li, *J. Am. Chem. Soc.*, 2003, **125**, 5248-5249.

(e) S. M. Langenegger, R. Häner, *Helv. Chim. Acta*, 2002, **85**, 3414-3421.

(f) S. M. Langenegger, R. Häner, *Chem. Commun.*, 2004, 2792-2793.

(g) N. Bouquin, V. L. Malinovskii, X. Guégano, S.-X Liu, S. Decurtins, R. Häner, *Chem. Eur. J.*, 2008, **14**, 5732-5736.

[23]   N. Conway, L. McLaughlin, *Bioconjug. Chem.,* 1991, **2**, 452-457.

[24]   (a) I. Bouamaied, T. Nguyen, T. Rühl, E. Stulz, *Org. Biomol. Chem.*, 2008, **6**, 3888-3891.

(b) K. Ebata, M. Masuko, H. Ohtani, M. Kashiwasake-Jibu, *Photochem. Photobiol.*, 1995, **62**, 836-839.

(c) R. Varghese, H.-A. Wagenknecht, *Chem. Eur. J.*, 2010, **16**, 9040-9046.

(d) N. C. Chaudhuri, R. X.-F. Ren, E. T. Kool, *Synlett.*, 1997, **4**, 341-347.

[25]   (a) R. E. Blankenship, *Molecular Mechanisms of Photosynthesis*, 2nd Edition, Wiley, Hoboken, NJ, USA, 2014.

(b) R. Croce, H. van Amerongen, *Nat. Chem. Biol.*, 2014, **10**, 492-501.

[26]   (a) T. Förster, *Ann. Phys.*, 1948, **437**, 55-75.

(b) E. Rabinowitch, *J. Phys. Chem.*, 1957, **61**, 870-878.

[27]   (a) G. S. Engel, T. R. Calhoun, E. L. Read, T.-K. Ahn, T. Mančal, Y.-C. Cheng, R. E. Blankenship, G. R. Fleming, *Nature*, 2007, **446**, 782-786.

(b) Y.-C. Cheng, G. R. Fleming, *Annu. Rev. Phys. Chem.*, 2009, **60**, 241-262.

(c) E. Collini, *Chem. Soc. Rev.*, 2013, **42**, 4932-4947.

(d) A. Ishizaki, G. R. Fleming, *Annu. Rev. Condens. Matter Phys.*, 2012, **3**, 333-361.

(e) F. Fassioli, R. Dinshaw, P. C. Arpin, G. D. Scholes, *J. R. Soc. Interface*, 2014, **11**, 20130901.

(f) J. M. Anna, G. D. Scholes, R. van Grondelle, *BioScience*, 2014, **64**, 14-25.

(g) A. Chenu, G. D. Scholes, *Annu. Rev. Phys. Chem.*, 2015, **66**, 69-96.

Chapter 1: Supramolecular Phenanthrene Nanotubes as Light-Harvesting Antennae

Work described in this chapter is published in:

Light-Harvesting Nanotubes Formed by Supramolecular Assembly of Aromatic Oligophosphates

C. D. Bösch, S. M. Langenegger, R. Häner, *Angew. Chem. Int. Ed.*, 2016, **55**, 9961-9964.

Abstract

A 2,7-disubstituted phosphodiester-linked phenanthrene trimer was synthesized which forms tubular structures in aqueous medium. The chromophores are arranged in H-aggregates. The combination with an acceptor leads to the formation of light-harvesting nanotubes in which the assembled phenanthrene units transfer their excitation energy to the acceptor. The efficiency depends on excitation wavelength. Direct excitation at the phenanthrene H-band leads to a higher increase of fluorescence intensity.

Introduction

The construction of artificial light-harvesting complexes has received much attention in recent years.[28] In light-harvesting systems energy is absorbed by numerous chromophores and transferred to an acceptor. Polymers[29] and dendrimers[30] were used to arrange multiple organic chromophores around acceptor molecules. Efficient transport of the excitation energy is a key aspect for the construction of effective light-harvesting systems.[31] The degree of structural order determines the level of electronic coupling and, thus, the efficiency of energy transfer in chromophore arrays.[32] One way of assembling highly organized molecular arrays is provided by supramolecular polymerization.[33] Inspired by the unique electronic properties of carbon nanotubes,[34] supramolecular organic nanotubes appear as particularly attractive scaffolds for the molecular organization of chromophore aggregates. Owing to the non-covalent nature of interaction, supramolecular polymers offer a high degree of modularity and, hence, flexibility for their construction and potential functionalization. The assembly of supramolecular nanotubes with light-harvesting properties has been shown for amphiphilic monomers[35] and aromatic peptides.[36] In

previous work we described the formation of supramolecular one-dimensional polymers from 3,6-disubstituted phenanthrene oligomers.[37] In combination with an acceptor the assembled phenanthrene units act as an antenna which effectively transfers its excitation energy to a pyrene acceptor. The use of two-dimensional polymers would allow extending the number of structurally organized, energy collecting chromophores. The assembly of two-dimensional polymers was demonstrated previously with 1,6- and 2,7-disubstituted pyrene oligomers.[38] The appearance of self-assembled nanostructures seems to depend on the substitution geometry of the phosphodiester-linked monomers. Therefore, a 2,7-disubstitued phenanthrene oligomer was synthesized and studied. AFM and TEM measurements revealed tubular assemblies which were further studied for their light-harvesting properties.
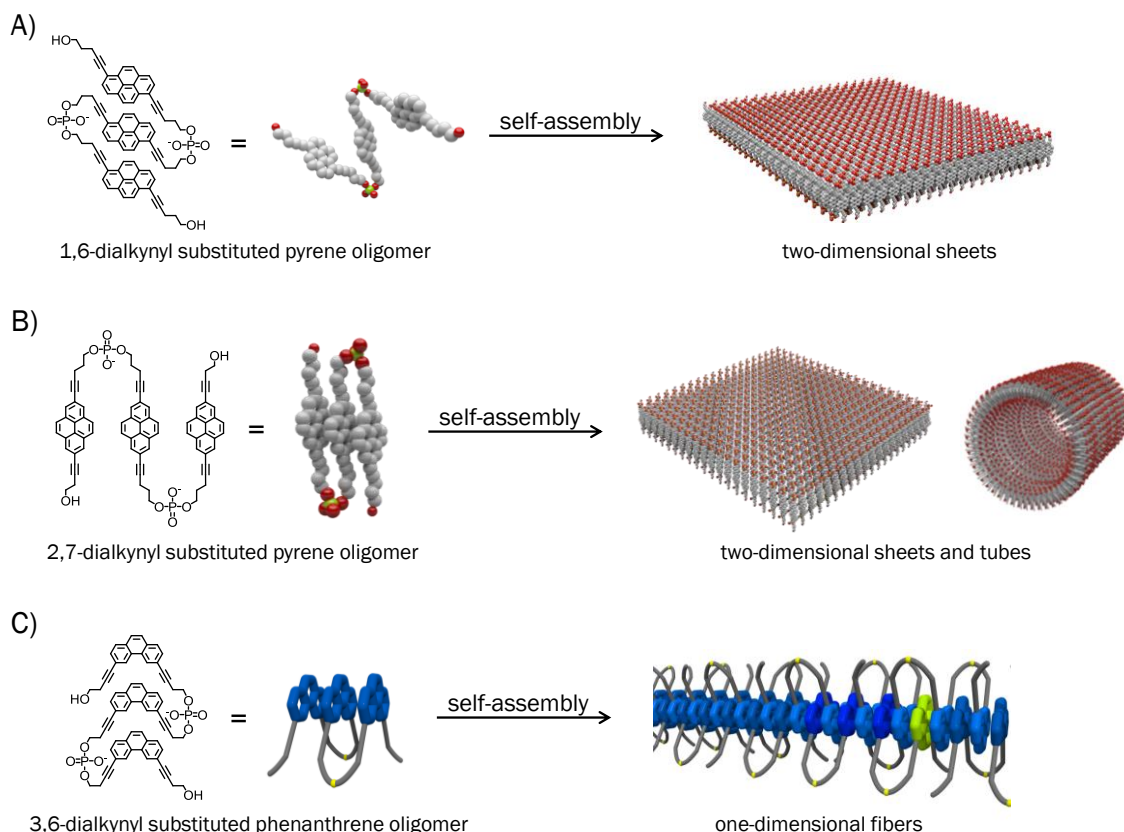

Figure 7: Previously investigated oligomers which self-assemble in aqueous medium. A) 1,6-Dialkynyl pyrene oligomer.[38a] B) 2,7-Dialkynyl pyrene oligomer.[38c] C) 3,6-Dialkynyl phenanthrene;[37] the fibers act as light-harvesting antennae with an incorporated acceptor (pyrene is highlighted in green).

Results

Oligomer Synthesis

Oligomers **1** and **2** were synthesized on a phenanthrene-modified solid support using standard phoshoramidite chemistry. Syntheses of the required phosphoramidites and solid support are described in the supporting information of this chapter. Oligomer **1** consists of three phenanthrene units which are joined by phosphodiester groups attached via butynol linkers in positions 2 and 7. The acceptor oligomer **2** has a similar structure, except that the phenanthrene in the central position has been replaced by a pyrene.
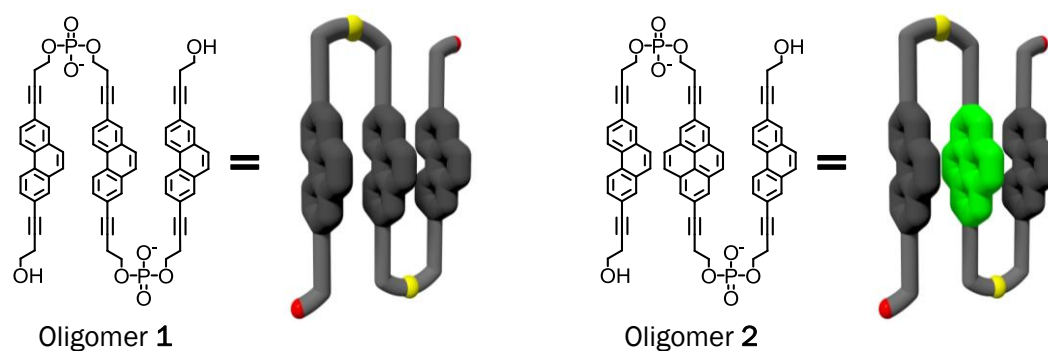

Figure 8: Structures and illustrative model representations of oligomers **1** and **2**. Pyrene is highlighted in green.

Photophysical Properties of Phenanthrene Nanotubes

The aggregation behavior of oligomer **1** is influenced by solvent polarity, and can be indirectly observed by changes in the absorption spectra. Figure 9 shows the absorption spectra of **1** in ethanol and in aqueous medium. In ethanol (black), oligomer **1** is very soluble and the phenanthrene units are not aggregated, therefore the absorption pattern looks similar to the one measured of the monomer (see supporting information, Figure 45). In a more polar, aqueous medium some changes are observed. First, there is a general hypochromicity, especially at 270 and 316 nm, indicating a strong aggregation behavior.[39] Further there is the appearance of a new band at 243 nm, which is considered to be an H-band.[40] When the aqueous solution is heated to 80°C the H-band disappears and the whole spectrum has almost the same shape as the one measured in ethanol. Those observations suggest that supramolecular polymers of **1** are formed in aqueous medium,

which can be disassembled again by heating the solution. For measurements in aqueous solution (10 mM sodium phosphate buffer pH 7.0) 10 vol% of ethanol were added to ensure the reversibility of the aggregation.
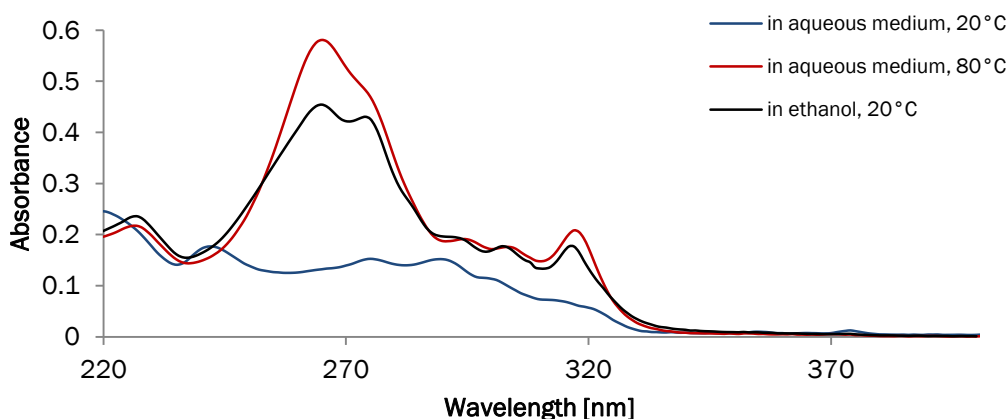

Figure 9: Absorption specta of **1**, in 10 mM sodium phosphate buffer pH 7.0, 10 vol% ethanol (blue: at 20°C, red: at 80°C) and in ethanol at 20°C (black), concentration: 1μM.

Fluorescence measurement of oligomer **1** in aqueous medium shows a structured emission band with maxima at 371 and 391 nm if excited at 316 nm (Figure 10, solid). If the sample is excited at 243 nm (H-band) the emission band looks different (Figure 10, dashed). The maxima are shifted 5 nm to the red (376 and 396 nm, respectively) and a broad band appears around 425 nm, which most likely arises from excimer formation.[41] This excitation wavelength dependent fluorescence of phenanthrene has been reported previously and was attributed to solvation effects.[42] Also the quantum yield depends on excitation wavelength. For excitation at 316 nm a value of 7% was obtained (with quinine sulfate in 0.5 M H_2SO_4 as standard), whereas excitation at 243 nm yielded only 3%. This red-shifted fluorescence and low quantum yield are known features of H-aggregates.[43]
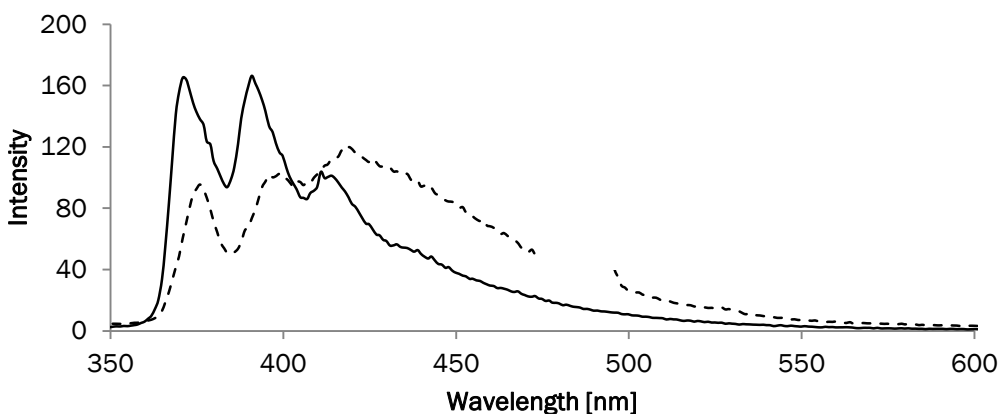
Figure 10: Fluorescence spectra of assembled **1** with different excitation wavelengths. Conditions: 1 µM in 10 mM sodium phosphate buffer pH 7.0, 10 vol% ethanol; λexc. 316 nm (solid) and 243 nm (dashed).

Excitation spectra further illustrate the influence of excitation wavelength on the emission. The excitation spectra of **1** are not the same over the whole emission (Figure 11). Excitation spectra were recorded for three emission wavelengths. For emission at 391 nm a spectrum was obtained which resembles the absorption spectrum of **1** in ethanol (not aggregated phenanthrenes). When the emission wavelength is changed to 412 nm the excitation spectrum shows a peak at 243 nm which coincides with the H-band in the absorption spectrum of **1**. Further to the red, when the emission wavelength is fixed to 437 nm, the excitation spectrum looks again different. This time the spectrum can be compared to the absorption spectrum of **1** in aqueous medium, with the H-band at 243 nm and comparatively low intensity at 265 and 316 nm. Thus, H-aggregation of phenanthrene leads to a red-shifted and low fluorescence.
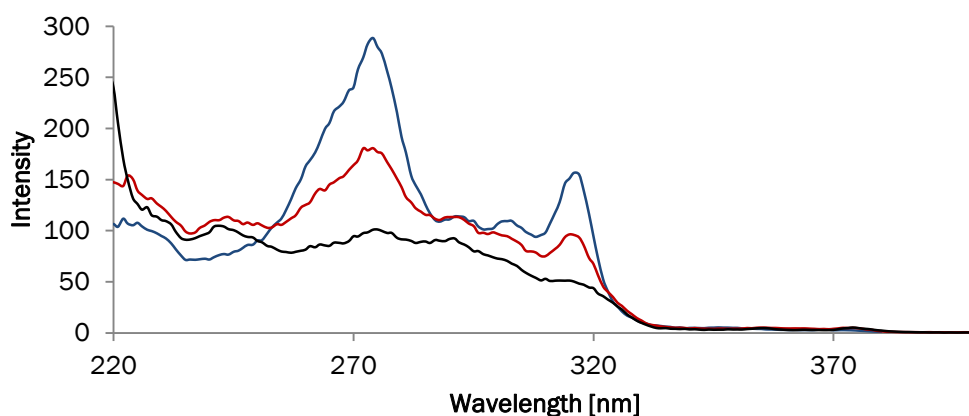
17

Figure 11: Excitation spectra of assembled **1** recorded for different emission wavelengths, 1 µM in 10 mM sodium phosphate buffer pH 7.0, 10 vol% ethanol. λem. 391 nm (blue), 412 nm (red) and 437 nm (black).

Visualization of Phenanthrene Nanotubes

Oligomer **1** forms tubular supramolecular polymers in aqueous medium. Atomic force microscopy (AFM) and transmission electron microscopy (TEM) reveal elongated objects with lengths up to several micrometers (Figure 12). The measured height in AFM is in the range of 4-4.5 nm. This value corresponds to a double layer of phenanthrenes, as the tubes flatten on the surface during the deposition.[38c] The diameter of the nanotubes varies in the range of 50-150 nm. Polymerization of **1** exclusively results in the formation of nanotubes. This is in contrast to findings with oligomers consisting of 2,7-linked pyrenes which formed simultaneously nanosheets and nanotubes in aqueous medium.[38c]
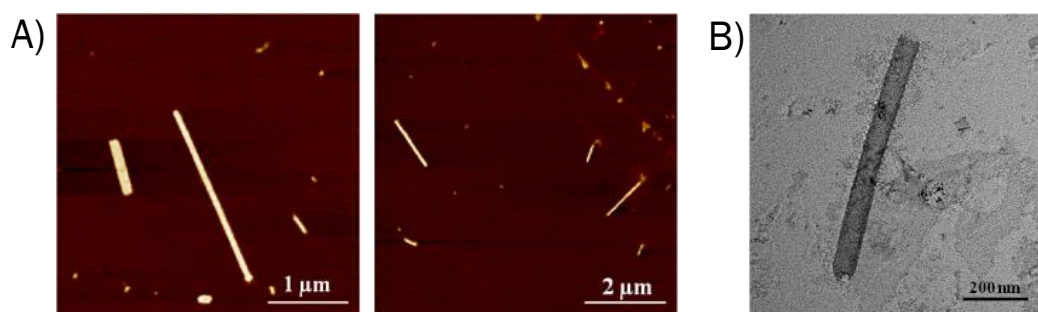

Figure 12: A) Tapping mode AFM images of assembled **1** in aqueous solution, deposited on mica using $NiCl_2$ as surface binding agent. B) TEM image of a phenanthrene nanotube.

18

Figure 13 shows an illustration of the self-assembled phenanthrene nanotube. As the tubes are formed in aqueous medium, hydrophobic phenanthrene units are located in a sheet-like manner with hydroxyl-groups (red) and phosphates (yellow) located on its inner and outer surfaces.
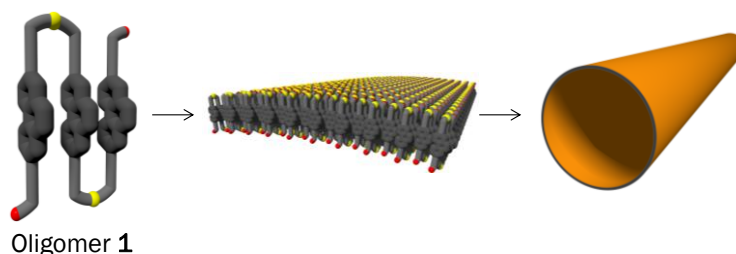

Oligomer **1**

Figure 13: Schematic illustration of the self-assembly of phenanthrene oligomer **1** into tubular supramolecular polymers.

Light-Harvesting Antenna with a Pyrene Oligomer

Excitation energy transfer in one-dimensional supramolecular polymers of 3,6-dialkynyl phenanthrene have been observed previously.[37] A titration experiment was carried out to test if the nanotubes formed of 2,7-dialkynyl phenanthrene also have light-harvesting properties. Oligomer **2** was chosen as the acceptor, as it has the same structure as **1**, with the exception that the phenanthrene in the middle is replaced by pyrene. Measurements were carried out after the addition of small quantities of oligomer **2** and subsequent reassembly of the polymer (solution heated to 80°C, then cooled to 20°C). This process leads to the formation of supramolecular phenanthrene nanotubes with randomly distributed pyrene acceptors.
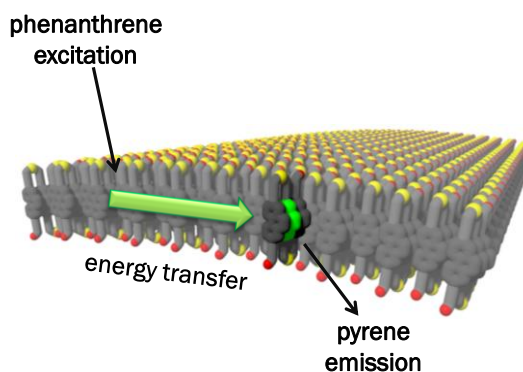

Figure 14: Illustration of excitation energy transfer from phenanthrene to pyrene in phenanthrene nanotubes doped with oligomer **2**.

Figure 15 (left) shows a comparison of the fluorescence of phenanthrene nanotubes before and after the reassembly with 1.2% pyrene. Already with a small quantity of acceptor a sharp increase of pyrene fluorescence is observable upon irradiation at 243 nm (H-band in the spectrum of the phenanthrene polymer). The effect of increasing pyrene content on the intensity of pyrene fluorescence is shown in Figure 15 (right). The maximal intensity is reached with a ratio of about 7% pyrene per phenanthrene. This shows that the supramolecular nanotube functions as a light-harvesting antenna in which the assembled phenanthrene moieties transfer their excitation energy to pyrene acceptors. Excitation of phenanthrene at 316 nm also leads to an increase of pyrene emission, although not as much as direct excitation of the H-band (Figure 16). The ratio of pyrene/phenanthrene emission is higher if the antenna is excited at 243 nm. This coincides with the theory that the increased radiative lifetime for the relaxed excited state in H-aggregates is beneficial for efficient energy transfer.[44] The quantum yield of the antenna with 7.3% pyrene, however, is the same (23%) for both excitation wavelengths.
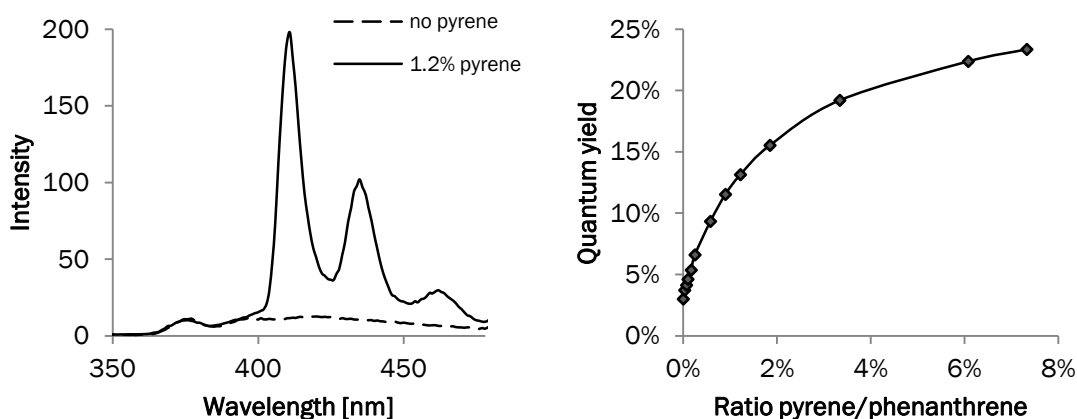

Figure 15: Left: Fluorescence spectra of assembled phenanthrene nanotubes in the absence (dashed) and in the presence of 1.2% pyrene (solid). Right: Quantum yield of light-harvesting supramolecular nanotubes as a function of pyrene/phenanthrene ratio. Conditions: 0.5 µM **1** in 10 mM sodium phosphate buffer pH 7.0, 10 vol% ethanol, λexc. 243 nm; excitation slit: 2.5 nm, emission slit: 5 nm.
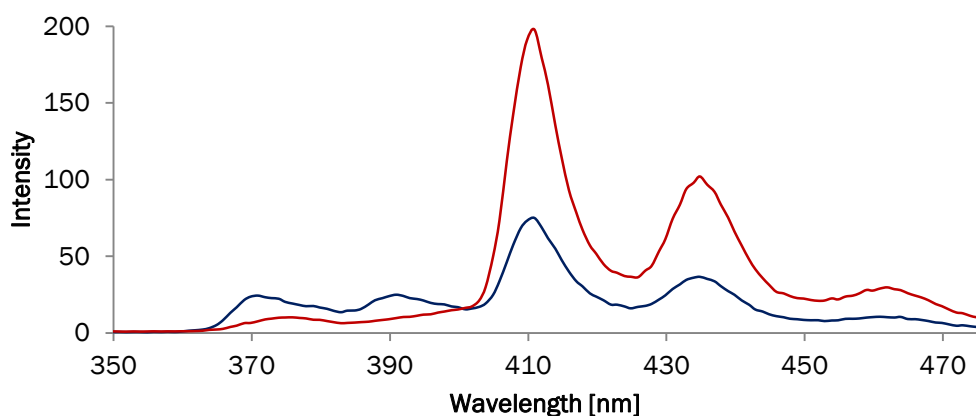
Figure 16: Fluorescence spectra of light-harvesting antenna with excitation wavelength 316 nm (blue) and 243 nm (red), conditions as in Figure 15.

It is important to note that oligomer **2** is only incorporated into the nanotube if oligomer **1** is reassembled in the prescence of **2** (heating of the solution to 80°C, and then cooling to 20°C). No energy transfer from phenanthrene to pyrene was observed upon addition of **2** to preformed nanotubes at ambient temperature. Figure 17 shows the measurement of the phenanthrene nanotubes after the addition of 0.03% pyrene before and after reassembly.
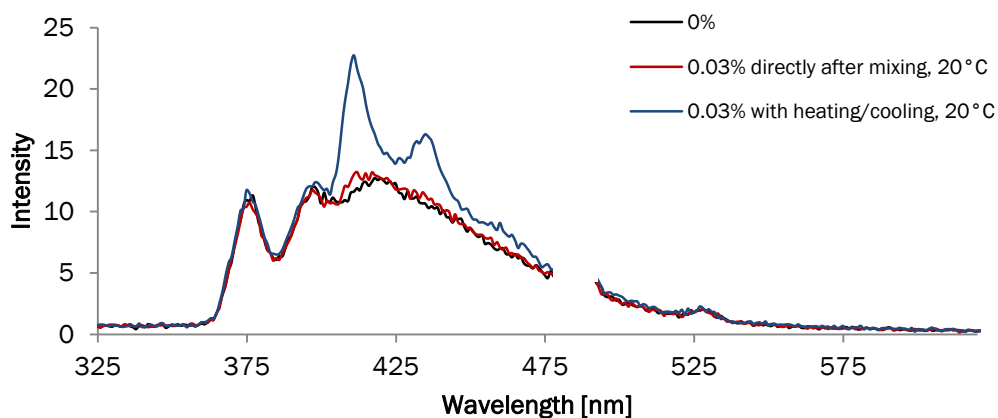

Figure 17: Fluorescence spectra to illustrate the importance of heating/cooling the sample to observe incorporation of **2**. Conditions: 0.5 µM **1** in 10 mM sodium phosphate buffer pH 7.0, 10 vol% ethanol. Addition of **2** represented as pyrene/phenanthrene (%). λexc. 243 nm; excitation slit: 2.5 nm; emission slit: 5 nm.

To prove that **2** alone does not exhibit the measured fluorescence, the titration experiment was also carried out with a solution which does not contain **1**. Figure 18 shows the measurements for the addition of "1.2%" pyrene to a solution without phenanthrene nanotubes for both excitation wavelengths. It shows that the fluorescence signal from the acceptor alone at this low concentration is negligible. Therefore the acceptor itself is not responsible for the high fluorescence intensity observed in pyrene-doped nanotubes (Figure 15).
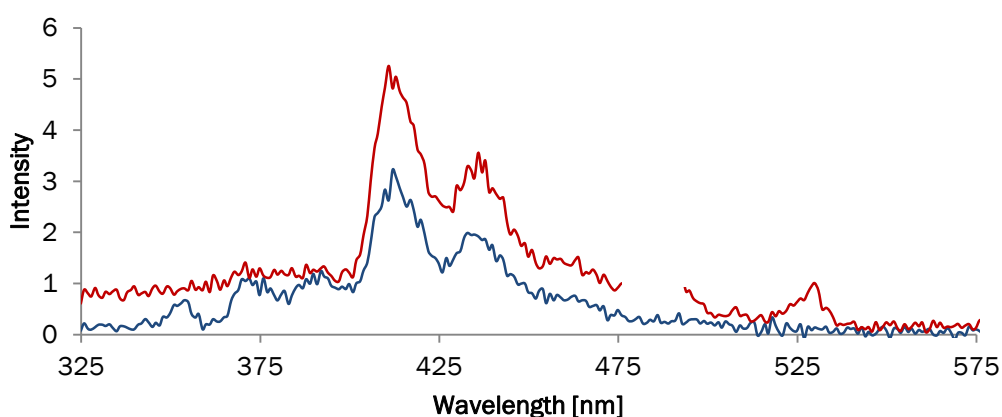

Figure 18: Reference fluorescence spectra of oligomer **2** ("1.2%" pyrene/phenanthrene). λexc. 316 nm (blue) and 243 nm (red); excitation slit: 2.5 nm; emission slit: 5 nm.

Finally, the incorporation of **2** does not change the morphology of the supramolecular polymers. AFM measurements of a sample containing 0.5 µM **1** and 0.5 nM **2** (0.1% pyrene/phenanthrene) revealed objects of identical shape as those formed of oligomer **1** alone (see supporting information, Figure 56).

Light-Harvesting Antenna with Cationic Dyes

Further, acridine orange and rhodamine 6G were tested for their acceptor efficiency. Both are positively charged, fluorescent dyes which are known as DNA intercalators. Figure 20 shows the fluorescence measurements before and after the addition of 1% of the respective dyes. In both cases the fluorescence intensity does not increase as much as in the case with pyrene, but again, the intensities are higher when the phenanthrenes are excited at the H-band. The maximal values are already reached with concentration of 1.7% of dye (quantum yields of 10% with excitation wavelength 243 nm).

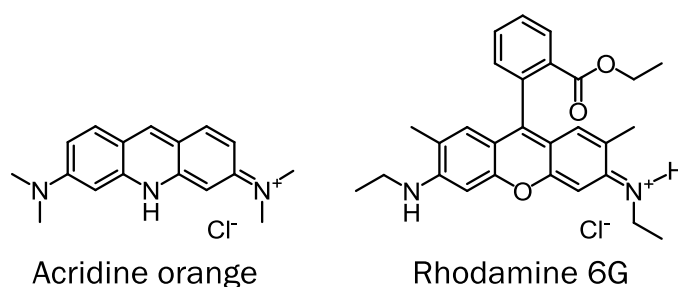Acridine orange   Rhodamine 6G

Figure 19: Chemical structures of acridine orange and rhodamine 6G which were used as acceptors for phenanthrene light-harvesting nanotubes.
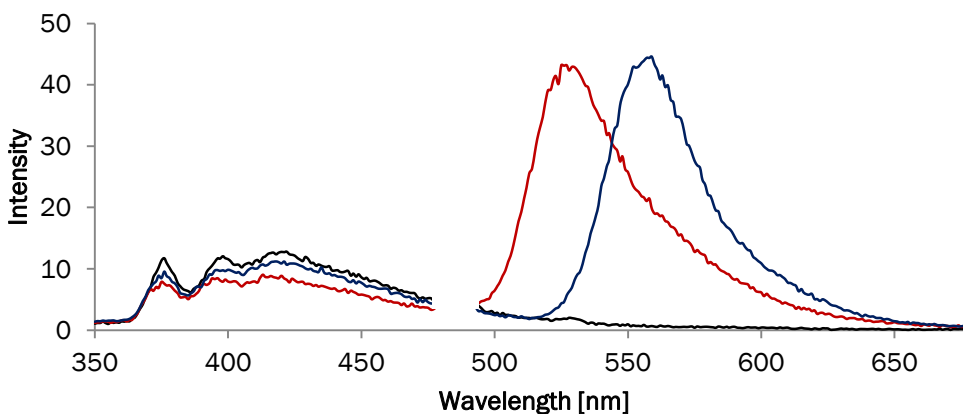

Figure 20: Fluorescence spectra of phenanthrene nanotubes without acceptor (black), with 1% acridine orange (red), and with 1% rhodamine 6G (blue), conditions as in Figure 15.

Conclusion

The self-assembly of aromatic oligomers into nanotubes with light-harvesting properties was demonstrated. 2,7-Phosphodiester-linked phenanthrene oligomers form H-aggregated supramolecular polymers in aqueous medium which were revealed as tubular objects in AFM and TEM imaging. Those phenanthrene nanotubes exhibit only weak fluorescence. By incorporating minute amounts of acceptor, an increase of the corresponding acceptor fluorescence is observed. The π-stacked phenanthrene units function as light-harvesting antennae in which the excitation energy is efficiently transferred to the acceptor. By exciting the phenanthrene H-band directly, a higher increase of acceptor fluorescence is observed. In the case of pyrene, this is illustrated with a higher increase in quantum yield and a higher ratio of pyrene emission to phenanthrene emission. The fluorescence quantum yields of the light-harvesting antenna (with 7.3% pyrene/phenanthrene) are the same for both excitation wavelengths. This leads to the conclusion that excitation of the H-band yields lower quantum yield, but with an acceptor present, the excited phenanthrenes transfer the energy more effective.

Supporting Information

Organic Synthesis

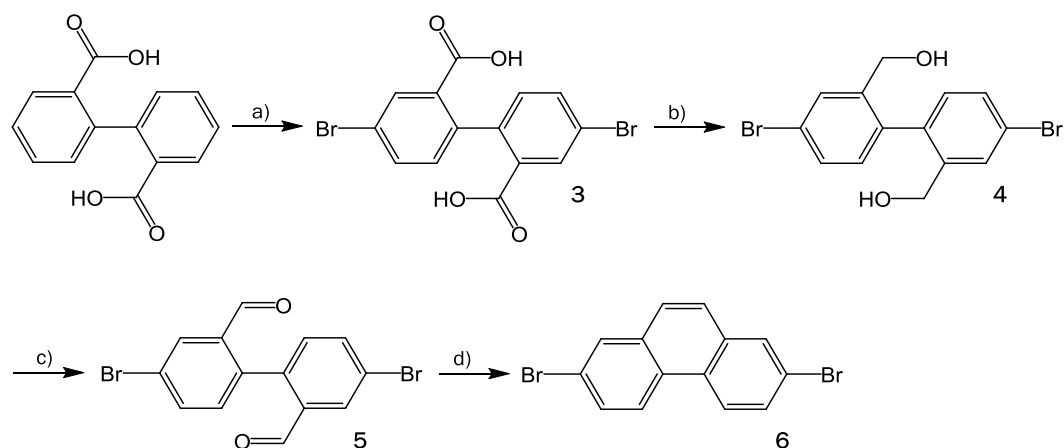Synthesis of 2,7-dibromophenanthrene (**6**, Figure 21) is described in literature.[45]

Figure 21: Synthetic approach for 2,7-dibromophenanthrene **6**. Conditions: a) Dibromoisocyanuric acid, H_2SO_4, r.t., 18 h; b) $NaBH_4$, I_2, THF, 80°C, 1 h, 45%; c) Oxalyl chloride, DMSO, Et_3N, DCM, -78°C, 1.5 h, 96%; d) N_2H_4, CH_3CO_2H, 120°C, 1.5 h, 91%.
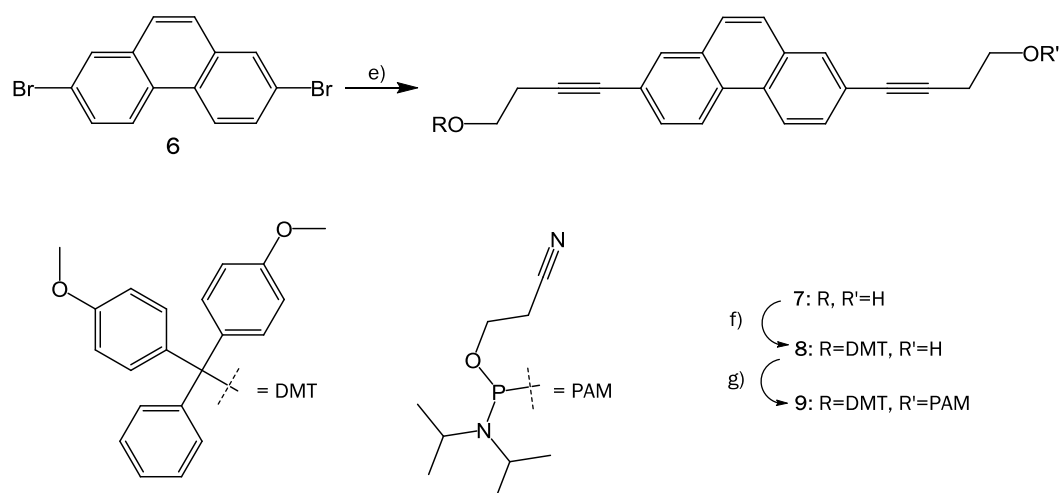

Figure 22: Synthetic approach for phenanthrene phosphoramidite **9**. Conditions: e) 3-butyn-1-ol, Pd[PPh3]2Cl2, CuI, THF, Et_3N, 80°C, 24 h, 63%; f) DMT-Cl, THF, Et_3N, r.t., 4 h, 42%; g) PAM-Cl, DIPEA, DCM, r.t., 2 h, 90%.
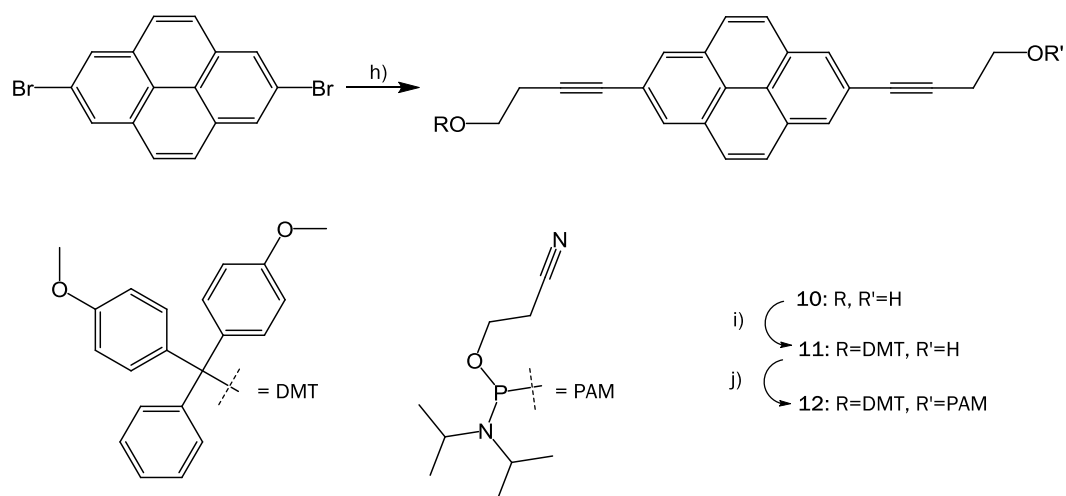
Figure 23: Synthetic approach for pyrene phosphoramidite **12**. Conditions: h) 3-butyn-1-ol, Pd[PPh$_3$]$_2$Cl$_2$, CuI, THF, Et$_3$N, 80°C, 24 h, 72%; i) DMT-Cl, THF, Et$_3$N, r.t., 16 h, 37%; j) PAM-Cl, DIPEA, DCM, r.t., 2 h, 56%.

4,4'-Dibromo-2,2'-bis(carboxyl)-1,1'-biphenyl (3): Diphenic acid (4.67 g, 19.29 mmol) was dissolved in 150 ml H$_2$SO$_4$ and cooled in an ice bath to 0°C. Dibromoisocyanuric acid (5.64 g, 19.66 mmol) was added portionwise to the solution. The reaction mixture was allowed to warm to r.t. and stirred for 18 h. The reaction was then poured over 800 ml of ice. The precipitate was filtered off, washed with water and dried under high vacuum. The product was used without further purification for the next step (crude yield: 7.1 g).

4,4'-Dibromo-2,2'-bis(hydroxymethyl)-1,1'-biphenyl (4): Compound **3** (2 g, 5.03 mmol) was dissolved in 15 ml THF. NaBH$_4$ (0.72 g, 19.03 mmol) was added slowly. After gas evolution stopped I$_2$ (1.3 g, 5.07 mmol) in 10 ml THF was added portionwise. The reaction mixture was stirred under reflux for 1 h. TLC (hexane/ethyl acetate 7:3) showed disappearance of starting material. The reaction was quenched with 2% HCl and extracted with hexane (3x). The combined organic phases were washed with 10% NaOH (3x), brine (1x) and dried with MgSO$_4$. After filtration the solvent was removed in vacuo and the residue was dried under high vacuum. Silica gel chromatography (hexane/ethyl acetate 7:3) gave **4** as a white solid (0.85 g, 45%). ^{1}H NMR (300 MHz, DMSO) δ 7.70 (d, J = 2.0 Hz, 2H), 7.49 (dd, J = 8.1, 2.1 Hz, 2H), 7.03 (d, J = 8.1 Hz, 2H), 5.24 (t, J = 5.4 Hz, 2H), 4.17 – 4.03 (m, 4H). ^{13}C NMR (75 MHz, DMSO) δ 142.52, 135.91, 131.02, 129.53, 129.21, 121.09, 60.10. HRMS-NSI (*m/z*): [M-H]$^-$ calcd for C$_{14}$H$_{11}$O$_2$Br$_2$, 368.9120; found, 368.9135.

4,4'-Dibromo-2,2'-diformyl-1,1'-biphenyl (5): A solution containing oxalyl chloride (0.54 ml, 6.19 mmol) in 15 ml DCM was cooled down to -78°C (cooling bath: dry CO_2 in aceton/ethanol 1:1). DMSO (0.62 ml, 8.68 mmol) was added, followed by **4** (0.85 g, 2.28 mmol) dissolved in 15 ml DCM. The reaction mixture was stirred for 1.5 h. Et_3N (2.6 ml, 14.05 mmol) was added and the reaction mixture was allowed to warm to r.t. The reaction mixture was put into a separation funnel and was washed with 5% HCl, saturated $NaHCO_3$ and brine. The solvent was removed in vacuo and the residue was dried under high vacuum to yield **4** as an orange solid (0.81 g, 96%). ^1H NMR (300 MHz, DMSO) δ 9.70 (s, 2H), 8.12 (d, J = 2.2 Hz, 2H), 7.94 (dd, J = 8.2, 2.2 Hz, 2H), 7.38 (d, J = 8.2 Hz, 2H). ^{13}C NMR (75 MHz, DMSO) δ 190.58, 138.39, 135.94, 135.57, 133.71, 131.87, 122.13.

2,7-Dibromophenanthrene (6): Compound **5** (1.62 g, 4.4 mmol) was dissolved in 40 ml glacial acetic acid and heated up to reflux. Hydrazine monohydrate (0.3 ml, 6.18 mmol) in 5 ml glacial acetic acid was added dropwise to the solution. A precipitate started to form instantly. The reaction mixture was stirred for 1.5 h, until TLC (hexane/ethyl acetate 8:2) showed completeness of the reaction. After cooling down to r.t., the reaction mixture was poured over ice (~400 ml) and the brown precipitate was filtered off. After washing with H_2O, the filter cake was dried under high vacuum to yield **6** (1.35 g, 91%). ^1H NMR (300 MHz, DMSO) δ 8.79 (d, J = 8.9 Hz, 2H), 8.29 (d, J = 2.1 Hz, 2H), 7.90 (s, 2H), 7.84 (dd, J = 8.9, 2.1 Hz, 2H). ^{13}C NMR (75 MHz, DMSO) δ 133.13, 130.51, 129.95, 128.18, 127.07, 125.40, 120.44.

2,7-Bis(4-hydroxybut-1-yn-1-yl)phenanthrene (7): 2,7-dibromophenanthrene (0.43 g, 1.28 mmol) was dissolved in THF (10 ml) and Et_3N (5 ml) under argon. CuI (20 mg) and $Pd[PPh_3]_2Cl_2$ (50 mg) were added, followed by 3-butyn-1-ol (0.3 ml, 3.96 mmol). The reaction mixture was heated to reflux and stirred for 24 h. TLC (DCM/methanol 95:5) showed disappearance of starting material. The solvent was removed in vacuo and the residue was purified by silica gel chromatography (DCM, then DCM/methanol 99:1). Compound **7** was isolated as a white solid (255 mg, 63 %). ^1H NMR (300 MHz, DMSO) δ 8.76 (d, J = 8.7 Hz, 2H), 8.05 (d, J = 1.5 Hz, 2H), 7.84 (s, 2H), 7.65 (dd, J = 8.5, 1.7 Hz, 2H), 4.95 (t, J = 5.6 Hz, 2H), 3.67 – 3.60 (m, 4H), 2.63 (t, J = 6.8 Hz, 4H). ^{13}C NMR (75 MHz, DMSO) δ 131.59, 131.27, 129.49, 128.59, 126.97, 123.44, 121.76, 89.82, 81.01, 59.73, 23.38. HRMS-NSI (*m/z*): $[M+H]^+$ calcd for $C_{22}H_{19}O_2$, 315.1380; found, 315.1372.

2-[4-(4,4'-Dimethoxytriphenylmethyloxy)but-1-yn-1-yl]-7-(4-hydroxyhex-1-yn-1-yl)phenanthrene (8): Compound **7** (379.1 mg, 1.21 mmol) was dissolved in THF (10 ml) and Et_3N (2 ml). DMT-Cl (410 mg, 1.21 mmol) was added in two portions. The reaction mixture was stirred at r.t. for 4 h. The solvent was removed in vacuo and the residue was purified by

silica gel chromatography (hexane/ethyl acetate/Et₃N 1:1:0.02) to give **8** as a white foam (310.9 mg, 42%). ^{1}H NMR (300 MHz, DMSO) δ 8.77 (dd, J = 8.7, 6.5 Hz, 2H), 8.06 (s, 2H), 7.84 (s, 2H), 7.70 – 7.62 (m, 2H), 7.47 (d, J = 7.4 Hz, 2H), 7.34 – 7.30 (m, 6H), 7.23 (t, J = 7.1 Hz, 1H), 6.90 (d, J = 8.8 Hz, 4H), 4.95 (t, J = 5.6 Hz, 1H), 3.73 (s, 6H), 3.67 – 3.61 (m, 2H), 3.19 (t, J = 6.5 Hz, 2H), 2.78 (t, J = 6.3 Hz, 2H), 2.63 (t, J = 6.8 Hz, 2H). ^{13}C NMR (75 MHz, DMSO) δ 158.09, 144.90, 135.67, 131.63, 131.31, 131.27, 129.66, 129.54, 129.41, 128.73, 128.61, 127.85, 127.67, 127.08, 126.97, 126.71, 123.60, 123.50, 121.83, 121.56, 113.21, 89.88, 89.54, 85.53, 81.29, 81.03, 61.60, 59.75, 55.01, 23.40, 20.34. HRMS-NSI (m/z): [M+Na]$^+$ calcd for $C_{43}H_{36}O_4Na$, 639.2506; found, 639.2511.

Phosphoramidite (9): Compound **8** (150.4 mg, 0.24 mmol) was dissolved in DCM (2.2 ml) and DIPEA (0.2 ml). PAM-Cl (60 mg, 0.25 mmol) was added and the reaction mixture was stirred at r.t. for 2 h until TLC (hexane/ethylacetate/Et₃N 6:4:0.1) showed disappearance of starting material. After removing the solvent in vacuo the product was purified by silica gel chromatography (hexane/ethyl acetate/Et₃N 7:3:0.1). Phosphoramidite **9** was isolated as a white foam (178.8 mg, 90%). ^{1}H NMR (300 MHz, CDCl₃) δ 8.53 (d, J = 8.6 Hz, 2H), 7.94 (s, 2H), 7.68 – 7.61 (m, 4H), 7.55 (d, J = 7.7 Hz, 2H), 7.43 (d, J = 8.7 Hz, 4H), 7.31 (t, J = 7.4 Hz, 2H), 7.26 – 7.19 (m, 1H), 6.85 (d, J = 8.8 Hz, 4H), 3.98 – 3.81 (m, 4H), 3.78 (s, 6H), 3.73 – 3.60 (m, 2H), 3.36 (t, J = 6.8 Hz, 2H), 2.86 – 2.74 (m, 4H), 2.68 – 2.62 (m, 2H), 1.23 (dd, J = 6.7, 3.4 Hz, 12H). ^{13}C NMR (75 MHz, CDCl₃) δ 158.55, 145.15, 136.37, 132.01, 131.98, 131.82, 131.77, 130.16, 129.75, 129.72, 129.36, 129.27, 128.28, 127.91, 127.13, 127.09, 126.84, 122.89, 122.29, 122.06, 117.76, 113.20, 88.87, 87.80, 86.19, 81.94, 81.62, 62.15, 62.06, 61.82, 58.75, 58.50, 55.28, 43.34, 43.17, 24.80, 24.77, 24.70, 24.68, 22.69, 22.60, 21.26, 20.51, 20.43. ^{31}P NMR (121 MHz, CDCl₃) δ 148.23. HRMS-NSI (m/z): [M+H]$^+$ calcd for $C_{52}H_{54}O_5N_2P$, 817.3765; found, 817.3784.

Phenanthrene-modified solid support: Compound **8** (30 mg, 0.05 mmol) was dissolved in DCM (0.25 ml). Succinic anhydride (5 mg, 0.05 mmol) and DMAP (9.16 mg, 0.075 mmol) were added. The reaction mixture was stirred for 4 h at r.t., and then transferred into a separation funnel. The organic phase was washed once with 10% citric acid and once with brine. After drying with MgSO₄ and filtration, the solvent was removed in vacuo. The residue was dissolved in 6.5 ml of acetonitrile. 2 ml (~0.015 mmol of ester) of this solution were transferred into a round bottom flask. LCAA-CPG (500 Å, 300 mg) were added, followed by BOP (13.3 mg, 0.03 mmol) and N-methylimidazol (5 µl, 0.06 mmol). The suspension was stirred for 20 h. The solid support was filtered and washed with DCM. A solution of pyridine

and acetic acid anhydride (3:1, 2.4 ml) was prepared, to which were added DMAP (30 mg) and the solid support. After 2 h of stirring, the solid support was filtered and washed with DCM.

Determination of loading: A small sample of solid support (2.3 mg) was treated with 10 ml of 3% trichloroacetic acid in DCM. The absorption was measured at 498 nm. For the calculation of the loading, the absorption coefficient ε = 70'000 for the DMT cations was used.

2,7-Bis(4-hydroxybut-1-yn-1-yl)pyrene (10): 2,7-dibromopyrene (1.00 g, 2.78 mmol) was dissolved in THF (25 ml) and Et$_3$N (5 ml) under argon. CuI (20 mg) and Pd[PPh$_3$]$_2$Cl$_2$ (50 mg) were added, followed by 3-butyn-1-ol (0.65 ml, 8.59 mmol). The reaction mixture was heated to reflux and stirred for 18 h. TLC (hexane/ethyl acetate 4:6) showed still remaining starting material, therefore the same amount of reagent and catalysts were added. The reaction mixture was stirred for another 5 h under reflux, until TLC showed disappearance of starting material. The solvent was removed in vacuo and the residue was purified by silica gel chromatography (hexane/ethyl acetate 4:6). Compound **10** was isolated as a yellowish solid (673.2 mg, 72 %). ^{1}H NMR (300 MHz, DMSO) δ 8.32 (s, 4H), 8.17 (s, 4H), 4.98 (t, J = 5.6 Hz, 2H), 3.72 – 3.65 (m, 4H), 2.68 (t, J = 6.8 Hz, 4H). ^{13}C NMR (75 MHz, DMSO) δ 130.70, 127.84, 127.49, 122.64, 121.27, 89.62, 81.41, 59.81, 23.44. HRMS-NSI (*m/z*): [M+H]$^+$ calcd for C$_{24}$H$_{19}$O$_2$, 339.1380; found, 339.1375.

2-[4-(4,4'-Dimethoxytriphenylmethyloxy)but-1-yn-1-yl]-7-(4-hydroxyhex-1-yn-1-yl)pyrene (11): Compound **10** (301 mg, 0.89 mmol) was dissolved in THF (12 ml) and Et$_3$N (2.5 ml). DMT-Cl (303 mg, 0.89 mmol) was added in two portions. The reaction mixture was stirred at r.t. for 3 h. The solvent was removed in vacuo and the residue was purified by silica gel chromatography (hexane/ethyl acetate/Et$_3$N 6:4:0.1) to give **11** as a white foam (197 mg, 35%). ^{1}H NMR (300 MHz, DMSO) δ 8.32 (s, 4H), 8.17 (s, 4H), 7.49 (d, J = 7.2 Hz, 2H), 7.37 – 7.30 (m, 6H), 7.24 (t, J = 7.2 Hz, 1H), 6.91 (d, J = 8.9 Hz, 4H), 4.98 (t, J = 5.6 Hz, 1H), 3.73 (s, 6H), 3.71 – 3.65 (m, 2H), 3.24 (t, J = 6.5 Hz, 2H), 2.84 (t, J = 6.4 Hz, 2H), 2.68 (t, J = 6.8 Hz, 2H). ^{13}C NMR (75 MHz, DMSO) δ 158.10, 144.92, 135.68, 130.74, 130.71, 129.68, 127.88, 127.76, 127.69, 127.57, 127.46, 126.73, 122.71, 122.61, 121.32, 121.04, 113.22, 89.65, 89.26, 85.58, 81.66, 81.40, 61.68, 59.80, 55.00, 23.44, 20.37. HRMS-NSI (*m/z*): [M+H]$^+$ calcd for C$_{45}$H$_{36}$O$_4$, 640.2608; found, 640.2604.

Phosphoramidite (12): Compound **11** (230 mg, 0.36 mmol) was dissolved in DCM (3.5 ml) and DIPEA (0.2 ml). PAM-Cl (90 mg, 0.38 mmol) was added and the reaction mixture was stirred at r.t. for 2 h until TLC (hexane/ethylacetate/Et$_3$N 6:4:0.1) showed disappearance of

starting material. After removing the solvent in vacuo the product was purified by silica gel chromatography (hexane/ethyl acetate/Et$_3$N 7:3:0.1). Phosphoramidite **12** was isolated as a white foam (175.7 mg, 58%). ^{1}H NMR (300 MHz, CDCl$_3$) δ 8.18 (d, *J* = 1.6 Hz, 4H), 7.95 (s, 4H), 7.57 (d, *J* = 7.6 Hz, 2H), 7.45 (d, *J* = 8.7 Hz, 4H), 7.32 (t, *J* = 7.5 Hz, 2H), 7.26 – 7.20 (m, 1H), 6.86 (d, *J* = 8.8 Hz, 4H), 4.03 – 3.82 (m, 4H), 3.78 (s, 6H), 3.73 – 3.61 (m, 2H), 3.41 (t, *J* = 6.8 Hz, 2H), 2.90 – 2.78 (m, 4H), 2.69 – 2.63 (m, 2H), 1.24 (t, *J* = 6.2 Hz, 12H). ^{13}C NMR (75 MHz, CDCl$_3$) δ 158.56, 145.18, 136.39, 131.11, 130.18, 128.31, 128.17, 127.93, 127.54, 127.51, 126.86, 123.75, 123.68, 121.69, 121.45, 117.78, 113.21, 88.55, 87.46, 86.22, 82.37, 82.05, 62.22, 62.11, 61.87, 58.77, 58.52, 55.28, 43.35, 43.19, 24.81, 24.80, 24.71, 22.73, 22.64, 21.31, 20.53, 20.44. ^{31}P NMR (121 MHz, CDCl$_3$) δ 148.25. HRMS-NSI (*m/z*): [M+H]$^+$ calcd for C$_{54}$H$_{54}$O$_5$N$_2$P, 841.3765; found, 841.3787.

NMR Spectra
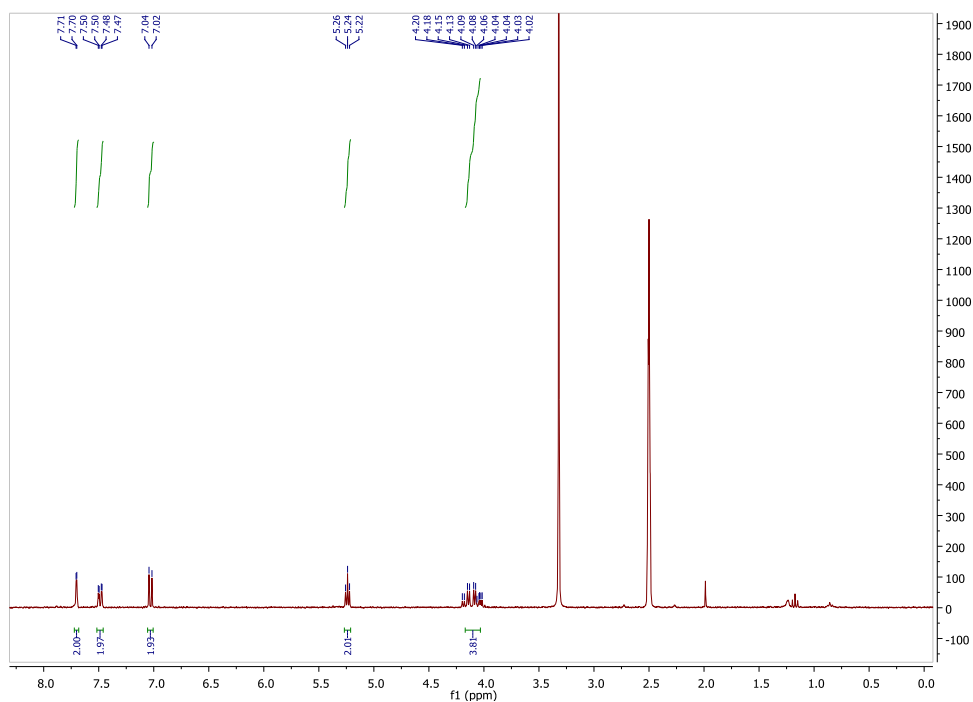
Figure 24: ^{1}H NMR of compound **4** in DMSO-d$_6$.
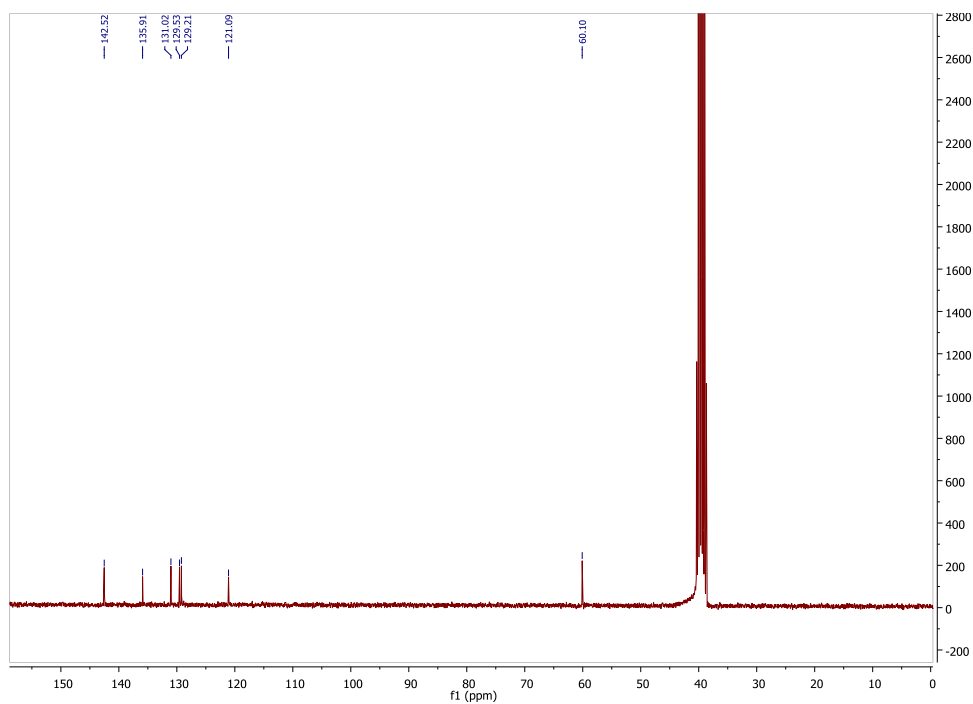
Figure 25: ^{13}C NMR of compound **4** in DMSO-d$_6$.
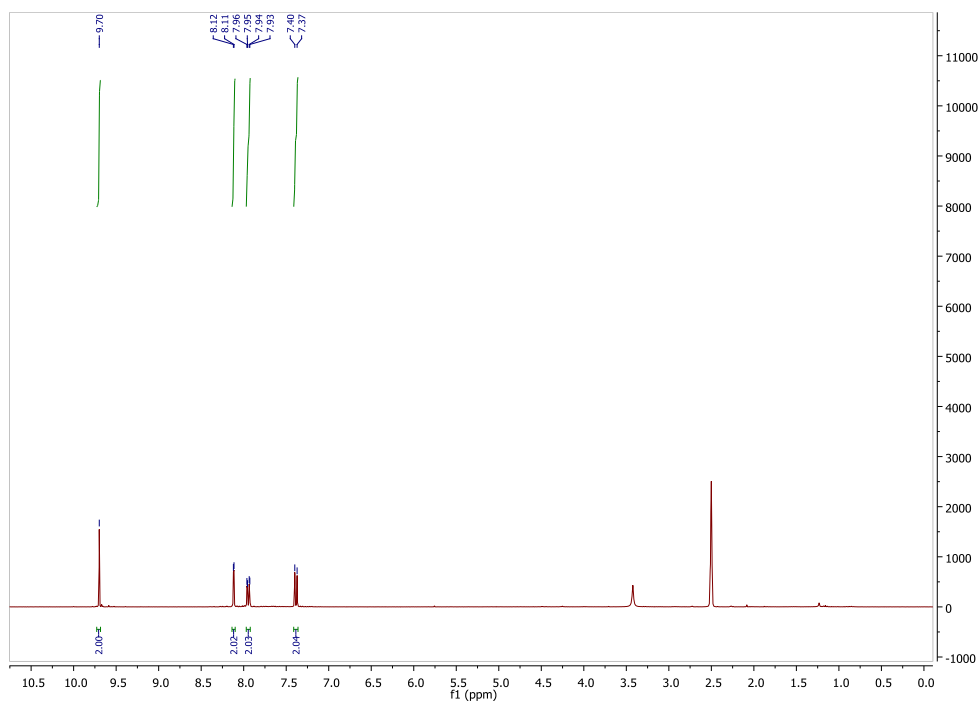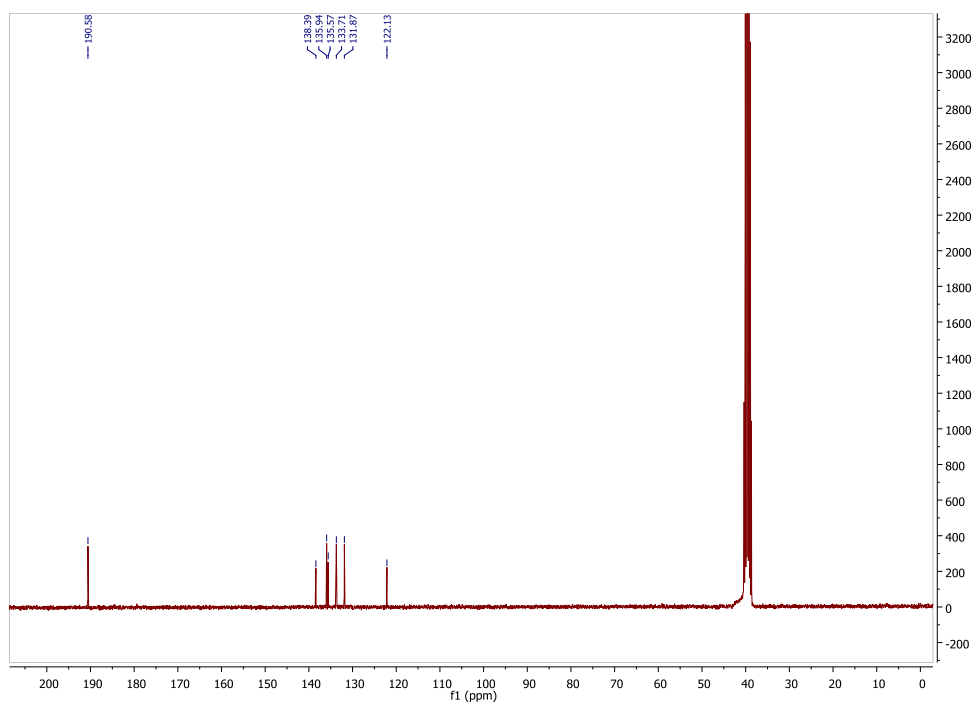

Figure 26: ^{1}H NMR of compound **5** in DMSO-d$_6$.

Figure 27: ^{13}C NMR of compound **5** in DMSO-d$_6$.

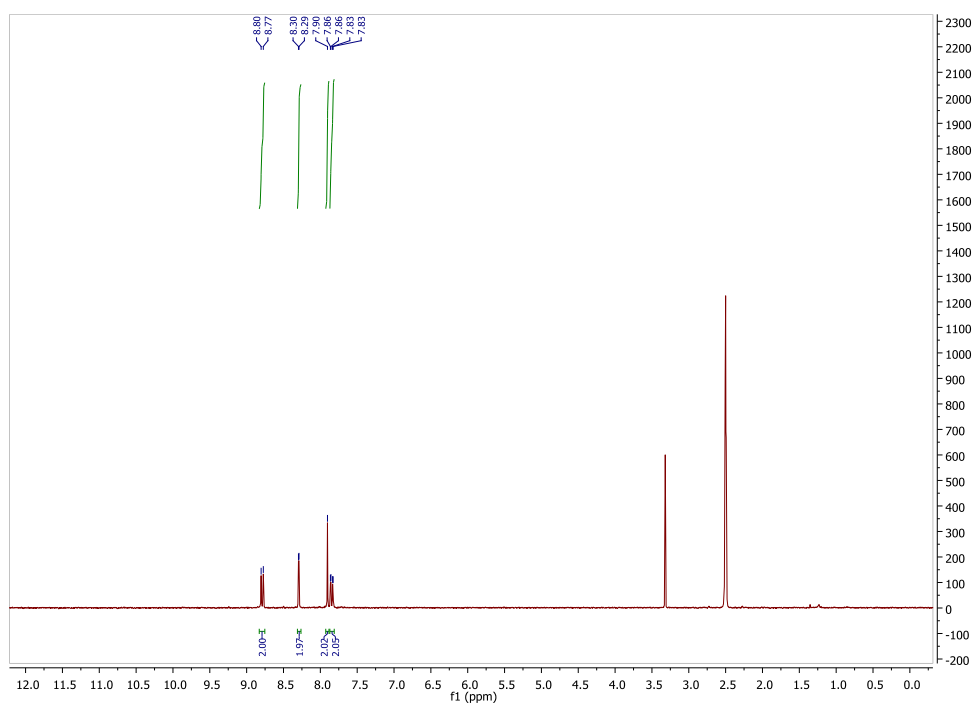

Figure 28: ^{1}H NMR of compound **6** in DMSO-d$_6$.
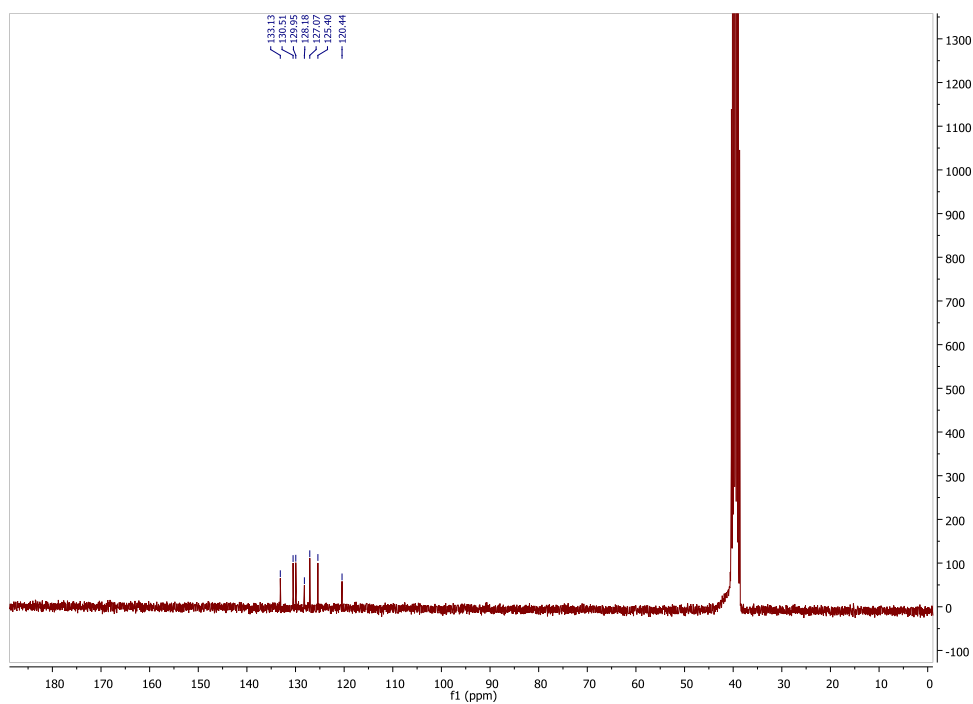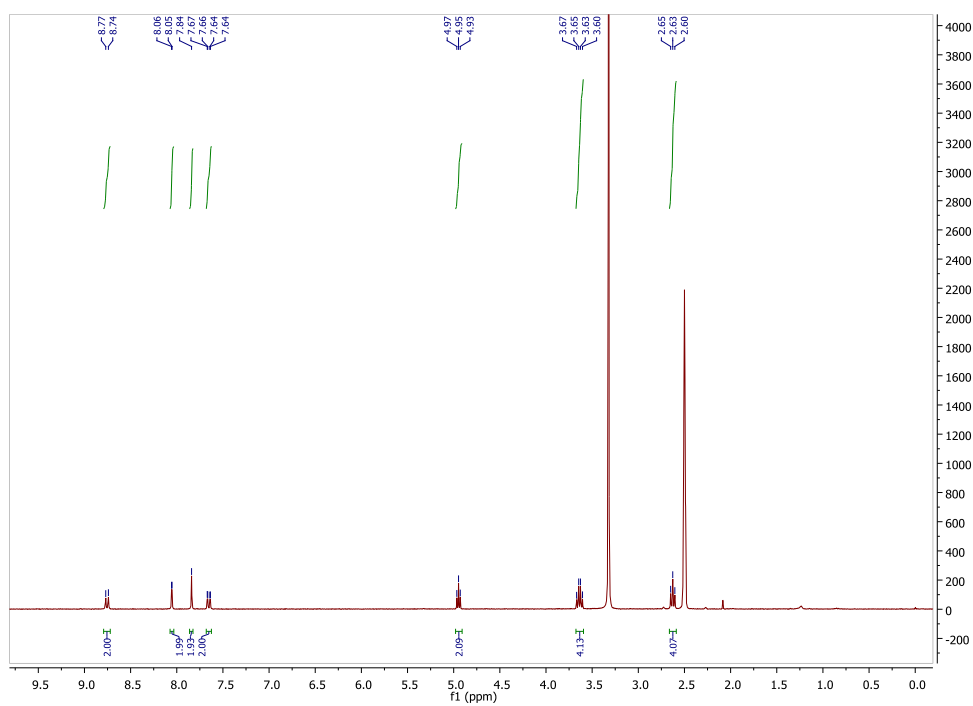
Figure 29: ^{13}C NMR of compound **6** in DMSO-d$_6$.

Figure 30: ^{1}H NMR of compound **7** in DMSO-d$_6$.
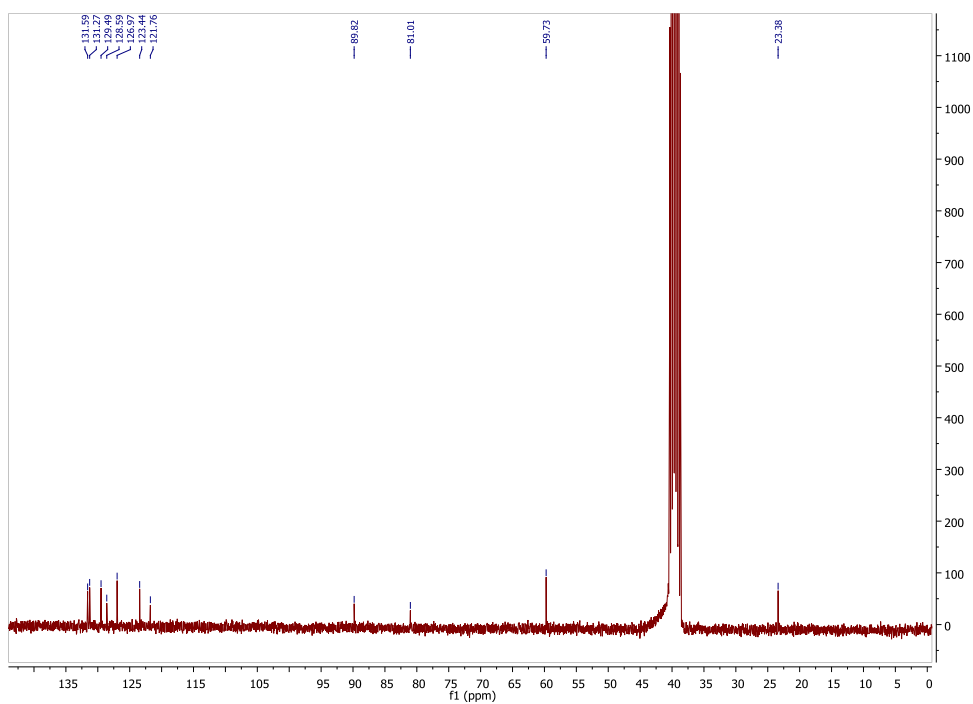
Figure 31: ^{13}C NMR of compound **7** in DMSO-d$_6$.

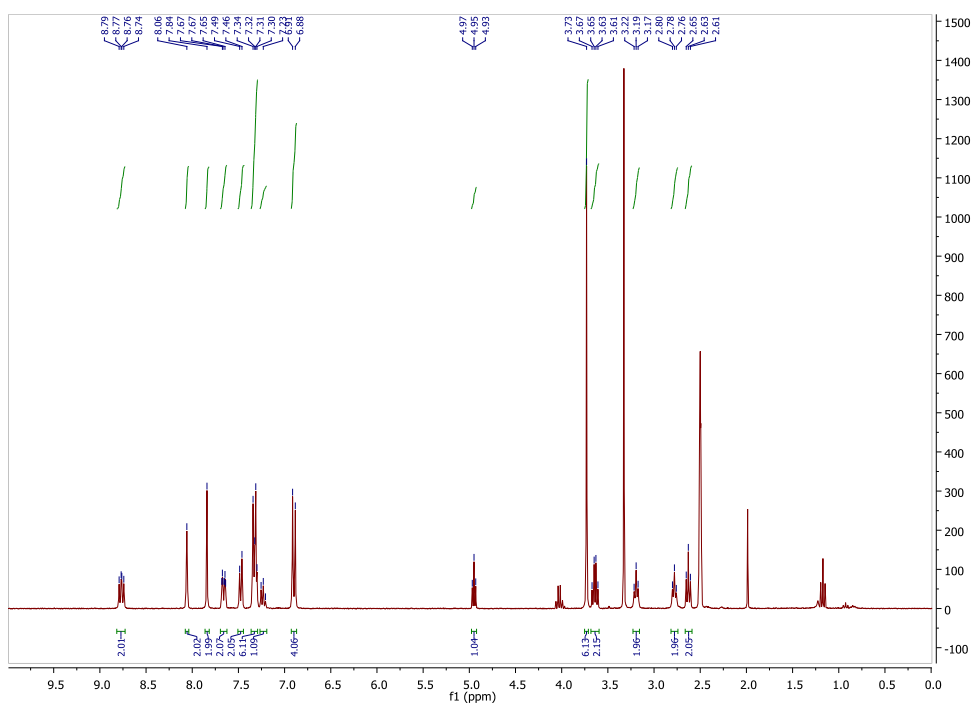Figure 32: ^{1}H NMR of compound **8** in DMSO-d$_6$.
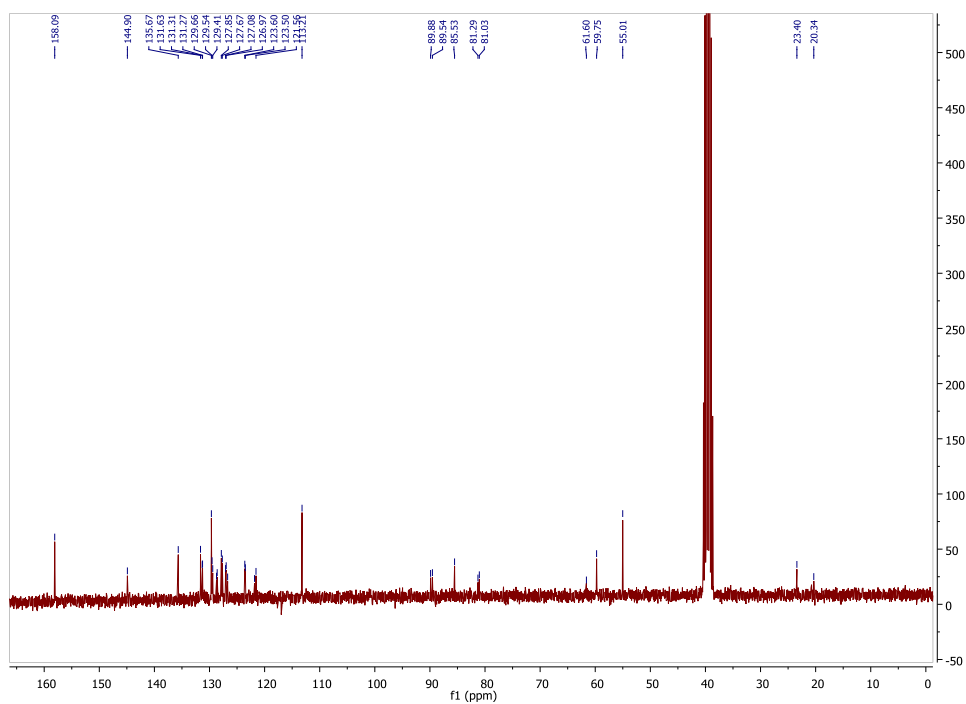
Figure 33: ^{13}C NMR of compound **8** in DMSO-d$_6$.
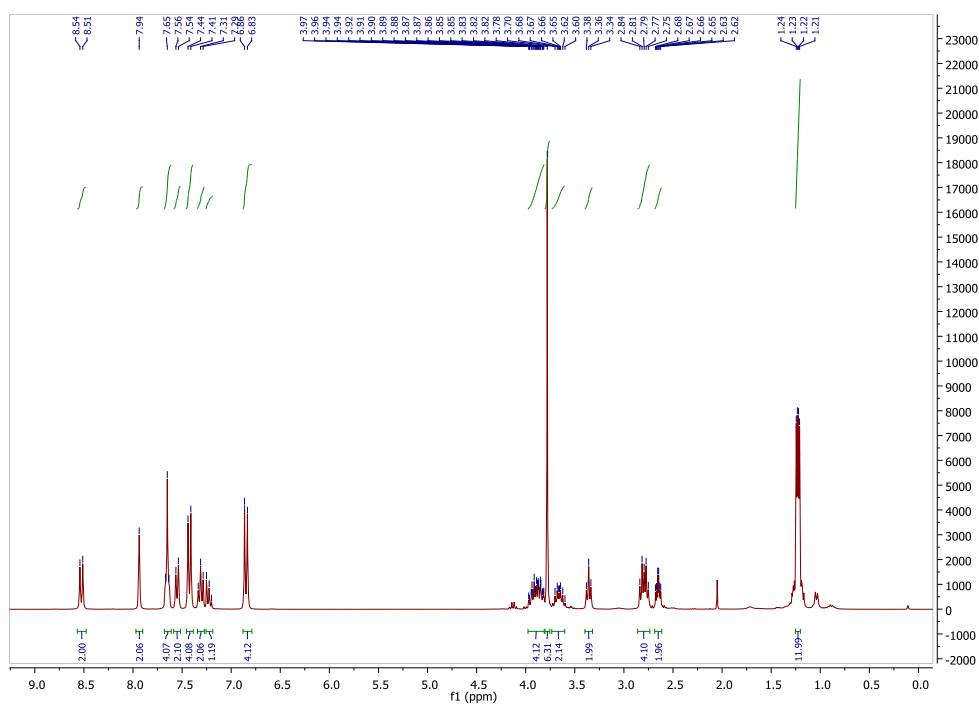
Figure 34: ^{1}H NMR of compound **9** in CDCl$_3$.
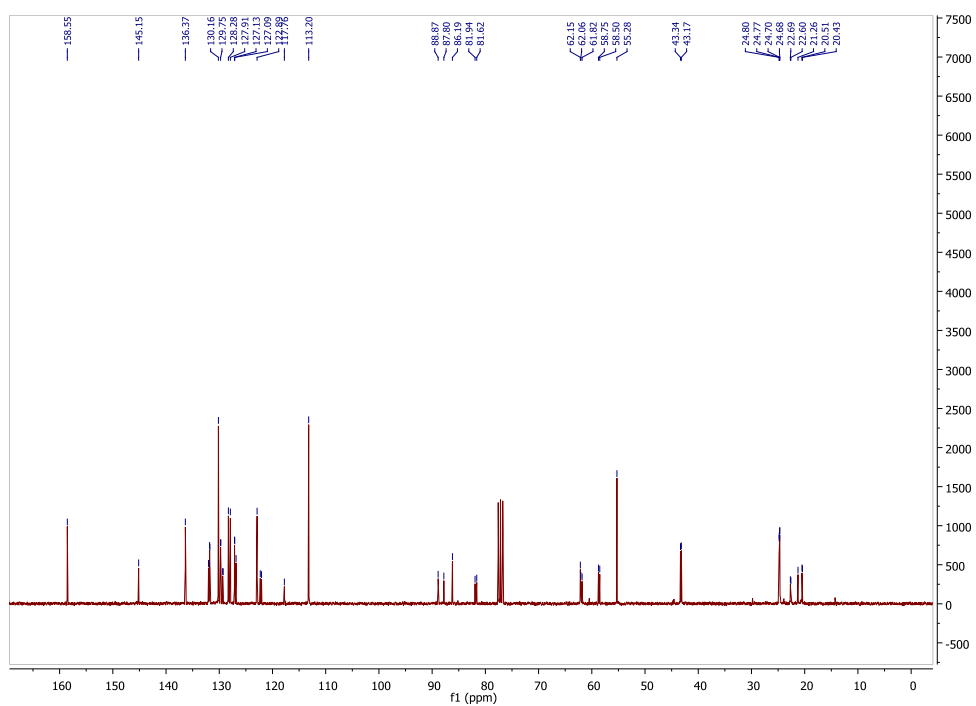
Figure 35: ^{13}C NMR of compound **9** in CDCl₃.
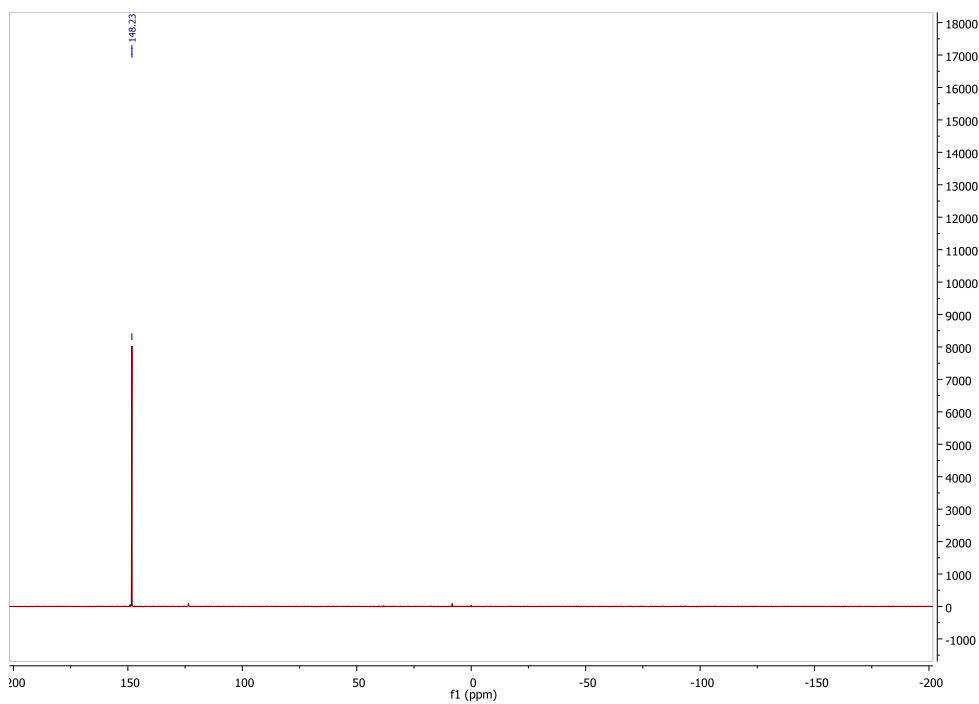
Figure 36: ^{31}P NMR of compound **9** in CDCl₃.
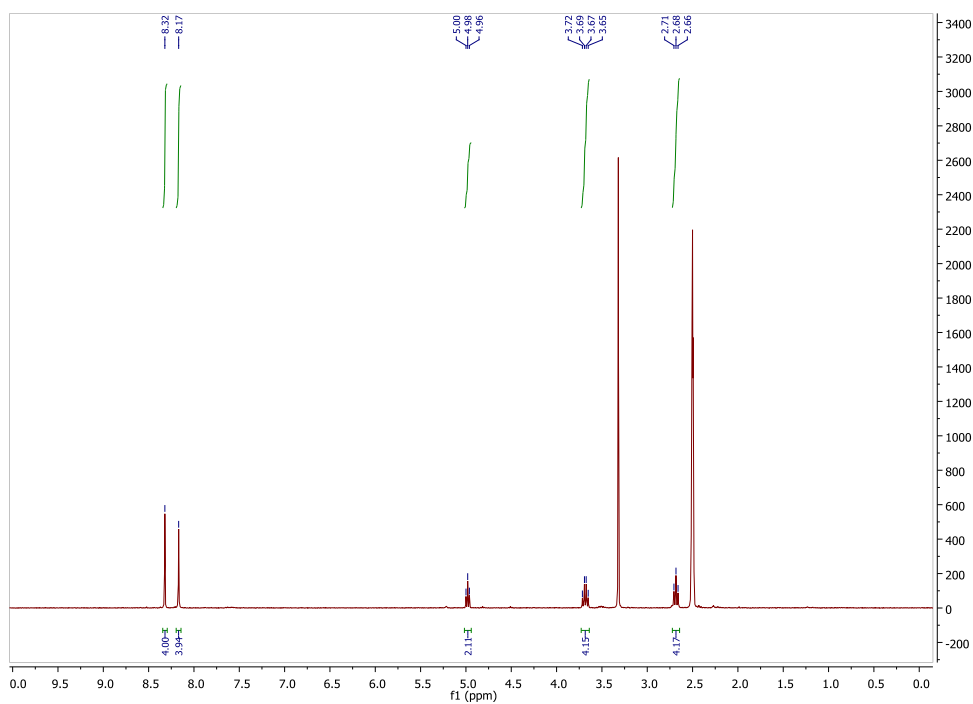
Figure 37: ^{1}H NMR of compound **10** in DMSO-d$_6$.
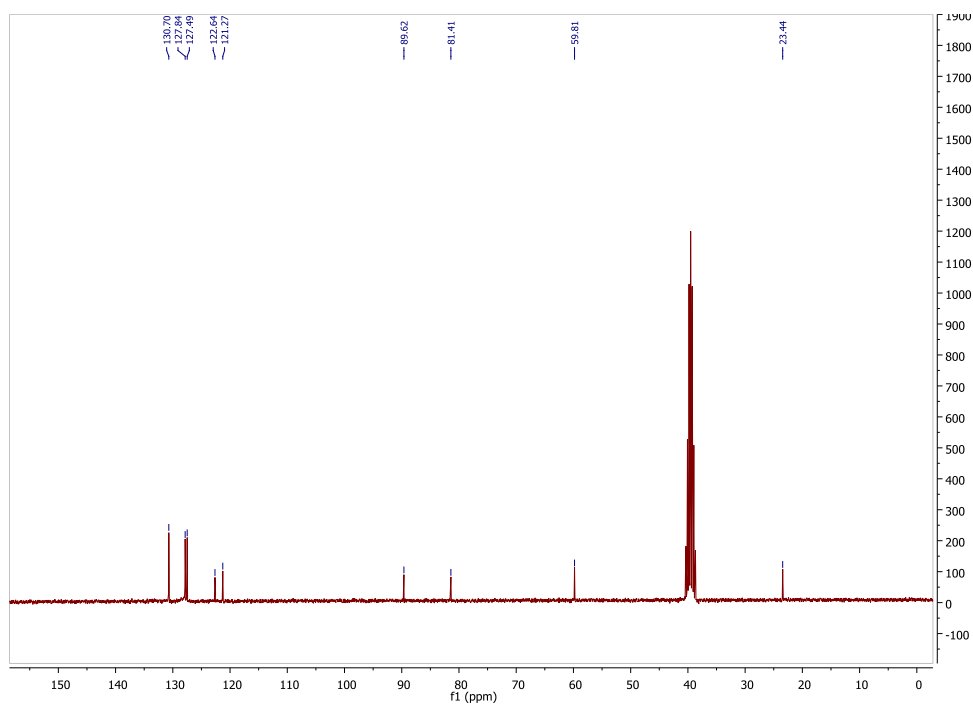
Figure 38: ^{13}C NMR of compound **10** in DMSO-d$_6$.
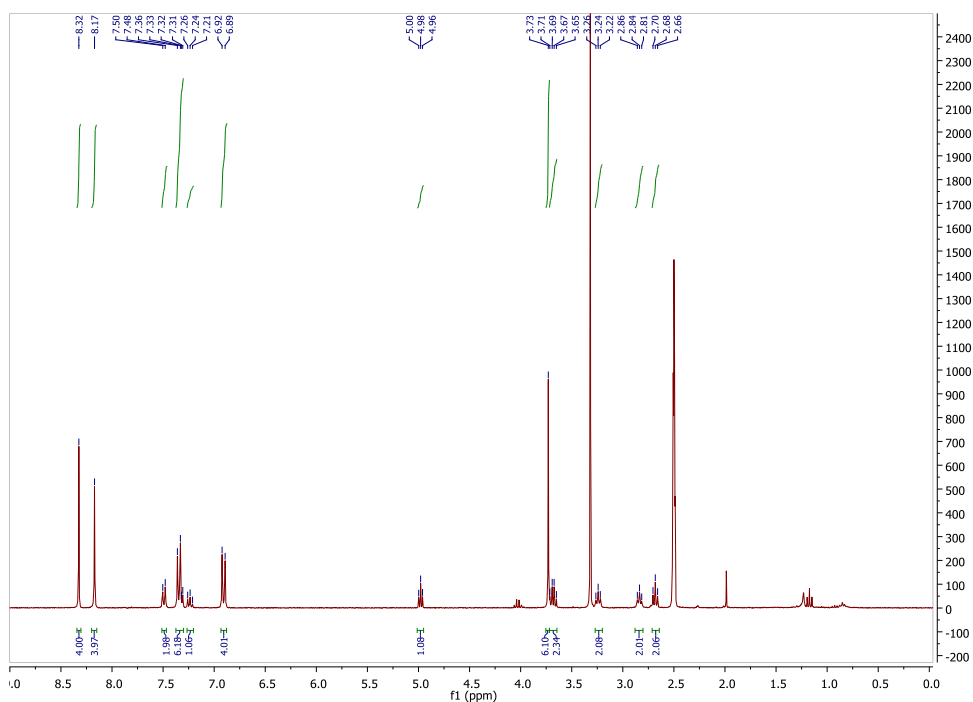
Figure 39: ^{1}H NMR of compound **11** in DMSO-d$_6$.
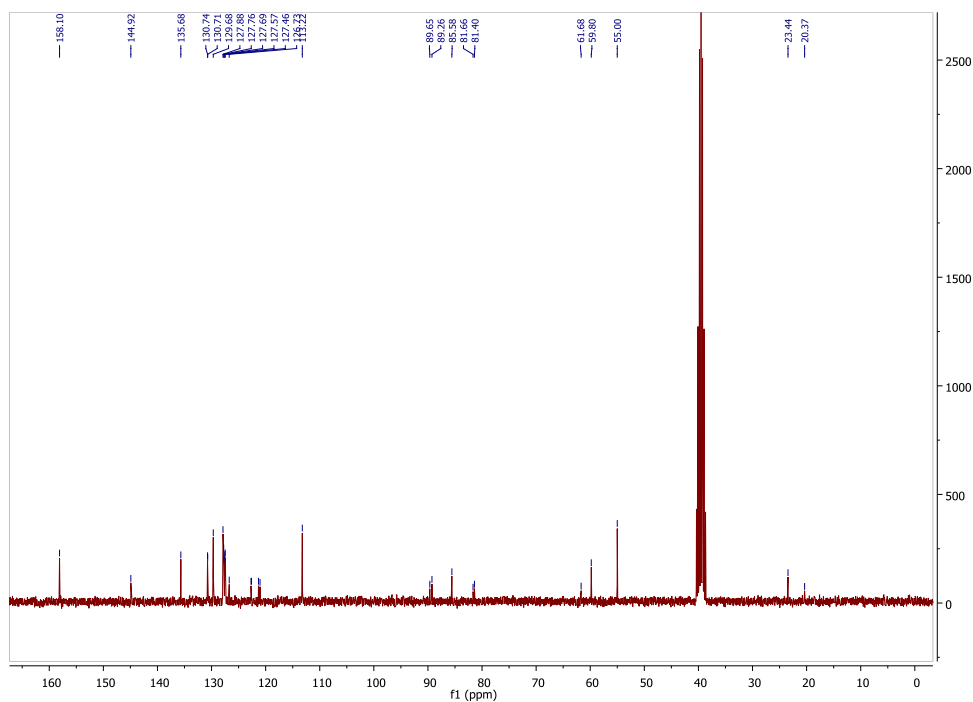
Figure 40: ^{13}C NMR of compound **11** in DMSO-d$_6$.
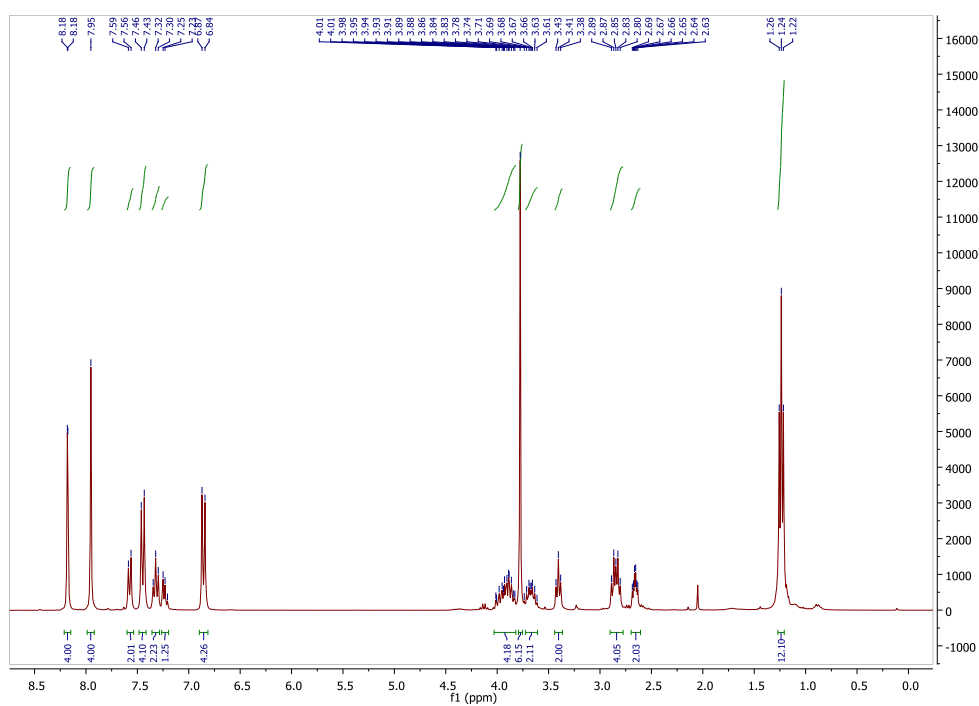
Figure 41: ¹H NMR of compound **12** in CDCl₃.

Figure 42: ¹³C NMR of compound **12** in CDCl₃.
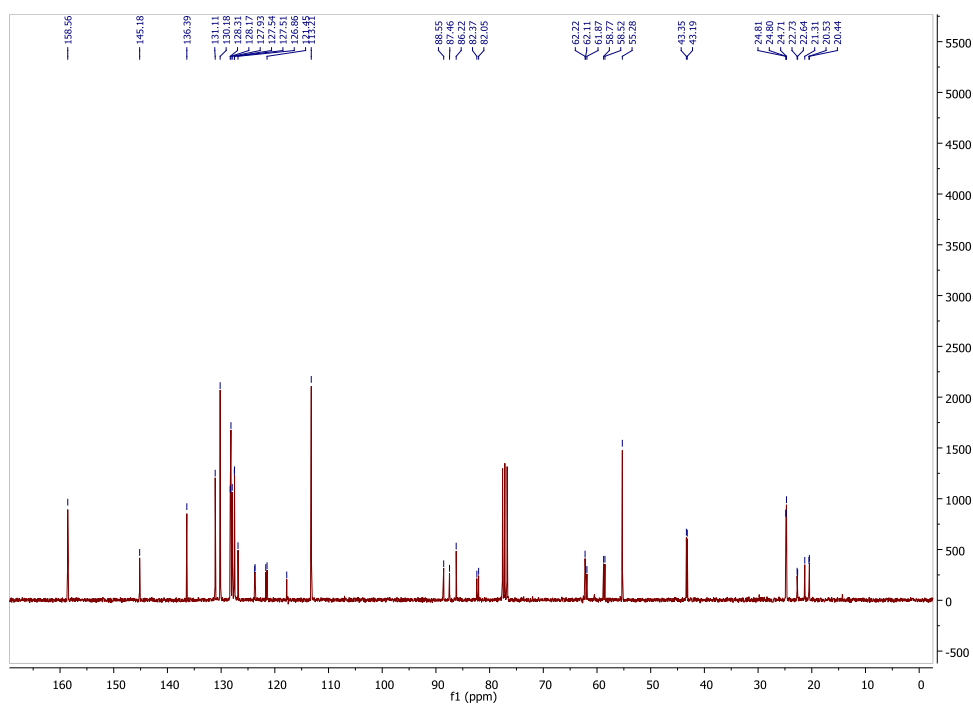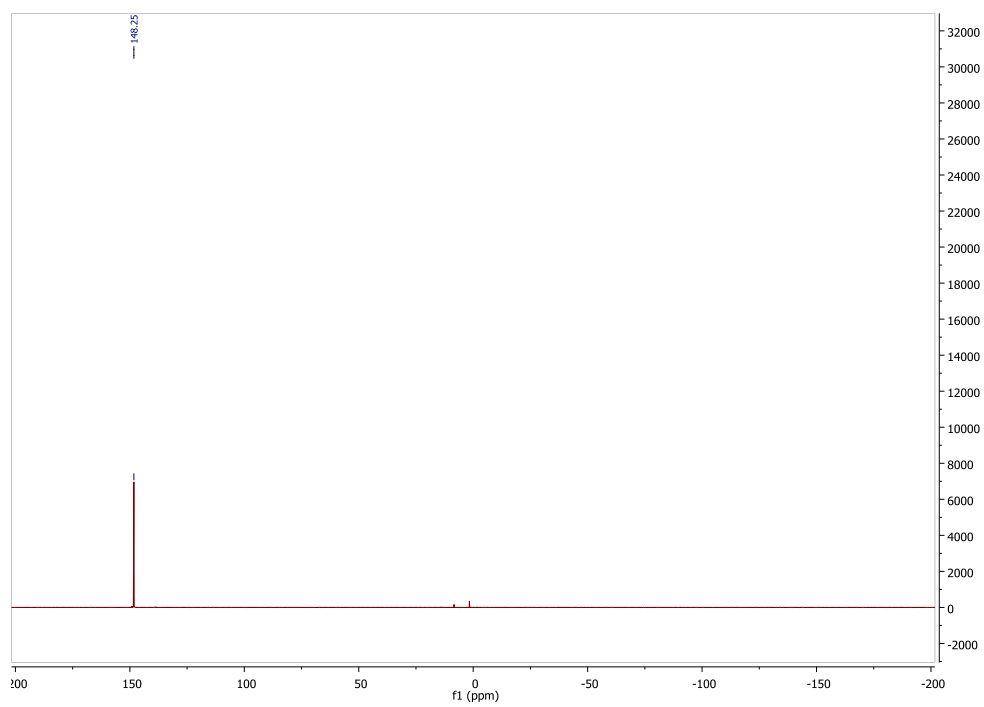
Figure 43: ^{31}P NMR of compound **12** in CDCl$_3$.

Spectra of 2,7-Dialkynyl Phenanthrene Monomer

The phenanthrene diol (**7**) shows an absorption spectrum with well-resolved vibronic bands. The absorption maximum is found at 316 nm with an absorption coefficient ε of 60'000. Around 350 nm a forbidden transition is visible. The fluorescence spectrum shows a high intensity and a well-resolved structure. The two highest intensities are found at 371 nm and 390 nm. The quantum yield of **7**, measured in ethanol, is 5%.

Figure 44: Absorption (solid) and fluorescence (dashed) spectra of compound **7**. Conditions: 1 μM in ethanol, 20°C; λexc. 316 nm.

Figure 45: Normalized absorption (solid) and fluorescence (dashed) spectra of compound **7** (monomer, blue) and oligomer **1** (black) in ethanol, 20°C; λexc. 316 nm.

Spectra of 2,7-Dialkynyl Pyrene Monomer

The absorption spectrum of the pyrene diol (**10**) shows an absorption maximum at 337 nm with an absorption coefficient ε of 30'000. The vibronic bands of the first electronic transition between 300 and 340 nm are well-resolved. The second electronic transition has a higher absorption at 283 nm, with ε=200'000. The fluorescence spectrum shows well-resolved vibronic bands, with the highest intensity peak found at 404 nm. Quantum yield was measured to be 4% in ethanol.
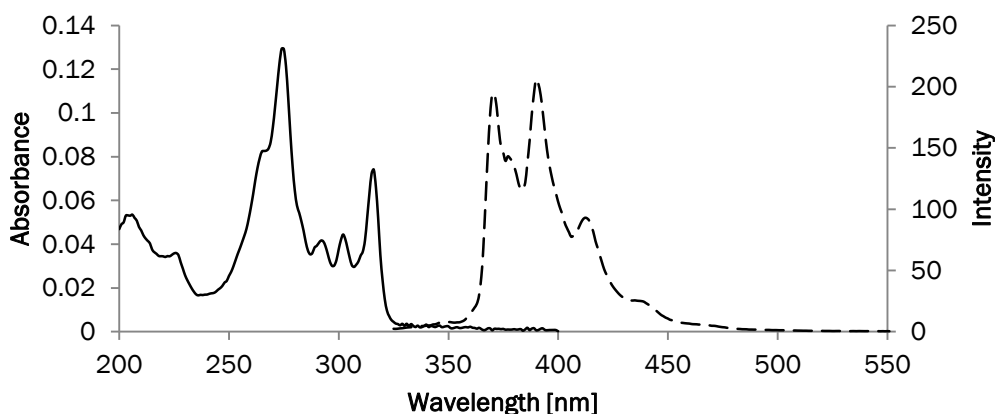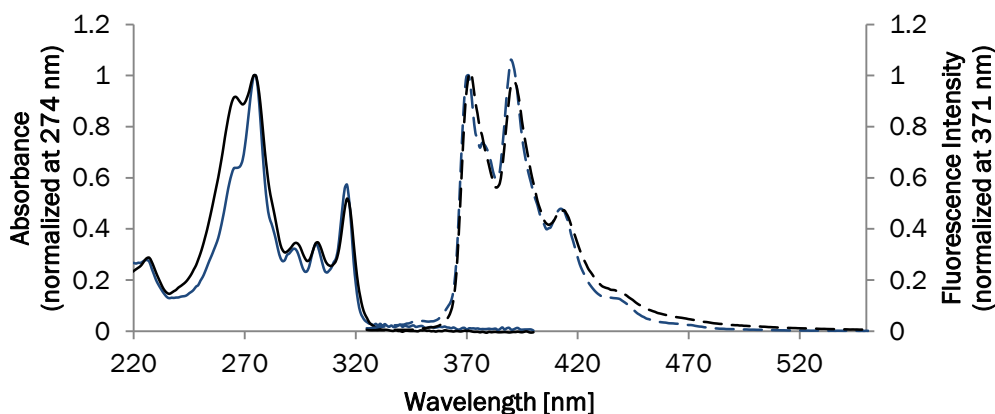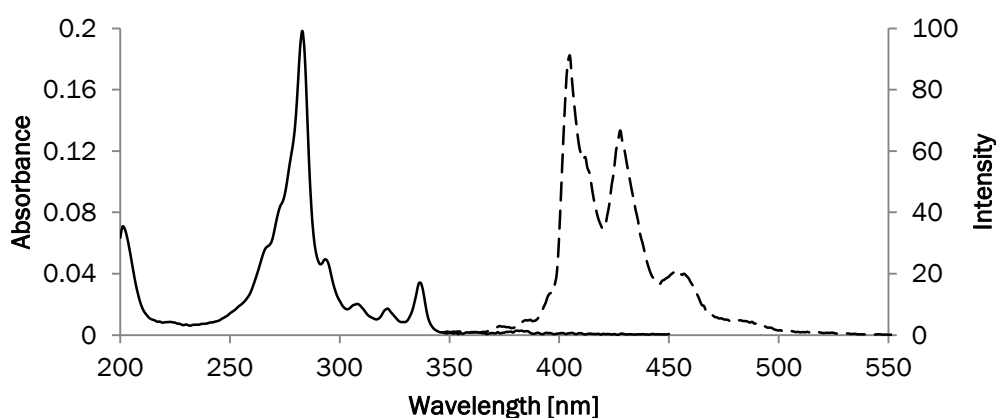

Figure 46: Absorption (solid) and fluorescence (dashed) spectra of compound **10**. Conditions: 1 µM in ethanol, 20°C; λexc. 337 nm.

Oligomer Synthesis

Oligomers were prepared on an Applied Biosystems 394 DNA/RNA synthesizer. A standard cyanoethyl phosphoramidite coupling protocol was used beginning with phenanthrene-loaded controlled pore glass (CPG) support. Compounds **9** and **12** were dissolved in 1,2-dichloroethane to yield 0.1 M solutions. After synthesis, the CPG-bound oligomers were cleaved and deprotected by treatment with 28-30% NH_4OH (aq) at 55°C for 6 h. The supernatants were collected and the debris' were washed three times with 1 ml $EtOH/H_2O$ 1:1.

After lyophilization the crude oligomers were purified by reversed phase HPLC (Merck LiChroCART 250-4; LiChrospher 100, RP-8, 5 µm); Solvent A: 0.1 M aqueous ammonium acetate; Solvent B: CH_3CN; 1 ml/min; T = 50°C; B[%] (t_R [min]) = 50 (0); 50 (2); 80 (17).

Purities were confirmed by ESI mass spectrometry. The samples were measured in negative ion mode in mixtures of water/acetonitrile/triethylamine.

The purified oligomers were dissolved in 1 ml ethanol. Samples of the stock solutions were diluted 100 times and the absorbance at 316 nm (phenanthrene) or 337 (pyrene) was measured. The molar absorption coefficients of the oligomers were calculated using the ε_{316}=60'000 for phenanthrene and ε_{337}=30'000 for pyrene.

Table 1: Calculated and found masses (negative ion mode) of oligomers **1** and **2**.

Oligomer	Chemical formula	Calculated mass	Found mass
1	$C_{66}H_{52}O_{10}P_2$	1066.30	532.14 (z=2)
2	$C_{68}H_{52}O_{10}P_2$	1090.30	544.14 (z=2)

Mass Spectra of Oligomers
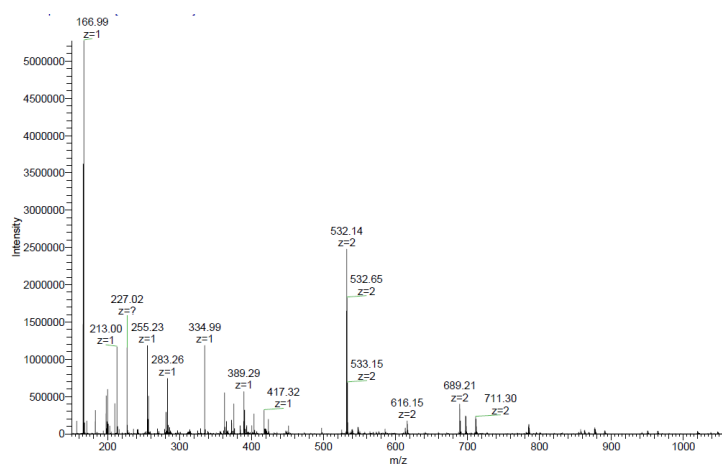
Figure 47: Mass spectrum of oligomer **1**.
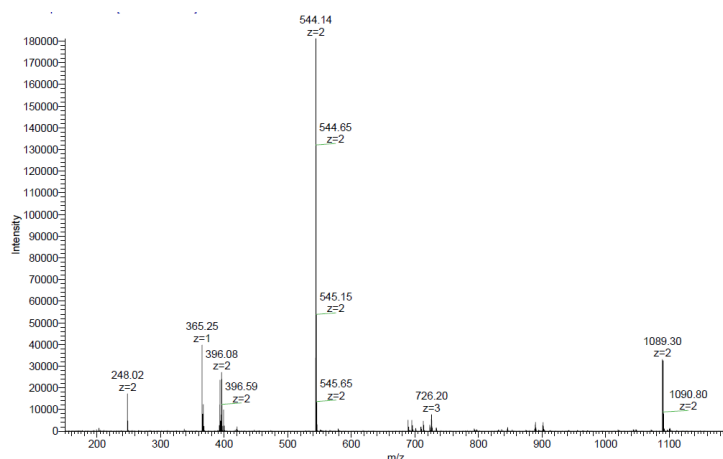
Figure 48: Mass spectrum of oligomer **2**.

Quantum Yield Determination

The quantum yield of phenanthrene nanotubes (λexc. 316 nm) in aqueous medium (10 mM sodium phosphate buffer pH 7.0, 10% ethanol) was determined relative to quinine sulfate in 0.5 M H_2SO_4 as a standard following the procedure described in literature.[46] Quantum yield for excitation at 243 nm was determined by using the fluorescence quantum yield of **1** with excitation wavelength 316 nm as a standard; under assumption the quantum yield is not dependent on excitation wavelength.

Table 2: Absorption values of **1** at 316 nm and 243 nm and corresponding fluorescence integrals upon excitation at those wavelengths. Quantum yield for excitation wavelength 243 nm was calculated by the discrepancy between the measured integral and the theoretical fluorescence integral if the quantum yield was not dependent on excitation wavelength.

Wavelength	Absorption	Fluorescence integral	Fluorescence integral (theo.)	Quantum yield
316 nm	0.067	9652.078	-	7%
243 nm	0.176	9242.669 (cut-off at 470 nm)	25354.712	3%

Additional Spectra of Titration Experiment

Figure 49: Fluorescence spectra of light-harvesting antenna. Conditions: 0.5 µM oligomer **1** in 10 mM sodium phosphate buffer pH 7.0, 10 vol% ethanol. Addition of oligomer **2** represented as pyrene/phenanthrene (%). λexc. 316 nm; excitation slit: 2.5 nm, emission slit: 5 nm.
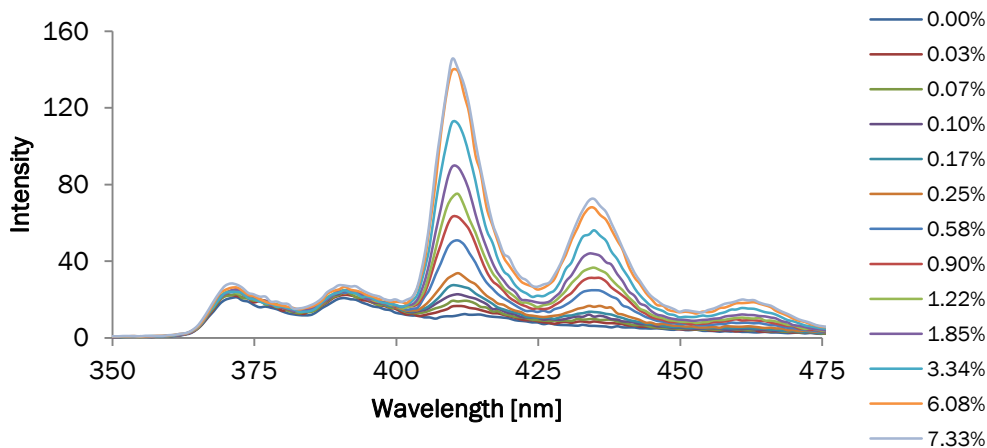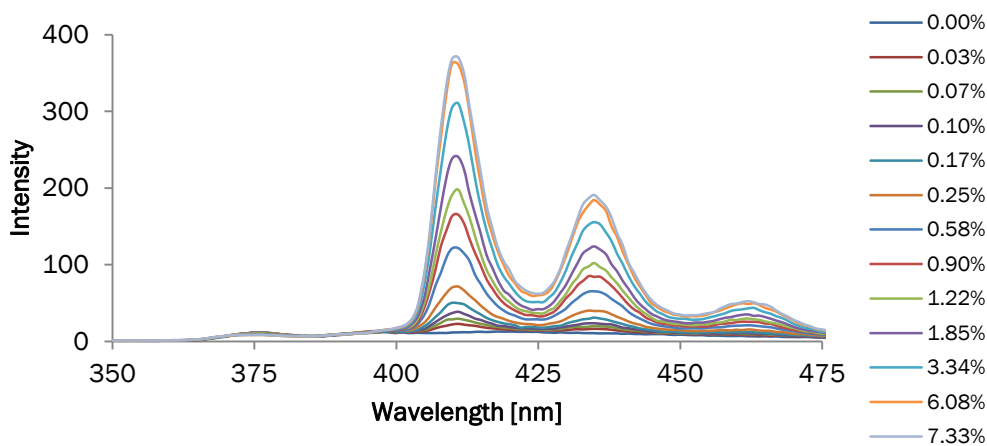

Figure 50: Fluorescence spectra of light-harvesting antenna. Conditions: 0.5 µM oligomer **1** in 10 mM sodium phosphate buffer pH 7.0, 10 vol% ethanol. Addition of oligomer **2** represented as pyrene/phenanthrene (%). λexc. 243 nm; excitation slit: 2.5 nm, emission slit: 5 nm.
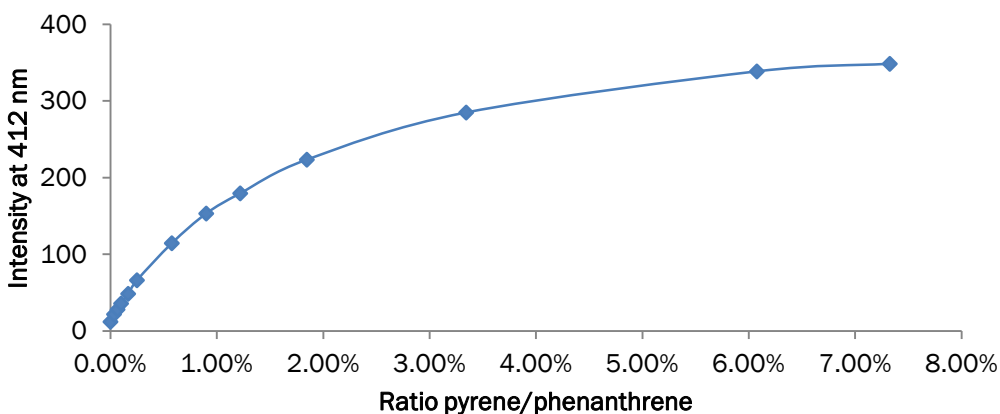
Figure 51: Fluorescence intensity at 412 nm as a function of ratio pyrene/phenanthrene. λexc. 243 nm; excitation slit: 2.5 nm, emission slit: 5 nm.
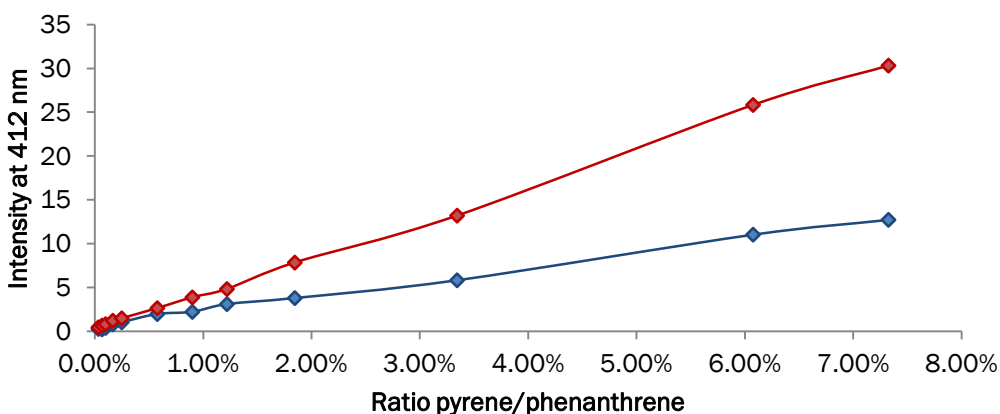
Figure 52: Reference experiment: Titration of oligomer **2** to a solution without oligomer **1**. Fluorescence intensity at 412 nm as a function of ratio pyrene/phenanthrene. λexc. 316 nm (blue), 243 nm (red); excitation slit: 2.5 nm, emission slit: 5 nm.

Excitation Spectra of Light-Harvesting Antenna

An excitation spectrum was recorded after each addition of **2** for emission at 412 nm. The contribution from direct excitation of pyrene is negligible. It is more likely that the observed emission is a result of exciting phenanthrene. The signal at 243 nm (H-band) increases and gets more distinct with higher concentrations of the acceptor.

Figure 53: Excitation spectra of light-harvesting antenna. Conditions: 0.5 µM oligomer **1** in 10 mM sodium phosphate buffer pH 7.0, 10 vol% ethanol. Addition of oligomer **2** represented as pyrene/phenanthrene (%). λem. 412 nm; excitation slit: 2.5 nm, emission slit: 5 nm.

AFM Measurements

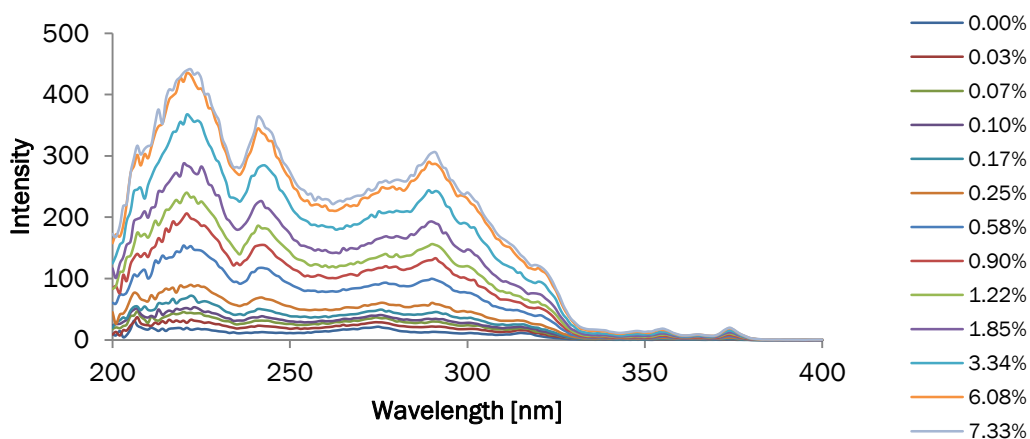AFM images were recorded under ambient conditions in air with a Nanosurf FlexAFM instrument. The measurements were carried out in tapping mode. Tubular structures of oligomer **1** were found with two different AFM sample preparation methods.

Method 1: An aqueous solution containing the assembled oligomer (5 µM in 10 mM sodium phosphate buffer pH 7.0, 10% ethanol) was mixed with a 2 mM $NiCl_2$ solution (ratio 1:2). 20 µl of the prepared solution were dropped on a freshly cleaved mica sheet (Glimmer "V1", 20 mm x 20 mm, G250-7, Plano GmbH). After an incubation time of 10 minutes, the mica sheet was rinsed with 2 ml of Milli-Q water and dried under an argon stream.

Method 2: To ensure that not Ni^{2+} ions are responsible for the tube formation, mica sheets were functionalized with 3-aminopropyltriethoxy silane (APTES). Freshly cleaved mica sheets were fixed on top of a 3 l desiccator with tape. The desiccator was flushed with argon. Two plastic caps (from Eppendorf tubes) were placed at the bottom; one was the filled with 30 µl of APTES, the other one with 10 µl of DIPEA. The desiccator was closed, and the chemicals were allowed to evaporate. The plastic caps were removed after two hours and the desiccator was purged with argon. The mica sheets were let for 1 day in the desiccator to cure. 20 µl of assembled oligomer (1 µM in 10 mM sodium phosphate buffer pH 7.0, 10% ethanol) were dropped on the modified mica sheet and let to incubate for 10

minutes. After rinsing with 2 ml of Milli-Q water, the sample was dried under an argon stream.

TEM Measurements

TEM images were recorded on a Philips CM12 using an operating voltage of 80 kV. Samples were prepared by dropping 4 µl of a 5 µM oligomer **1** solution on a carbon-coated grid (300 mesh Cu, AGS160-3, Agar Scientific). The solution was blotted with a filter paper after 30 seconds. Then the grid was dipped into Milli-Q water and the water was blotted. The washing step was repeated twice. Afterwards the grid was dipped into a 0.8% aqueous uranyl acetate solution, which was blotted directly. The grid was then dipped again into a 0.8% aqueous uranyl acetate solution, which was blotted after 30 seconds.

Additional AFM and TEM Images
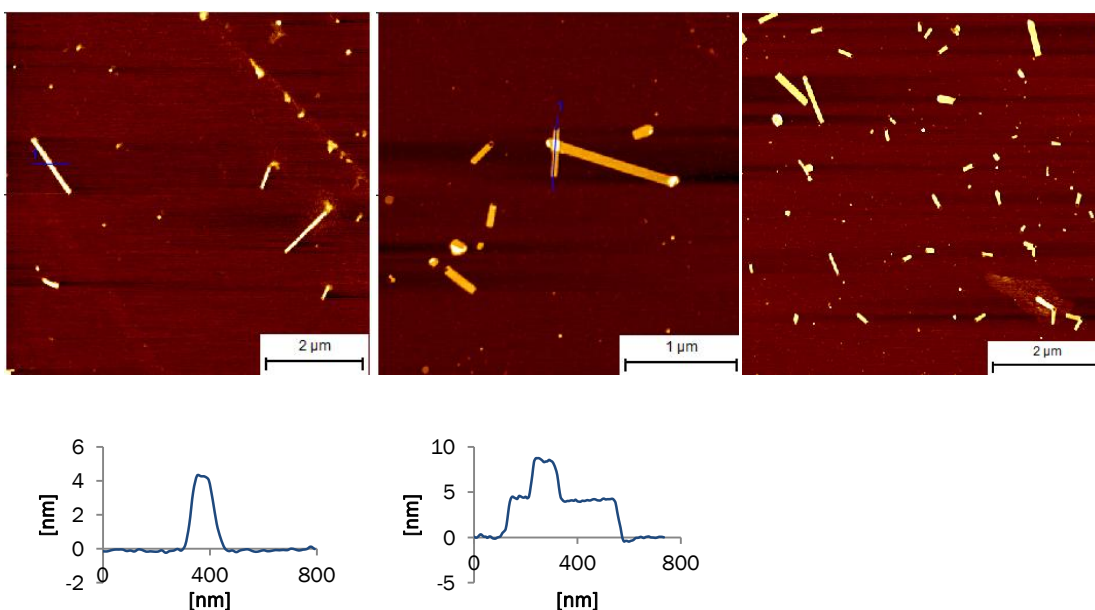
Figure 54: Additional AFM images of nanotubes formed by oligomer **1** (left: preparation method 1, middle and right: preparation method 2) with corresponding cross-sections.
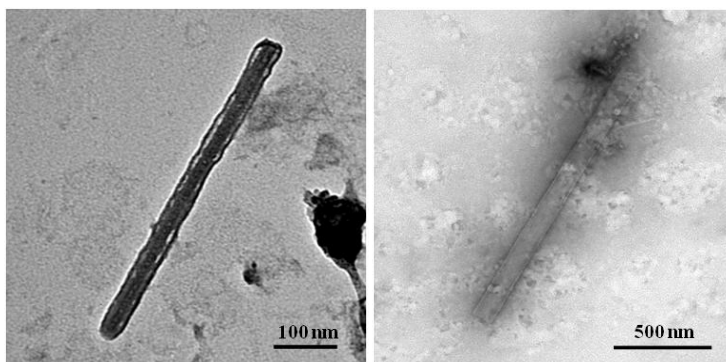
Figure 55: Additional TEM images of phenanthrene nanotubes.
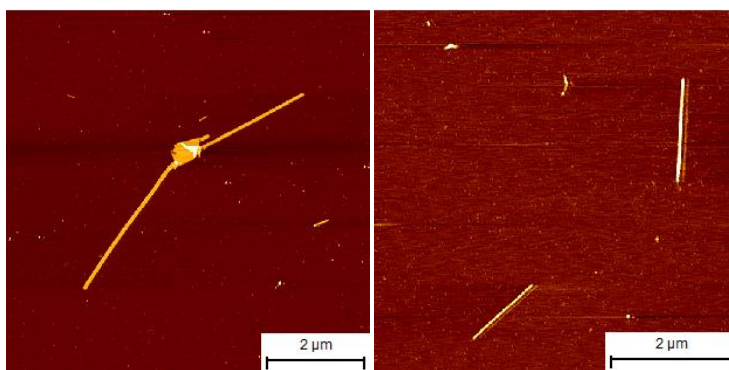
Figure 56: AFM images of assembled light-harvesting antenna (0.5 µM oligomer **1** and 0.5 nM oligomer **2**); deposited on APTES-modified mica.

Measurements of Acceptor Oligomer

The absorption spectrum of **2** shows differences when measured in different solvents (Figure 57). In ethanol (black) the vibronic band of phenanthrene at 316 nm is clearly visible. Absorption of pyrene is seen around 340 nm. In aqueous medium pyrene absorption is shifted to the red, so that the maximum is found at 350 nm. Further, the phenanthrene H-band at 243 nm is again visible and a strong hypochromicity is observable. Those changes are reversible if the aqueous sample is heated up.
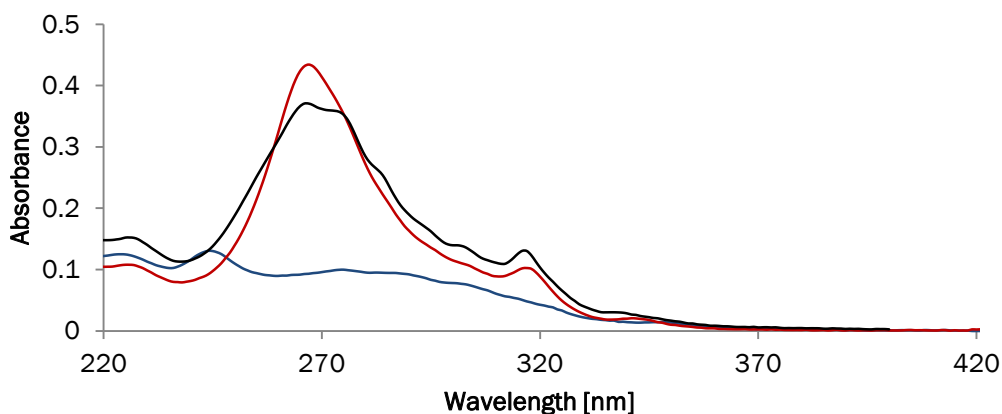
Figure 57: Absorption spectra of oligomer **2** in 10 mM sodium phosphate buffer pH 7.0, 10% ethanol (blue: at 20°C, red: at 80°C) and in ethanol at 20°C (black), concentration: 1µM.

Fluorescence of **2** was measured for three excitation wavelengths (Figure 58). At 350 nm pyrene is excited directly and monomer emission is visible with the maximal intensity at 412 nm. To see if there is again an excitation wavelength dependence of phenanthrene the sample was excited at 316 nm and 243 nm. The fluorescence measurement for 316 nm excitation shows emission from phenanthrene and from pyrene, whereas the latter has a higher relative intensity (I_{412}/I_{371} = 4). If the excitation wavelength is set to 243 nm one can again observe that excitation energy transfer is more efficient. The ratio of pyrene/phenanthrene fluorescence intensity increases (I_{412}/I_{371} = 30). For the fluorescence quantum yield it does not make a difference where phenanthrene is excited, for both excitation wavelengths a quantum yield of 11% was calculated. If pyrene is excited directly at 350 nm the quantum yield is only slightly lower (9%).

Figure 59 shows excitation spectra of **2** recorded for three different emission wavelengths. The spectrum measured for emission wavelength 391 nm shows a similar structural pattern as unassembled phenanthrene absorption. The measurements for emission wavelengths 412 and 437 nm are different. A contribution from pyrene is visible around 350 nm. Between 260 and 330 nm is a broad signal and at 243 nm one sees again the contribution of the phenanthrene H-band.
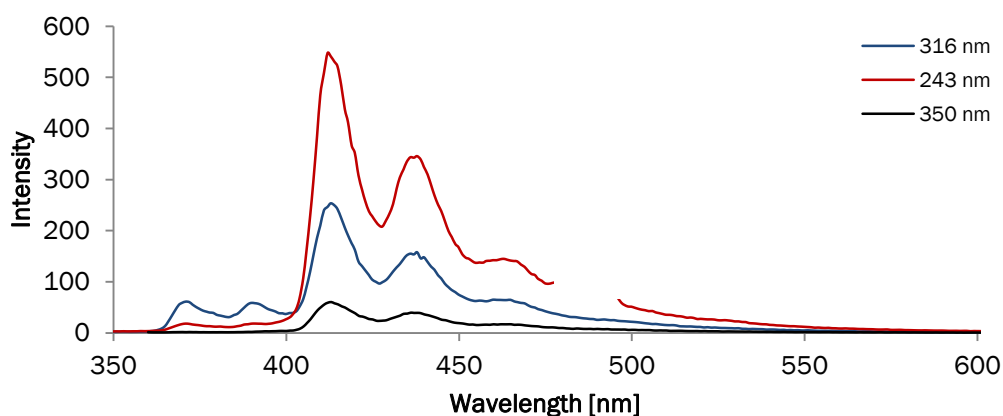
Figure 58: Fluorescence spectra of oligomer **2**. Conditions: 1 μM in 10 mM sodium phosphate buffer pH 7.0, 10 vol% ethanol; λexc. 316, 243, and 350 nm.
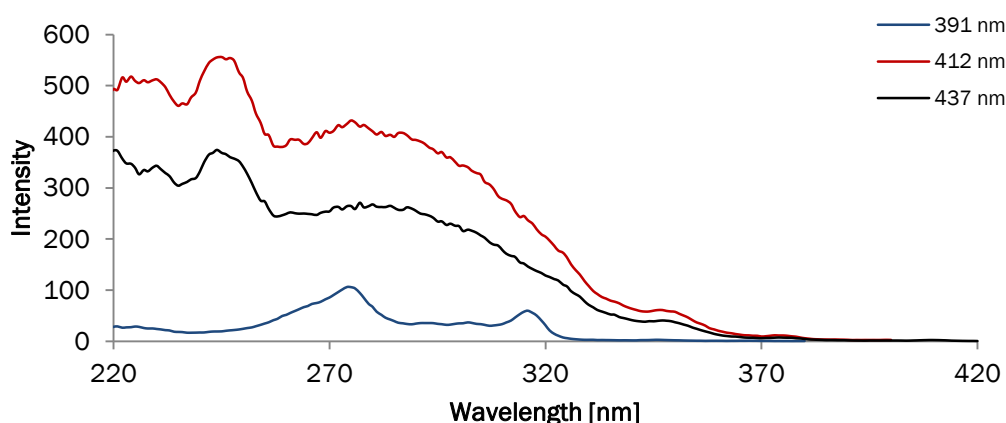
Figure 59: Excitation spectra of oligomer **2**, 1 μM in 10 mM sodium phosphate buffer pH 7.0, 10 vol% ethanol; λem. 391, 412, and 437 nm.

The acceptor alone does not form tubes. AFM experiments showed that it assembles into sheets (Figure 60). The sheets have a height of 2.5 nm which corresponds to a monolayer. Although no tubes are formed, it is still likely that single molecules of **2** are incorporated into a phenanthrene tube, as fluorescence measurements show the excitation energy transfer from phenanthrene to pyrene. In Figure 17 it was shown that fluorescence of pyrene is only observed when the polymer is newly assembled (heating and cooling of the sample). More precise analysis of AFM images of **2** reveals that sheets often appear as

pairs. And rarely there are found some sheets with heights of 5 nm. So it seems that **2** rather forms double layers that are not very stable and fall apart during the deposition. This could explain the often found pairs of round sheets on the AFM images.
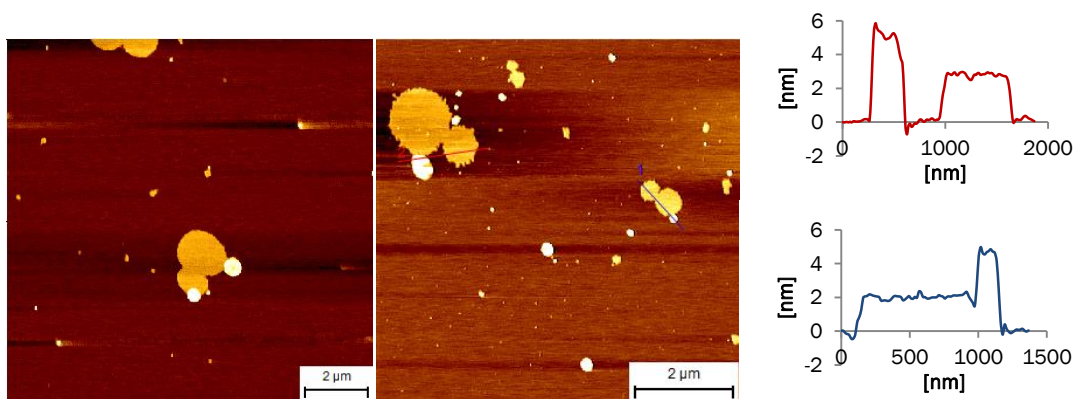
Figure 60: AFM images of **2**; deposited on APTES-modified mica and cross-sections.

UV-vis Cooling Curves of Oligomers 1 and 2

Figure 61: Normalized UV-vis cooling curves of oligomers **1** (blue) and **2** (red) measured at 265 nm, showing both a cooperative polymerization mechanism starting at roughly the same temperature, cooling gradient: 0.5 °C/min.

52

References

[28]   (a) D. Gust, T. A. Moore, A. L. Moore, *Acc. Chem. Res.*, 2001, **34**, 40-48.
(b) M. R. Wasielewski, *Acc. Chem. Res.*, 2009, **42**, 1910-1921.
(c) G. D. Scholes, G. R. Fleming, A. Olaya-Castro, R. van Grondelle, *Nat. Chem.*, 2011, **3**, 763-774.
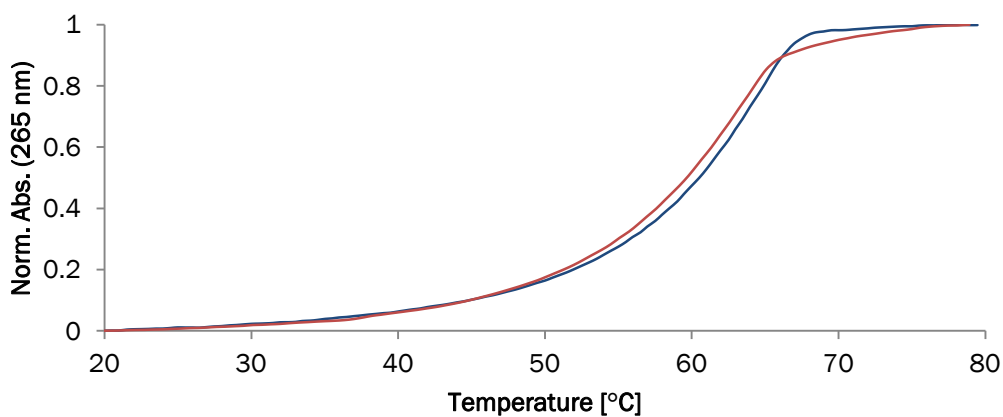(d) I. McConnell, G. H. Li, G.W. Brudvig, *Chem. Biol.*, 2010, **17**, 434-447.
(e) N. Aratani, D. Kim, A. Osuka, *Acc. Chem. Res.*, 2009, **42**, 1922-1934.
(f) W. Su, V. Bonnard, G. A. Burley, *Chem. Eur. J.*, 2011, **17**, 7982-7991.
(g) K. Rao, V. K. Datta, M. Eswaramoorthy, S. J. George, *Chem. Eur. J.*, 2012, **18**, 2184-2194.
(h) R. Ziessel, A. Harriman, *Chem. Commun.*, 2011, **47**, 611-631.
(i) D. Holten, D. F. Bocian, J. S. Lindsey, *Acc. Chem. Res.*, 2002, **35**, 57-69.
(j) M. S. Choi, T. Yamazaki, I. Yamazaki, T. Aida, Angew. Chem. Int. Ed., 2004, **43**, 150-158.
(k) H. Imahori, J. *Phys. Chem. B*, 2004, **108**, 6130-6143.

[29]   (a) S. E. Webber, *Chem. Rev.*, 1990, **90**, 1469-1482.
(b) D. Ng, J. E. Guillet, *Macromolecules*, 1982, **15**, 724-727.
(c) V. S. Lin, S. G. DiMagno,M. J. Therien, *Science*, 1994, **264**, 1105-1111.
(d) R. W. Wagner, J. S. Lindsey, *J. Am. Chem. Soc.*, 1994, **116**, 9759-9760.
(e) M. A. Fox, *Acc. Chem. Res.*, 1992, **25**, 569-574.
(f) D. M. Watkins, M. A. Fox*, J. Am. Chem. Soc.*, 1994, **116**, 6441-6442.
(g) I. Hwang, G. D. Scholes, *Chem. Mater.*, 2011, **23**, 610-620.
(h) E. Collini, G. D. Scholes, *Science*, 2009, **323**, 369-373.

[30]   (a) V. Balzani, A. Credi, M. Venturi, *ChemSusChem*, 2008, **1**, 26-58.
(b) C. Devadoss, P. Bharathi, J. S. Moore, *J. Am. Chem. Soc.*, 1996, **118**, 9635-9644.
(c) S. L. Gilat, A. Adronov, J. M. J. Fréchet, *Angew. Chem. Int. Ed.*, 1999, **38**, 1422-1427.
(d) A. Adronov, J. M. J. Fréchet, *Chem. Commun.*, 2000, 1701-1710.
(e) J. F. Galindo, E. Atas, A. Altan, D. G. Kuroda, S. Fernandez-Alberti, S. Tretiak, A. E. Roitberg, V. D. Kleiman, *J. Am. Chem. Soc.*, 2015, **137**, 11637-11644.
(f) C. Giansante, P. Ceroni, V. Balzani, F. Voegtle, *Angew. Chem. Int. Ed.*, 2008, **47**, 5422-5425.
(g) H. Lee, Y. H. Jeong, J. H. Kim, I. Kim, E. Lee, W. D. Jang *J. Am. Chem. Soc.*, 2015, **137**, 12394-12399.

[31]   A. N. Melkozernov, J. Barber, R. E. Blankenship, *Biochemistry*, 2006, **45**, 331-345.

[32]   (a) Z. G. Fetisova, A. M. Freiberg, K. E. Timpmann, *Nature*, 1988, **334**, 633-634.
(b) N. Sakai, S. Matile, *Beilstein J. Org. Chem.*, 2012, **8**, 897-904.

[33]   (a) T. F. A. de Greef, M. M. J. Smulders, M. Wolffs, A. P. H. J. Schenning, R. P. Sijbesma, E. W. Meijer, *Chem. Rev.*, 2009, **109**, 5687-5754.
(b) F. J. M. Hoeben, P. Jonkheijm, E.W. Meijer, A. P. H. J. Schenning, *Chem. Rev.*, 2005, 105, 1491-1546.
(c) H. Cui, M. J. Webber, S. I. Stupp, *Biopolymers*, 2010, **94**, 1-18.
(d) T. Aida, E. Meijer, S. I. Stupp, *Science*, 2012, **335**, 813-817.

(e) D. Görl, X. Zhang, F. Würthner, *Angew. Chem. Int. Ed.*, 2012, **51**, 6328-6348.

(f) M. J. Webber, E. A. Appel, E.W. Meijer, R. Langer, *Nat. Mater.*, 2016, **15**, 13-26.

(g) E. Krieg, M. M. C. Bastings, P. Besenius, B. Rybtchinski, *Chem. Rev.*, 2016, **116**, 2414-2477.

[34]   (a) R. H. Baughman, A. A. Zakhidov, W. A. de Heer, *Science*, 2002, **297**, 787-792.

(b) X. Zang, Q. Zhou, J. Chang, Y. Liu, L. Lin, *Microelectron. Eng.*, 2015, **132**, 192-206.

[35]   (a) N. Kameta, K. Ishikawa, M. Masuda, M. Asakawa, T. Shimizu, *Chem. Mater.*, 2012, **24**, 209-214.

(b) D. Eisele, C. Cone, E. Bloemsma, S. Vlaming, C. van der Kwaak, R. Silbey, M. Bawendi, J. Knoester, J. Rabe, D. Vanden Bout, *Nat. Chem.*, 2012, **4**, 655-662.

(c) H. Shao, J. Seifert, N. C. Romano, M. Gao, J. J. Helmus, C. P. Jaroniec, D. A. Modarelli, J. R. Parquette, *Angew. Chem. Int. Ed.*, 2010, **49**, 7688-7691.

[36]   J. H. Kim, M. Lee, J. S. Lee, C. B. Park, *Angew. Chem. Int. Ed.*, 2012, **51**, 517-520.

[37]   C. B. Winiger, S. Li, G. R. Kumar, S. M. Langenegger, R. Häner, *Angew. Chem. Int. Ed.*, 2014, **53**, 13609-13613.

[38]   (a) M. Vybornyi, A. V. Rudnev, S. M. Langenegger, T. Wandlowski, G. Calzaferri, R. Häner, *Angew. Chem. Int. Ed.*, 2013, **52**, 11488-11493.

(b) M. Vybornyi, A. Rudnev, R. Häner, *Chem. Mater.*, 2015, **27**, 1426-1431.

(c) M. Vybornyi, Y. B.-C. Hechevarria, M. Glauser, A. V. Rudnev, R. Häner, *Chem. Commun.*, 2015, **51**, 16191-16193.

[39]   (a) A. E. Clark, C. Y. Qin, A. D. Q. Li, *J. Am. Chem. Soc.*, 2007, **129**, 7586-7595.

(b) H. Bittermann, D. Siegemund, V. L. Malinovskii, R. Häner, *J. Am. Chem. Soc.*, 2008, **130**, 15285-15287.

(c) M. Hariharan, K. Siegmund, Y. Zheng, H. Long, G. C. Schatz, F. D. Lewis, *J. Phys. Chem. C*, 2010, **114**, 20466-20471.

(d) C. B. Winiger, S. M. Langenegger, G. Calzaferri, R. Häner, *Angew. Chem. Int. Ed.*, 2015, **54**, 3643-3647.

(e) P. S. Rukin, A. Y. Freidzon, A. V. Scherbinin, V. A. Sazhnikov, A. A. Bagaturyants, M. V. Alfimov, *Phys. Chem. Chem. Phys.*, 2015, **17**, 16997-17006.

[40]   (a) F. C. Spano, *Acc. Chem. Res.*, 2010, **43**, 429-439.

(b) A. Eisfeld, J. S. Briggs, *Chem. Phys.*, 2006, **324**, 376-384.

[41]   J. B. Birks, *Rep. Prog. Phys.*, 1975, **38**, 903-974.

[42]   E. Lendvay, I. Hornyak, *J. Lumin.*, 1974, **9**, 18-31.

[43]   M. Sauer, J. Hofkens, J. Enderlein, *Basic Principles of Fluorescence Spectroscopy*, Wiley-VCH, Weinheim, 2011.

[44]   A. T. Haeder, K. Kreger, A. Issac, B. Wittmann, M. Kivala, N. Hammer, J. Köhler, H.-W. Schmidt, R. Hildner, *Nature*, 2015, **523**, 196-200.

[45]   (a) J.W. Ciszek, J. M. Tour, *Tetrahedron Letters*, 2004, **45**, 2801-2803.

(b) J.W. Simek, T. Tuck, K. Courter Bush, *J. Chem. Educ.*, 1997, **74**, 107-108.

[46]   S. Fery-Forgues, D. Lababre, *J. Chem. Educ.*, 1999, **76**, 1260-1264.

Chapter 2: Energy Transfer over Base Pairs in DNA based Light-Harvesting Antennae

Abstract

DNA based light-harvesting antennae with light absorbing phenanthrenes and pyrene acceptors were synthesized. By exciting phenanthrene, the excitation energy is transferred to pyrene. Energy transfer is still detected when the phenanthrene antenna is separated by base pairs. Quantum yield measurements indicate that the observed energy transfer cannot be explained by a Förster resonance energy transfer mechanism alone. Coherent energy transfer is more reasonable as the incorporated phenanthrene units should couple strong enough. Investigation of the energy transfer mechanism is done by DUV-to-vis femtosecond transient absorption spectroscopy.

Introduction

DNA is a useful scaffold for the arrangement of molecules in nanomaterials.[47] In light-harvesting systems, energy is absorbed by chromophores and subsequently transferred to an acceptor. The design and construction of efficient artificial systems is a continuing field of study.[48] In previous work we described different light-harvesting systems based on DNA-organized chromophores.[49] In one approach 3,6-dicarboxamide phenanthrene and 1,8-dicarboxamide pyrene were incorporated into DNA duplexes to build up light-harvesting antennae (Figure 62 B).[49a] Light is absorbed by a stack of phenanthrenes and subsequently transferred to a phenanthrene-pyrene exciplex. The fluorescence intensity showed to be proportional to the number of light-absorbing phenanthrene (up to eight phenanthrenes were used in a duplex). Another system describes the use of 1,8-dicarboxamide pyrene and a cyanine dye (Cy5) as DNA building blocks (Figure 62 C).[49b] Duplexes with different numbers of pyrene at one end were prepared with a 5'-terminally attached Cy5 unit. By exciting pyrene the excitation energy is transferred via FRET from pyrene excimers to the Cy5 acceptor. Lastly, also a DNA three-way junction was used for the arrangement of chromophores for the construction of light-harvesting antennae (Figure 62 D).[49c] A 3,6-dicarboxamide phenanthrene antenna is located in one of the three stems and an exchangeable acceptor is brought into proximity through the annealing of the third strand.
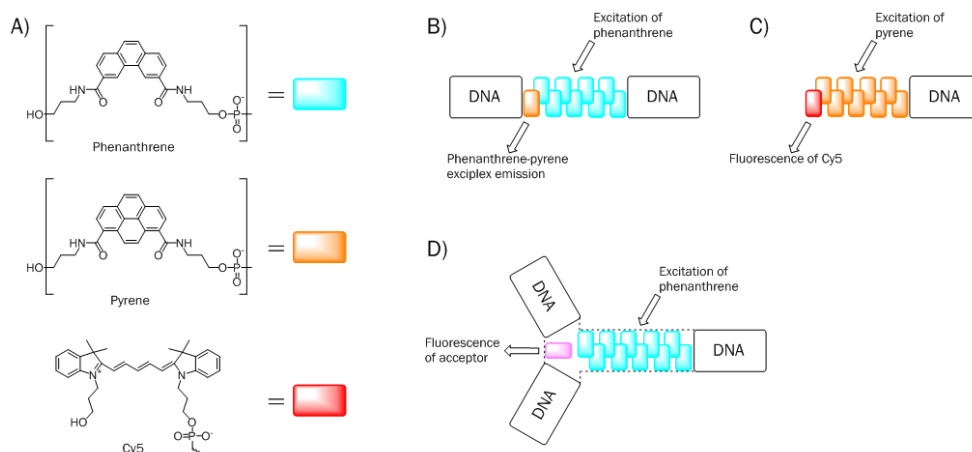
Figure 62: Overview of already investigated DNA based light-harvesting systems.[49] A) Some structures of already incorporated chromophores; B) Schematic illustration of DNA based light-harvesting antennae composed of light-harvesting phenanthrenes and a pyrene acceptor; C) Schematic illustration of antenna composed of a stack of pyrenes at the end of a DNA duplex with a cyanine (Cy5) at the end of the stack; D) DNA three-way junction with a phenanthrene stack and an exchangeable acceptor chromophore (pink).

In this chapter a DNA based light-harvesting antenna is presented which consist of a stack of light-harvesting phenanthrene units and one pyrene as acceptor (Figure 63). In contrast to previous projects 3,6-dialkynyl phenanthrene is used as the light-absorber as it has a higher absorption coefficient than the carboxamide counterpart and is expected to stack more efficiently. Conveniently, 1,8-dialkynyl pyrene was used as the acceptor. Further, it will be investigated if the excitation energy can be transferred over base pairs. Therefore, duplexes are prepared in which the phenanthrene antenna is separated by different numbers of base pairs (see Figure 63 B).
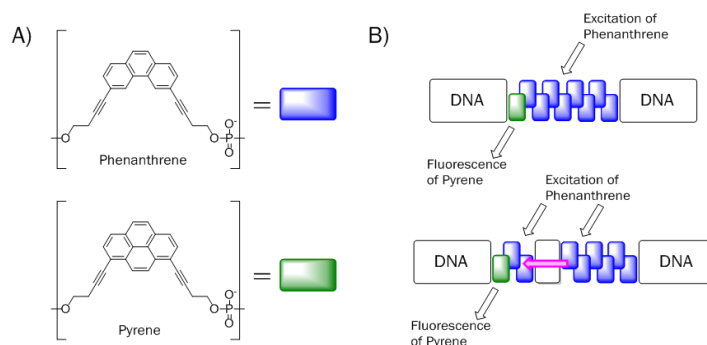

Figure 63: A) Structures of incorporated phenanthrene and pyrene building blocks; B) Schematic illustration of DNA based light-harvesting antennae without (top) and with (below) separating base pairs between phenanthrene units. Pink arrow indicates energy transfer over base pairs.
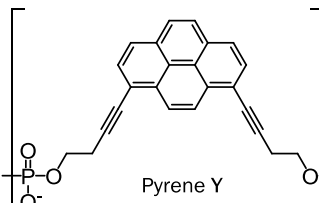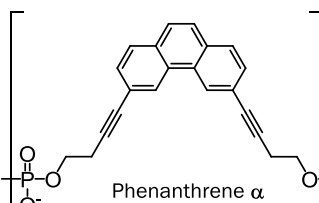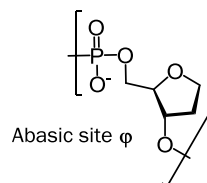
Results

DNA Sequences

(DNA strands for duplexes **0-3** and **Ref1** were synthesized by Elif Abay.)

DNA strands were synthesized by phosphoramidite chemistry using phenanthrene, pyrene and abasic site building blocks. Complementary DNA single strands were hybridized to yield duplexes with eight light collecting phenanthrene units and one pyrene acceptor (Table 3, duplexes **0-5**). An abasic site was introduced opposite pyrene to ensure its positioning at the end of the stack. Only A-T base pairs were used in the vicinity of the chromophores, as the quenching effect of G is well known.[50] However, G-C base pairs were used at the ends of the duplexes to increase the stability. In duplex **0** all phenanthrenes are next to each other, whereas in duplexes **1-5** the stack of phenanthrenes is separated by one to five A-T base pairs. Additionally two control duplexes were prepared: Duplex **Ref1** contains only the acceptor part which consists of two phenanthrenes and one pyrene; and duplex **Ref2** contains only the block of six phenanthrenes.

Table 3: Sequences of synthesized DNA strands and structures of unnatural building blocks.

Duplex	Sequences	
0	5' GGC TAA φαα ααA TTA AAT CGC 3' 3' CCG ATT Yαα ααT AAT TTA GCG 5'	Pyrene Y
1	5' GGC TAA φαT ααα TTA AAT CGC 3' 3' CCG ATT YαA ααα AAT TTA GCG 5'	
2	5' GGC TAA φαT Aαα αTA AAT CGC 3' 3' CCG ATT YαA Tαα αAT TTA GCG 5'	
3	5' GGC TAA φαT ATα ααA AAT CGC 3' 3' CCG ATT YαA TAα ααT TTA GCG 5'	Phenanthrene α
4	5' GGC TAA φαT ATA ααα AAT CGC 3' 3' CCG ATT YαA TAT αααTTA GCG 5'	
5	5' GGC TAA φαT ATA Tαα αAT CGC 3' 3' CCG ATT YαA TAT Aαα αTA GCG 5'	
Ref1	5' GGC TAA φαT ATA TTA AAT CGC 3' 3' CCG ATT YαA TAT AAT TTA GCG 5'	Abasic site φ
Ref2	5' GGC TAA ATα ααA TTA AAT CGC 3' 3' CCG ATT TAα ααT AAT TTA GCG 5'	

Spectroscopic Measurements

Figure 64 shows the absorption spectra of the investigated duplexes. The vibronic bands at 391 and 370 nm result from pyrene, those at 335 and 316 nm from phenanthrene absorption. Absorption around 260 nm is from the nucleobases, phenanthrene and pyrene. The spectra do not differentiate much from each other. Duplexes **0-5** contain all the same number of different building blocks and show roughly the same absorption band. **Ref1** contains six phenanthrenes less; therefore the vibronic bands around 320 and 260 nm are much lower. The other reference duplex (**Ref2**) contains only phenanthrene and DNA and shows the corresponding absorption peaks.
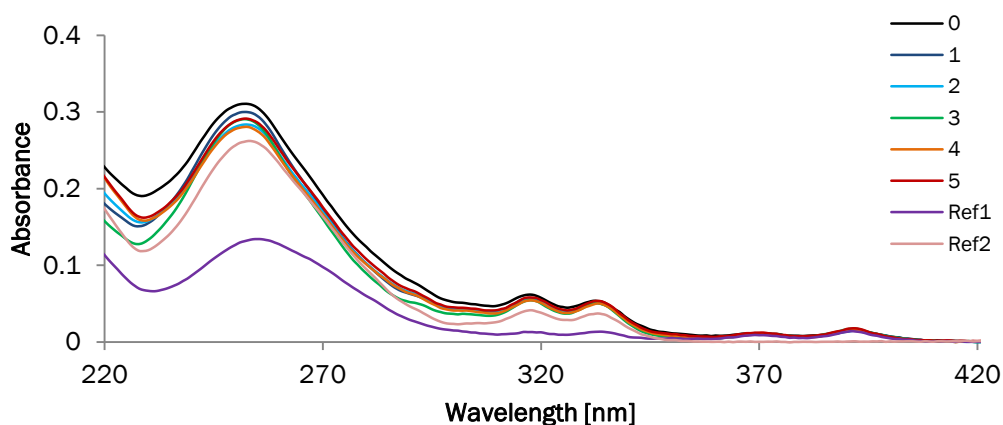

Figure 64: Absorption spectra of duplexes. Conditions: 0.25 µM each strand, 10 mM sodium phosphate buffer pH 7.0, 100 mM NaCl, 20°C.

Fluorescence spectra of the duplexes were recorded by exciting phenanthrene at 316 nm (Figure 65). For all duplexes mainly pyrene emission is observable with maxima at 403 and 425 nm. The ratio of intensities of those two peaks is not the same for all duplexes. Duplexes **0-2** show higher intensity at 425 nm compared to 403 nm, duplex **3** shows roughly the same intensities, whereas for duplexes **4** and **5** the emission at 403 nm is the highest. This phenomenon can be explained by different environments for pyrene which can lead to different vibronic band intensities. A similar effect was observed for pyrene in different solvents.[51]

In general the duplexes with no separating base pairs, with one and with two have about the same fluorescence intensities. If the stack of phenanthrene is separated by three base pairs the intensity decreases. With four or five base pairs the pyrene emission decreases even more, whereas there is no significant difference between those two duplexes. At the same time phenanthrene monomer emission around 380 nm increases if the stack of phenanthrene is separated by more than three base pairs (see inset Figure 65).
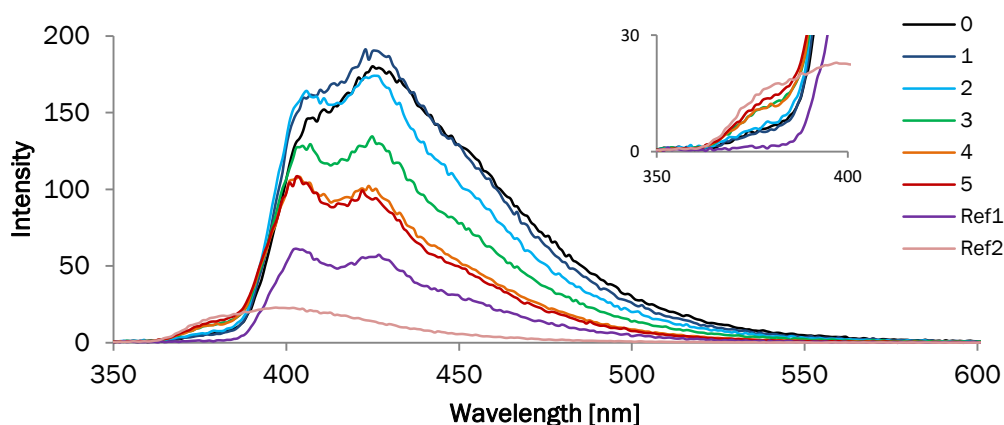

Figure 65: Fluorescence spectra of duplexes. Conditions: 0.25 μM each strand, 10 mM sodium phosphate buffer pH 7.0, 100 mM NaCl, λexc. 316 nm, 20°C. Excitation slit: 2.5 nm, emission slit: 5 nm.

Excitation spectra were measured to visualize which excitation wavelengths lead to the observed pyrene emission at 425 nm (Figure 66). For all duplexes the contribution from pyrene (360-400 nm) is the same. Contribution from phenanthrene (310-340 nm) differs: duplexes **0**, **1**, and **2** show roughly the same intensities, whereas a lower one is observed for duplex **3** and the lowest for duplexes **4** and **5**. The intensities get not as low as it is for **Ref1**, indicating that there is still more excitation energy than from only two phenanthrenes.
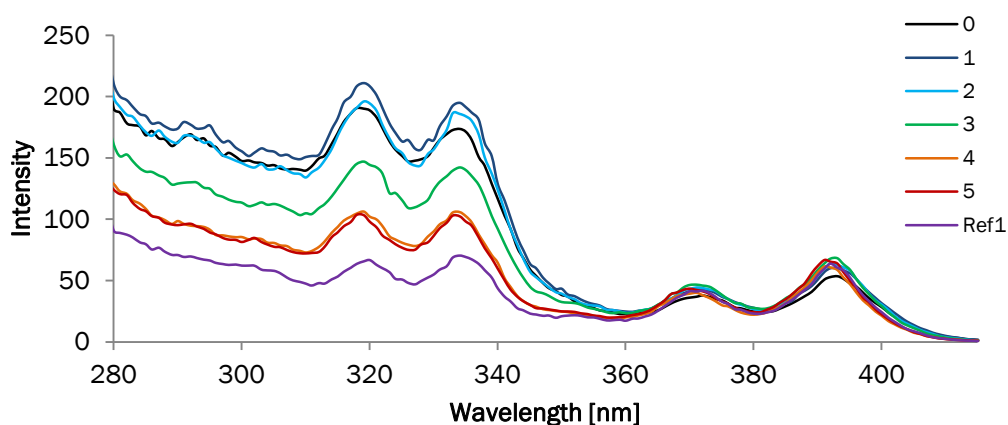
Figure 66: Excitation spectra of duplexes. Conditions: 0.25 µM each strand, 10 mM sodium phosphate buffer pH 7.0, 100 mM NaCl, λem. 425 nm, 20°C. Excitation slit: 2.5 nm, emission slit: 5 nm.

Quantum Yields

Quantum yields (Φ_F) were measured for all single strands and duplexes (Table 4) by exciting phenanthrene at 316 nm with quinine sulfate in 0.5 M H_2SO_4 as a standard. Single strands containing only phenanthrene have values around 5%, whereas single strands with pyrene have significant higher quantum yields (29-46%) due to excitation energy transfer from phenanthrene to pyrene. Average values were calculated by using the quantum yields of complementary strands. The measured quantum yields of the duplexes deviate from theoretical ones. This increase in quantum yield cannot be explained by FRET theory.[52] The observed efficiency of excitation energy transfer can be explained by quantum coherence.[53] The stacked phenanthrenes in the DNA duplexes should couple strong enough to enable coherent energy transfer. This theory could also explain why the quantum yield of duplex **0** is lower than that of duplex **1**. In duplex **0** the phenanthrene units are not separated by base pairs, therefore the electronic coupling could be very large which then rather leads to relaxation instead of excitation energy transfer.[54] Figure 67 illustrates the measured (black) and calculated (blue) quantum yields of the duplexes. The deviation between the two values decreases with increasing number of separating base pairs.

Table 4: Quantum yields of DNA single strands and corresponding DNA duplexes (average value of single strands and measured).

	Sequences	Φ_F (single strands)	Φ_F (avg. of single strands)	Φ_F (duplexes)
0	5' GGC TAA φαα ααA TTA AAT CGC 3'	6%	22%	45%
	3' CCG ATT Υαα ααT AAT TTA GCG 5'	37%		
1	5' GGC TAA φαT ααα TTA AAT CGC 3'	4%	23%	50%
	3' CCG ATT ΥαA ααα AAT TTA GCG 5'	42%		
2	5' GGC TAA φαT Aαα αTA AAT CGC 3'	5%	23%	45%
	3' CCG ATT ΥαA Tαα αAT TTA GCG 5'	41%		
3	5' GGC TAA φαT ATα ααA AAT CGC 3'	6%	22%	36%
	3' CCG ATT ΥαA TAα ααT TTA GCG 5'	38%		
4	5' GGC TAA φαT ATA ααα AAT CGC 3'	5%	17%	27%
	3' CCG ATT ΥαA TAT αααTTA GCG 5'	29%		
5	5' GGC TAA φαT ATA Tαα αAT CGC 3'	4%	19%	24%
	3' CCG ATT ΥαA TAT Aαα αTA GCG 5'	33%		
Ref1	5' GGC TAA φαT ATA TTA AAT CGC 3'	6%	26%	56%
	3' CCG ATT ΥαA TAT AAT TTA GCG 5'	46%		
Ref2	5' GGC TAA ATα ααA TTA AAT CGC 3'	5%	5%	8%
	3' CCG ATT TAα ααT AAT TTA GCG 5'	5%		

Theoretical value for no energy transfer:

$\Phi_{no\ ET} = \Phi_{Ref1}/4 + \Phi_{Ref2} = 22\%$

Explanation: This quantum yield is based on the determined value of **Ref1** with the additional fluorescence from **Ref2**. As **Ref1** contains only two phenanthrenes, the absorption is four times lower than in duplexes **0-5**. Therefore the absorption is multiplied by the factor 4. The quantum yield of **Ref2** is added, because the block of phenanthrenes still emits light if the energy is not transferred to pyrene.
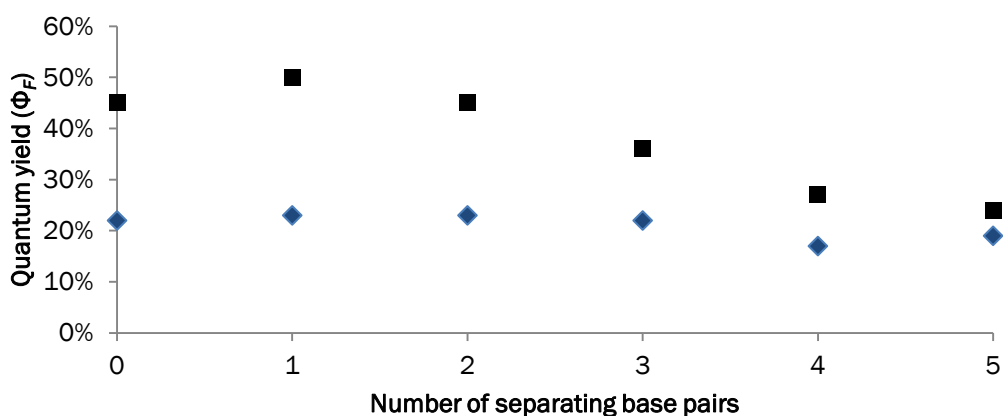
Figure 67: Quantum yields of duplexes. Comparison of measured values (black) and calculated quantum yields (average of both single strands, blue).

Using the quantum yields of duplexes **Ref1** and **Ref2**, the theoretical quantum yield for no energy transfer was calculated to be 22% (see footnote in Table 4); a value the quantum yield of duplex **5** approaches. Still, the measured value of duplex **5** is higher than the average of both single strands. Additionally, as can be seen in Figure 68, duplex **5** (red) shows a higher pyrene and lower phenanthrene fluorescence than the arithmetic sum of duplexes **Ref1** and **Ref2** (black, solid). This indicates that although the phenanthrene units are separated by five base pairs, there is still some excitation energy transferred.
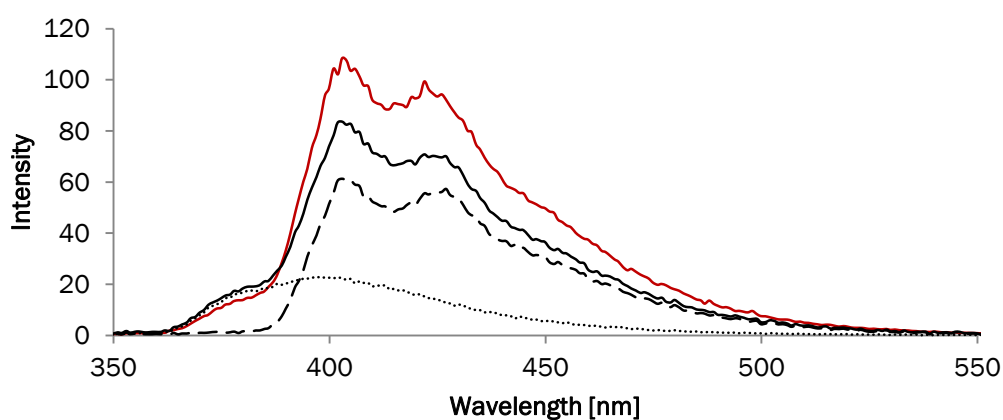

Figure 68: Comparison of the measured fluorescence spectrum of duplex **5** (red) with the arithmetic sum of **Ref1** and **Ref2** (black, solid); fluorescence spectra of **Ref1** (dashed) and **Ref2** (dotted). Conditions: 0.25 µM each strand, 10 mM sodium phosphate buffer pH 7.0, 100 mM NaCl, λexc. 316 nm, 20°C. Excitation slit: 2.5 nm, emission slit: 5 nm.

Transient Absorption Spectroscopy

(Transient absorption spectroscopy was done by the groups of Prof. Thomas Feurer and Prof. Andrea Cannnizzo, simulation of the relaxation processes was done by Prof. Antonio Monari.)

Transient absorption spectroscopy is a method to investigate energy transfer mechanisms in light-harvesting systems.[55] Briefly, a sample is excited with a laser beam (pump pulse) and a probe pulse (white light probe) is then sent through the sample with different time delays τ to measure an absorption spectrum (experimental set-up shown in the supporting information, Figure 111). A difference absorption spectrum is then calculated (absorption of the excited state minus absorption of the ground state). Generally, such a spectrum contains the following contributions:

- Ground state bleaching (GSB): This signal is observed because a fraction of the sample is excited to higher state and fewer molecules remain in the ground state. Therefore, the ground state absorption in the excited sample is less and the result is a negative signal in the spectrum in the region of the ground state absorption.

- Excited state absorption (ESA): After excitation, molecules can be excited to higher states with optically allowed transitions. Thus, the probe beam will be absorbed at these wavelengths in the excited sample and a positive signal is observed in the difference spectrum.

- Stimulated emission: This contribution is only observed for fluorescent samples. Emission of a photon from the excited molecule is induced by a photon from the probe pulse. This leads to an increased light intensity on the detector and consequently, to a negative signal in the difference spectrum.

Figure 69 shows the transient absorption (TA) measurement of 3,6-dialkynyl phenanthrene (phenanthrene monomer) and selected TA spectra at different times after excitation. There are three ESA bands present which are populated at time zero. A small rise of signal is observed below 500 nm at early dynamics with a simultaneous narrowing of the band centered at 600 nm. GSB of phenanthrene is observed below 340 nm which decays in the time window of the measurement. The decrease of the signal after 3 ps is considered as cooling and relaxation which is still present after 300 ps.

Time components of different dynamics are defined and clarified by decay associated spectra (DAS) calculated from the analysis of TA signals (Figure 70, left) and the sum of DASes (Figure 70, right) to signify the importance of the presence of each DAS for the

illustration of the dynamics. Time components τ_1 = 0.04 ps, τ_2 = 0.13 ps, τ_3 = 3.06 ps, τ_4 = 69.8 ps, τ_5 = ∞ have been calculated to explain the important dynamics. The result of the analysis shows a fast decay of the bright ESA which is populated at time zero (τ_1). The calculated DAS for this time component has a higher amplitude compared to the other DASes. It is noteworthy that τ_1 is very close to the temporal resolution (40 fs) and therefore the corresponding DAS amplitude can be easily overestimated. The fast dynamic is followed by a slower dynamic around 130 fs, illustrating the narrowing of the ESA at time zero and a small amplification of the bands at 500 and 380 nm. The 3.06 ps dynamics shows small cooling and relaxation of the lower ESA followed by a rotational diffusion around 69.8 ps which decreases the signal from 1.5 mOD to 1 mOD. The infinity component explains the recovery of the ground state.
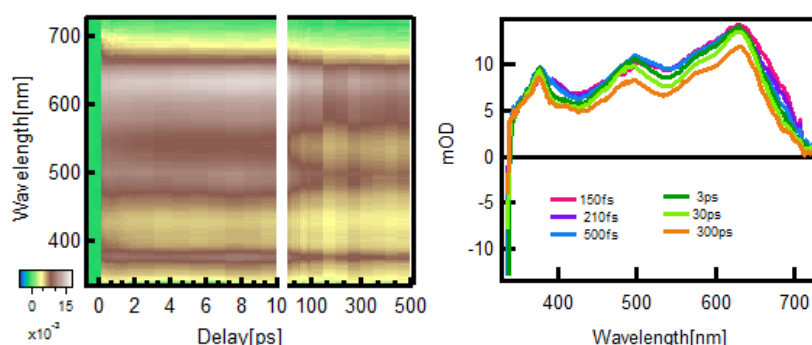

Figure 69: Two-dimensional transient absorption spectrum of phenanthrene monomer (left) and selected transient absorptions at different time delays (right).
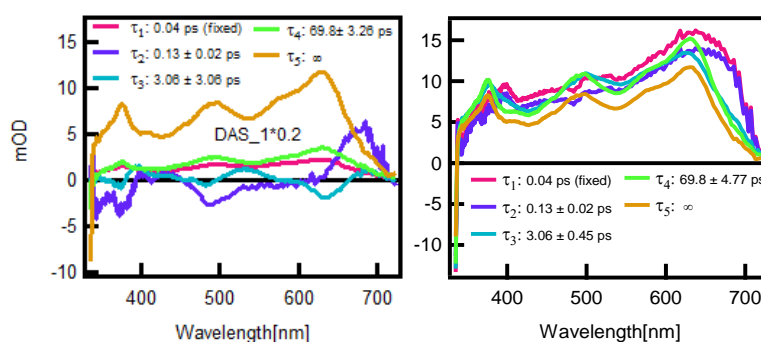

Figure 70: Decay associated spectra calculated from transient absorption signals of phenanthrene monomer (left) and calculated sum of the spectra (right). To depict all the DASes in one graph, DAS_1 was multiplied by a factor of 0.2. This arbitrary manipulation was also executed in the sum of all the DASes. (pink curves).

TD-DFT calculation and simulation of the photocycle were performed for a 3,6-dicarboxamide linked phenanthrene, but the results are also applicable for the dialkynyl derivative. The excited levels in phenanthrene are two singlet states (S_A and S_B, see Figure 71). S_B is higher in term of energy but has more oscillator strength than S_A and therefore it is optically accessible while the first level is not. The model presented in Figure 71 shows that at the beginning the higher lever (S_B) is excited. This state decays in less than 100 fs via IVR (intramolecular vibrational-energy redistribution) and populates at the intersection partially S_B and S_A via pulse limited IC (internal conversion). The population in S_B passes through the intersection barrier (system is hot) and via a slower IC (~400 fs) giving rise to the population of S_A. The dynamic is followed by relaxation due to non-radiative channels and rotational diffusion.
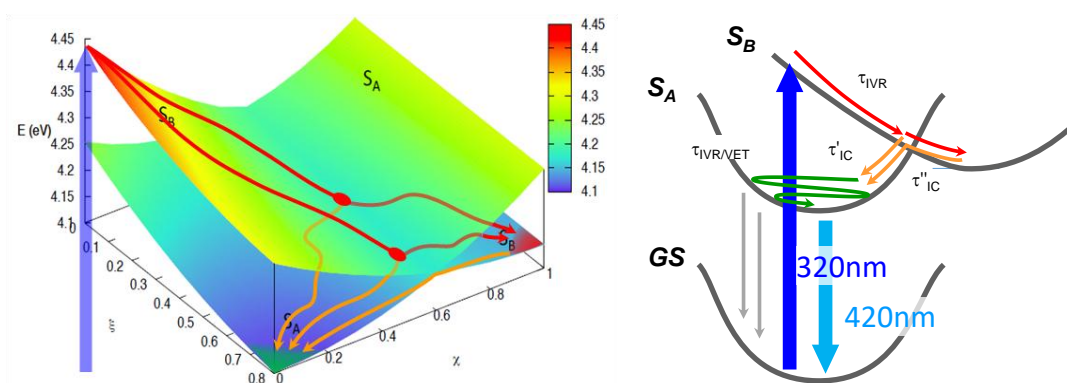

Figure 71: 2D potential energy surfaces connecting Franck-Condon region with the two excited state minima. Energies are given in eV with respect to the ground state in Franck-Condon.

Figure 72 (left) shows the TA measurements for duplex **0** where there is no gap between the phenanthrenes. The spectrum at 140 fs after excitation shows a negative signal below 340 nm which corresponds to phenanthrene absorption and the ESA of phenanthrene around 360 nm. Also observed is the presence of negative signals at 370 nm and 390 nm (vibronic bands of pyrene) on top of a positive ESA. During the measurement the phenanthrene signals go to almost zero and at the same time GSB of pyrene (350-400 nm) increases. This confirms that the energy absorbed by phenanthrene is transferred to pyrene. Another observation is the small stimulated emission of pyrene at 450 nm on top of the positive ESA at time zero.
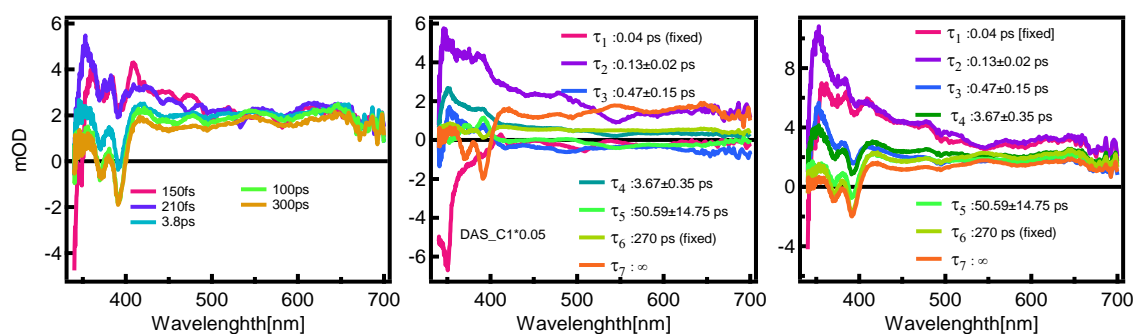
Figure 72: Transient absorption at different time delays of duplex **0** (left), calculated decay associated spectra (middle) and sum of decay associated spectra (right).

Figure 73 (left) shows the selected spectra at different times after excitation of duplex **1**. The result indicates that a complete transfer of excitation energy from excited phenanthrene to pyrene occurs. The negative signal corresponding to phenanthrene absorption is not observed and the ESA at 360 nm clearly disappears after 300 ps. There is again the presence of GSB of pyrene (370 nm, 390 nm) at 150 fs after excitation which continuously rises. Half of the total pyrene signal is immediately present and the other half rises via slower dynamics which is very likely due to FRET. Relaxation of ESA of phenanthrene above 450 nm is less evident since the dynamic is mixed with the rise of ESA of pyrene.
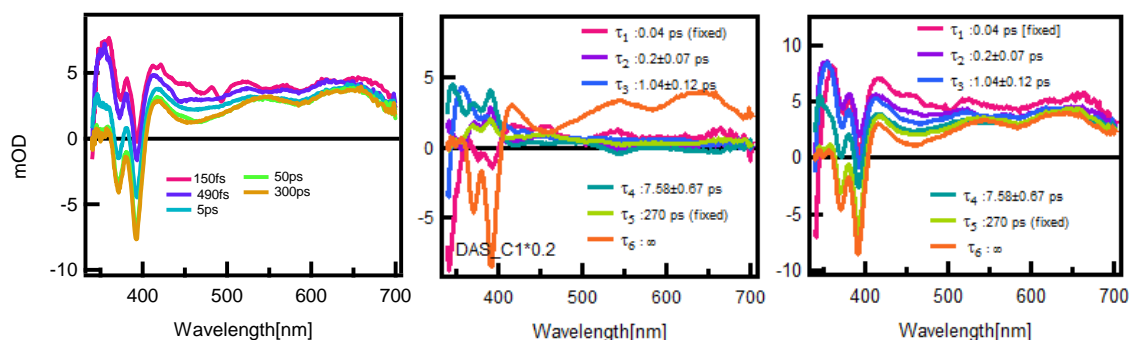

Figure 73: Transient absorption at different time delays of duplex **1** (left), calculated decay associated spectra (middle) and sum of decay associated spectra (right).

Figure 74 and Figure 75 show the results of the TA measurements of duplexes **2** and **3**, respectively. The phenanthrene signals do not disappear completely after 300 ps, indicating that not all phenanthrene molecules have transferred their energy to pyrene. Those measurements confirm the observations in the fluorescence spectra where pyrene emission was lower due to less energy transfer from phenanthrene.
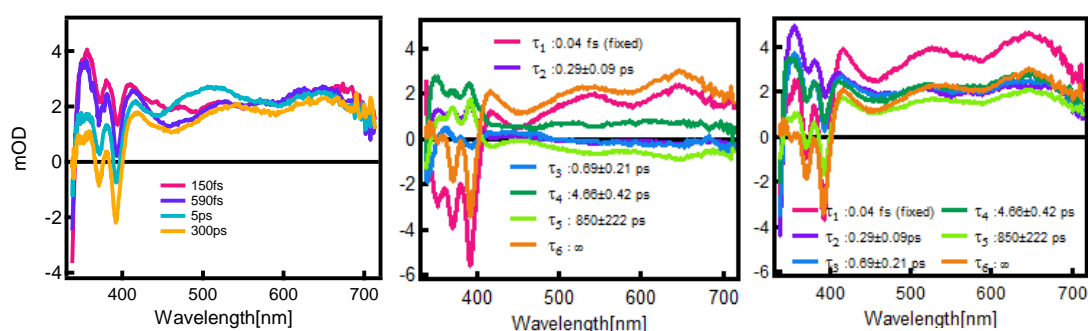

Figure 74: Transient absorption at different time delays of duplex **2** (left), calculated decay associated spectra (middle) and sum of decay associated spectra (right).
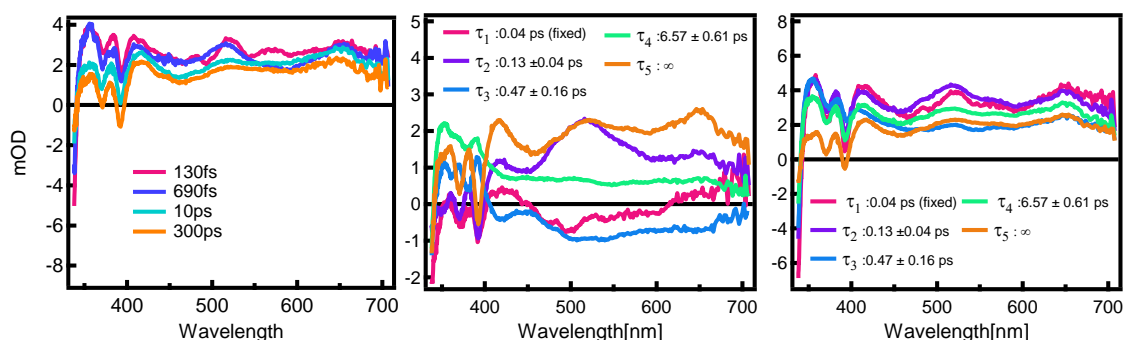

Figure 75: Transient absorption at different time delays of duplex **3** (left), calculated decay associated spectra (middle) and sum of decay associated spectra (right).

Figure 76 shows a model for the energy transfer over base pairs. Phenanthrene as the light-harvester has a higher excited state with delocalizing character and a lower excited state with a non-delocalizing character. The transient delocalized state mediates the energy transfer with high efficiency and collapses into a long-lived localized state. When an acceptor is present an important fraction (more than 50%) is instantaneously localized on the acceptor. The rest of the energy populates the acceptor with slower mechanisms, most likely FRET. The photocycle of the DNA based light-harvesting antenna is the following: At the beginning only one phenanthrene is excited, this localized energy is transferred to a delocalized excited state of the multichromophoric stack in less than 100 fs and finally, it is transferred to pyrene which then emits light by going back to the ground state. The transfer over the delocalized state of phenanthrene is affected by separating base pairs and is interrupted by the presence of two or three DNA base pairs.
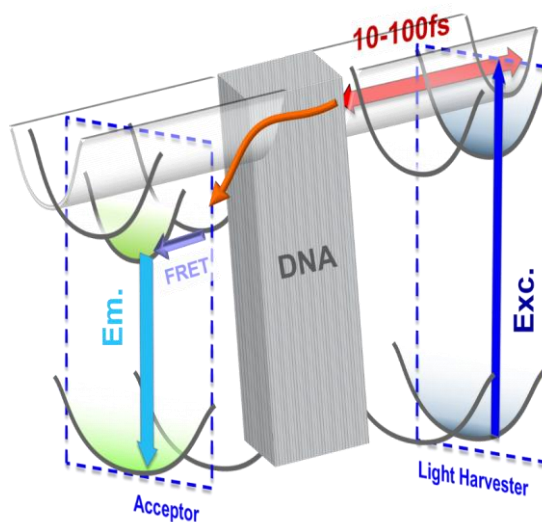
Figure 76: Model of the proposed mechanism of excitation energy transfer over base pairs in DNA based light-harvesting antennae.

Stability of Duplexes

Table 5 shows the determined melting temperatures (T_m). Generally, the duplexes are less stable with separating base pairs between the phenanthrenes. The lowest values were determined for duplexes **2** and **3** in which the phenanthrenes are separated by two and three base pairs, respectively. Spectra are shown in the supporting information (Figure 103 - Figure 110). They show all little hysteresis as duplex formation and disassembly are at thermodynamic equilibrium.[56] The curves are all not perfectly sigmoid possibly due to the additional absorption of phenanthrene at 260 nm.

Table 5: Melting temperatures (T_m) of duplexes.

Duplex	Sequences	T_m
0	5' GGC TAA φαα ααA TTA AAT CGC 3' 3' CCG ATT Yαα ααT AAT TTA GCG 5'	51°C
1	5' GGC TAA φαT ααα TTA AAT CGC 3' 3' CCG ATT YαA ααα AAT TTA GCG 5'	49°C
2	5' GGC TAA φαT Aαα αTA AAT CGC 3' 3' CCG ATT YαA Tαα αAT TTA GCG 5'	45°C
3	5' GGC TAA φαT ATα ααA AAT CGC 3' 3' CCG ATT YαA TAα ααT TTA GCG 5'	45°C
4	5' GGC TAA φαT ATA ααα AAT CGC 3' 3' CCG ATT YαA TAT αααTTA GCG 5'	46°C
5	5' GGC TAA φαT ATA Tαα αAT CGC 3' 3' CCG ATT YαA TAT Aαα αTA GCG 5'	48°C
Ref1	5' GGC TAA φαT ATA TTA AAT CGC 3' 3' CCG ATT YαA TAT AAT TTA GCG 5'	51°C
Ref2	5' GGC TAA ATα ααA TTA AAT CGC 3' 3' CCG ATT TAα ααT AAT TTA GCG 5'	54°C

Conclusion and Outlook

DNA based light-harvesting antennae composed of light collecting phenanthrenes and pyrene acceptors have been investigated. Excitation of phenanthrene leads to energy transfer to pyrene which then results in pyrene emission. This is in contrast to DNA based light-harvesting antennae composed of dicarboxamide phenanthrenes which form an exciplex with pyrene.[49a,c] Quantum yield measurements and transient absorption spectroscopy indicate that the energy is transferred over a delocalized excited state of the phenanthrenes. The energy transfer over this delocalized state is sensitive to the DNA bridge and the efficiency gets lower when the phenanthrenes are separated by more than three base pairs. More detailed studies on the mechanism by transient absorption spectroscopy are in progress, especially also systems where the pyrene is positioned in the middle of a stack of phenanthrene.

The presented concept would allow constructing DNA architectures with defined numbers of light-harvesters and defined distances (see Figure 77). Previously presented supramolecular light-harvesting polymers have presumably a random distribution of acceptors. Introducing DNA into those systems could control the number and positioning of acceptors due to specific base pairing. One, two or three dimensional architectures could be designed. Further it would be possible to arrange different chromophores in a certain order to enable an energy cascade.
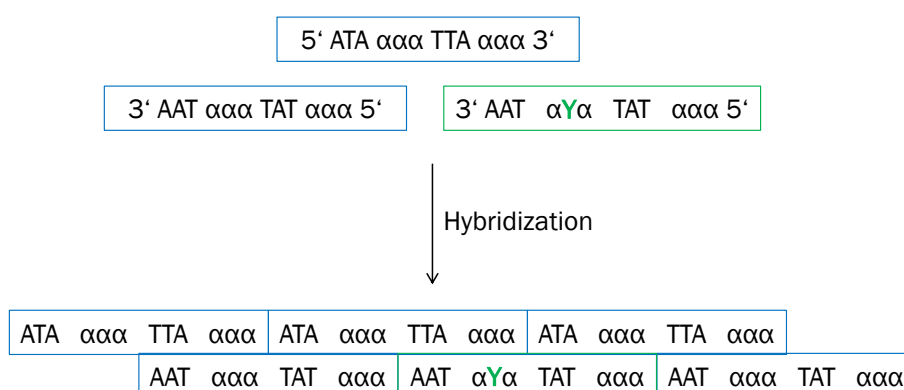

Figure 77: Schematic illustration of a DNA architecture composed of DNA single strands which hybridize over sticky ends. Light collecting phenanthrenes (α) are separated by three A-T base pairs, so that the expected excitation energy transfer to pyrene (Y) still can take place.

Supporting Information

Syntheses of Phosphoramidites

Syntheses of phenanthrene and pyrene phosphoramidites were described previously.[57] Abasic site building block is commercially available (Glen Research).

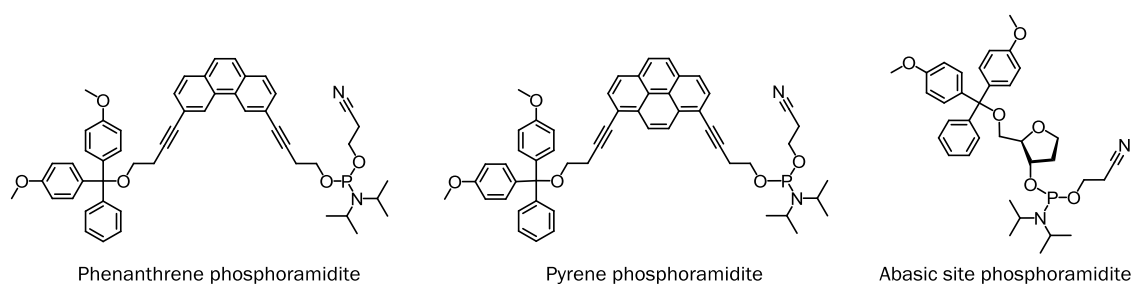Phenanthrene phosphoramidite   Pyrene phosphoramidite   Abasic site phosphoramidite

Figure 78: Chemical structures of phosphoramidites used to synthesize DNA based light-harvesting antennae presented in this chapter.

DNA Synthesis

DNA strands were prepared on an Applied Biosystems 394 DNA/RNA synthesizer. A standard cyanoethyl phosphoramidite coupling protocol was used beginning with nucleoside-loaded controlled pore glass (CPG) support. After synthesis, the CPG-bound strands were cleaved and deprotected by treatment with 28-30% NH_4OH (aq) at 55°C overnight. The supernatants were collected and the debris' were washed three times with 1 ml $EtOH/H_2O$ 1:1. After lyophilization the crude oligomers were purified by reversed phase HPLC (Merck LiChroCART 250-4; LiChrospher 100, RP-18, 5 μm); Solvent A: 0.1 M aqueous ammonium acetate; Solvent B: CH_3CN; 1 ml/min; T = 40°C; B[%] (t_R [min]) = 0 (0); 5 (2); 50 (22). Purities were confirmed by ESI mass spectrometry. The samples were measured in negative ion mode in mixtures of water/acetonitrile/triethylamine.

The purified oligomers were dissolved in 1 ml Milli-Q H_2O. Samples of the stock solutions were diluted and the absorbance at 326 nm was measured to determine the concentrations. The molar absorption coefficients of the oligomers were calculated using the ε_{326} value of 35'400 for phenanthrene.

71

Table 6: Calculated and found masses (negative ion mode) of DNA strands.

| Strand	Sequence	Calculated mass	Found mass
0_a	5' GGC TAA φαα ααA TTA AAT CGC 3'	6574.72	656.42 (z=10)
0_b	3' CCG ATT Υαα ααT AAT TTA GCG 5'	6777.04	676.62 (z=10)
1_a	5' GGC TAA φαT ααα TTA AAT CGC 3'	6565.71	655.52 (z=10)
1_b	3' CCG ATT ΥαA ααα AAT TTA GCG 5'	6786.05	677.52 (z=10)
2_a	5' GGC TAA φαT Aαα αTA AAT CGC 3'	6574.72	656.42 (z=10)
2_b	3' CCG ATT ΥαA Tαα αAT TTA GCG 5'	6777.04	676.62 (z=10)
3_a	5' GGC TAA φαT ATα ααA AAT CGC 3'	6574.72	656.42 (z=10)
3_b	3' CCG ATT ΥαA TAα ααT TTA GCG 5'	6777.04	676.62 (z=10)
4_a	5' GGC TAA φαT ATA ααα AAT CGC 3'	6574.72	656.42 (z=10)
4_b	3' CCG ATT ΥαA TAT αααTTA GCG 5'	6777.04	676.62 (z=10)
5_a	5' GGC TAA φαT ATA Tαα αAT CGC 3'	6565.71	655.52 (z=10)
5_b	3' CCG ATT ΥαA TAT Aαα αTA GCG 5'	6786.05	677.52 (z=10)
Ref1_a	5' GGC TAA φαT ATA TTA AAT CGC 3'	6367.24	635.61 (z=10)
Ref1_b	3' CCG ATT ΥαA TAT AAT TTA GCG 5'	6578.57	656.81 (z=10)
Ref2_a	5' GGC TAA ATα ααA TTA AAT CGC 3'	6635.73	662.52 (z=10)
Ref2_b	3' CCG ATT TAα ααT AAT TTA GCG 5'	6617.71	1322.24 (z=5)

Mass Spectra of Oligomers
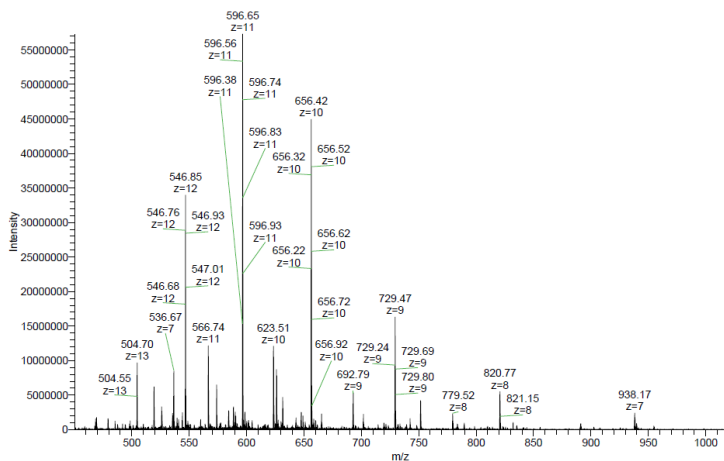
Figure 79: Mass spectrum of single strand **0_a**.
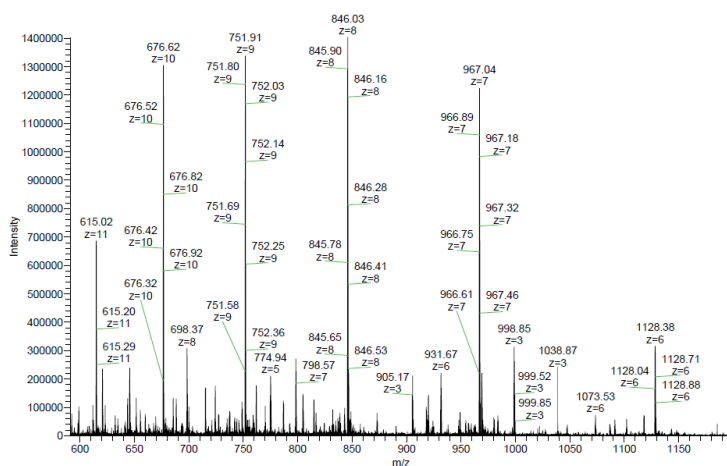

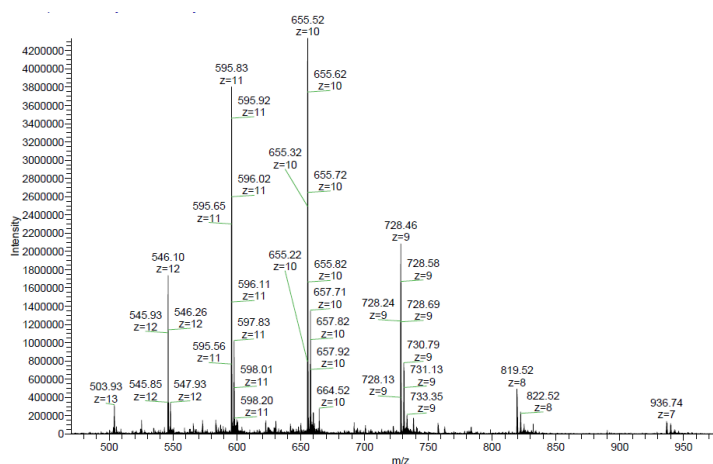Figure 80: Mass spectrum of single strand **0_b**.
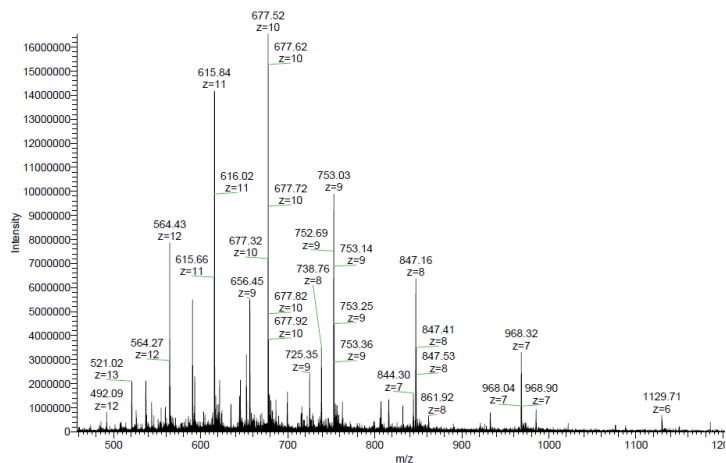
Figure 81: Mass spectrum of single strand **1_a**.
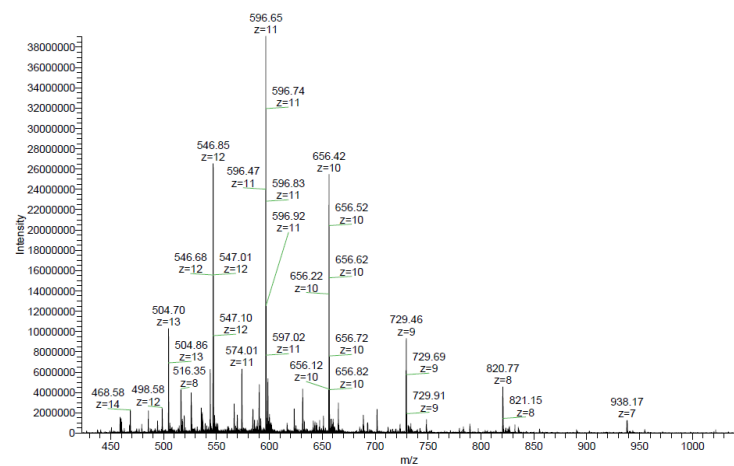

Figure 82: Mass spectrum of single strand **1_b**.
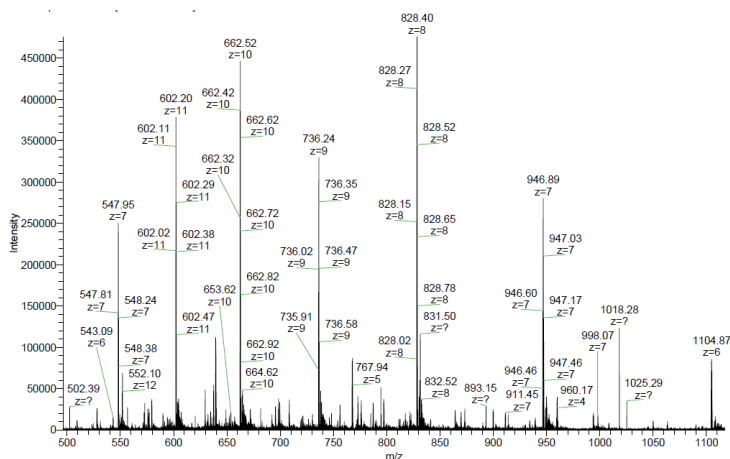

Figure 83: Mass spectrum of single strand **2_a**.
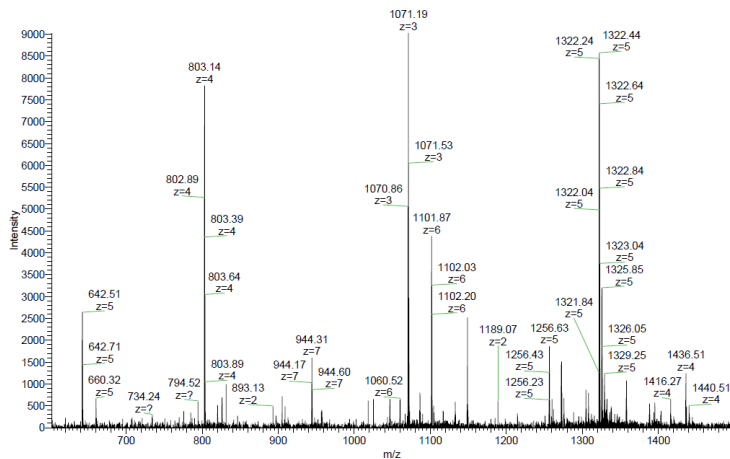
Figure 84: Mass spectrum of single strand **2_b**.

Figure 85: Mass spectrum of single strand **3_a**.

Figure 86: Mass spectrum of single strand **3_b**.

Figure 87: Mass spectrum of single strand **4_a**.

Figure 88: Mass spectrum of single strand **4_b**.

Figure 89: Mass spectrum of single strand **5_a**.

Figure 90: Mass spectrum of single strand **5_b**.

Figure 91: Mass spectrum of single strand **Ref1_a**.

Figure 92: Mass spectrum of single strand **Ref1_b**.

Figure 93: Mass spectrum of single strand **Ref2_a**.

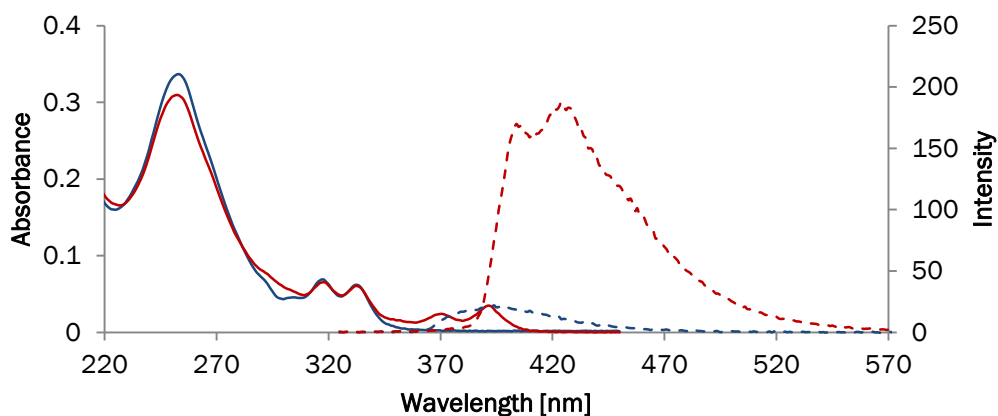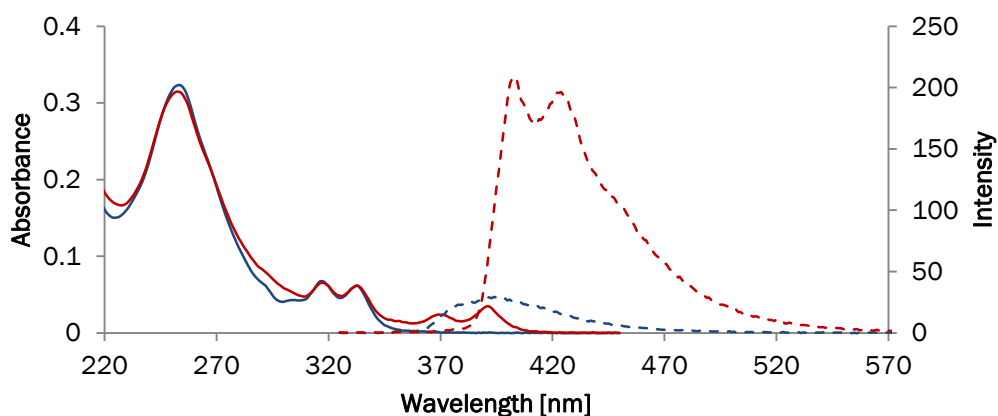Figure 94: Mass spectrum of single strand **Ref2_b**.

Spectra of Single Strands
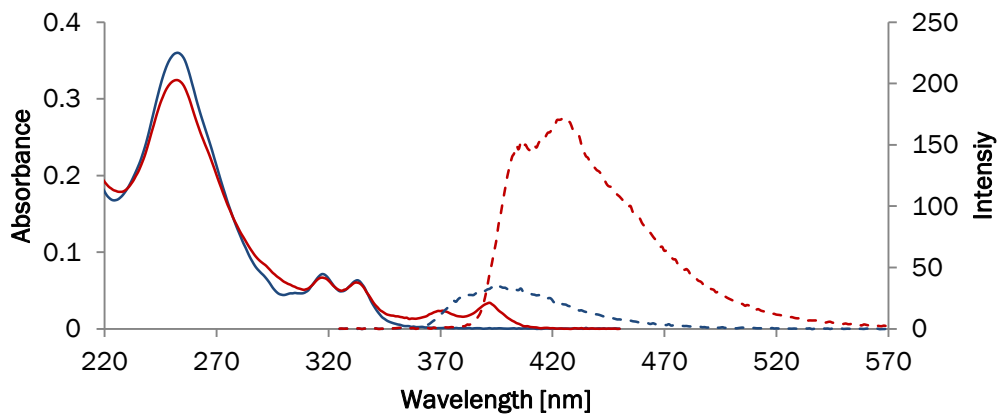
Figure 95: Absorption (solid) and fluorescence (dashed) spectra of single strands **0_a** (blue) and **0_b** (red). Conditions: 0.5 μM in 10 mM sodium phosphate buffer pH 7.0, 100 mM NaCl, λexc. 316 nm, 20°C. Excitation slit: 2.5 nm, emission slit: 5 nm.

Figure 96: Absorption (solid) and fluorescence (dashed) spectra of single strands **1_a** (blue) and **1_b** (red). Conditions: 0.5 μM in 10 mM sodium phosphate buffer pH 7.0, 100 mM NaCl, λexc. 316 nm, 20°C. Excitation slit: 2.5 nm, emission slit: 5 nm.
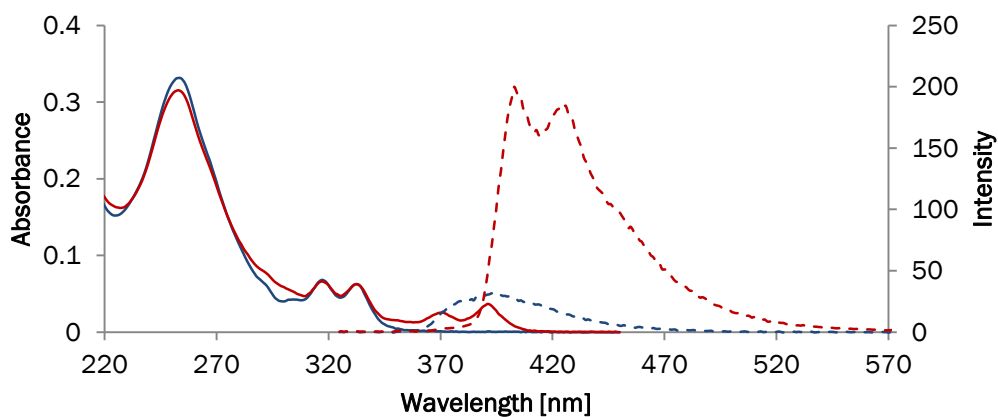
Figure 97: Absorption (solid) and fluorescence (dashed) spectra of single strands **2_a** (blue) and **2_b** (red). Conditions: 0.5 µM in 10 mM sodium phosphate buffer pH 7.0, 100 mM NaCl, λexc. 316 nm, 20°C. Excitation slit: 2.5 nm, emission slit: 5 nm.

Figure 98: Absorption (solid) and fluorescence (dashed) spectra of single strands **3_a** (blue) and **3_b** (red). Conditions: 0.5 µM in 10 mM sodium phosphate buffer pH 7.0, 100 mM NaCl, λexc. 316 nm, 20°C. Excitation slit: 2.5 nm, emission slit: 5 nm.
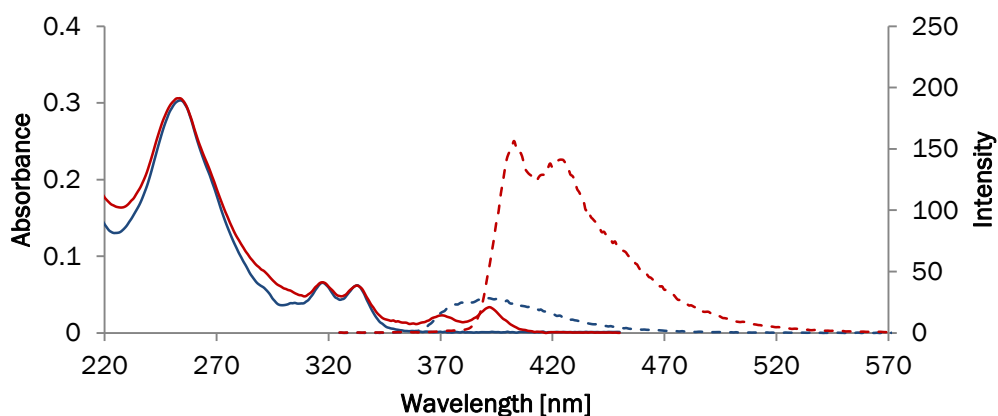
Figure 99: Absorption (solid) and fluorescence (dashed) spectra of single strands **4_a** (blue) and **4_b** (red). Conditions: 0.5 µM in 10 mM sodium phosphate buffer pH 7.0, 100 mM NaCl, λexc. 316 nm, 20°C. Excitation slit: 2.5 nm, emission slit: 5 nm.
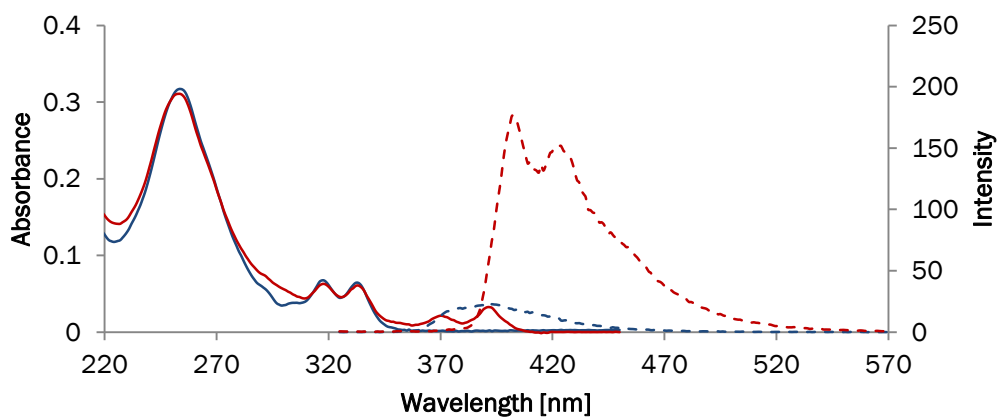

Figure 100: Absorption (solid) and fluorescence (dashed) spectra of single strands **5_a** (blue) and **5_b** (red). Conditions: 0.5 µM in 10 mM sodium phosphate buffer pH 7.0, 100 mM NaCl, λexc. 316 nm, 20°C. Excitation slit: 2.5 nm, emission slit: 5 nm.
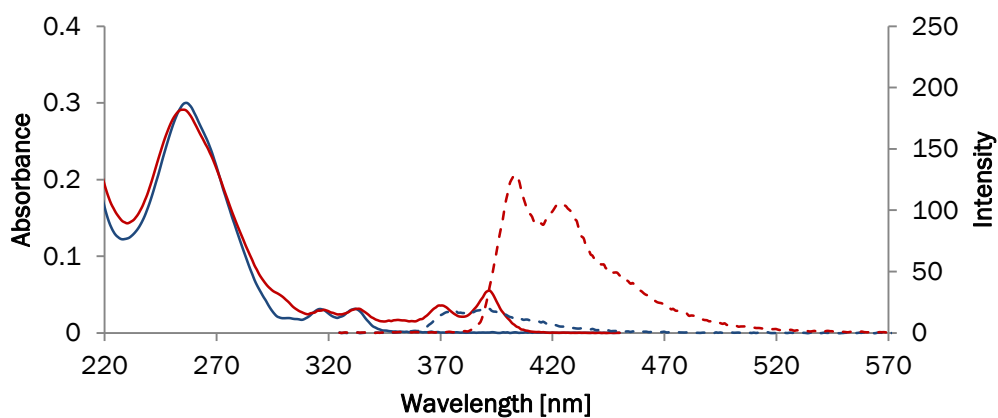
Figure 101: Absorption (solid) and fluorescence (dashed) spectra of single strands **Ref1_a** (blue) and **Ref1_b** (red). Conditions: 1 μM in 10 mM sodium phosphate buffer pH 7.0, 100 mM NaCl, λexc. 316 nm, 20°C. Exc. slit: 2.5 nm, em. slit: 5 nm.
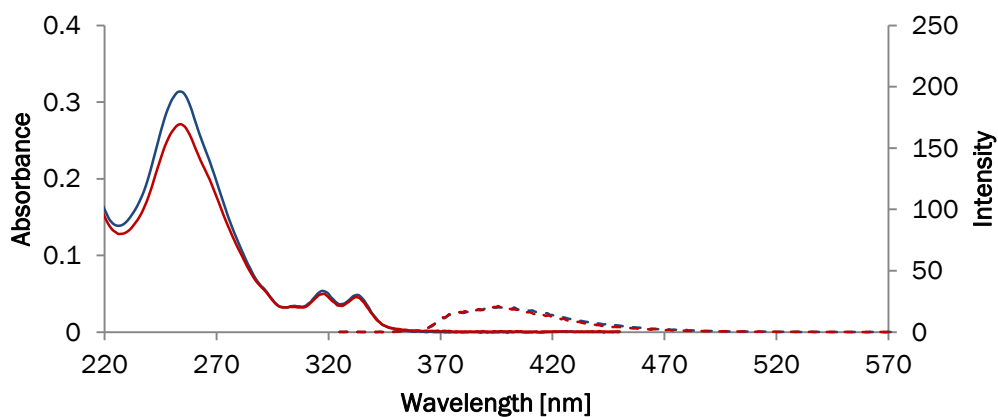

Figure 102: Absorption (solid) and fluorescence (dashed) spectra of single strands **Ref2_a** (blue) and **Ref2_b** (red). Conditions: 0.5 μM in 10 mM sodium phosphate buffer pH 7.0, 100 mM NaCl, λexc. 316 nm, 20°C. Exc. slit: 2.5 nm, em. slit: 5 nm.

Spectra of T$_m$ Measurements

Figure 103: Cooling-heating-cooling curves of duplex **0** while measuring the absorption at 260 nm. Concentration: 1 µM each strand, 10 mM sodium phosphate buffer pH 7.0, 100 mM NaCl. (Cooling: blue; heating: red)
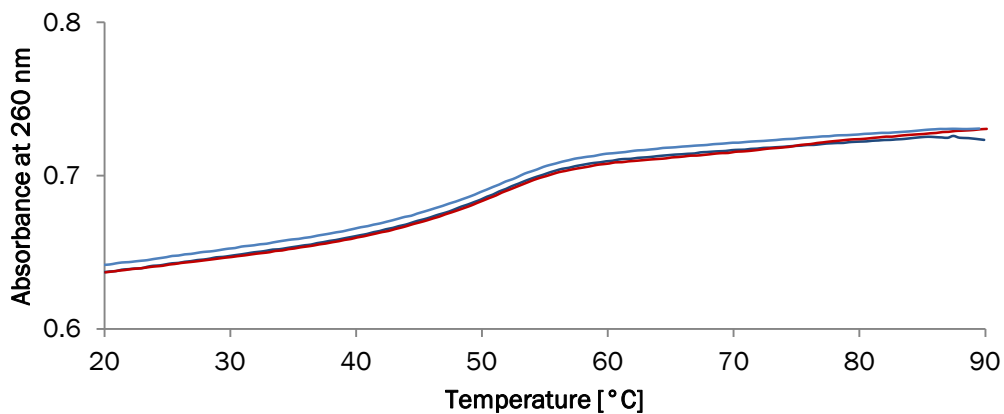

Figure 104: Cooling-heating-cooling curves of duplex **1** while measuring the absorption at 260 nm. Concentration: 1 µM each strand, 10 mM sodium phosphate buffer pH 7.0, 100 mM NaCl. (Cooling: blue; heating: red)

Figure 105: Cooling-heating-cooling curves of duplex **2** while measuring the absorption at 260 nm. Concentration: 1 µM each strand, 10 mM sodium phosphate buffer pH 7.0, 100 mM NaCl. (Cooling: blue; heating: red)

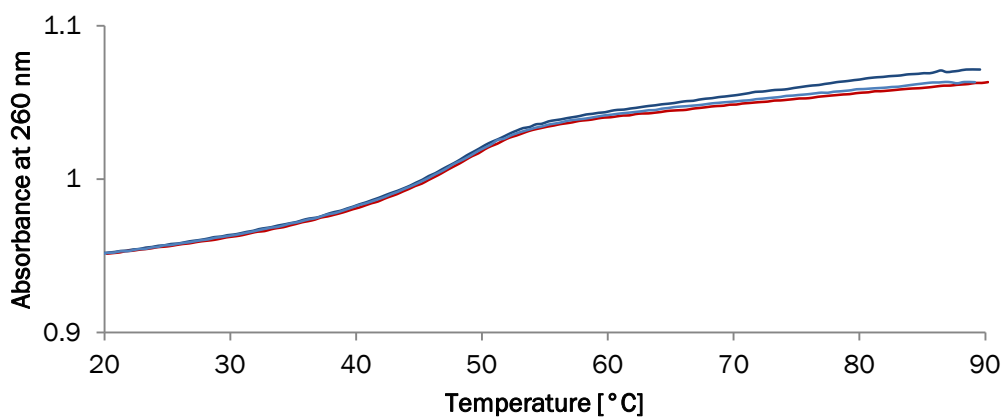Figure 106: Cooling-heating-cooling curves of duplex **3** while measuring the absorption at 260 nm. Concentration: 1 µM each strand, 10 mM sodium phosphate buffer pH 7.0, 100 mM NaCl. (Cooling: blue; heating: red)
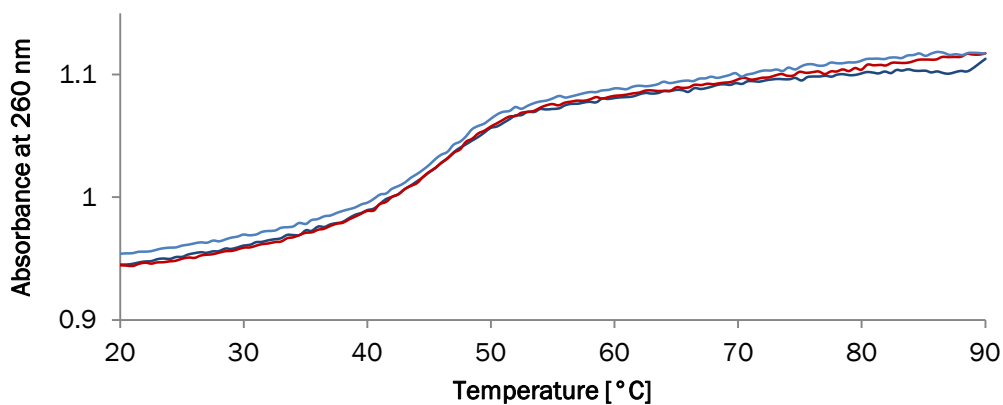
Figure 107: Cooling-heating-cooling curves of duplex **4** while measuring the absorption at 260 nm. Concentration: 1 µM each strand, 10 mM sodium phosphate buffer pH 7.0, 100 mM NaCl. (Cooling: blue; heating: red)
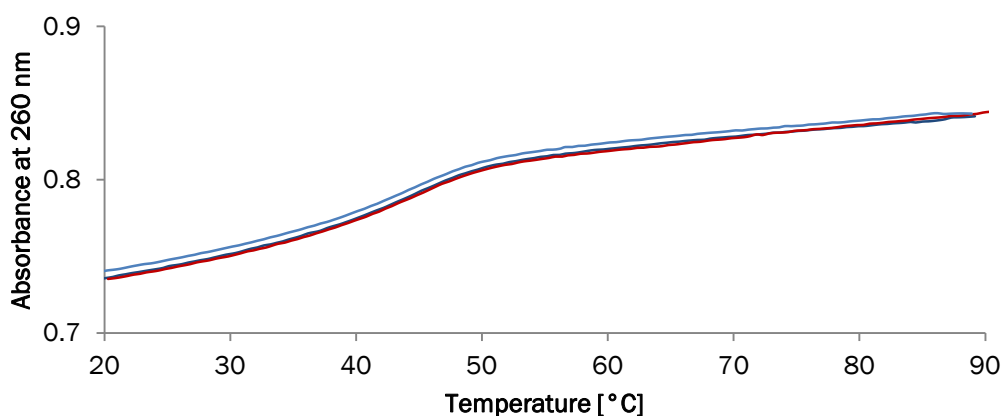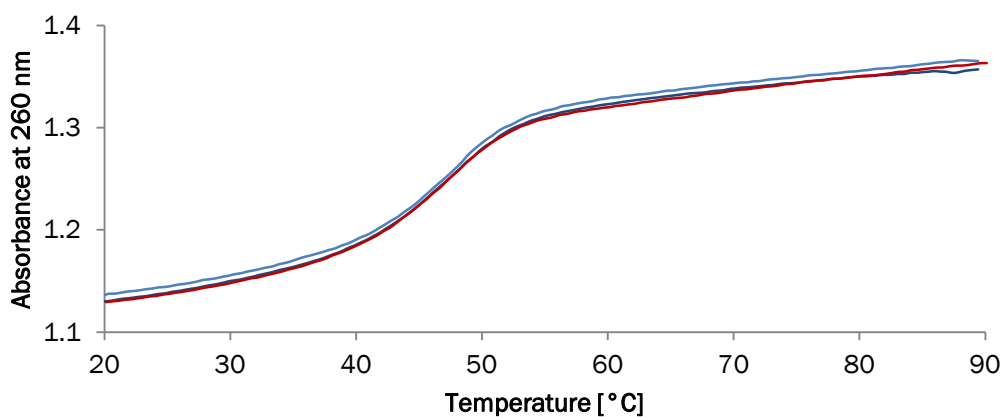

Figure 108: Cooling-heating-cooling curves of duplex **5** while measuring the absorption at 260 nm. Concentration: 1 µM each strand, 10 mM sodium phosphate buffer pH 7.0, 100 mM NaCl. (Cooling: blue; heating: red)

Figure 109: Cooling-heating-cooling curves of duplex **Ref1** while measuring the absorption at 260 nm. Concentration: 1 µM each strand, 10 mM sodium phosphate buffer pH 7.0, 100 mM NaCl. (Cooling: blue; heating: red)
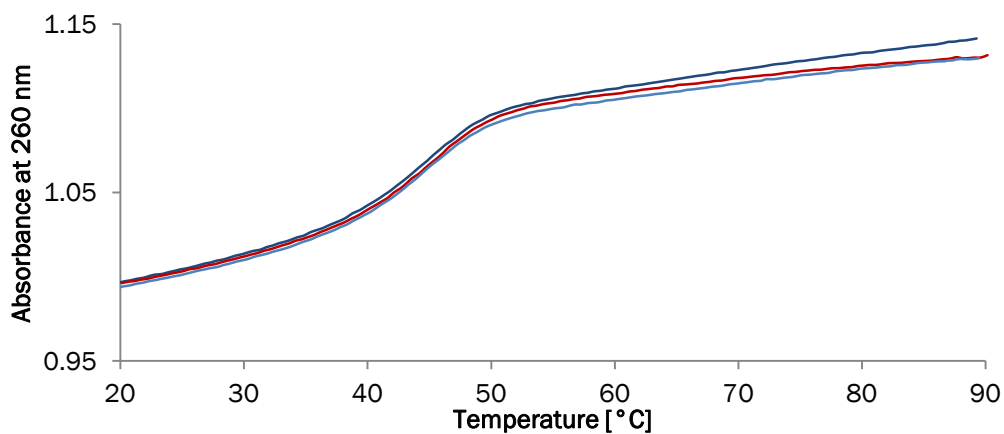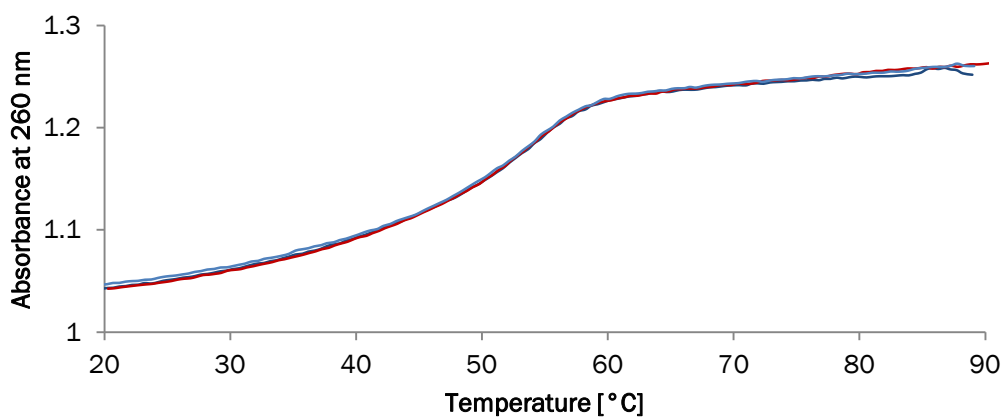

Figure 110: Cooling-heating-cooling curves of duplex **Ref2** while measuring the absorption at 260 nm. Concentration: 1 µM each strand, 10 mM sodium phosphate buffer pH 7.0, 100 mM NaCl. (Cooling: blue; heating: red)

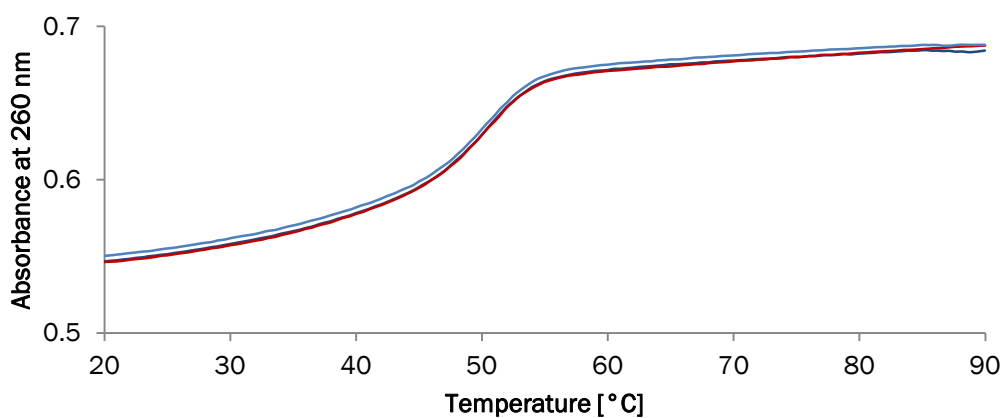## Set-Up for Transient Absorption Measurements

Samples were excited at 324 nm with a power of 1.5 mW. Radius of the pump beam at the sample position was measured to be about 36 µm² (50% of the radius of the beam profile). The sample handling was provided by a jet flow in air. Aqueous solutions were prepared to have phenanthrene absorption of 0.2-0.3, assuming a light path of 0.02-0.03 cm. Time resolution of the measurement has been calculated with a 50 fs standard deviation with a time window extended to 400 ps.

Figure 111: Experimental set-up of single shot time-resolved spectroscopy (illustration was done by Maryam Nazari Haghighi Pashaki).

References

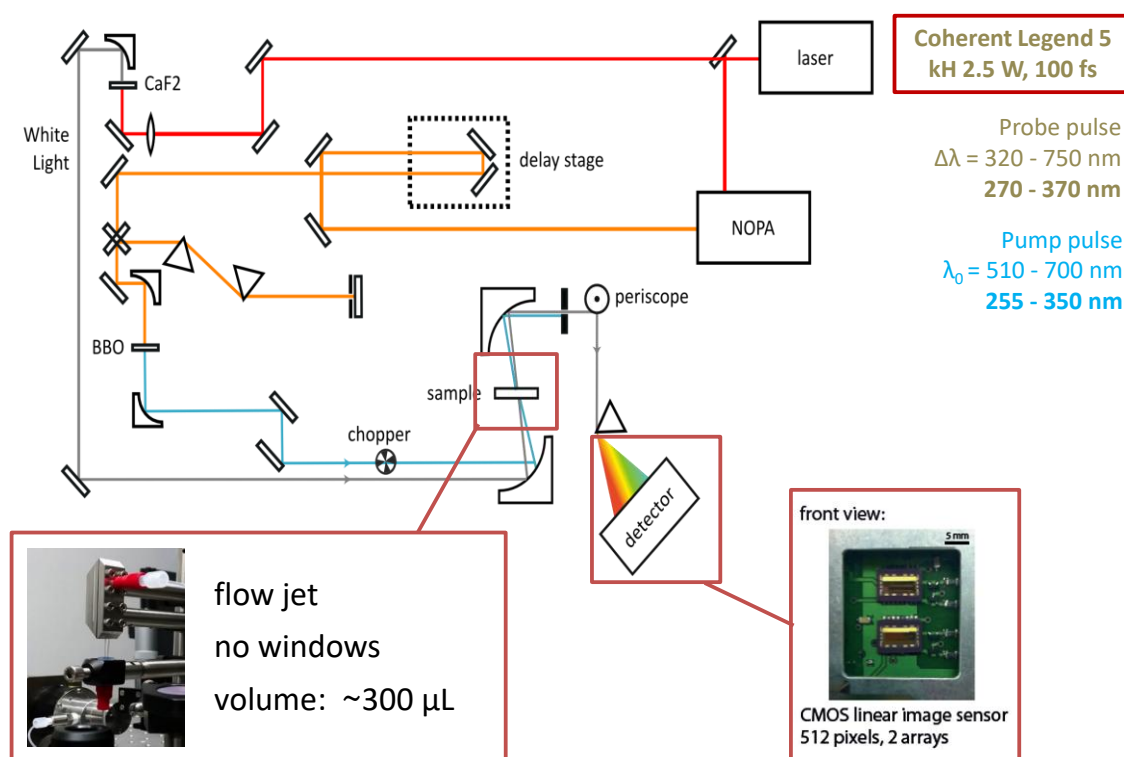[47] (a) E. Stulz, G. H. Clever, *DNA in Supramolecular Chemistry and Nanotechnology*, Wiley, Hoboken, NJ, USA, 2015.
(b) L.-A. Fendt, I. Bouamaied, S. Thöni, N. Amiot, E. Stulz, *J. Am. Chem. Soc.*, 2007, **129**, 15319-15329.
(c) F. A. Aldaye, A. L. Palmer, H. F. Sleiman, *Science*, 2008, **321**, 1795-1799.
(d) N. C. Seeman, *Annu. Rev. Biochem.*, 2010, **79**, 65-87.
(e) E. Stulz, *Chem. Eur. J.*, 2012, **18**, 4456-4469.
(f) W. Pfeifer, B. Saccà, *ChemBioChem*, 2016, **17**, 1063-1080.
(g) C. K. McLaughlin, G. D. Hamblin, H. F. Sleiman, *Chem. Soc. Rev.*, 2011, **40**, 5647-5656.
(h) T. J. Bandy, A. Brewer, J. R. Burns, G. Marth, T. Nguyen, E. Stulz, *Chem. Soc. Rev.*, 2011, **40**, 138-148.
(i) A. V. Pinheiro, D. Han, W. M. Shih, H. Yan, *Nat. Nanotechnol.*, 2011, **6**, 763-772.

[48] (a) D. Gust, T. A. Moore, A. L. Moore, *Acc. Chem. Res.*, 2001, **34**, 40-48.
(b) M. S. Choi, T. Yamazaki, I. Yamazaki, T. Aida, Angew. Chem. Int. Ed., 2004, **43**, 150-158.
(c) H. Yeo, K. Tanaka, Y. Chujo, *RSC Adv.*, 2017, **7**, 10869-10874.
(d) X. Feng, X. Ding, L. Chen, Y. Wu, L. Liu, M. Addicoat, S. Irle, Y. Dong, D. Jiang, *Scientific Reports*, 2016, **6**, 32944.
(e) H. Li, Y. Liu, T. Huang, M. Qi, Y. Ni, J. Wang, Y. Zheng, Y. Zhou, D. Yan, *Macromol. Rapid Commun.*, 2017, **38**, 1600818.
(f) A. Uetomo, M. Kozaki, S. Suzuki, K. Yamanaka, O. Ito, K. Okada, *J. Am. Chem. Soc.*, 2011, **133**, 13276-13279.
(g) R. K. Dubey, D. Inan, S. Sengupta, E. J. R. Sudhölter, F. C. Grozema, W. F. Jager, *Chem. Sci.*, 2016, **7**, 3517-3532.
(h) C. F. Calver, K. S. Schanze, G. Cosa, *ACS Nano*, 2016, **10**, 10598-10605.
(i) J.-J. Li, Y. Chen, J. Yu, N. Cheng, Y. Liu, *Adv. Mater.*, 2017, **29**, 1701905.

[49] (a) F. Garo, R. Häner, *Angew. Chem. Int. Ed.*, 2012, **51**, 916-919.
(b) O. O. Adeyemi, V. L. Malinovskii, S. M. Biner, G. Calzaferri, R. Häner, *Chem. Commun.*, 2012, **48**, 9589-9591.
(c) M. Probst, S. M. Langenegger, R. Häner, *Chem. Commun.*, 2014, **50**, 159-191.

[50] (a) S. O. Kelley, J. K. Barton, *Science*, 1999, 283, 375-381.
(b) F. Garo, R. Häner, *Bioconjug. Chem.*, 2012, **23**, 2105-2113.

[51] K. Kalyanasundaram, J. K. Thomas, *J. Am. Chem. Soc.*, 1977, **99**, 2039-2044.

[52] (a) T. Förster, *Ann. Phys.*, 1948, **2**, 55-75.
(b) C. Berney, G. Danuser, *Biophys. J.*, 2003, **84**, 3992-4010.

[53] (a) E. Collini, *Chem. Soc. Rev.*, 2013, **42**, 4932-4947.
(b) E. Collini, G. D. Scholes, *Science*, 2009, **323**, 369-373.
(c) J. Strümpfer, M. Şener, K. Schulten, *J. Phys. Chem. Lett.*, 2012, **3**, 536-542.
(d) G. S. Engel, T. R. Calhoun, E. L. Read, T.-K. Ahn, T. Mančal, Y.-C. Cheng, R. E. Blankenship, G. R. Fleming, *Nature*, 2007, **446**, 782-786.
(e) G. R. Fleming, G. D. Scholes, *Nature*, 2004, **431**, 256-257.
(f) I. Hwang, G. D. Scholes, *Chem. Mater.*, 2011, **23**, 610-620.

[54] A. Chenu, G. D. Scholes, *Annu. Rev. Phys. Chem.*, 2015, **66**, 69-96.

[55]   (a) R. Berera, R. van Grondelle, J. T. M. Kennis, *Photosynth. Res.*, 2009, **101**, 105-118.
(b) J. P. Connelly, M. G. Müller, R. Bassi, R. Croce, A. R. Holzwarth, *Biochemistry*, 1997, **36**, 281-287.
(c) S. Honda, S. Yokoya, H. Ohkita, H. Benten, S. Ito, *J. Phys. Chem. C*, 2011, **115**, 11306-11317.

[56]   R. A. J. Darby, M. Sollogoub, C. McKeen, L. Brown, A. Risitano, N. Brown, C. Barton, T. Brown, K. R. Fox, *Nucleic Acids Res.*, 2002, **30**, e39.

[57]   (a) C. Winiger, S. M. Langenegger, G. Calzaferri, R. Häner, Angew. Chem. Int. Ed., 2015, **54**, 3643-3647.
(b) H. Bittermann, D. Siegemund, V. L. Malinovskii, R. Häner, *J. Am. Chem. Soc.*, 2008, **130**, 15287-15287.

Chapter 3: Formation of Functionalizable DNA Sheets via Phenanthrene Sticky Ends

Abstract

Complementary DNA strands with each three phosphate-linked 2,7-dialkynyl phenanthrenes at their 3' ends form duplexes with amphiphilic overhangs. In presence of spermine, those overhangs act as sticky ends which link the duplexes. Supramolecular two-dimensional sheets with altering DNA and phenanthrene parts are formed. Fluorescence measurements show that the assembled phenanthrene units act as light-harvesting antennae and transfer absorbed energy to an acceptor which is either directly added to the polymer or added attached to a complementary DNA strand. Those DNA architectures allow constructing and investigating light-harvesting antennae with acceptors at defined distances to the donors. In addition, the DNA part opens other possibilities for functionalization.

Introduction

In nanotechnology DNA is used to create one-, two-, or three-dimensional assemblies due to its unique molecular recognition properties which opens opportunities to precisely organize materials within those structures.[58] Combining DNA building blocks with other molecules can influence the structure and introduce other functionalities.[59] Such functional supramolecular polymers have potential for biomedical, biomimetic and electronic applications.[60] There are diverse approaches to build up DNA assemblies. DNA origami describes the preparation of well-defined nanosized objects by assembling a long DNA strand with short staple strands (see Figure 112 A).[61] This makes it a useful tool for the spatial arrangement of molecules at the nanoscale and is therefore suitable for the development of solid state devices or nanomedicine.[62] Another way to construct large DNA assemblies is to use duplexes with unpaired nucleotides at the ends which can then pair with other single-stranded overhangs to form longer structures (sticky end approach, Figure 112 B).[63] Moreover, two- and three-dimensional structures can be implemented with sticky ends.[63b,64] With the additional incorporation of terpyridine substituted thymidines into short

DNA strands with sticky ends it was possible to form long duplexes which are then bundled together via metal complexation interactions.[65]
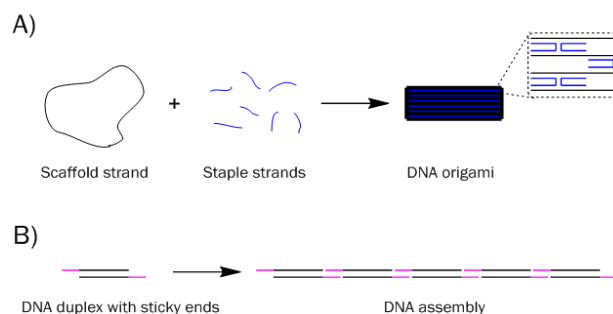

Figure 112: A) Schematic illustration of DNA origami formation. A circular DNA single strand (scaffold strand, black) is annealed with staple strands (blue) to form a predesigned assembly. B) Schematic illustration of DNA assembly via sticky ends (pink).

Further methods to prepare DNA assemblies comprise the incorporation of chemical modifications or hydrophobic aromatic molecules. DNA-pyrene hybrid oligomers showed to self-assemble into nanoribbons with addressable DNA strands at the surfaces.[66] Similarly, DNA-porphyrine hybrid amphiphiles self-assemble into spherical nanostructures.[67] DNA dumbbells (duplexes in which the single strands are linked on both ends) with a perylenediimide (PDI) on each end form one-dimensional DNA supramolecular polymers via PDI stacking.[68] Also a cationic dye triplet has been attached as sticky ends on DNA single strands to form long duplexes.[69] Oligoethylene glycol dendrons were introduced into DNA strands which then self-assemble in organic solvent and form long DNA nanofibers (block copolymer approach).[70] Condensation of DNA into tightly packed structures can be induced by the addition of polycations like spermidine, spermine or cobalthexamine.[71] Those polyamines are protonated under physiological pH and can therefore electrostatically interact with the phosphate backbone. Spermine, specifically, is known precipitate DNA at relatively low concentrations.[72] With spermidine it was shown that the precipitation of DNA is stepwise and formation of fibers, fiber bundles and a highly condensed phase can be observed.[73] It has also been used to fold DNA origami structures which showed to be more stable in the presence of high electric field pulses.[74]
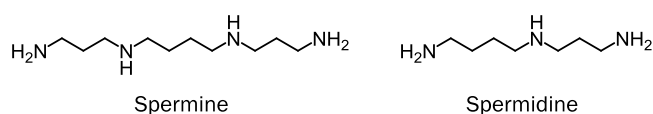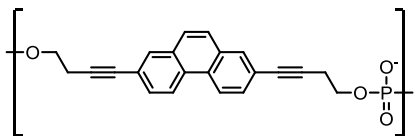

Figure 113: Chemical structures of polyamines spermine and spermidine.

Results and Discussion

DNA Sequences

Table 7 shows DNA strands which were used for the work presented in this chapter. Complementary strands were hybridized to yield duplexes with three or no 2,7-dialkynyl phenanthrene at either both or only one 3' end. In each duplex 20 base pairs are formed which corresponds to two turns of the DNA duplex. Single strands were analyzed as well for their aggregation behavior.

Table 7: Sequences of DNA strands and structure of unnatural building block phenanthrene (**Ph**).

	Sequences
1	5' CAA GGT CCG ATG CAA GGA AG (**Ph**)$_3$ 3'
2	3' (**Ph**)$_3$ GTT CCA GGC TAC GTT CCT TC 5'
3	5' CAA GGT CCG ATG CAA GGA AG 3'
4	3' GTT CCA GGC TAC GTT CCT TC 5'

Phenanthrene (**Ph**)

Spectroscopic and Microscopic Measurements

Figure 114 (left) shows the temperature dependent absorption spectrum of duplex **1*2** in the presence of 0.1 mM spermine tetrahydrochloride. 20 vol% of ethanol was added to ensure reversibility of the assembly process. The vibronic bands between 300 and 340 nm are from the absorption of the incorporated phenanthrene units. The absorbance around 260 nm comes from the DNA bases and from phenanthrene. The measured absorption bands at different temperatures show a clear aggregation behavior. At elevated temperatures the two single strands are expected to be separated. By lowering the temperature, the absorption at 260 nm gets lower and slightly blue-shifted. At the same time the vibronic band at 318 nm is red-shifted. This indicates hybridization of the two single strands, and at the same time assembly of the phenanthrene units. Another indication for DNA aggregation is the increase in the region 320-400 nm due to Tyndall scattering.[75] Two isobestic points can be seen at 285 nm and 322 nm. In contrast, another

behavior is observed for the measurement under conditions which are usually used for DNA (10 mM sodium phosphate buffer pH 7.0, 100 mM NaCl); hypochromicity at 260 nm, but otherwise no shifts (Figure 114, right). In this case it is assumed that the duplex is formed but the phenanthrenes do not interact with each other. This could be due to the lack of spermine which is known to stabilize DNA duplexes. Additionally, as a polycation it can shield the negative charge from the phosphates, and therefore diminish the repulsive forces and promote phenanthrene aggregation.
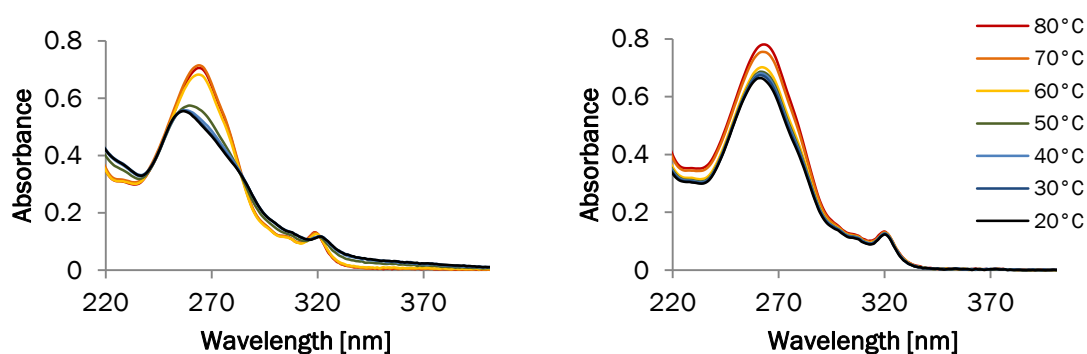

Figure 114: Temperature-dependent absorption spectra of **1*2**. Left: Conditions: 1 µM each strand, 10 mM sodium phosphate buffer pH 7.0, 0.1 mM spermine tetrahydrochloride, 20 vol% ethanol. Right: Conditions: 1 µM each strand, 10 mM sodium phosphate buffer pH 7.0, 100 mM NaCl.

AFM images of **1*2** on APTES-modified mica show large and equally high sheet structures (1.2-1.4 nm). Those sheets are mainly round and often grown together. They are only observed when the duplex is assembled in the presence of spermine. Under standard conditions only disparate aggregates are observed (supporting information, Figure 128). Also in the case where phenanthrenes are only on one side of the duplex (**1*4, 2*3**) those large sheets are not formed; smaller and higher sheets are observed (500 nm in diameter, 3 nm high, see Figure 132 and Figure 133).
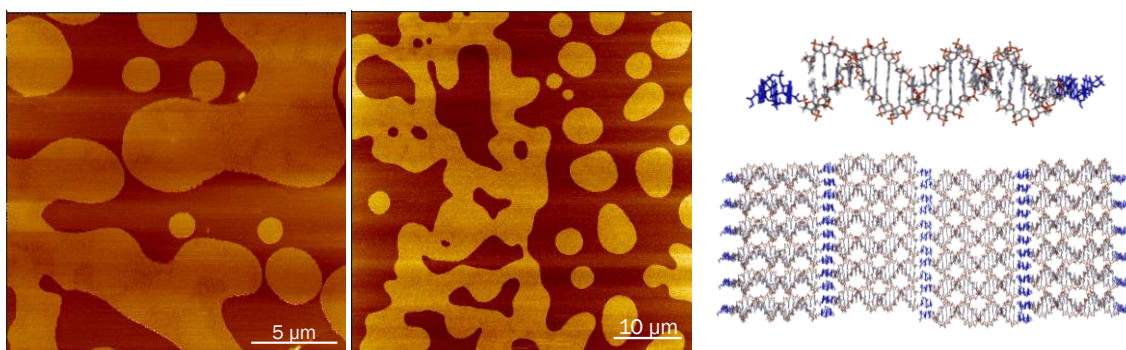
Figure 115: Left and middle: AFM images of **1*2** deposited on APTES-modified mica. Conditions: 1 µM each strand, 10 mM sodium phosphate buffer pH 7.0, 0.1 mM spermine tetrahydrochloride, 20 vol% ethanol. Right: Model of assembled duplexes via phenanthrene sticky ends.

Melting temperatures (T_m) can give insights into the self-assembly mechanism of the DNA sheets. A control duplex which does not contain phenanthrene overhangs was prepared to determine the T_m of solely the DNA part (as the phenanthrene units in **1*2** also absorb at 260 nm); a value of 53°C was determined. Then, the absorbance of **1*2** at 318 nm was measured while cooling/heating the sample to determine the T_m of the phenanthrene part. This measurement does not show an isodesmic mechanism like for the DNA, its looks more like a cooperative mechanism (nucleation-elongation polymerization) which starts at 57°C, so roughly at the same temperature as the DNA part (see Figure 116). In the model shown in Figure 115 the duplexes are arranged in a regular way. Phenanthrene overhangs interact in a way, so that altering lines of solely phenanthrene and solely DNA arise. Non-normalized spectra of T_m measurements are shown in Figure 141 - Figure 146.
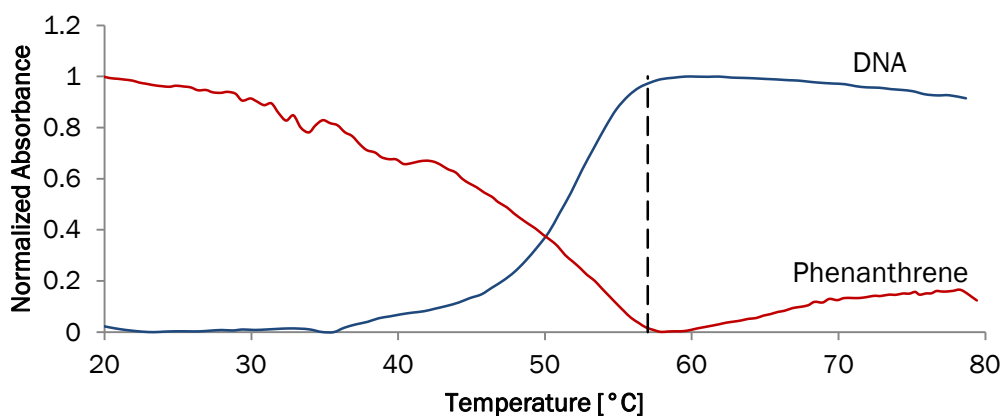

Figure 116: Normalized absorption of DNA part at 260 nm (**3*4**, blue) and of phenanthrene part at 318 nm (**1*2**, red). Dashed line indicates 57°C where both entities start to assemble.

94

Light-Harvesting DNA Sheets

Fluorescence measurements were performed to further prove that phenanthrenes in the observed sheets are arranged in a well-defined order and also to show they act as light-harvesting antenna. The structural order of chromophores and the resulting high electronic coupling between them is a prerequisite for efficient energy transfer.[76] The DNA sheet can be functionalized with acceptor molecules in different ways, either by adding a suitable chromophore which can intercalate in the DNA or phenanthrene part, or by adding a DNA strand with a replaced nucleotide.

Functionalization with a Pyrene-Containing Oligomer

Here we will show first the possibility to add an acceptor which will be incorporated directly into the phenanthrene bands. A pyrene-containing oligomer has already been used as an acceptor for a tubular phenanthrene supramolecular polymer (see Chapter 1).[77] Figure 117 shows the fluorescence measurements after adding 1% of pyrene per phenanthrene (solution is heated to 80°C and cooled to 20°C before measurement). It clearly shows that phenanthrene emission (378 nm and 398 nm) decreases, whereas pyrene emission increases (412 nm, 435 nm and 462 nm). In a duplex which contains only one phenanthrene overhang (**1*4**) or just the single strand (**1**) no such energy transfer was observed. Pyrene fluorescence is visible but the relative intensities (412 nm/378 nm) are much lower (0.77 and 1.07, compared to 2.23). Also the measurement of **1*2** with 1% pyrene under other conditions (10 mM sodium phosphate buffer pH 7.0, 100 mM NaCl) does not show a mentionable pyrene emission (Figure 118).
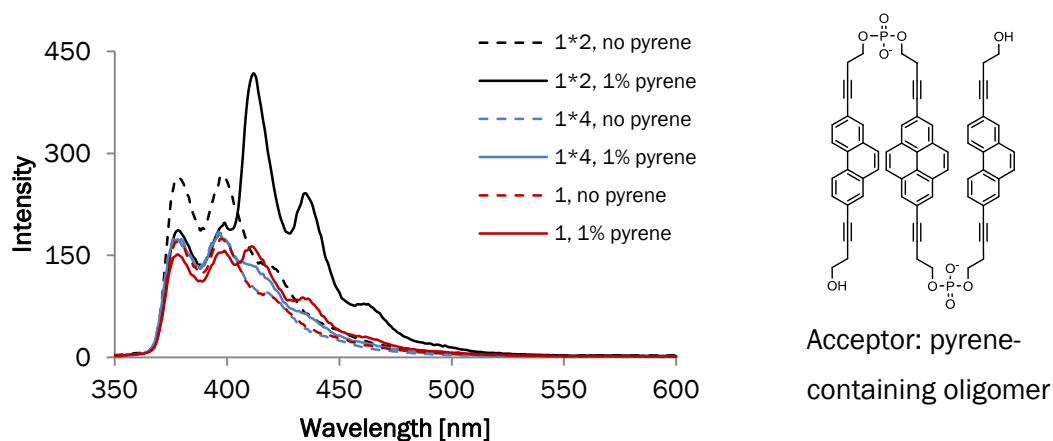
Figure 117: Left: Fluorescence measurements without (dashed) and with acceptor (solid). Addition of acceptor represented as 1 mol% of pyrene per total phenanthrene content in the samples. Conditions: 1 µM of each strand (duplexes: 1 µM + 1 µM), 10 mM sodium phosphate buffer pH 7.0, 0.1 mM spermine tetrahydrochloride, 20 vol% ethanol, 20°C, λexc. 321 nm. Right: Structure of acceptor oligomer.

Table 8: Effective phenanthrene (378 nm) and pyrene (412 nm) fluorescence intensities and their ratios. (Values from Figure 117)

	Intensity at 378 nm	Intensity at 412 nm	Ratio of intensities (412 nm/378 nm)	Relative ratio
1*2	186.66	417.13	2.23	1
1*4	173.35	133.55	0.77	0.34
1	151.68	161.83	1.07	0.48

A comparison of the light-harvesting properties of **1*2** with different conditions is shown in Figure 118. In black is the measurement with spermine (as shown in Figure 117) and in red without spermine. Without spermine almost no pyrene emission is visible, further demonstrating that no well-ordered assemblies are formed which would enable energy transfer.
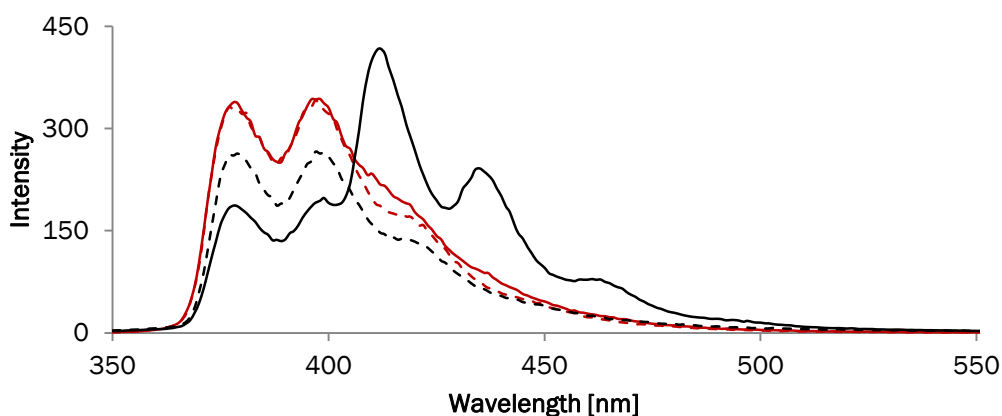
Figure 118: Fluorescence measurements without (dashed) and with acceptor (solid) of assembled **1*2**. Addition of acceptor represented as 1 mol% of pyrene per total phenanthrene content in the samples. Black: Conditions: 1 µM each strand, 10 mM sodium phosphate buffer pH 7.0, 0.1 mM spermine tetrahydrochloride, 20 vol% ethanol, λexc. 321 nm. Red: Conditions: 1 µM each strand, 10 mM sodium phosphate buffer pH 7.0, 100 mM NaCl, λexc. 321 nm.

Incorporation of the pyrene-containing oligomer is exceedingly improved when the supramolecular polymer is reassembled (heating the solution to 80°C, then cooling down to 20°C). Figure 119 shows the measurement of the assembled DNA sheet before addition of pyrene, after the addition of pyrene (without reassembly), at 80°C with pyrene, and again at 20°C after the heating (reassembled). It can be seen clearly that after the reassembly process pyrene emission is enhanced while at the same time phenanthrene emission decreases, leading to the conclusion that the aggregated phenanthrenes in the sheet have to be disrupted to allow efficient incorporation of the additional oligomer. Further, the measurement at 80°C shows no observable energy transfer, as the characteristic peaks of pyrene are missing. At this temperature the DNA sheet is completely disassembled and the phenanthrenes in the single strands cannot act as a light-harvesting antenna.
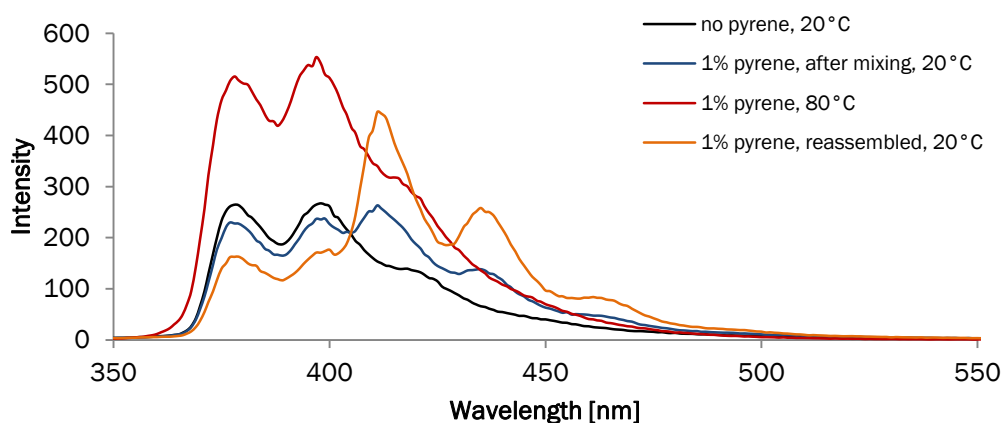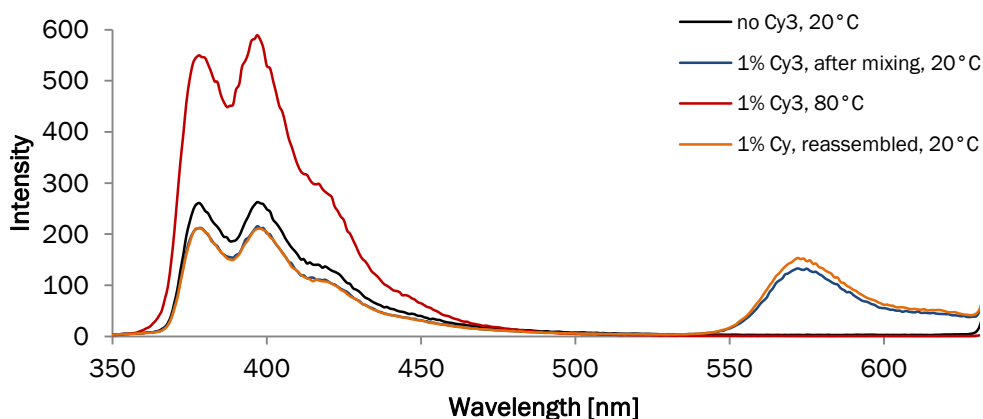
Figure 119: Fluorescence measurement of DNA sheet alone (black) and with added pyrene acceptor before reassembly (blue), at 80°C (red) and after reassembly (orange). Conditions: see Figure 117.

Functionalization with a Cyanine(Cy3)-Containing DNA Single Strand

The supramolecular polymer can also be functionalized by adding modified DNA strands. A strand which is complementary to strand **1** with a cyanine (Cy3) modification at the 5' end was chosen as an acceptor (3' GTT CCA GGC TAC GTT CCT TC(Cy3) 5'). Also in this case energy transfer is observed, as the emission of phenanthrene decreases and Cy3 emission at 573 nm appears (Figure 120). Duplex **1*2** shows the highest ratio of intensity between Cy3 emission and phenanthrene emission (573 nm/378 nm). Single strand **1** shows a lower ratio and duplex **1*4** the lowest.

Cy3:

Acceptor:

3' GTT CCA GGC TAC GTT CCT TC(Cy3) 5'
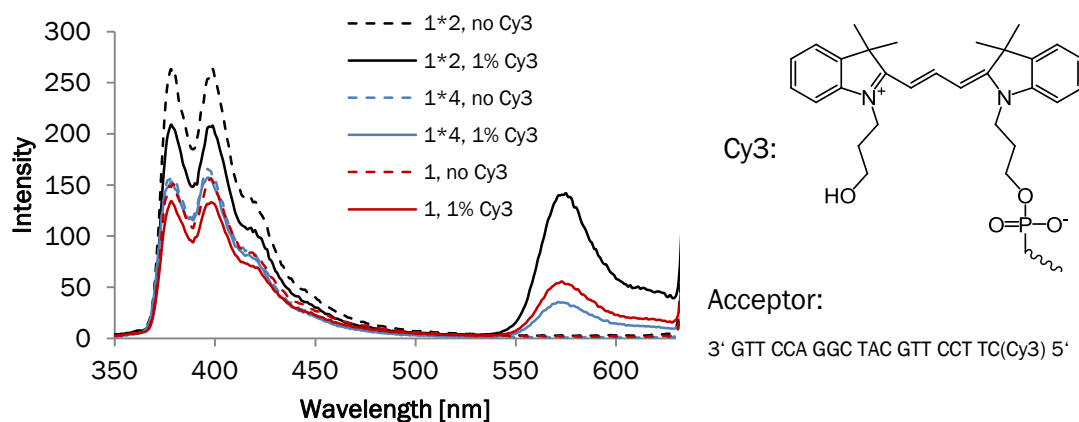
Figure 120: Fluorescence measurements without (dashed) and with acceptor (solid). Addition of acceptor represented as 1 mol% of Cy3 per total phenanthrene content in the samples. Conditions: see Figure 117.

Table 9: Effective phenanthrene (378 nm) and Cy3 (573 nm) fluorescence intensities and their ratios. (Values from Figure 120)

	Intensity at 378 nm	Intensity at 573 nm	Ratio of intensities (573 nm/378 nm)	Relative ratio
1*2	208.91	140.49	0.67	1
1*4	153.20	35.02	0.23	0.34
1	134.12	55.61	0.41	0.62

In contrast to the example with the pyrene-oligomer, the system with the Cy3-containing DNA strand as acceptor does not necessarily need to be heated and cooled to ensure efficient energy transfer. Figure 121 shows the fluorescence measurements of the DNA sheet without acceptor, with added Cy3 acceptor before and after resassembly, and at elevated temperature. Both measurements at 20°C (before and after reassembly) show similar fluorescence intensities. Only a slight increase in Cy3 emission is observed for the reassembled system. Addition of a complementary strand to the systems leads to spontaneous DNA strand exchange.[78] At 80°C no Cy3 emission is observed at all which is in agreement with the expected complete disassembly of the DNA sheet and the loss of energy transfer capacity.

Figure 121: Fluorescence measurement of DNA sheet alone (black) and with added Cy3 acceptor before reassembly (blue), at 80°C (red) and after reassembly (orange). Conditions: see Figure 117.

Reversibility of Light-Harvesting Effect

The self-assembly of the DNA sheets and the resulting light-harvesting properties are reversible; either by heating the solution (as shown in the temperature-dependent UV-vis and fluorescence spectra) or by adding NaCl. The stabilizing efficacy of spermine can be reduced by increasing the ionic strength.[78a,79] Figure 122 and Figure 123 show the fluorescence spectra of pyrene- and Cy3-doped DNA sheets with increasing concentrations of NaCl, respectively. In both cases the emission of the acceptor decreases, whereas phenanthrene emission increases. In DNA sheets with pyrene a NaCl concentration of 200 mM is needed to remove pyrene-emission. With the acceptor attached to a DNA strand (Cy3), a minimum was reached after the addition of 100 mM NaCl. The residual Cy3-emission is attributed to duplexes formed by single strand **1** and the complementary Cy3-strand.
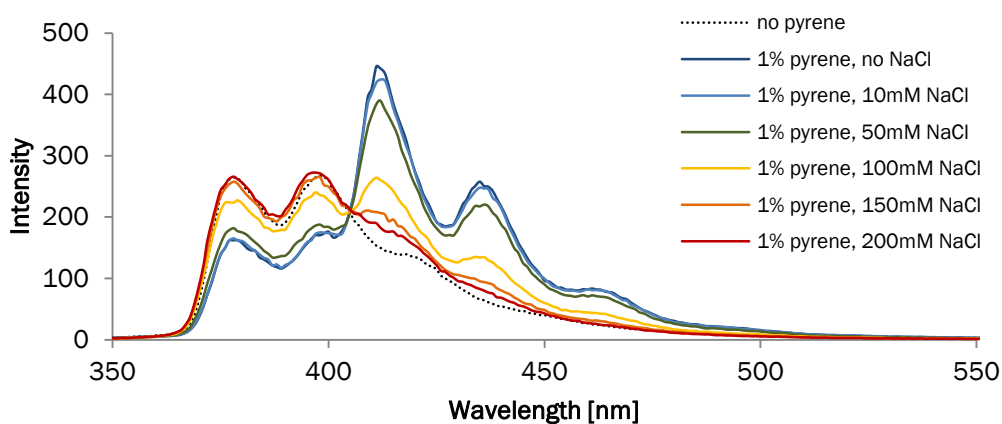
Figure 122: Fluorescence measurements with added NaCl. Addition of acceptor represented as 1 mol% of pyrene per total phenanthrene content in the sample. Conditions: see Figure 117.
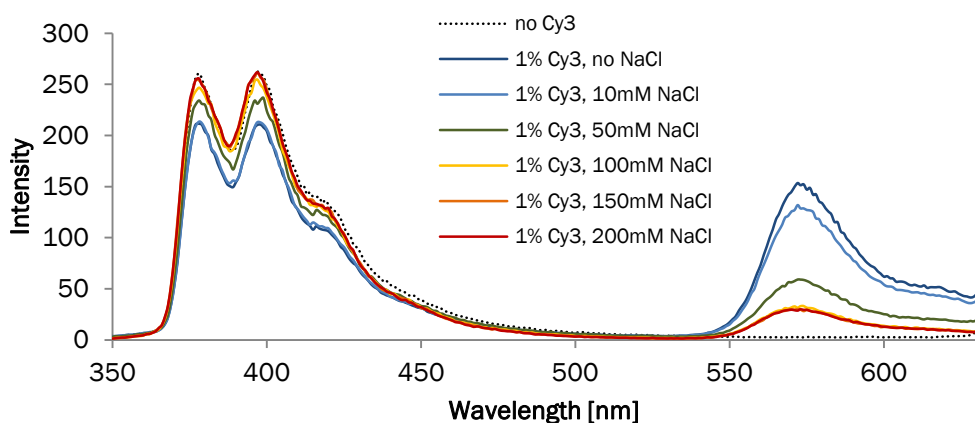
Figure 123: Fluorescence measurements with added NaCl. Addition of acceptor represented as 1 mol% of Cy3 per total phenanthrene content in the sample. Conditions: see Figure 117.

Changes upon NaCl addition are also observed in the absorption spectra (Figure 124 and Figure 125) where the measurements show a red-shift in the 260 nm region and a blue-shift in the 320 nm region. The changes coincide with the measured absorption of the non-aggregated DNA sheet (measurement at 80°C, or without spermine). In both measurements the absorption maximum shifts from 257 to 261 nm by increasing the NaCl concentration from 50 to 100 mM. Concluding that between those salt concentrations a transition takes place which results in the disassembly the DNA aggregates (duplexes are not dehybridized).
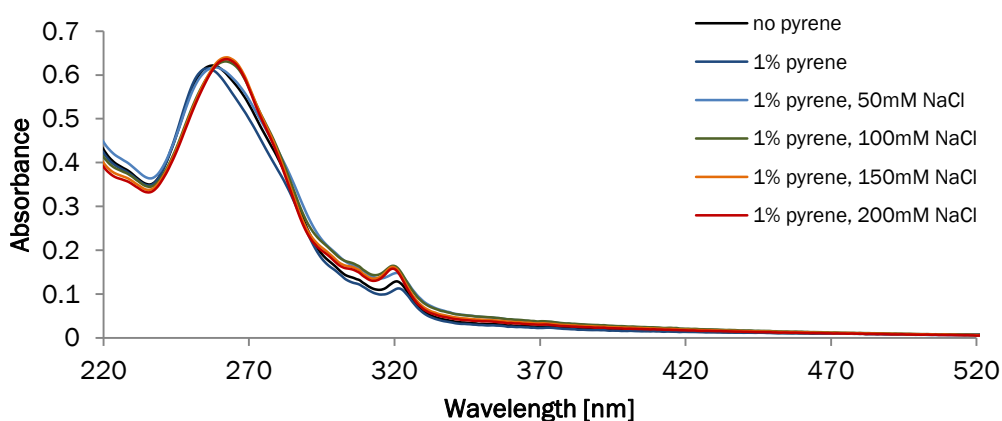
Figure 124: Absorption spectra of **1*2** with 1% pyrene/phenanthrene with different concentrations of NaCl. Conditions: 1 µM of each strand, 10 mM sodium phosphate buffer pH 7.0, 0.1 mM spermine tetrahydrochloride, 20 vol% ethanol, 20°C.

101
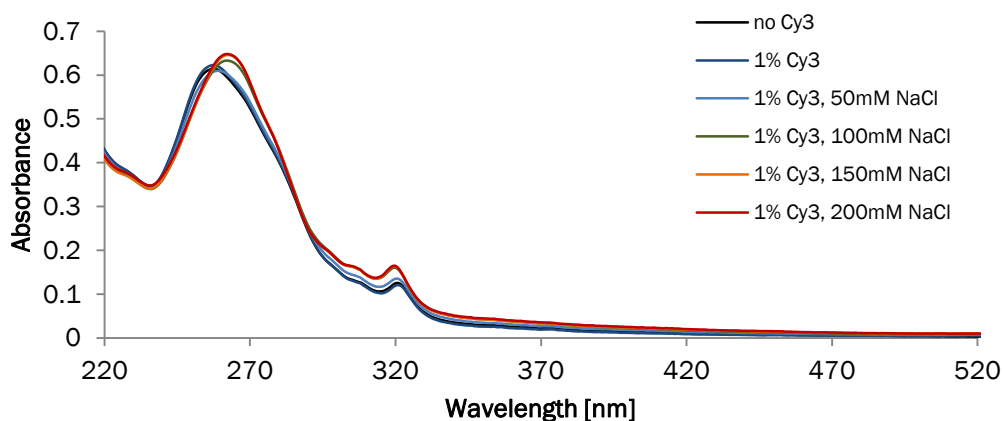
Figure 125: Absorption spectra of **1*2** with 1% Cy3/phenanthrene with different concentrations of NaCl. Conditions: 1 µM of each strand, 10 mM sodium phosphate buffer pH 7.0, 0.1 mM spermine tetrahydrochloride, 20 vol% ethanol, 20°C.

Conclusion and Outlook

The formation of supramolecular DNA sheets via phenanthrene sticky ends has been presented. Duplexes with phenanthrene overhangs self-assemble in the presence of spermine. The addition of the polycation is crucial for the self-assembly as the UV-vis and AFM measurements under standard DNA conditions do not indicate formation of aggregates.

The assembled phenanthrene units act as light-harvesting antennae and transfer absorbed energy to an acceptor which is either directly added to the polymer or attached to a complementary DNA strand. The light-harvesting effect of those sheets is reversible by adding NaCl which is presumably due to disassembly of the aggregates.

Duplexes with no or just one phenanthrene overhang on one side do not show the formation of such large assemblies in the presence of spermine.

Those DNA architectures allow constructing and investigating light-harvesting antennae with acceptors at defined distances to the donors by varying the number of base pairs in between. Further, the introduction of DNA into supramolecular polymers opens other possibilities for functionalization.

Supporting Information

DNA Synthesis and Purification

DNA strands **3**, **4** and Cy3-modified acceptor strand were purchased from Microsynth. Syntheses of 2,7-phenanthrene phosphoramidite and phenanthrene-loaded support are described in the supporting information of Chapter 1. DNA strands **1** and **2** were prepared on an Applied Biosystems 394 DNA/RNA synthesizer. A standard cyanoethyl phosphoramidite coupling protocol was used beginning with phenanthrene-loaded controlled pore glass (CPG) support. After synthesis, the CPG-bound oligomers were cleaved and deprotected by treatment with 28-30% NH_4OH (aq) at 55°C overnight. The supernatants were collected and the debris' were washed three times with 1 ml $EtOH/H_2O$ 1:1. After lyophilization the crude oligomers were purified by reversed phase HPLC (Merck LiChroCART 250-4; LiChrospher 100, RP-18, 5 μm); Solvent A: 0.1 M aqueous ammonium acetate; Solvent B: CH_3CN; 1 ml/min; T = 40°C; B[%] (t_R [min]) = 0 (0); 5 (2); 50 (22). Purities were confirmed by ESI mass spectrometry. The samples were measured in negative ion mode in mixtures of water/acetonitrile/triethylamine.

Table 10: Calculated and found masses (negative ion mode) of DNA strands.

Strand	Chemical formula	Calculated mass	Found mass
1	$C_{262}H_{294}N_{86}O_{125}P_{22}$	7329.17	609.69 (z=12)
2	$C_{259}H_{299}N_{65}O_{135}P_{22}$	7164.03	715.32 (z=10)

The purified oligomers were dissolved in 1 ml Milli-Q H_2O. Samples of the stock solutions were diluted 100 times and the absorbance at 260 nm was measured to determine the concentrations. The molar absorption coefficients of the oligomers were calculated using the ε_{260} values of 15'300, 11'700, 7'400 and 9'000 for A, G, C and T bases, respectively, and 47'000 for phenanthrene.

Mass Spectra of Oligomers

Figure 126: Mass spectrum of single strand **1**.

Figure 127: Mass spectrum of single strand **2**.

AFM Measurements

AFM images were recorded under ambient conditions in air with a Nanosurf FlexAFM instrument. The measurements were carried out in tapping mode.

APTES-functionalized mica: Freshly cleaved mica sheets were fixed on top of a 3 l desiccator with tape. The desiccator was flushed with argon. Two plastic caps (from Eppendorf tubes) were placed at the bottom; one was the filled with 30 µl of 3-aminopropyltriethoxy silane (APTES), the other one with 10 µl of DIPEA. The desiccator was closed, and the chemicals were allowed to evaporate. The plastic caps were removed after two hours and the desiccator was purged with argon. The mica sheets were let for 1 day in the desiccator to cure. 10 µl of sample was dropped on the modified mica sheet and let to incubate for 10 minutes. After rinsing with 2 ml of Milli-Q water, the sample was dried under an argon stream.

Additional AFM Images

AFM of 1*2 with standard conditions
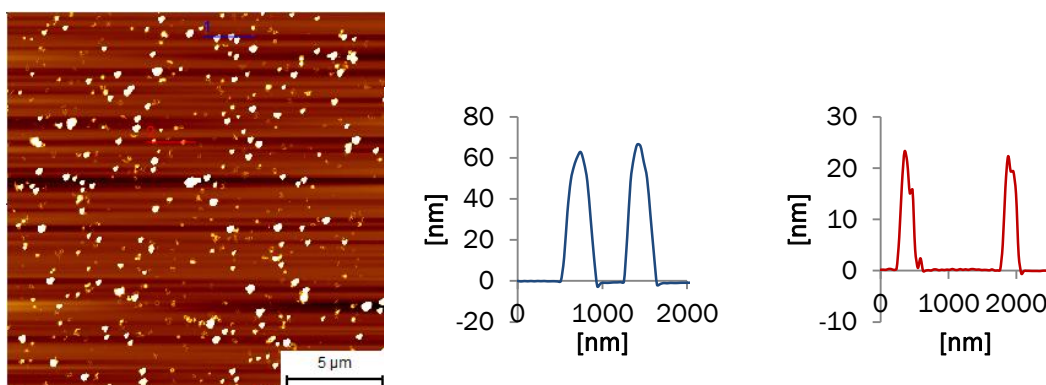
Figure 128: AFM image of **1***2 deposited on APTES-modified mica. Conditions: 1 µM each strand, 10 mM sodium phosphate buffer pH 7.0, 100 mM NaCl.

Additional AFM of 1*2 with spermine
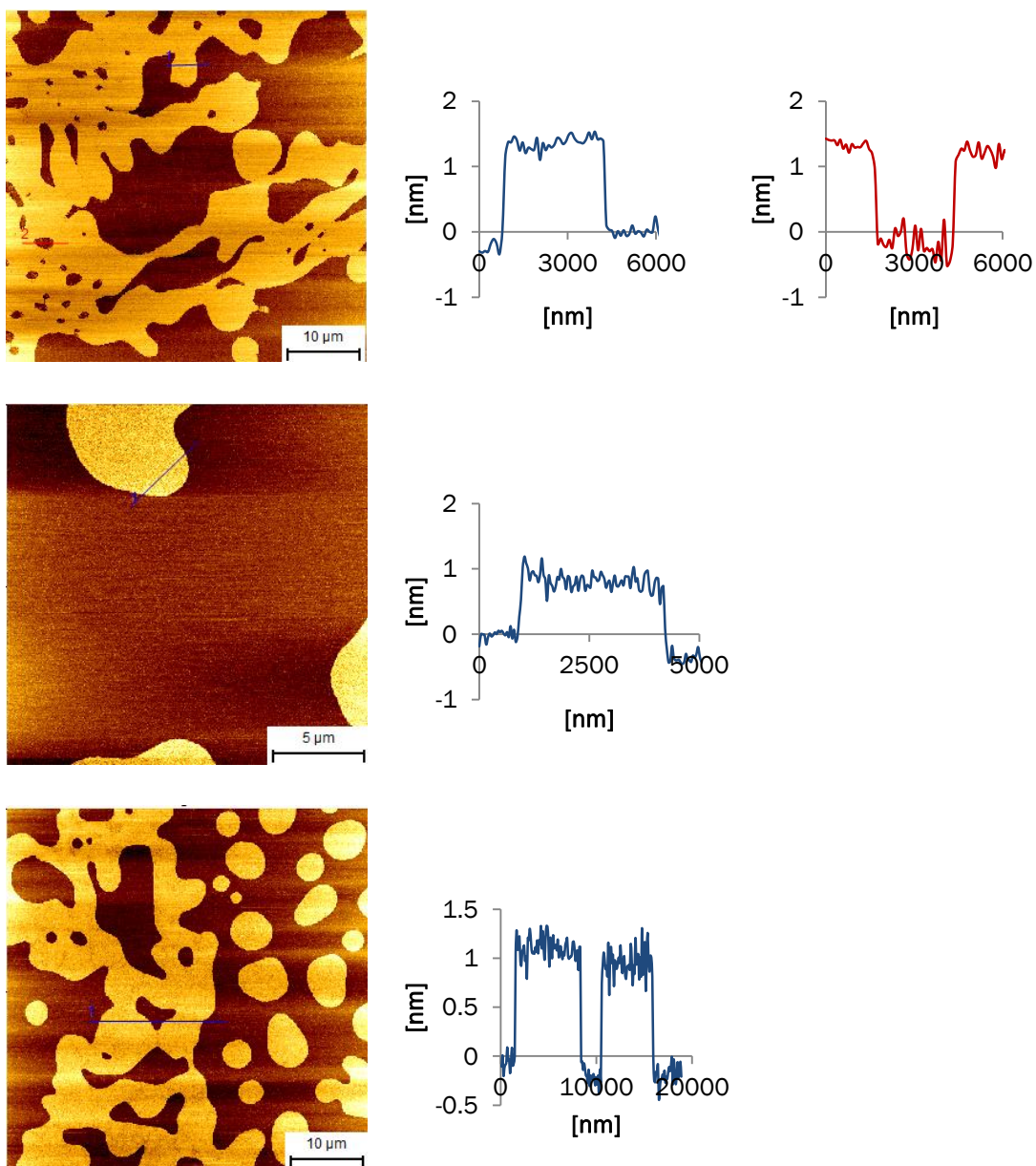
Figure 129: AFM images of **1*2** deposited on APTES-modified mica. Conditions: 1 μM each strand, 10 mM sodium phosphate buffer pH 7.0, 0.1 mM spermine tetrahydrochloride, 20 vol% ethanol.
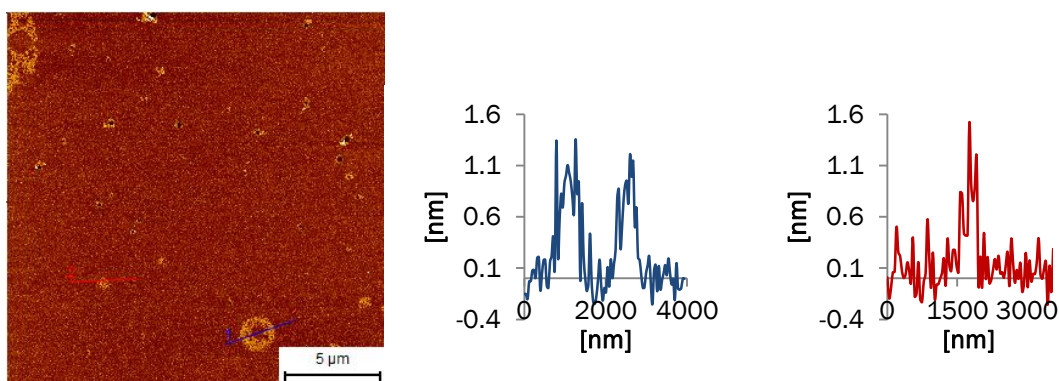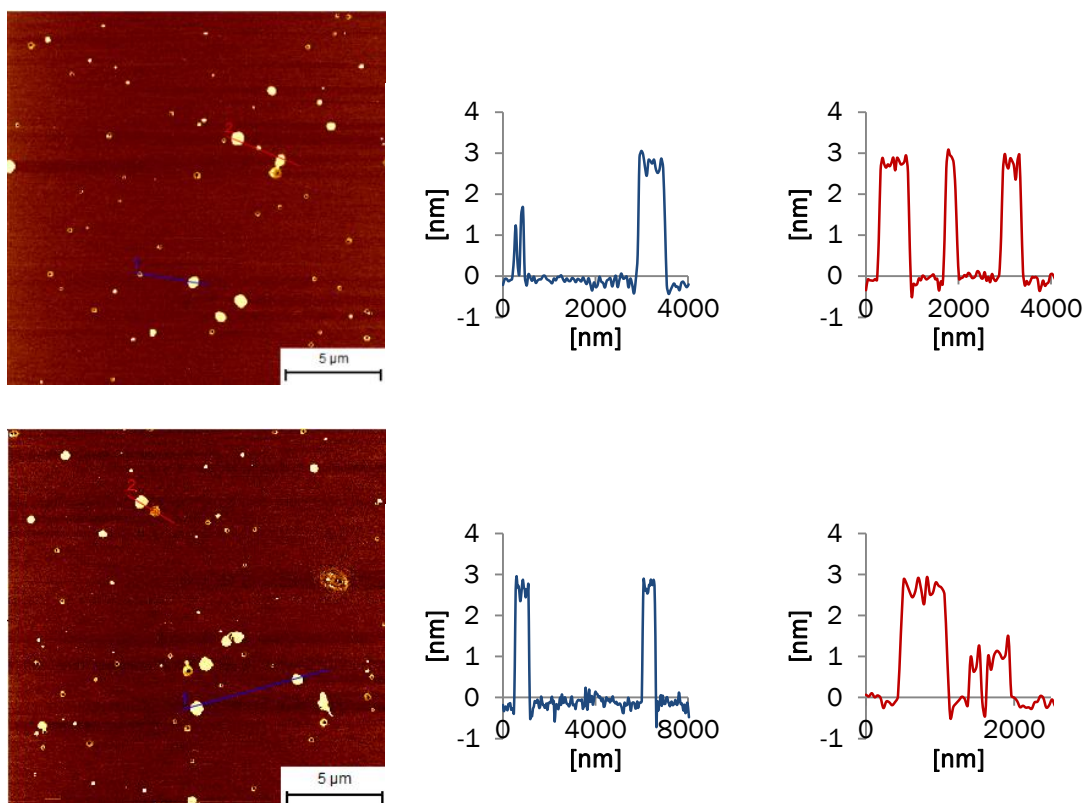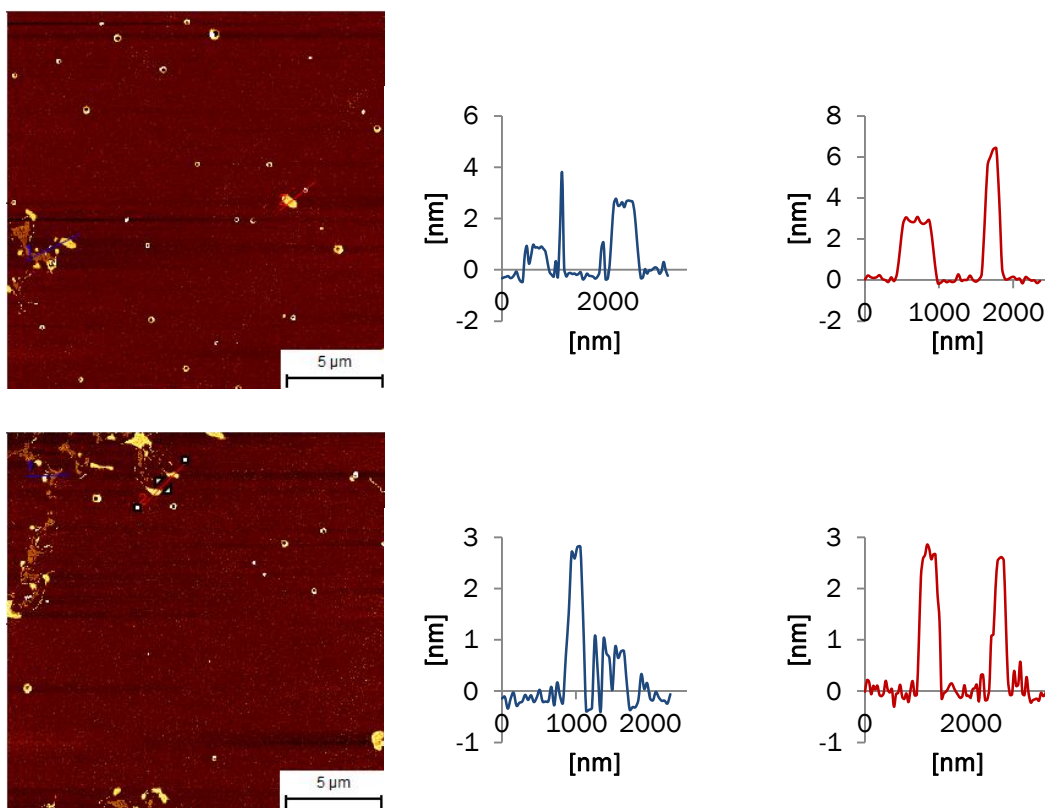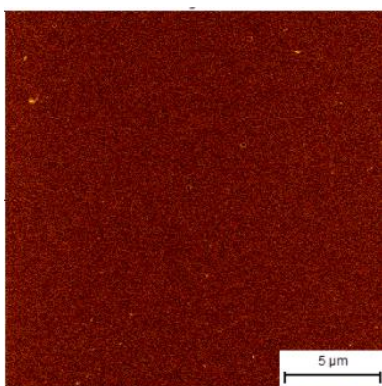
AFM of single strand 1 with spermine
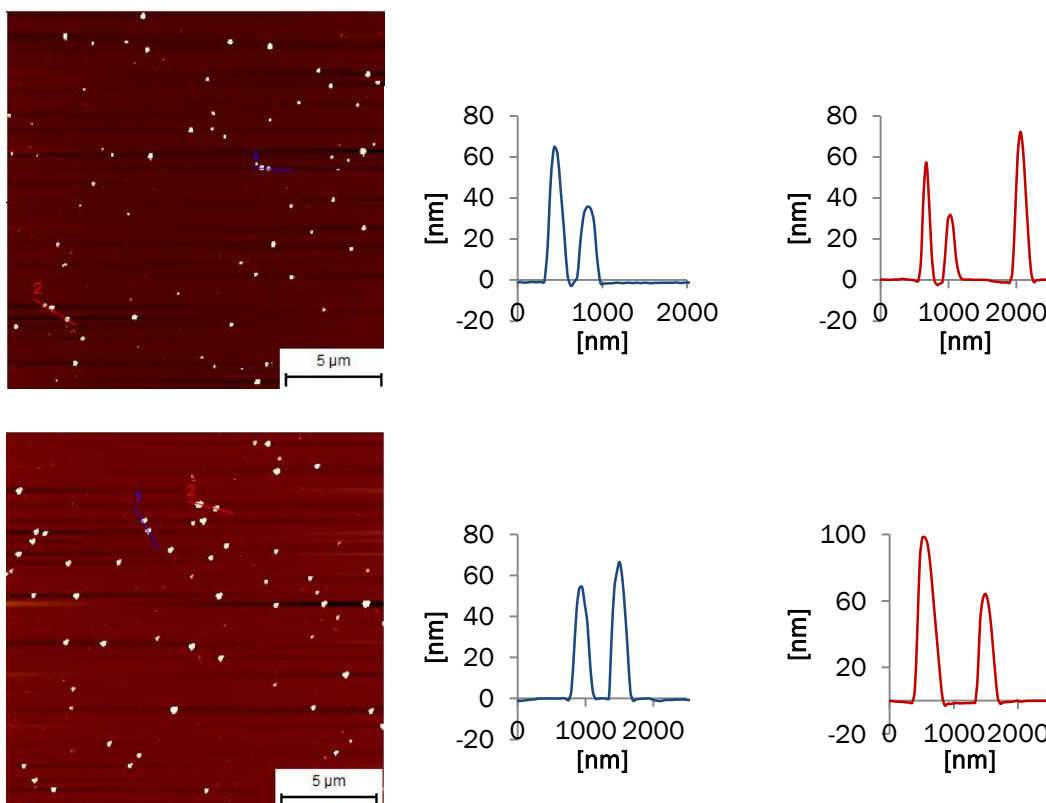
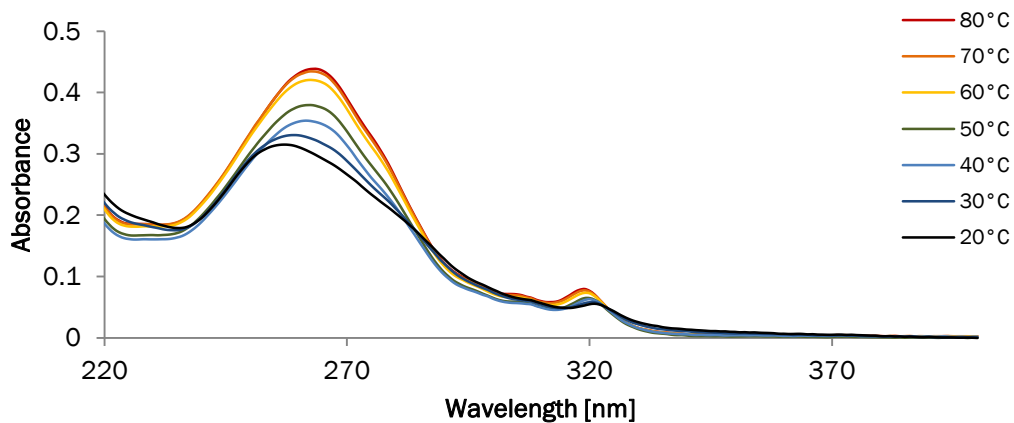Figure 130: AFM images of **1** deposited on APTES-modified mica. Conditions: 1 µM, 10 mM sodium phosphate buffer pH 7.0, 0.1 mM spermine tetrahydrochloride, 20 vol% ethanol.

AFM of single strand 2 with spermine

Figure 131: AFM image of **2** deposited on APTES-modified mica. Conditions: 1 µM, 10 mM sodium phosphate buffer pH 7.0, 0.1 mM spermine tetrahydrochloride, 20 vol% ethanol.

AFM of duplex 1*4 with spermine

Figure 132: AFM images of **1*4** deposited on APTES-modified mica. Conditions: 1 µM each strand, 10 mM sodium phosphate buffer pH 7.0, 0.1 mM spermine tetrahydrochloride, 20 vol% ethanol.

AFM of duplex 2*3 with spermine

Figure 133: AFM images of **2*3** deposited on APTES-modified mica. Conditions: 1 µM each strand, 10 mM sodium phosphate buffer pH 7.0, 0.1 mM spermine tetrahydrochloride, 20 vol% ethanol.

AFM of duplex 3*4 with spermine

Figure 134: AFM image of **3*4** deposited on APTES-modified mica. Conditions: 1 µM each strand, 10 mM sodium phosphate buffer pH 7.0, 0.1 mM spermine tetrahydrochloride, 20 vol% ethanol.

Temperature-Dependent UV-vis Spectra of Single Strands

Figure 135: Temperature-dependent absorption spectra of **1**. Conditions: 1 µM single strand, 10 mM sodium phosphate buffer pH 7.0, 0.1 mM spermine tetrahydrochloride, 20 vol% ethanol.
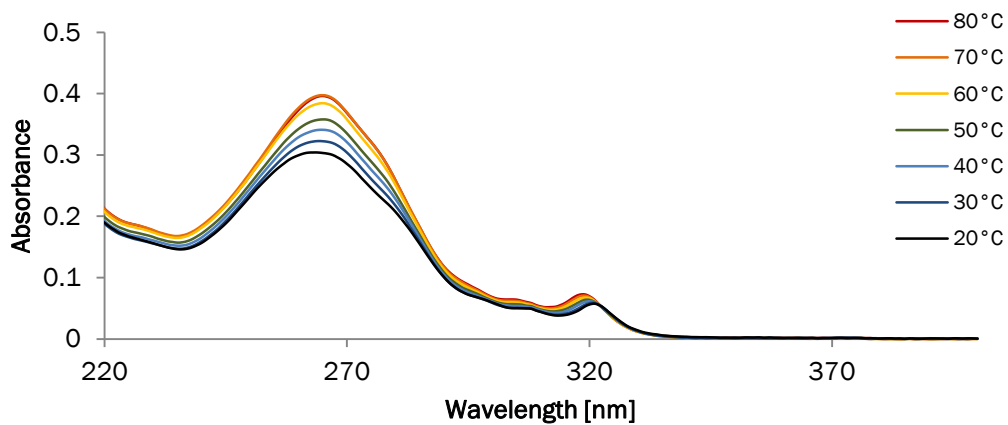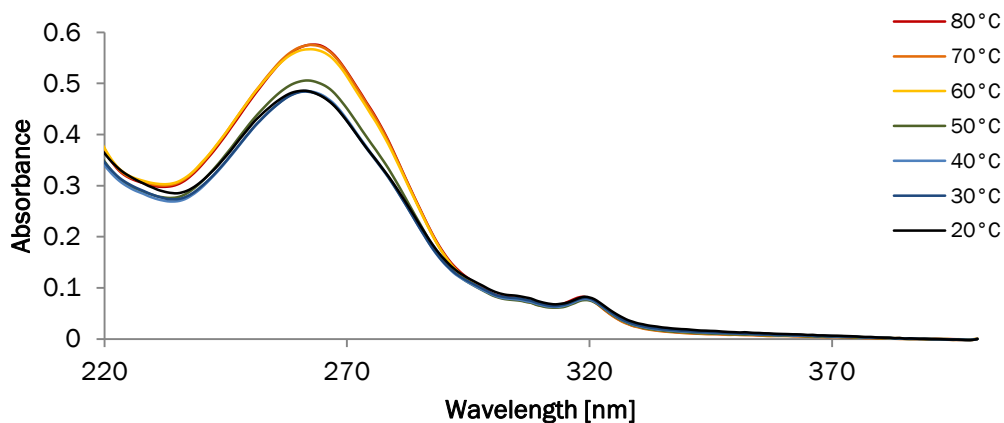

Figure 136: Temperature-dependent absorption spectra of **2**. Conditions: 1 µM single strand, 10 mM sodium phosphate buffer pH 7.0, 0.1 mM spermine tetrahydrochloride, 20 vol% ethanol.
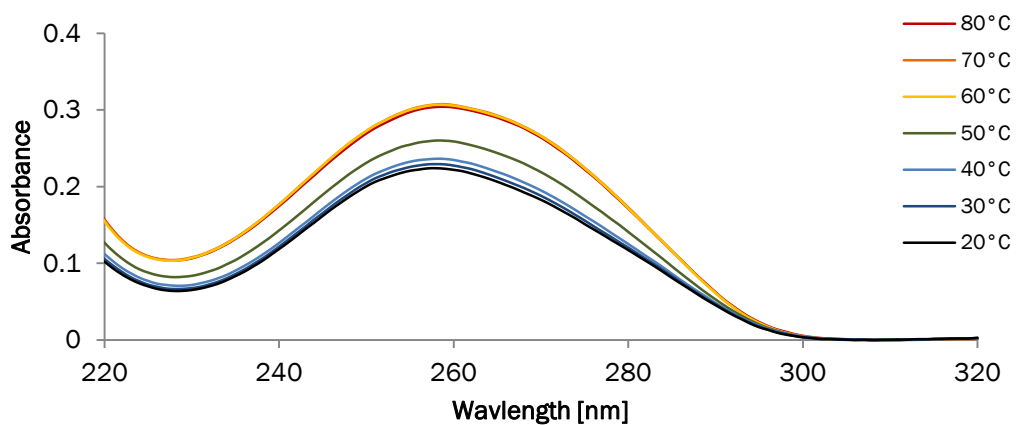
Temperature-Dependent UV-vis Spectra of Duplexes
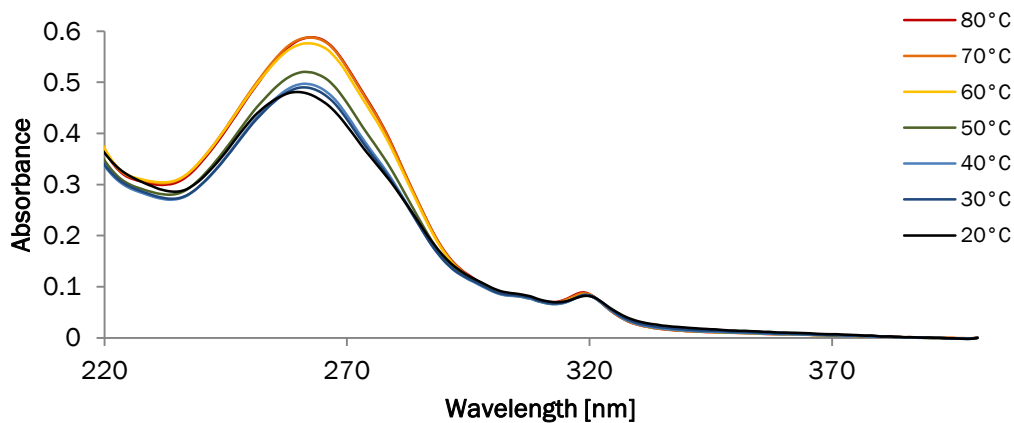
Figure 137: Temperature-dependent absorption spectra of **1*4**. Conditions: 1 µM each strand, 10 mM sodium phosphate buffer pH 7.0, 0.1 mM spermine tetrahydrochloride, 20 vol% ethanol.
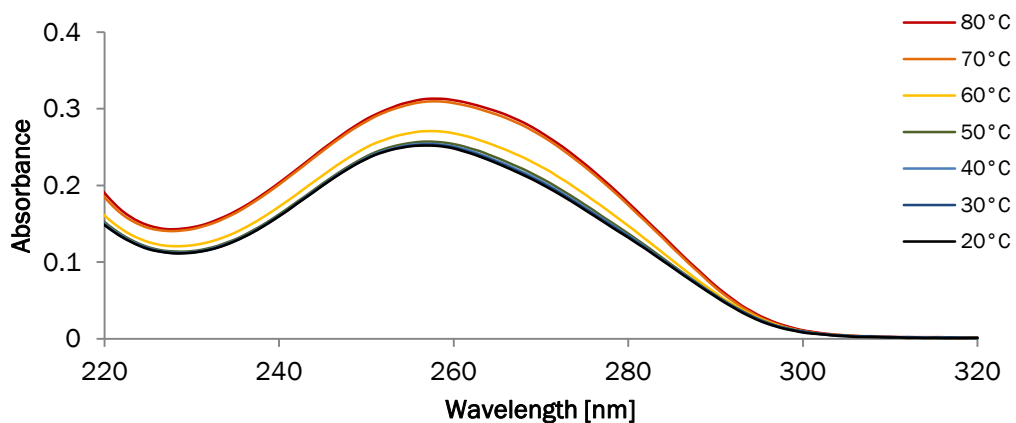

Figure 138: Temperature-dependent absorption spectra of **2*3**. Conditions: 1 µM each strand, 10 mM sodium phosphate buffer pH 7.0, 0.1 mM spermine tetrahydrochloride, 20 vol% ethanol.

Figure 139: Temperature-dependent absorption spectra of **3*4**. Conditions: 1 μM each strand, 10 mM sodium phosphate buffer pH 7.0, 0.1 mM spermine tetrahydrochloride, 20 vol% ethanol.

Figure 140: Temperature-dependent absorption spectra of **3*4**. Conditions: 1 μM each strand, 10 mM sodium phosphate buffer pH 7.0, 100 mM NaCl.
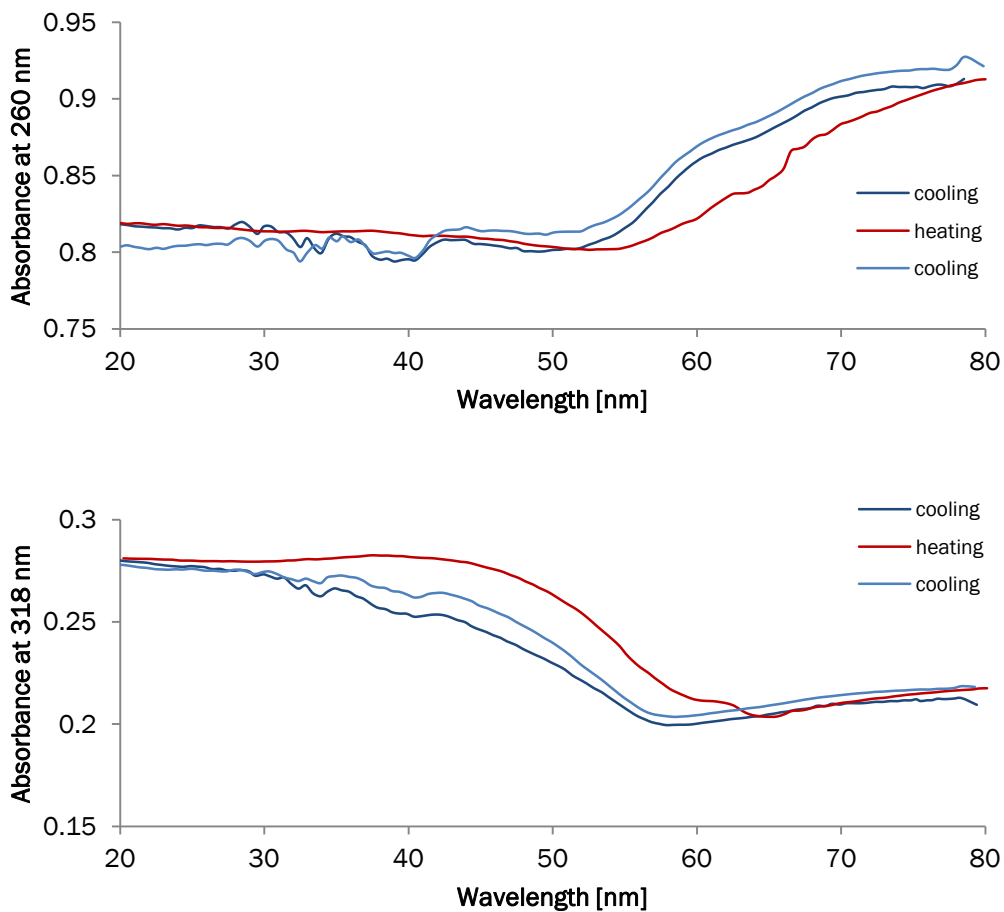
Spectra of T_m Measurements

Figure 141: UV-vis heating and cooling curves of duplex **1*2**. Conditions: 1 µM each strand, 10 mM sodium phosphate buffer pH 7.0, 0.1 mM spermine tetrahydrochloride, 20 vol% ethanol.

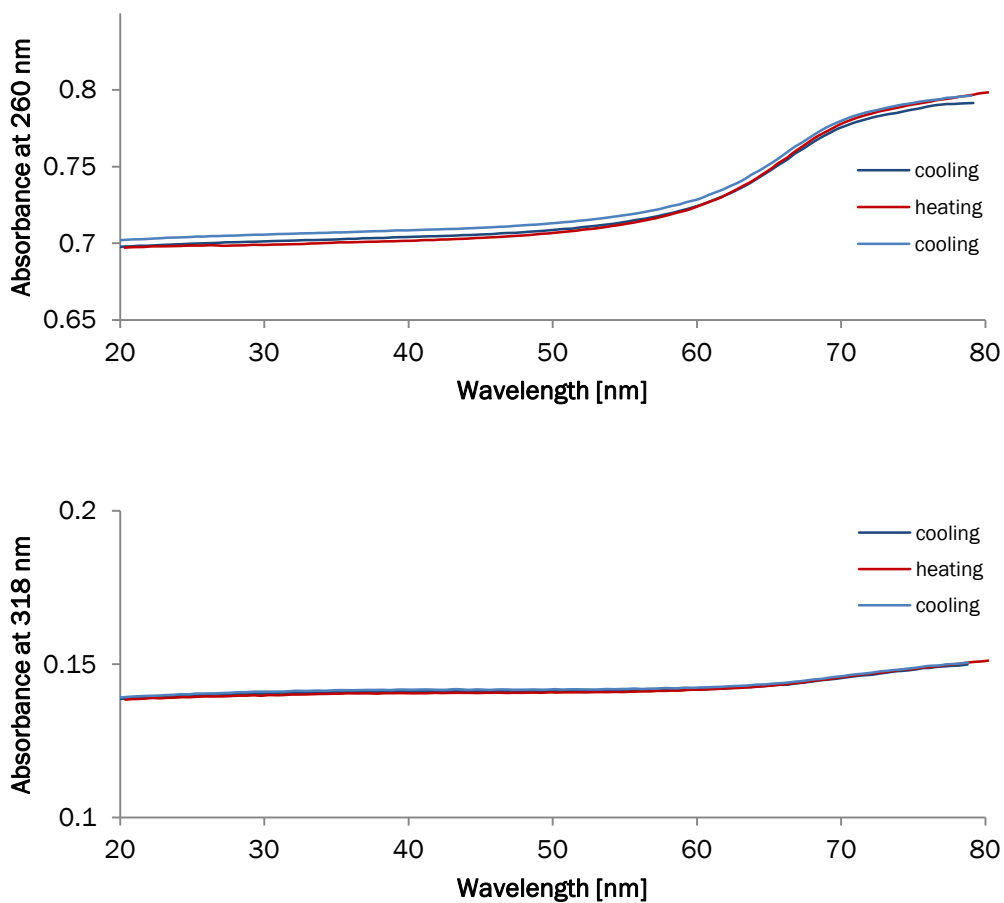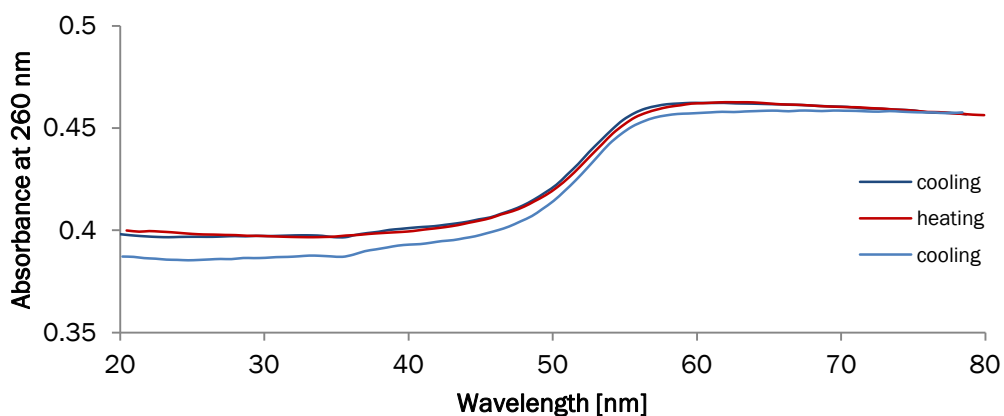Figure 142: UV-vis heating and cooling curves of duplex **1*2**. Conditions: 1 µM each strand, 10 mM sodium phosphate buffer pH 7.0, 100 mM NaCl.

Figure 143: UV-vis heating and cooling curves of duplex **3*4**. Conditions: 1 µM each strand, 10 mM sodium phosphate buffer pH 7.0, 0.1 mM spermine tetrahydrochloride, 20 vol% ethanol.
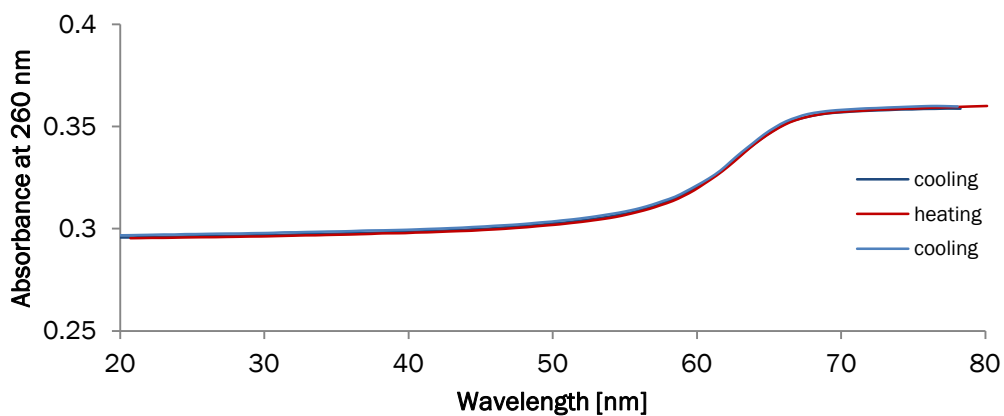
Figure 144: UV-vis heating and cooling curves of duplex **3*4**. Conditions: 1 µM each strand, 10 mM sodium phosphate buffer pH 7.0, 100 mM NaCl.
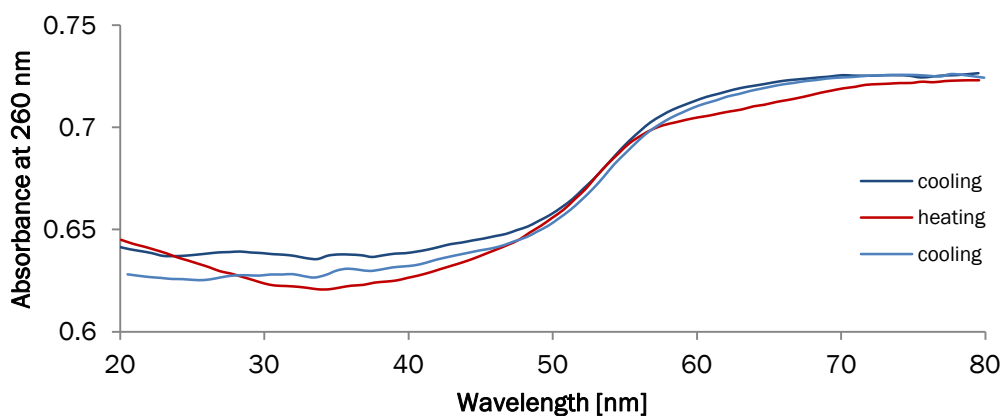

Figure 145: UV-vis heating and cooling curves of duplex **1*4**. Conditions: 1 µM each strand, 10 mM sodium phosphate buffer pH 7.0, 0.1 mM spermine tetrahydrochloride, 20 vol% ethanol.

Figure 146: UV-vis heating and cooling curves of duplex **2*3**. Conditions: 1 µM each strand, 10 mM sodium phosphate buffer pH 7.0, 0.1 mM spermine tetrahydrochloride, 20 vol% ethanol.

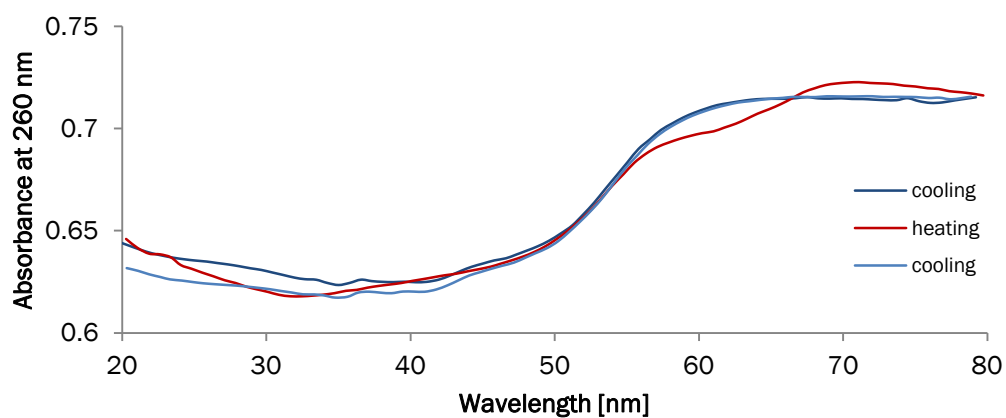## References

[58]   (a) F. A. Aldaye, A. L. Palmer, H. F. Sleiman, *Science*, 2008, **321**, 1795-1799.
(b) N. C. Seeman, *Annu. Rev. Biochem.*, 2010, **79**, 65-87.
(c) E. Stulz, *Chem. Eur. J.*, 2012, **18**, 4456-4469.
(d) W. Pfeifer, B. Saccà, *ChemBioChem*, 2016, **17**, 1063-1080.

[59]   (a) C. K. McLaughlin, G. D. Hamblin, H. F. Sleiman, *Chem. Soc. Rev.*, 2011, **40**, 5647-5656.
(b) T. J. Bandy, A. Brewer, J. R. Burns, G. Marth, T. Nguyen, E. Stulz, *Chem. Soc. Rev.*, 2011, **40**, 138-148.
(c) A. V. Pinheiro, D. Han, W. M. Shih, H. Yan, *Nat. Nanotechnol.*, 2011, **6**, 763-772.

[60]   T. Aida, E. W. Meijer, S. I. Stupp, *Science*, 2012, **335**, 813-817.

[61]   (a) T. Tørring, N. V. Voigt, J. Nangreave, H. Yan, K. V. Gothelf, *Chem. Soc. Rev.*, 2011, **40**, 5636-5646.
(b) B. Saccà, C. M. Niemeyer, *Angew. Chem. Int. Ed.*, 2012, **51**, 58-66.
(c) W. Liu, H. Zhong, R. Wang, N. C. Seeman, *Angew. Chem. Int. Ed.*, 2011, **50**, 264-267.

[62]   (a) A. R. Chandrasekaran, *J. Chem. Technol. Biotechnol.*, 2016, **91**, 843-846.
(b) I. Bald, A. Keller, *Molecules*, 2014, **19**, 13803-13823.
(c) A. Udomprasert, T. Kangsamaksin, *Cancer Sci.*, 2017, **108**, 1535-1543.
(d) I. H. Stein, C. Steinhauer, P. Tinnefeld, *J. Am. Chem. Soc.*, 2011, **133**, 4193-4195.

[63]   (a) E. Ban, C. R. Picu, *Biomacromolecules*, 2014, **15**, 143-149.
(b) N. C. Seeman, *DNA and Cell Biol.*, 1991, **10**, 475-486.
(c) J. Xu, E. A. Fogleman, S. L. Craig, *Macromolecules*, 2004, **37**, 1863-1870.

[64]   S. Venkadesh, P. K. Mandal, N. Gautham, *Biochem. Biophys. Res. Commun.*, 2011, **407**, 548-551.

[65]   J. R. Burns, J. Zekonyte, G. Siligardi, R. Hussain, E. Stulz, *Molecules*, 2011, **16**, 4912-4922.

[66]   (a) Y. Vyborna, M. Vybornyi, R. Häner, *J. Am. Chem. Soc.*, 2015, **137**, 14051-14054.
(b) Y. Vyborna, M. Vybornyi, R. Häner, *Chem. Commun.*, 2017, **53**, 5179-5181.

[67]   S. K. Albert, M. Golla, H. V. P. Thelu, N. Krishnan, P. Deepak, R. Varghese, *Org. Biomol. Chem.*, 2016, **14**, 6960-6969.

[68]   M. Hariharan, Y. Zheng, B. Rybtchinski, F. D. Lewis, *J. Phys. Chem. B*, 2013, **117**, 14649-14654.

[69]   H. Kashida, T. Hayashi, T. Fujii, H. Asanuma, *Chem. Eur. J.*, 2011, **17**, 2614-2622.

[70]   K. M. M. Carneiro, F. A. Aldaye, H. F. Sleiman, *J. Am. Chem. Soc.*, 2010, **132**, 679-685.

[71]   (a) G. Iacomino, G. Picariello, L. D'Agostino, *Biochim. Biophys. Acta*, 2012, **1823**, 1745-1755.
(b) J. Pelta, F. Lovolant, J.-L. Sikorav, *J. Biol. Chem.*, 1996, **271**, 5656-5662.
(c) M. Saminathan, T. Antony, A. Shirahata, L. H. Sigal, T. Thomas, T. J. Thomas, *Biochemistry*, 1999, **38**, 3821-3830.
(d) M.-H. Hou, S.-B. Lin, J.-M. P. Yuann, W.-C. Lin, A. H.-J. Wang, L.-S. Kan, *Nucleic Acids Res.*, 2001, **29**, 5121-5128.
(e) R. W. Wilson, V. A. Bloomfield, *Biochemistry*, 1979, **18**, 2192-2196.

(f) A. G. Cherstvy, *Phys. Chem. Chem. Phys.*, 2011, **13**, 9942-9968.

(g) I. Koltover, K. Wagner, C. R. Safinya, *Proc. Natl. Acad. Sci. U.S.A.*, 2000, **97**, 14046-14051.

[72] (a) S. Razin, R. Rosansky, *Arch. Biochem. Biophys.*, 1959, **81**, 36-54.

(b) B. C. Hoopes, W. R. McClure, *Nucleic Acids Res.*, 1981, **9**, 5493-5504.

(c) E. Raspaud, I. Chaperon, A. Leforestier, F. Livolant, *Biophys. J.*, 1999, **77**, 1547-1555.

(d) Y. Fu, X. Wang, J. Zhang, Y. Xiao, W. Li, J. Wang, *Biomacromolecules*, 2011, **12**, 747-756.

(e) C. Böttcher, C. Endisch, J.-H. Fuhrhop, C. Catterall, M. Eaton, *J. Am. Chem. Soc.*, 1998, **120**, 12-17.

(f) A. M. Katz, I. S. Tolokh, S. A. Pabit, N. Baker, A. V. Onufriev, L. Pollack, *Biophys. J.*, 2017, **112**, 22-30.

[73] (a) H. Kuramochi, Y. Yonezawa, *J. Biosci. Bioeng.*, 2001, **92**, 183-185.

(b) Y. Fang, J. H. Hoh, *J. Am. Chem. Soc.*, 1998, **120**, 8903-8909.

[74] A. Chopra, S. Krishnan, F. C. Simmel, *Nano Lett.*, 2016, **16**, 6683-6690.

[75] (a) F.-M Chen, *Biophys. J.*, 1997, **73**, 348-356.

(b) K. B. Roy, T. Antony, A. Saxena, H. B. Bohidar, *J. Phys. Chem. B*, 1999, **103**, 5117-5121.

[76] (a) Wasielewski, *Acc. Chem. Res.*, 2009, **42**, 1910-1921.

(b) G. D. Scholes, G. R. Fleming, A. Olaya, R. van Grondelle, *Nat. Chem.*, 2011, **3**, 763-774.

(c) Z. G. Fetisova, A. M. Freiberg, K. E. Timpmann, *Nature*, 1988, **334**, 633-634.

(d) N. Sakai, S. Matile*, Beilstein J. Org. Chem.*, 2012, **8**, 897-904.

[77] C. D. Bösch, S. M. Langenegger, R. Häner*, Angew. Chem. Int. Ed.*, 2016, **55**, 9961-9964.

[78] (a) W. J. Kim, T. Ishihara, T. Akaike, A. Maruyama, *Chem. Eur. J.*, 2001, **7**, 176-180.

(b) M. Weiser, H.-A. Wagenknecht, *Chem. Commun.*, 2015, **51**, 16530-16533.

[79] G.-L. Gan, H. Chao, X.-P. Cai, Z.-S. Jiang, H. Li, *J. Inorg. Biochem.*, 2013, **129**, 9-14.

Chapter 4: Exploration of Phenanthrene Derivatives for Light-Harvesting Antennae

Abstract

The synthesis and photophysical properties of phenanthrene derivatives are described. By extending the aromatic system of phenanthrene, chromophores with higher absorption coefficients and red-shifted absorptions are formed. The potential to use them as alternatives in light-harvesting antennae is discussed.

Introduction

Chapter 1 described a 2,7-disubstituted phenanthrene oligomer which forms supramolecular light-harvesting nanotubes in combination with an acceptor.[80] Also in DNA-based light-harvesting antenna phenanthrene is a favored building block as it efficiently transfers its excitation energy.[80,81] Construction of artificial light-harvesting complexes which will use sunlight work the most efficient if they absorb in the visible range as the sun emits there more light (see Figure 147).[82] Phenanthrene, however, absorbs only UV light (ε_{252}=64'100, ε_{294}=14'400, ε_{346}=220 in cyclohexane).[83] Adding carboxamide or alkynyl linkers to phenanthrene does not shift its absorption to the visible range.[80,81a,c] One possibility to influence the photophysical properties of a molecule is to extend its aromatic system and/or to add substituents.[84]

Figure 148 gives an overview of possible phenanthrene derivatives. Triphenylene has an additional aromatic ring (9,10-benzophenanthrene). Its functionalization and conjugation with other molecules lead to materials with distinct properties with applications as light-emitting or charge-transporting devices.[85] 1,4-Diazatriphenylene is a heterocyclic analog of triphenylene. Electrochemical properties of diazatriphenylene derivatives and potential applications as light-emitting devices have been studied as well.[86] By further enhancing the aromatic system of 1,4-diazatriphenylene one can obtain dibenzo[a,c]phenanzine. This building block has been investigated as core building block in π-conjugated electrochromic polymers where it shifted the absorption to the red.[87] Also its usage in solar cells has been investigated.[88] Carbon atoms in the homocyclic aromatic system of phenanthrene can be replaced by nitrogen to obtain 1,10-phenanthroline. This molecule and its versatile usage

for luminescent molecules, materials and metal complexes have been extensively studied.[89] The most distinguished property of 1,10-phenanthroline is its tunable fluorescence by conjugation and metal binding which makes it an ideal building block for light-emitting devices.[90] Adding substituents is another possibility to change the absorption of phenanthrene. In Figure 148 is shown the example of 9,10-dimethoxyphenanthrene.
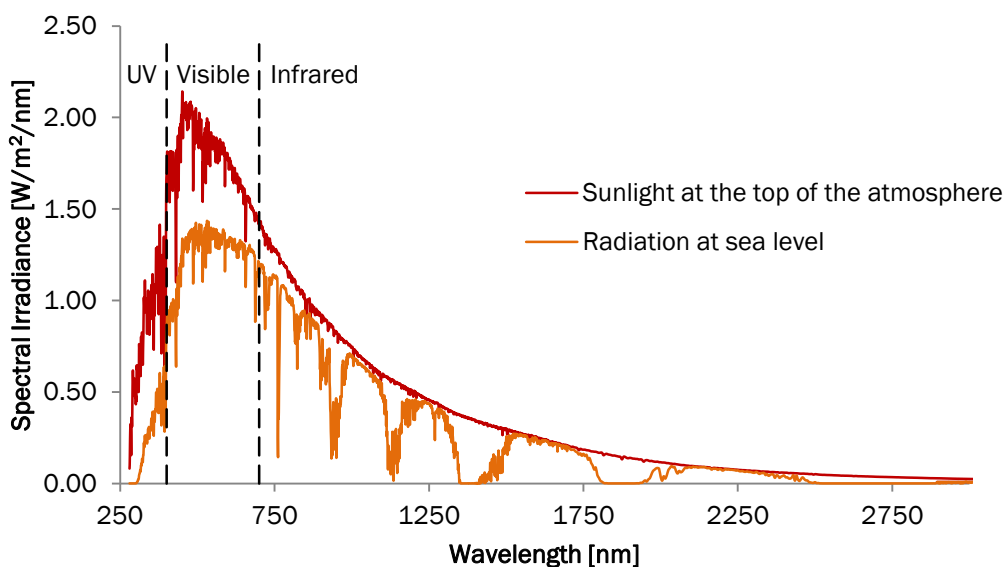

Figure 147: Spectral distribution of solar radiation at the top of the Earth's atmosphere (red) and at sea level (orange). By passing through the atmosphere, some light is absorbed by gases with specific absorption bands. (Data adapted from ref. [82d]).
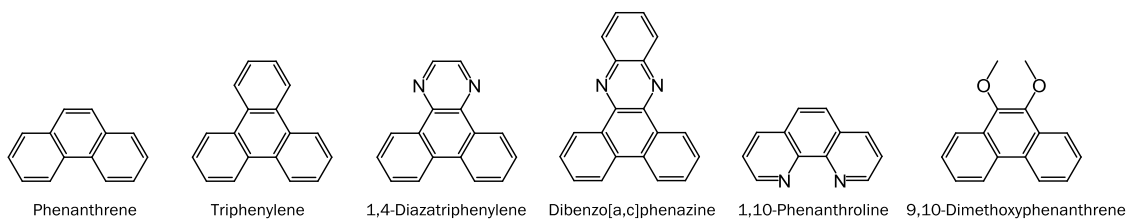
Figure 148: Chemical structure of phenanthrene and a selection of derivatives.

Results

Synthesis of Phenanthrene Derivatives

(The triphenylene derivative, corresponding phosphoramidite and oligomer were synthesized by Simon Rothenbühler.)

An overview of synthesized 2,7-dialkynyl phenanthrene derivatives **1-4** is shown in Figure 149. They were all investigated by UV-vis absorption and fluorescence spectroscopy. Further, derivative **1** and **2** were converted into their corresponding DMT-protected phosphoramidites. Some oligomers were synthesized and analyzed.
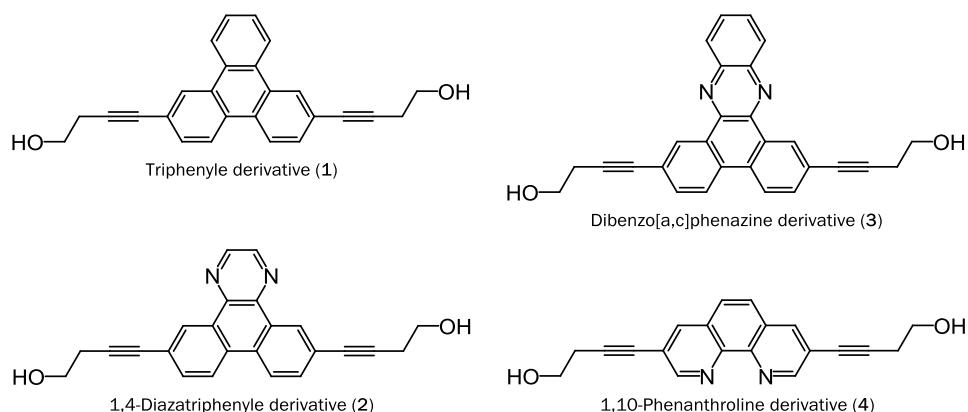

Figure 149: Chemical structures of synthesized chromophores.

The triphenylene derivative (**1**) was synthesized starting from 2,7-dibromotriphenylene. Butynyl-linkers were attached via Sonogashira coupling. Starting with 2,7-dibromophenanthrene-9,10-dione two different derivatives were synthesized. Intermediates 1,4-diaza-6,11-dibromotriphenylene (or 6,11-dibromodibenzo[f,h]quinoxaline) and 2,7-dibromodibenzo[a,c]phenazine were both synthesized according to literature. Further, butynyl-linkers were attached to yield the corresponding 1,4-diazatriphenylene (**2**) and dibenzo[a,c]phenazine (**3**) derivatives. 3,8-Dibromo-1,10-phenanthroline is commercially available and was further modified with 3-butyn-1-ol to yield the 1,10-phenanthroline derivative (**4**).

Photophysical Properties of the Derivatives

Figure 150 shows a comparison of the absorption spectra of 2,7-dialkynyl phenanthrene and its derivatives. For ease of comparison the values are normalized, the raw values can be found in the supporting information (Figure 158 - Figure 160). Phenanthrene has a structured absorption band with distinct peaks at 274, 292, 302 and 316 nm. The first electronic transition of phenanthrene is forbidden and located between 300 and 350 nm.[83,91] The second electronic transition is located between 320 and 280 nm, the third around 270 nm.
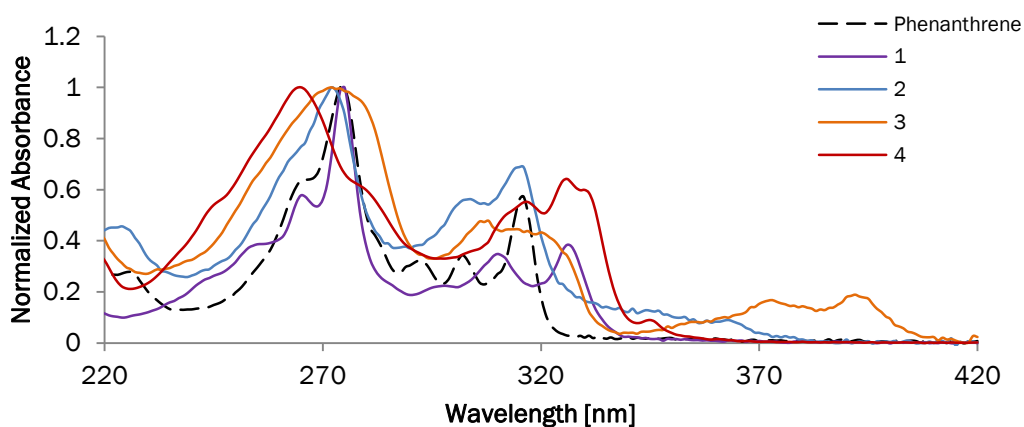
Figure 150: Normalized absorption spectra of 2,7-dialkynyl phenanthrene and derivatives **1**-**4**, measured in ethanol at 20°C.

The absorption pattern of the triphenylene derivative (**1**) looks pretty similar to the one of phenanthrene. Small changes are only observed in the second transition where the peaks are red-shifted; the values are 298, 310 and 326 nm. The heterocyclic compound **2** shows roughly the same absorption peaks as phenanthrene (272, 302 and 316 nm) but the assumed forbidden transition is more allowed. It is seen as a broad band located between 330 and 380 nm.

Further enhancing the aromatic system leads to an even more red-shifted absorption; compound **3** absorbs up to 400 nm. The first electronic transition shows peaks at 357, 372 and 393 nm. The other two transitions are located at the same wavelengths as the ones in phenanthrene, although broader and less structured.

The last compound in this series is the 2,7-dialkynyl 1,10-phenanthroline derivative (**4**). The nitrogen atoms in phenanthroline are able to coordinate metal atoms. To ensure that no complexes are formed the measurements were done in the presence of 20 µM Na$_2$EDTA. The measured absorption spectrum of **4** does not show much similarity with the other ones. Distinct peaks are located at 265, 317, 326, 330 and 345 nm. In the next section it will be shown that the absorption and as well the fluorescence of **4** can be changed by adding Zn^{2+} to the solution.

The normalized fluorescence spectra of phenanthrene and its derivatives **1**-**4** are summarized in Figure 151. The fluorescence peaks of phenanthrene are located at 371, 377, 390 and 412 nm. Compound **1** emits in the same region, but the peaks are less pronounced. The heterocyclic derivatives **2** and **3** show much different emissions. Both are broad and red-shifted; maxima are found at 465 and 505 nm, respectively. According to literature, the fluorescence of unmodified 1,4-diazatriphenylene looks similar to phenanthrene fluorescence.[92] Therefore the observed emission is presumably from excimer formation.[93] The even more red-shifted excimer emission of **4** can be explained with its more red-shifted absorption.
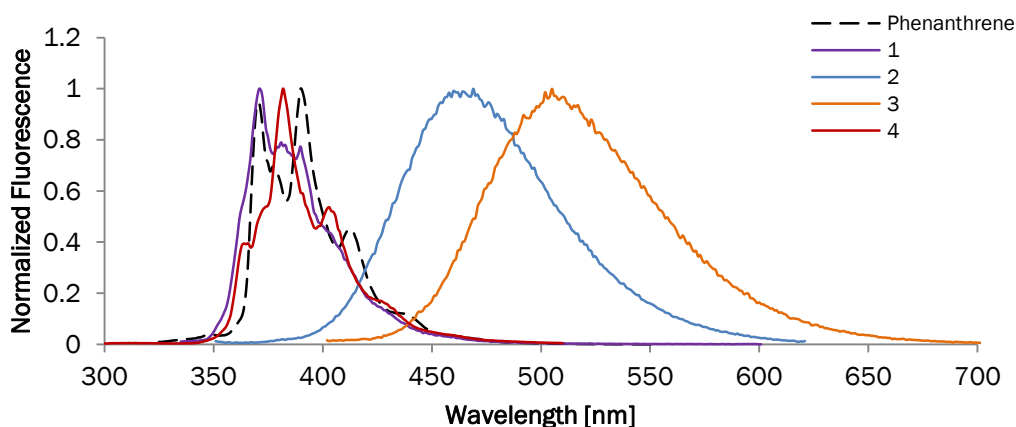
Figure 151: Normalized fluorescence spectra of 2,7-dialkynyl phenanthrene and its derivatives **1**-**4**, measured in ethanol at 20°C. λexc. 316 nm (phenanthrene and **2**), 326 nm (**1**), 393 (**3**), 265 (**4**).

Tunable Photophysical Properties of 1,10-Phenanthroline

A short experiment was done to show the influence of metal ions on the absorption and fluorescence of **4**. Measurements were first done in ethanol with the addition of 20 μM Na$_2$EDTA (black curves in Figure 152), then an excess of ZnCl$_2$ was added (red curves). The absorption spectrum shows a clear red-shift after the addition of the cation, confirming complex formation. The two peaks with the highest absorption shifted from 264 and 325 nm to 270 and 341 nm. Also in the fluorescence spectra some changes are observed. Three peaks can be identified which are located at 362, 382 and 403 nm in the measurement without ZnCl$_2$. In the complex those peaks are slightly shifted (368, 385 and 405 nm) and the ratio of intensities is different. The overall emission is in both measurements located between 350 and 470 nm.
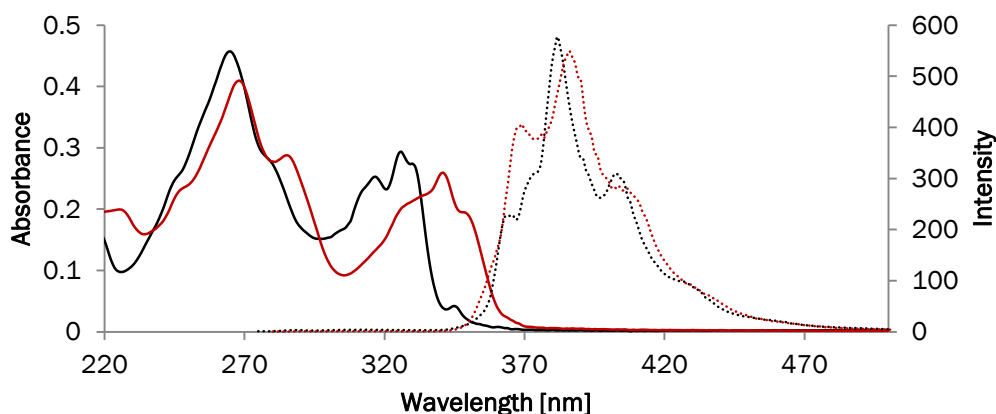
Figure 152: Absorption (solid) and fluorescence (dotted) of compound **4** before (black) and after the addition of an excess ZnCl$_2$ (red). Conditions: 5 μM in ethanol, 20 μM Na$_2$EDTA, 20°C, λexc. 265 nm (without ZnCl$_2$) and 268 (with ZnCl$_2$), <u>attention</u>: In the fluorescence measurement with ZnCl$_2$ the excitation slit width was set down from 5 nm to 2.5 nm due to higher quantum yield.

Quantum Yields

Quantum yields are summarized in Table 11. 2,7-Dialkynyl phenanthrene has a quantum yield of 5%. By adding another aromatic ring (derivative **1**) the quantum yield does not change. A huge increase to 22% is observed for the heteroaromatic 1,4-diazatriphenylene (**2**). Notably, the emission signal comes from assumed excimer formation. Then again, with an additional aromatic ring (derivative **3**) the quantum yield does not change (19%). Derivative **4** has very low quantum yield (3%) if it not complexed, with Zn^{2+} the quantum yield is enhanced (19%).

Table 11: Quantum yields measured in ethanol, determined by using quinine sulfate in 0.5 M H_2SO_4 as standard.

Compound	Quantum yield
2,7-Dialkynyl phenanthrene	5%
Derivative **1**	5%
Derivative **2**	22%
Derivative **3**	19%
Derivative **4**	3% (with $ZnCl_2$: 19%)

Syntheses of Phosphoramidites and Oligomers

Derivatives **1** and **2** were further converted into their corresponding DMT-protected phosphoramidites. Triphenylene and 1,4-diazatriphenylene modified solid support were synthesized as described for phenanthrene in Chapter 1.
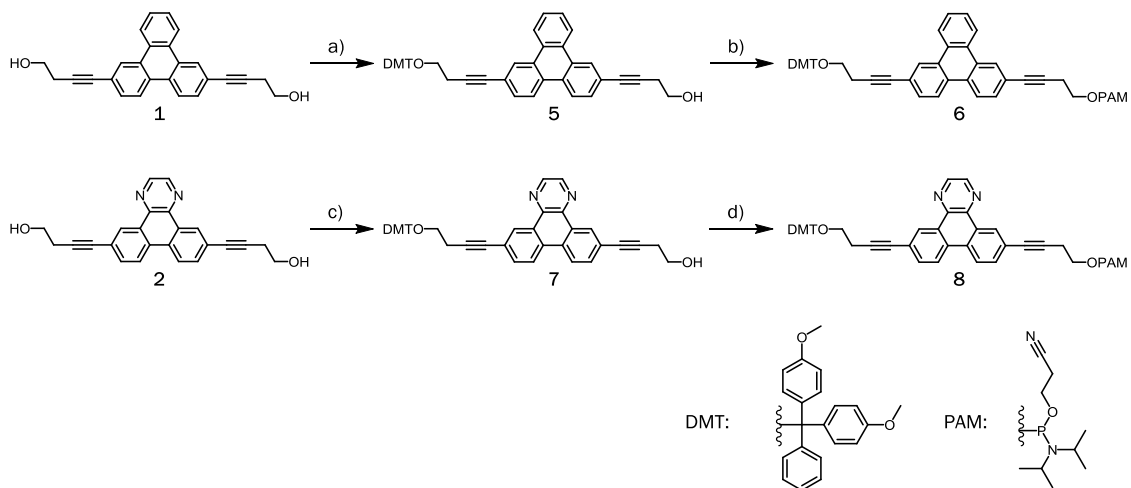
Figure 153: Synthesis of phosphoramidites **6** and **8**; a) DMT-Cl, Et₃N, DMT, 42%; b) PAM-Cl, DIPEA, DCM, 39%; c) DMT-Cl, pyridine, 51%; d) PAM-Cl, DIPEA, DCM, 58%.

Using those phosphoramidites several oligomers were synthesized on a DNA synthesizer (see Figure 154). Trimers of triphenylene and 1,4-diazatriphenylene were assembled on corresponding solid supports (oligomers **9** and **10**). Oligomer **11** is a combination of triphenylene and 1,4-diazatriphenylene which is a potential acceptor for a triphenylene antenna. Oligomers **12** and **13** contain two and four 1,4-diazatriphenylene units, respectively. With those one can study the influence of length on the photophysical properties and assembly behavior. The last oligomer in this series (oligomer **14**) is built up by a 1,4-diazatriphenylene and a phenanthrene linked by one phosphate group. Small amounts of this oligomer could be co-assembled with the phenanthrene nanotube to see if the absorbed energy is transferred to 1,4-diazatriphenylene. The oligomers were not purified after deprotection and cleavage from solid support. Although coupling on the DNA synthesizer looked promising, only small amounts could be cleaved from the solid supports, presumably to low solubility of the oligomers or sticking to the solid support. The right masses were found in mass spectrometry. Absorption and fluorescence measurements

were therefore done with solutions which may contain small amounts of monomers and dimers (or trimers in the case of **12**).
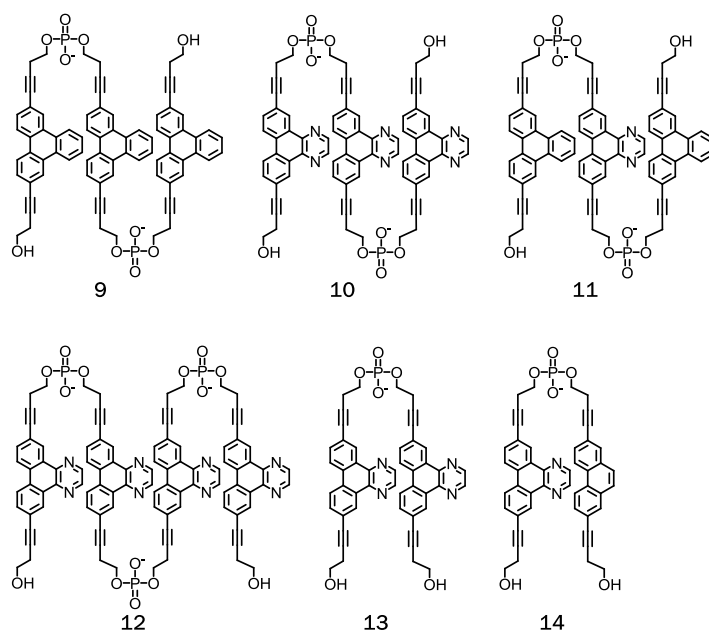
Figure 154: Structures of synthesized oligomers **9-14** consisting of phenanthrene derivatives.

Measurements of Triphenylene Oligomer

The absorption spectra of **9** in ethanol and in aqueous medium are shown in Figure 155. The absorption pattern in ethanol is similar to the monomer (compare with Figure 158 in the supporting information). Changes are observed in aqueous medium which indicate aggregation. The spectrum is almost featureless, only the peak at 274 can still be distinguished. The amount of ethanol in the solution was increased to 20 vol% to ensure the reversibility of the assembly/disassembly process (see supporting information Figure 166).
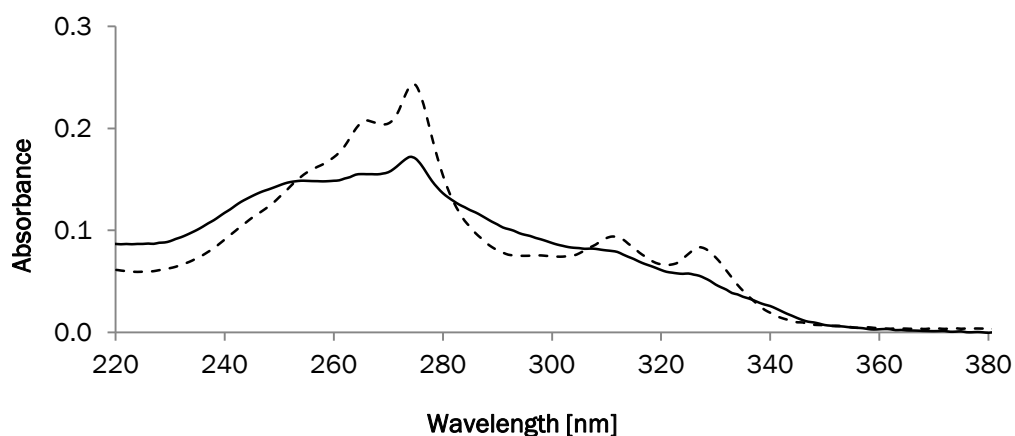
Figure 155: Absorption spectra of oligomer **9** (0.5 µM) in ethanol (dashed) and in aqueous medium (solid, 10 mM sodium phosphate buffer pH 7.0, 20 vol% ethanol), 20°C.

AFM measurements reveal fiber formation of **9** in aqueous medium. The lengths vary from a few nanometers up to 250 nm. Single fibers seem to be about 6 nm height (seldom fibers with heights of 3 nm are found), but they are often entangled and heights of a multiple of 6 nm are found (see cross-sections in Figure 156).
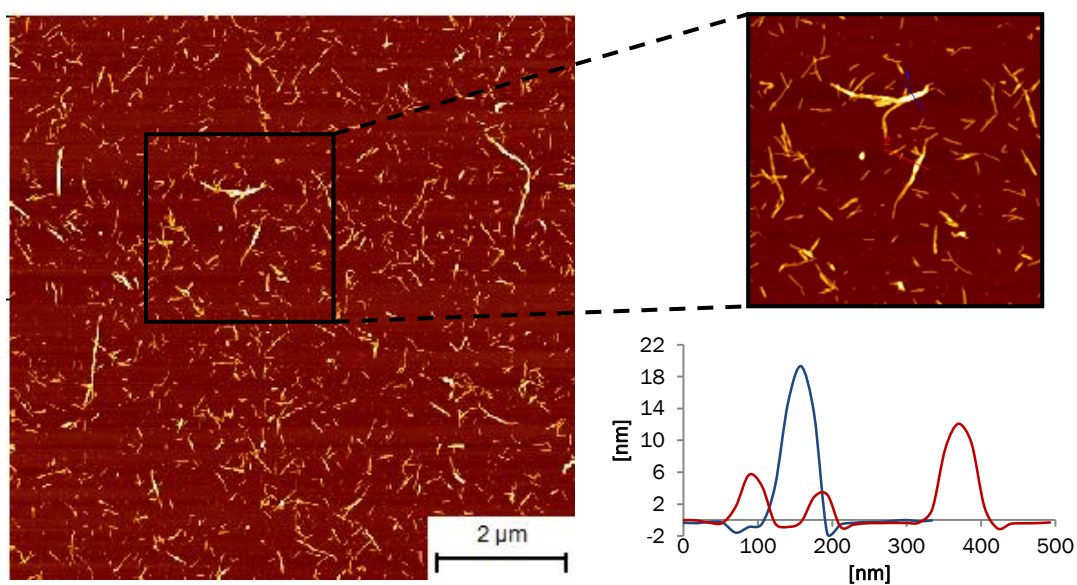
Figure 156: AFM image of assembled **9**. Conditions: 1 µM in 10 mM sodium phosphate buffer, pH 7.0, 20 vol% ethanol.

The supramolecular fibers formed by oligomer **9** were tested for their light-harvesting properties. So far, no energy transfer has been found if oligomer **11** (1,4-diazatriphenylene), acridine orange or rhodamine 6G were used as acceptor dyes.

Further Measurements

Absorption and fluorescence spectra of the other synthesized oligomers can be found in the supporting information of this chapter. Measurements in aqueous medium (10 mM sodium phosphate buffer pH 7.0, 10 vol% ethanol) do not show huge spectral changes in absorption, as can be seen for example in Figure 152 for **10** (1,4-diazatriphenylene trimer). Compared to the measurement at high temperature (80°C), the measurement at 20°C shows hypochromicity, but no significant blue- or red-shift or changes like the appearance of an H- or J-band. Otherwise no further experiments with those oligomers were done.
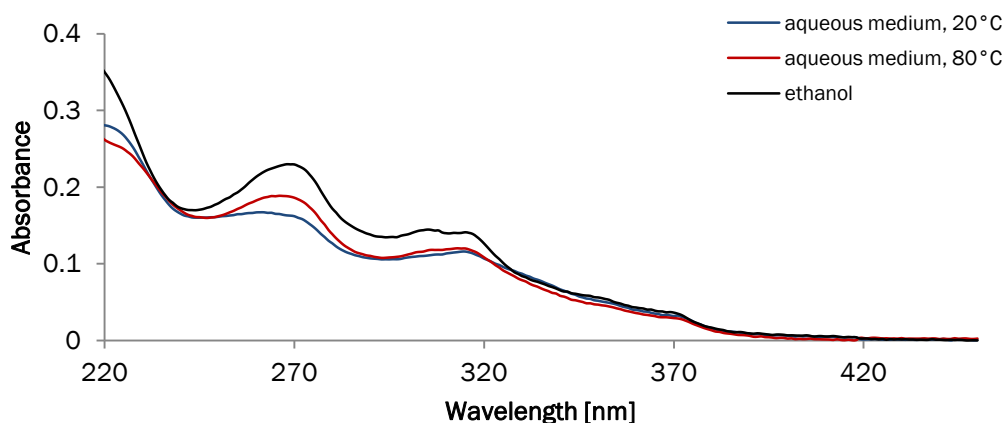
Figure 157: Absorption spectra of oligomer **10** (1,4-diazatriphenylene trimer) in ethanol and in aqueous medium (10 mM sodium phosphate buffer pH 7.0, 10 vol% ethanol). Concentration: 1 µM.

Conclusion and Outlook

Four different phenanthrene derivates have been synthesized and the photophysical properties of the monomers in ethanol have been measured. The absorption spectra do not change much; particularly it was not possible to shift the absorption to the visible range. 1,4-Diazatriphenylene and dibenzo[a,c]phenazine derivatives showed both red-shifted fluorescence emission, indicating excimer formation. Additionally, the fluorescence quantum yields were much higher compared to phenanthrene (19% and 22%, compared to 5%). The fluorescence spectra and quantum yields of triphenylene and 1,10-phenanthroline show less deviation. Additionally, the tunable photophysical properties of 1,10-phenanthroline was investigated by adding $ZnCl_2$. The absorption can be slightly red-shifted, but more interestingly, the quantum yield increases from 3% to 19%.

Oligomers containing triphenylene and 1,4-diazatriphenylene were synthesized and investigated, though the purification was incomplete, presumably due to low solubility or sticking of the oligomers to the solid support. AFM measurements of the triphenylene trimer in aqueous medium revealed that it self-assembles into fibers which bundle. Preliminary experiments using those fibers as antennae for light-harvesting were not successful.

Oligomers containing 1,10-phenanthroline would be of interest, as its ability to bind metal ions influences its photophysical properties. Also the self-assembly behavior and appearance of supramolecular polymers could be dependent on different cations. So, far the 1,10-phenanthroline derivative has not been converted into its corresponding phosphoramidite. For the oligomer synthesis it is not recommended to do it on a solid support, as the other derivatives showed low yields when trying to cleave or redissolve them. Synthesis of such short oligomers is also feasable in solution and is worth trying, especially as higher quantities can be produced.

The construction of a light-harvesting antenna which absorbs light in the visible range is still an objective. 1,10-Phenanthroline with an appropriate cation could lead to such an absorption. Otherwise, phenanthrenes with substituents are still candidates which should be investigated as electron withdrawing/donating groups can affect photophysical properties.
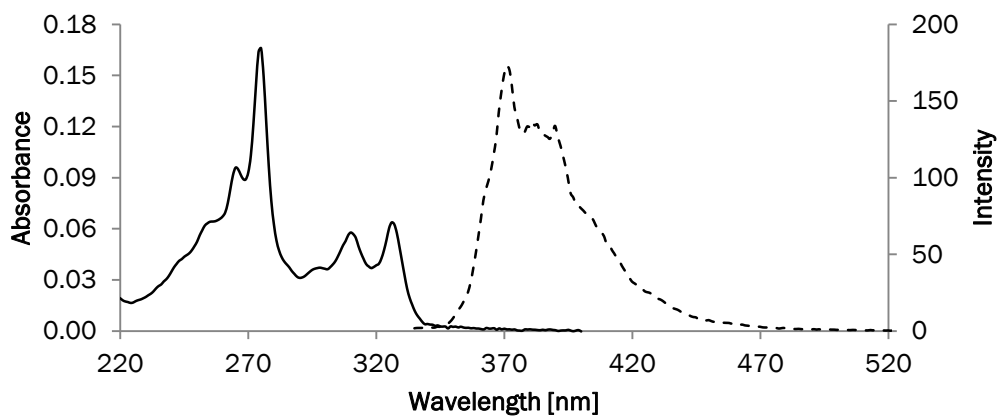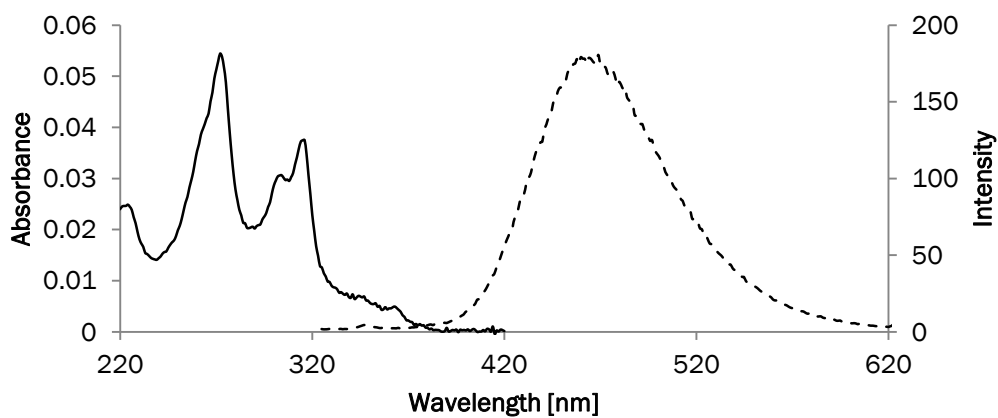
Supporting Information

Spectra of Monomers

Figure 158: Absorption (solid) and fluorescence (dashed) spectra of compound **1**. Conditions: 1 µM in ethanol, 20°C, λexc. 326 nm.

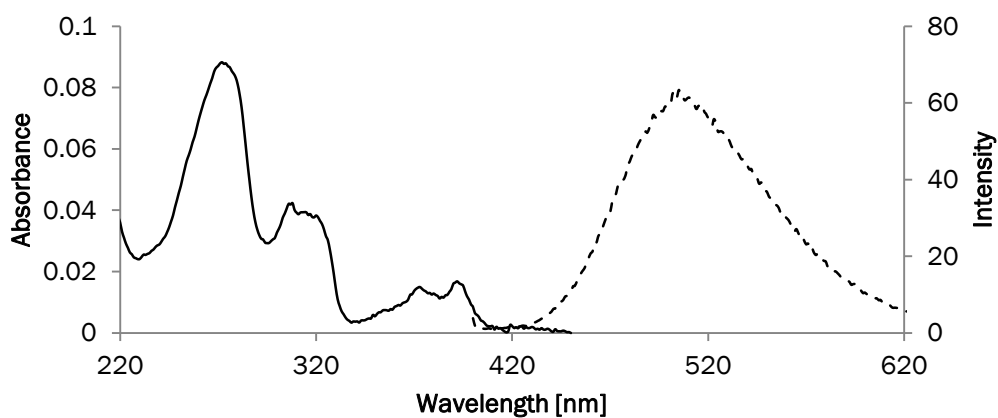Figure 159: Absorption (solid) and fluorescence (dashed) spectra of compound **2**. Conditions: 1 µM in ethanol, 20°C, λexc. 316 nm.

Figure 160: Absorption (solid) and fluorescence (dashed) spectra of compound **3**. Conditions: 1 µM in ethanol, 20°C, λexc. 393 nm.

Spectra of Oligomers
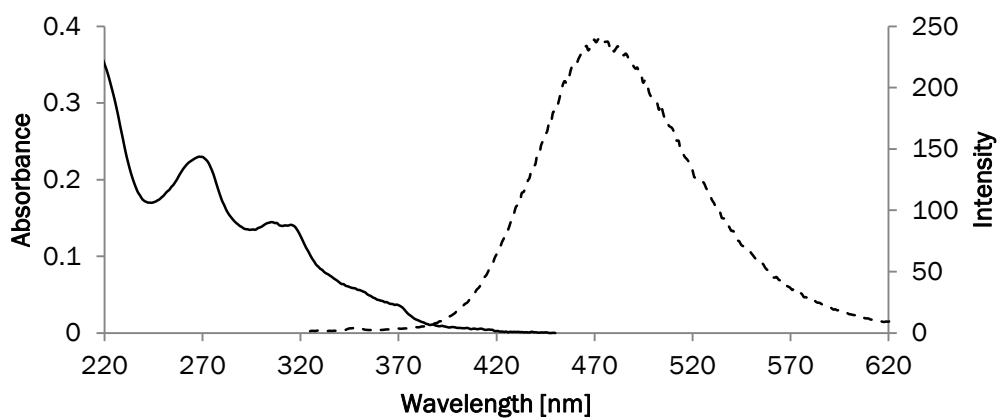
Figure 161: Absorption (solid) and fluorescence (dashed) spectra of **10** in ethanol, 1 µM, 20°C, λexc. 316 nm.
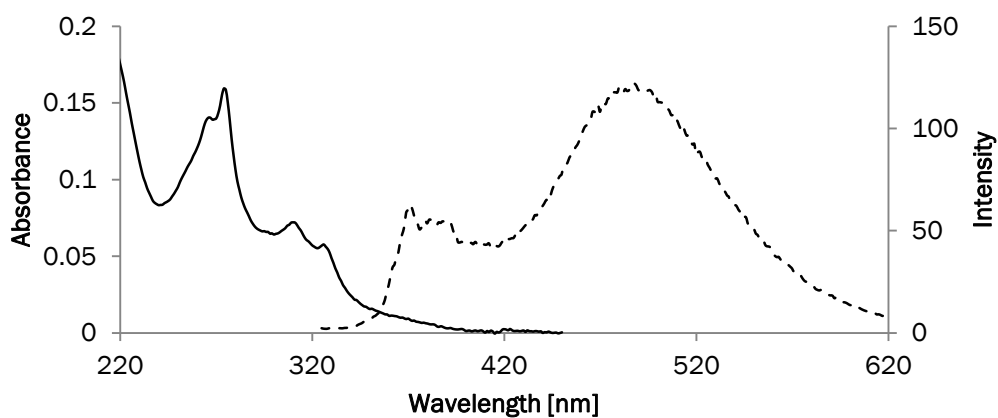
Figure 162: Absorption (solid) and fluorescence (dashed) spectra of **11** in ethanol, 1 µM, 20°C, λexc. 316 nm.
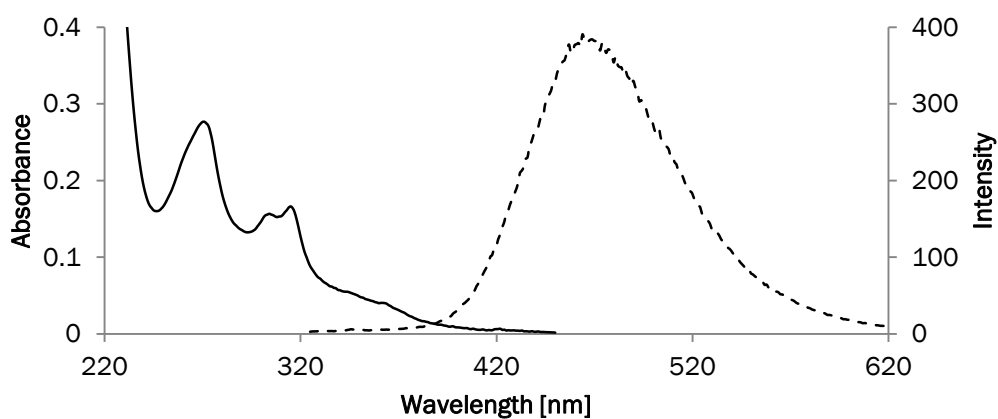
Figure 163: Absorption (solid) and fluorescence (dashed) spectra of **12** in ethanol, 1 µM, 20°C, λexc. 316 nm.
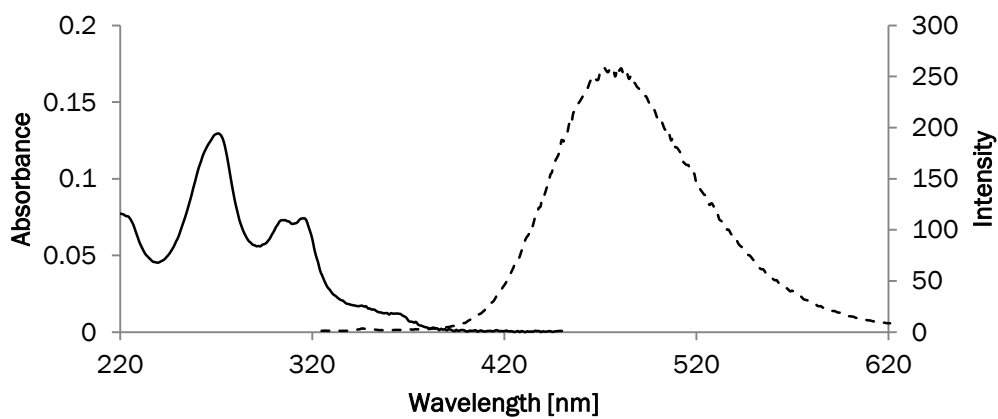
Figure 164: Absorption (solid) and fluorescence (dashed) spectra of **13** in ethanol, 1 µM, 20°C, λexc. 316 nm.

133
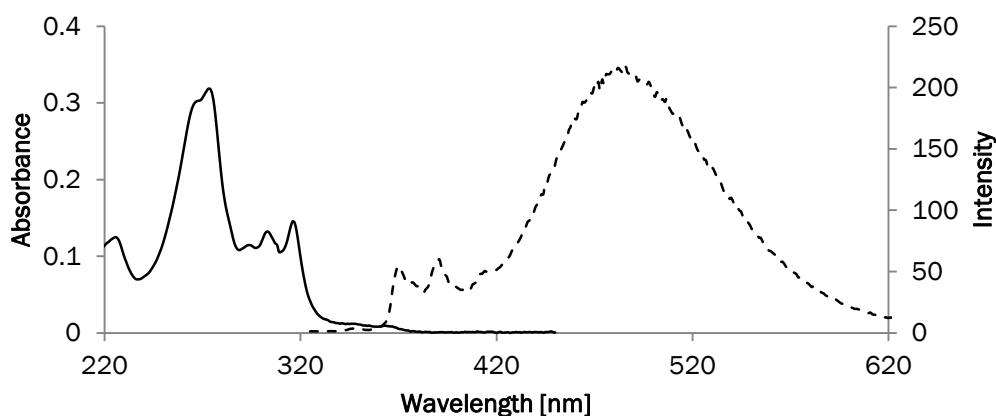
Figure 165: Absorption (solid) and fluorescence (dashed) spectra of **14** in ethanol, 1 µM, 20°C, λexc. 316 nm.
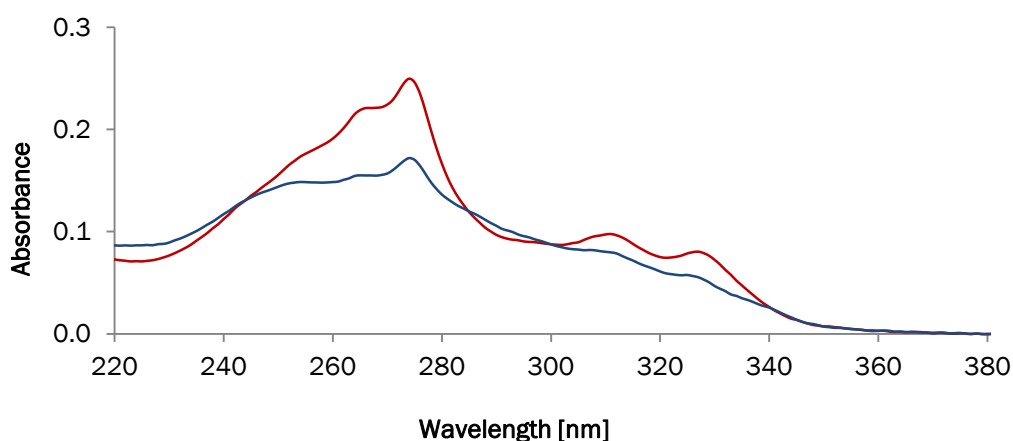
Figure 166: Absorption spectra of **9** at 20°C (blue) and 75°C (red). Conditions: 0.5 µM in 10 mM sodium phosphate buffer pH 7.0, 20 vol% ethanol.

Syntheses of Phenanthrene Derivatives and Phosphoramidites

6,11-Dibromo-1,4-diazatriphenylene was synthesized according to literature. [86a]

2,7-Dibromodibenzo[a,c]phenazine was synthesized according to literature. [87a]

Triphenylene derivative (1): 2,7-Dibromotriphenylene (403.5 mg, 1.05 mmol) was suspended in THF (9 ml) and Et$_3$N (4.7 ml). After degassing the solution with argon, CuI (20 mg) and Pd[PPh$_3$]$_2$Cl$_2$ (40 mg) were added. 3-Butyn-1-ol (0.25 ml, 3.30 mmol) was added and the reaction mixture was refluxed for 19 h at 75°C. TLC (DCM/methanol 95:5) showed

still mono-reacted and unreacted starting material, therefore equal amounts of catalysts and 3-butyn-1-ol (0.45 ml, 5.95 mmol) were added. The reaction mixture was stirred for further 23 h until TLC showed only product. The reaction mixture was concentrated in vacuo and the resulting black residue was purified by flash column chromatography on silica gel (DCM/methanol 99:1 → 95:5). After removing the solvent in vacuo, compound **1** was further purified by precipitation: The residue was dissolved in hot acetone (75 ml). Then, an excess of hexane was added. The white precipitate was filtered off, washed with hexane and dried (247.5 mg, 65%). ^{1}H NMR (300 MHz, DMSO) δ 8.84 – 8.81 (m, 4H), 8.74 (d, J = 8.6 Hz, 2H), 7.74 – 7.67 (m, 4H), 4.97 (t, J = 5.7 Hz, 2H), 3.67 (q, J = 12.5, 6.8 Hz, 4H), 2.66 (t, J = 6.8 Hz, 4H). ^{13}C NMR (75 MHz, DMSO) δ 130.72, 129.85, 129.11, 128.65, 128.57, 126.98, 124.70, 123.16, 117.48, 90.53, 81.84, 60.25, 23.99. HRMS-ESI (m/z): [M+H]$^+$ calculated for $C_{26}H_{21}O_2$, 365.1536; found, 365.1538.

1,4-Diazatriphenylene derivative (2): 6,11-Dibromo-1,4-diazatriphenylene (0.4 g, 1.03 mmol) was suspended in THF (8 ml) and Et$_3$N (2 ml) under argon. CuI (20 mg) and Pd[PPh$_3$]$_2$Cl$_2$ (50 mg) were added, followed by 3-butyn-1-ol (0.24 ml, 3.09 mmol). The reaction mixture was heated to reflux and stirred for 18 h. TLC (DCM/methanol 95:5) showed disappearance of starting material. The solvent was removed in vacuo and the residue was purified by silica gel chromatography (DCM/methanol 99:1 → 95:5). Compound **2** was isolated as a yellow solid (0.27 g, 71%). ^{1}H NMR (300 MHz, DMSO) δ 9.11 (d, J = 1.7 Hz, 2H), 9.09 (s, 2H), 8.81 (d, J = 8.5 Hz, 2H), 7.84 (dd, J = 8.4, 1.8 Hz, 2H), 4.99 (t, J = 5.6 Hz, 2H), 3.67 (dd, J = 12.4, 6.7 Hz, 4H), 2.66 (t, J = 6.7 Hz, 4H). ^{13}C NMR (75 MHz, DMSO) δ 158.11, 144.94, 139.71, 139.66, 135.68, 132.18, 132.06, 129.68, 129.64, 129.50, 129.24, 129.21, 127.87, 127.70, 127.48, 127.44, 127.40, 126.73, 124.15, 124.05, 123.00, 122.78, 113.22, 90.69, 90.52, 85.49, 81.04, 80.85, 61.54, 59.74, 55.01, 23.46, 20.41. HRMS-NSI (m/z): [M+H]$^+$ calcd for $C_{24}H_{19}O_2N_2$, 367.1441; found, 367.1437.

Dibenzo[a,c]phenazine derivative (3): 2,7-Dibromodibenzo[a,c]phenazine (0.39 g, 0.89 mmol) was dissolved in THF (7 ml) and Et$_3$N (2 ml) under argon. CuI (20 mg) and Pd[PPh$_3$]$_2$Cl$_2$ (50 mg) were added, followed by 3-butyn-1-ol (0.2 ml, 2.64 mmol). The reaction mixture was heated to reflux, whereat a precipitate started to form. TLC (DCM/methanol 95:5) after 5 h showed disappearance of starting material. The solvent was removed in vacuo and the residue was suspended in DCM, filtered and washed thoroughly with DCM. The colourless solid was dried under high vacuum (0.33 g, 89%). ^{1}H NMR (300 MHz, DMSO) δ 9.11 (d, J = 1.7 Hz, 2H), 8.63 (d, J = 8.6 Hz, 2H), 8.32 (dd, J = 6.5, 3.4 Hz, 2H), 7.99 (dd, J = 6.5, 3.4 Hz, 2H), 7.77 (dd, J = 8.4, 1.7 Hz, 2H), 5.02 (t, J =

5.6 Hz, 2H), 3.71 – 3.66 (m, 4H), 2.69 (t, J = 6.7 Hz, 4H). ^{13}C NMR (75 MHz, DMSO) δ 141.47, 140.65, 132.80, 130.73, 130.02, 129.25, 129.07, 128.06, 123.99, 123.02, 90.65, 80.80, 59.79, 23.50. HRMS-NSI (m/z): [M+H]$^+$ calcd for $C_{28}H_{21}O_2N_2$, 417.1598; found, 417.1604.

1,10-Phenanthroline derivative (4): 3,8-Dibromo-1,10-phenanthroline (500.6 mg, 1.48 mmol) was suspended in THF (14 ml) and Et$_3$N (7 ml) under argon. CuI (70 mg) and Pd[PPh$_3$]$_2$Cl$_2$ (105 mg) were added. An excess of catalysts was used due to possible complex formation with the nitrogens on 1,10-phenanthroline. Then, 3-butyn-1-ol (0.35 ml, 4.44 mmol) was added and the reaction was stirred under reflux for 24 h. TLC (DCM/toluene/methanol) showed still unreacted starting material, therefore more CuI (40 mg), Pd[PPh$_3$]$_2$Cl$_2$ (60 mg) and 3-butyn-1-ol (0.17 ml) were added and the reaction was stirred under reflux for another 4 h. After cooling down to r.t., aqueous KCN was added to complex and remove Cu.[94] The suspension was filtered off, washed with aqueous KCN, with cold H$_2$O and little cold DCM and then dried. Compound **4** was isolated as a yellow solid (371.7 mg, 79%). ^{1}H NMR (300 MHz, DMSO) δ 9.04 (d, J = 2.0 Hz, 2H), 8.55 (d, J = 2.0 Hz, 2H), 7.98 (s, 2H), 5.00 (t, J = 5.6 Hz, 2H), 3.67 (dd, J = 12.4, 6.6 Hz, 4H), 2.68 (t, J = 6.7 Hz, 4H). HRMS-NSI (m/z): [M+H]$^+$ calcd for $C_{20}H_{17}O_2N_2$, 317.1285; found, 317.1286.

Compound 5: Compound **1** (260 mg, 0.71 mmol) was dissolved in DMF (6 ml) and Et$_3$N (1 ml) under argon. DMT-Cl (245.2 mg, 0.72 mmol) was added in two equal portions. The reaction mixture was stirred at r.t. for 2 h. The yellowish reaction mixture was transferred into a separatory funnel and diluted with DCM/Et$_3$N 99:1 (10 ml). The organic layer was washed once with 5% aqueous citric acid (10 ml) and once with saturated NaHCO$_3$ (10 ml). After drying the organic phase over Na$_2$SO$_4$ and filtration, the solvent was removed in vacuo. The yellowish oil was dried and purified by flash column chromatography on silica gel (DCM + 1% Et$_3$N). Compound **5** was isolated as a white solid (200.4 mg, 42 %). ^{1}H NMR (300 MHz, DMSO) δ 8.85 – 8.74 (m, 6H), 7.73 – 7.68 (m, 4H), 7.50 (d, J = 7.3 Hz, 2H), 7.37 – 7.34 (m, 6H), 7.26 (d, J = 7.2 Hz, 1H), 6.92 (d, J = 8.9 Hz, 4H), 4.98 (t, J = 5.7 Hz, 1H), 3.73 (s, 6H), 3.68 (q, J = 12.5, 6.7 Hz, 2H), 3.24 (t, J = 6.6 Hz, 2H), 2.82 (t, J = 6.6 Hz, 2H), 2.67 (t, J = 6.8 Hz, 2H).

Compound 6: Compound **5** (200 mg, 0.30 mmol) was dissolved in dry DCM (2.7 ml) and DIPEA (0.3 ml) under argon. PAM-Cl (170 mg, 0.72 mmol) was added and the reaction mixture was stirred at r.t. for 2 h. The reaction mixture was concentrated in vacuo and the residue was purified by a short silica gel flash column chromatography (hexane/ethyl acetate/Et$_3$N 7:3:0.1). Compound **6** was isolated as a white foam (100.1 mg, 39 %). ^{1}H NMR (300 MHz, DMSO) δ 8.81 – 8.75 (m, 6H), 7.73 – 7.69 (m, 4H), 7.50 (d, J = 7.3 Hz,

2H), 7.37 – 7.31 (m, 6H), 7.26 – 7.24 (m, 1H), 6.92 (d, J = 8.9 Hz, 4H), 3.91 – 3.77 (m, 4H), 3.73 (s, 6H), 3.68 – 3.60 (m, 2H), 3.24 (t, J = 6.5 Hz, 2H), 2.85 – 2.73 (m, 6H), 1.18 (t, J = 6.6 Hz, 12H). ^{31}P NMR (121 MHz, DMSO) δ 147.19. HRMS-ESI (m/z): [M+H]$^+$ calculated for $C_{56}H_{56}O_5N_2P$, 867.3921; found, 867.3949.

Compound 7: Compound **2** (0.2 g, 0.55 mmol) was dissolved in pyridine (5.5 ml) and DMT-Cl (185 mg, 0.55 mmol) was added. The reaction mixture was stirred at r.t. for 1 h, and then transferred into a separatory funnel and diluted with DCM. The organic layer was washed once with 10% citric acid and once with H_2O. After drying with $MgSO_4$ and filtration, the solvent was removed in vacuo. The residue was purified by silica gel chromatography (hexane/ethyl acetate/Et$_3$N 6:4:0.1) to give **7** as a white solid (0.19 g, 51%). ^{1}H NMR (300 MHz, DMSO) δ 9.18 (d, J = 1.6 Hz, 1H), 9.12 (d, J = 1.7 Hz, 1H), 9.11 – 9.08 (m, 2H), 8.83 (dd, J = 8.8, 6.9 Hz, 2H), 7.86 (ddd, J = 8.5, 4.7, 1.8 Hz, 2H), 7.53 – 7.48 (m, 2H), 7.40 – 7.32 (m, 6H), 7.28 – 7.21 (m, 1H), 6.97 – 6.90 (m, 4H), 4.99 (t, J = 5.7 Hz, 1H), 3.73 (s, 6H), 3.67 (dd, J = 12.4, 6.7 Hz, 3H), 3.22 (t, J = 5.9 Hz, 2H), 2.81 (t, J = 6.2 Hz, 2H), 2.66 (t, J = 6.7 Hz, 2H). ^{13}C NMR (75 MHz, DMSO) δ 158.11, 144.94, 139.71, 139.66, 135.68, 132.18, 132.06, 129.68, 129.64, 129.50, 129.24, 129.21, 127.87, 127.70, 127.48, 127.44, 127.40, 126.73, 124.15, 124.05, 123.00, 122.78, 113.22, 90.69, 90.52, 85.49, 81.04, 80.85, 61.54, 59.74, 55.01, 23.46, 20.41. HRMS-NSI (m/z): [M+H]$^+$ calcd for $C_{45}H_{37}O_4N_2$, 669.2748; found, 669.2758.

Compound 8: Compound **7** (0.24 g, 0.36 mmol) was dissolved in DCM (3 ml) and DIPEA (0.6 ml). PAM-Cl (90 mg, 0.38 mmol) was added and the reaction mixture was stirred at r.t. for 3 h until TLC (hexane/ethylacetate/Et$_3$N 7:3:0.1) showed disappearance of starting material. After removing the solvent in vacuo the product was purified by silica gel chromatography (hexane/ethyl acetate/Et$_3$N 7:3:0.1). Phosphoramidite **8** was isolated as white foam (0.18 g, 58%). ^{1}H NMR (300 MHz, DMSO) δ 9.20 – 9.06 (m, 4H), 8.84 (s, 2H), 7.87 (d, J = 8.8 Hz, 2H), 7.51 (d, J = 7.5 Hz, 2H), 7.36 (d, J = 8.8 Hz, 6H), 7.26 (d, J = 7.0 Hz, 1H), 6.94 (d, J = 8.8 Hz, 4H), 3.84 (d, J = 9.0 Hz, 4H), 3.74 (s, 6H), 3.65 (d, J = 10.3 Hz, 2H), 3.23 (s, 2H), 2.88 – 2.78 (m, 6H), 1.19 (t, J = 6.6 Hz, 12H). ^{31}P NMR (121 MHz, DMSO) δ 147.26. HRMS-NSI (m/z): [M+H]$^+$ calcd for $C_{54}H_{54}O_5N_4P$, 869.3826; found, 869.3839.
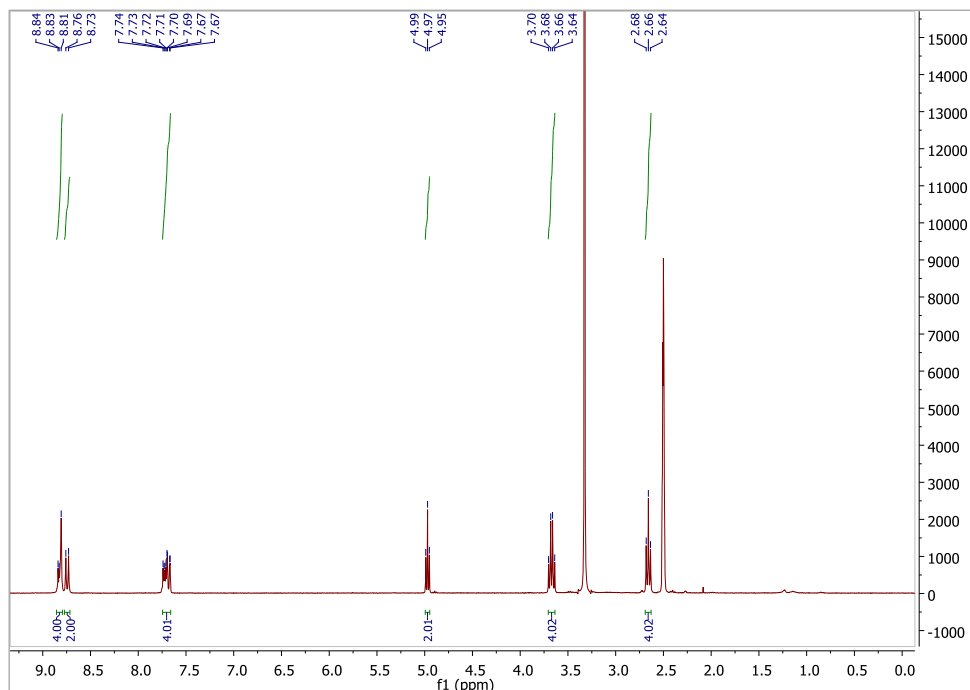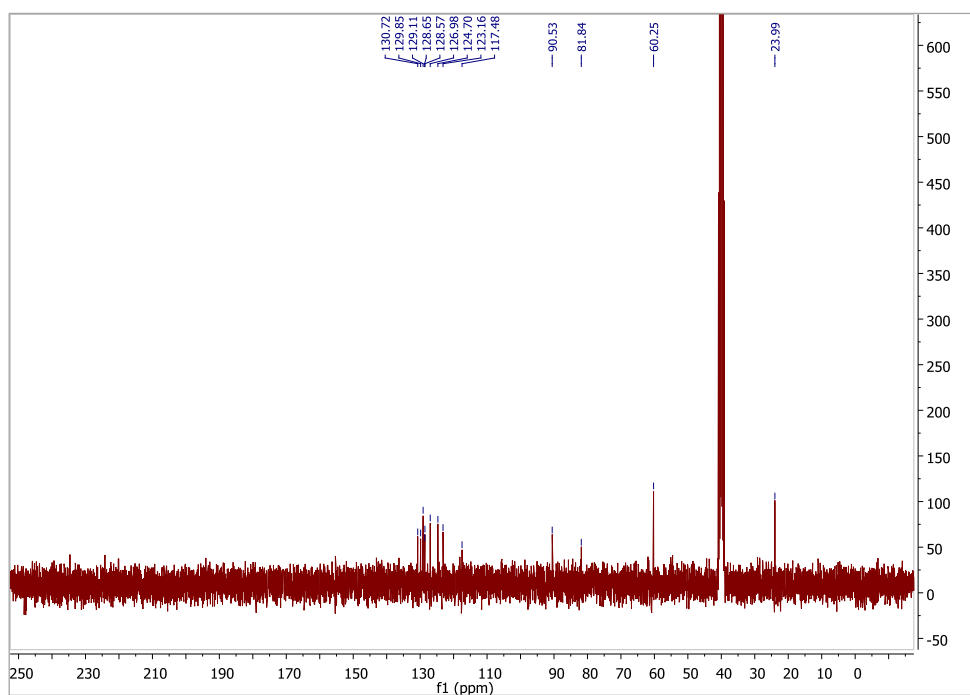
NMR Spectra

Figure 167: ^{1}H NMR of compound **1** in DMSO-d$_6$.

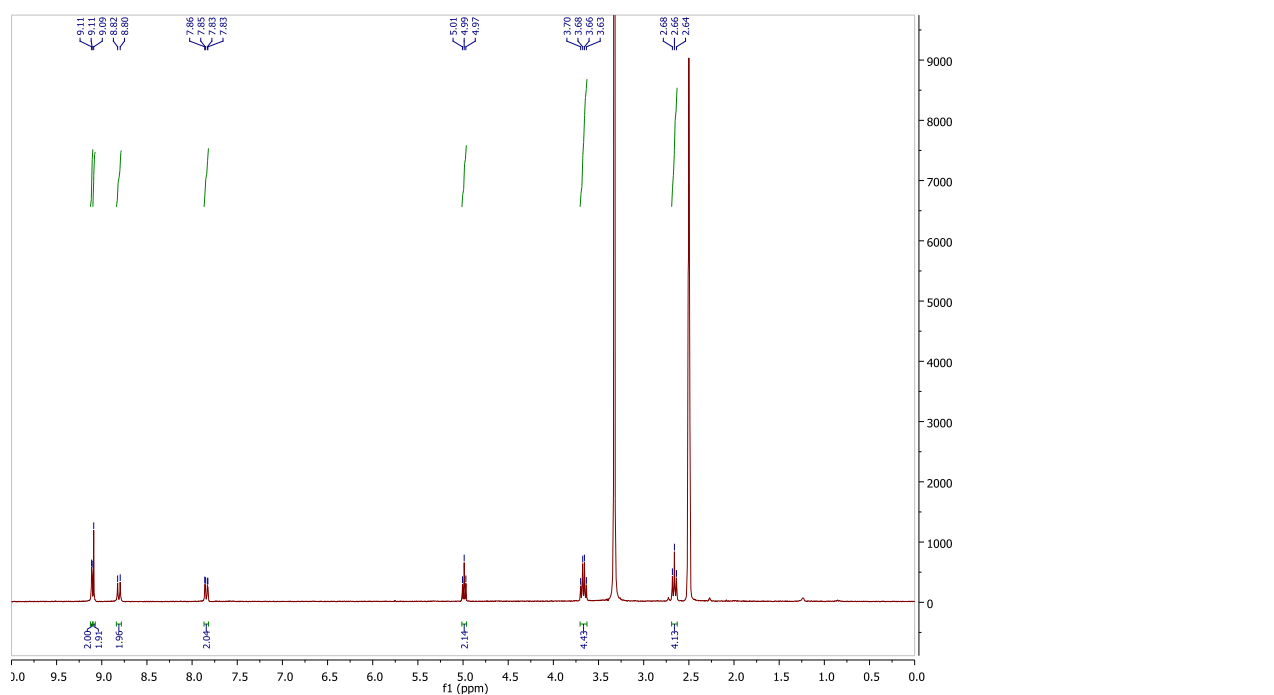

Figure 168: ^{13}C NMR of compound **1** in DMSO-d$_6$.
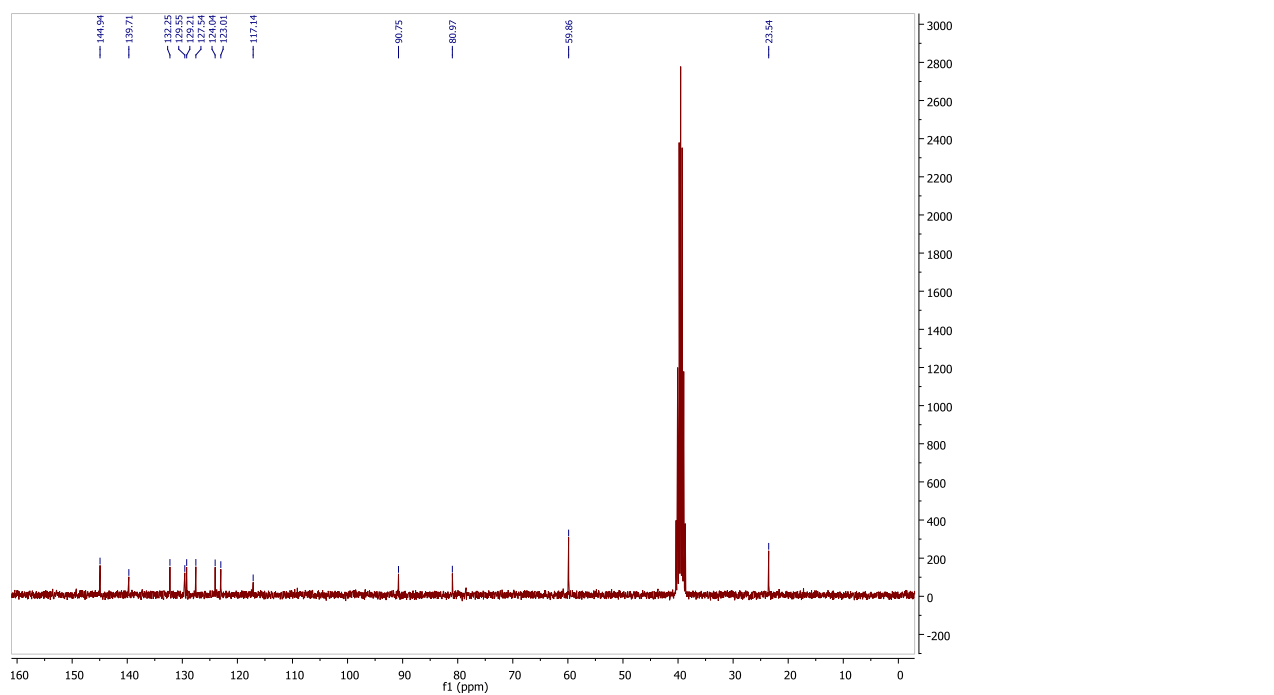
Figure 169: ^{1}H NMR of compound **2** in DMSO-d$_6$.

Figure 170: ^{13}C NMR of compound **2** in DMSO-d$_6$.
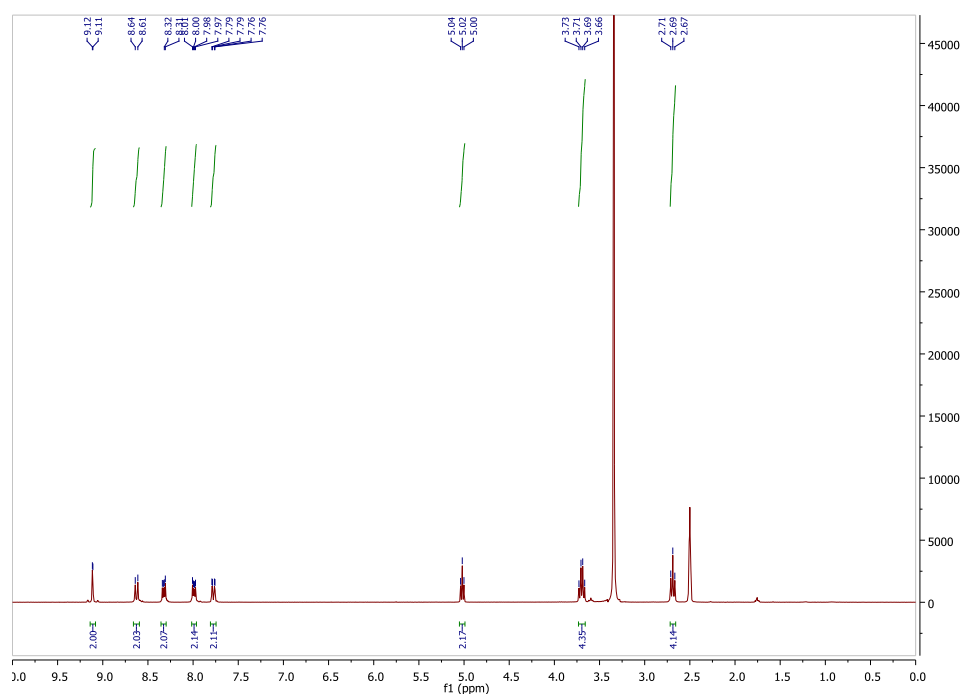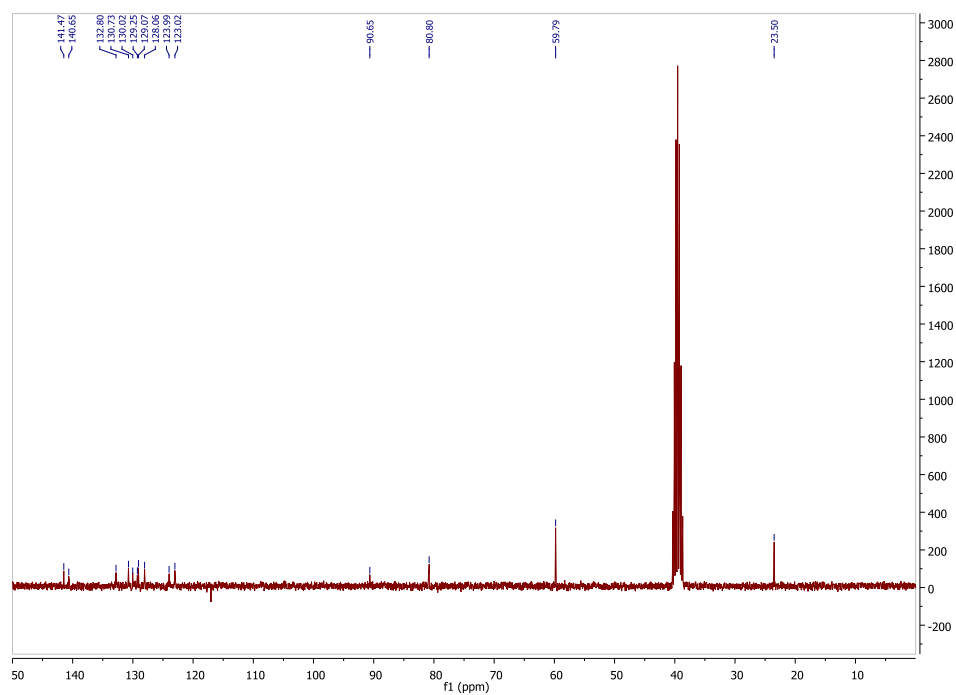
Figure 171: ^{1}H NMR of compound **3** in DMSO-d$_6$.

Figure 172: ^{13}C NMR of compound **3** in DMSO-d$_6$.
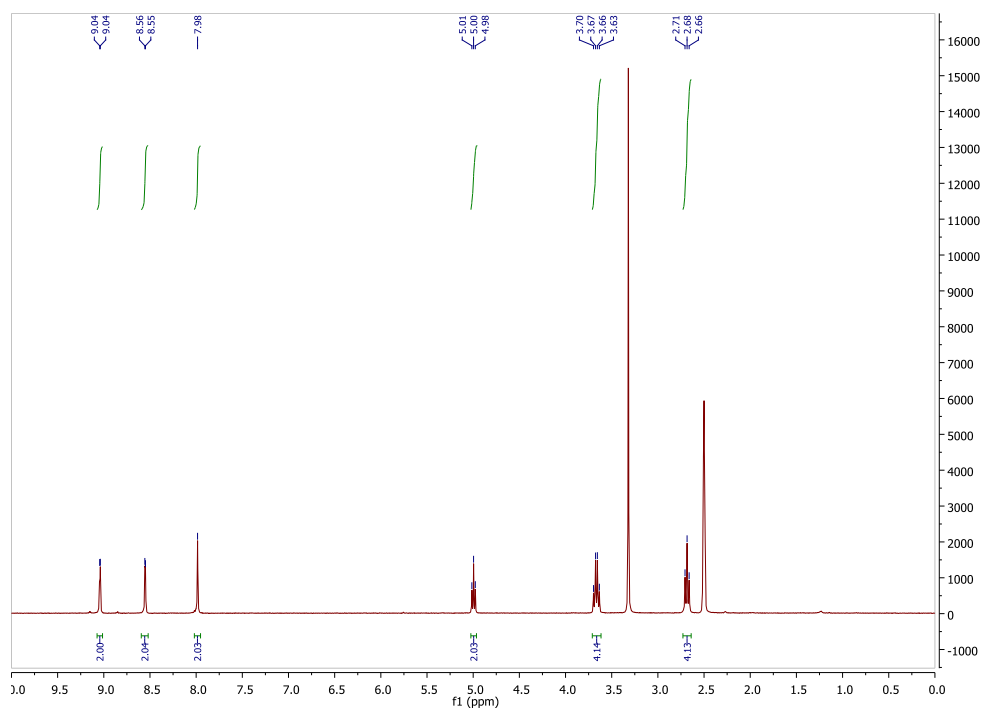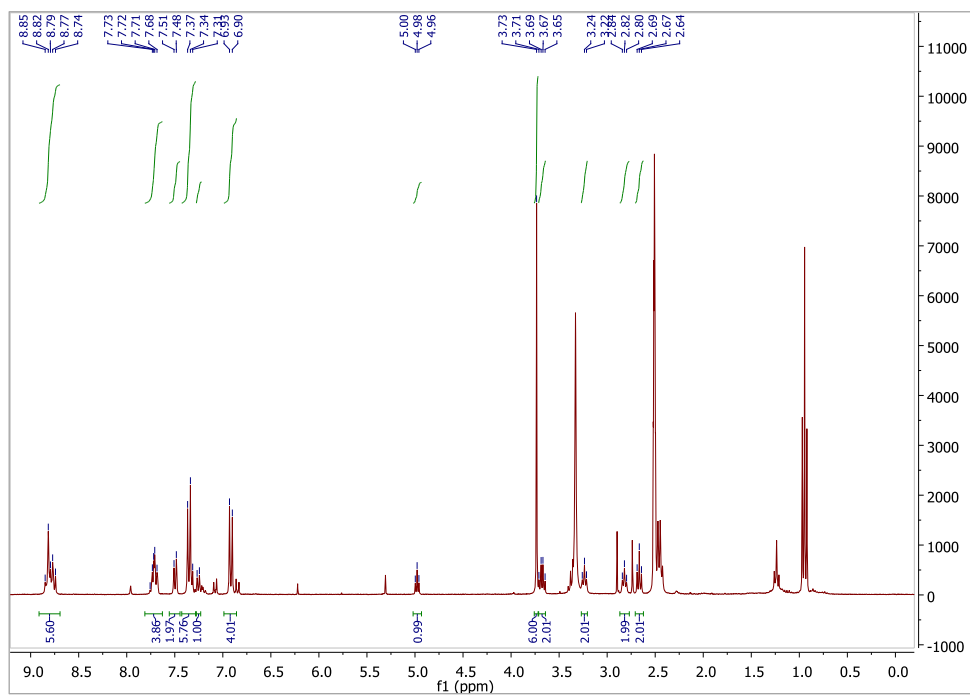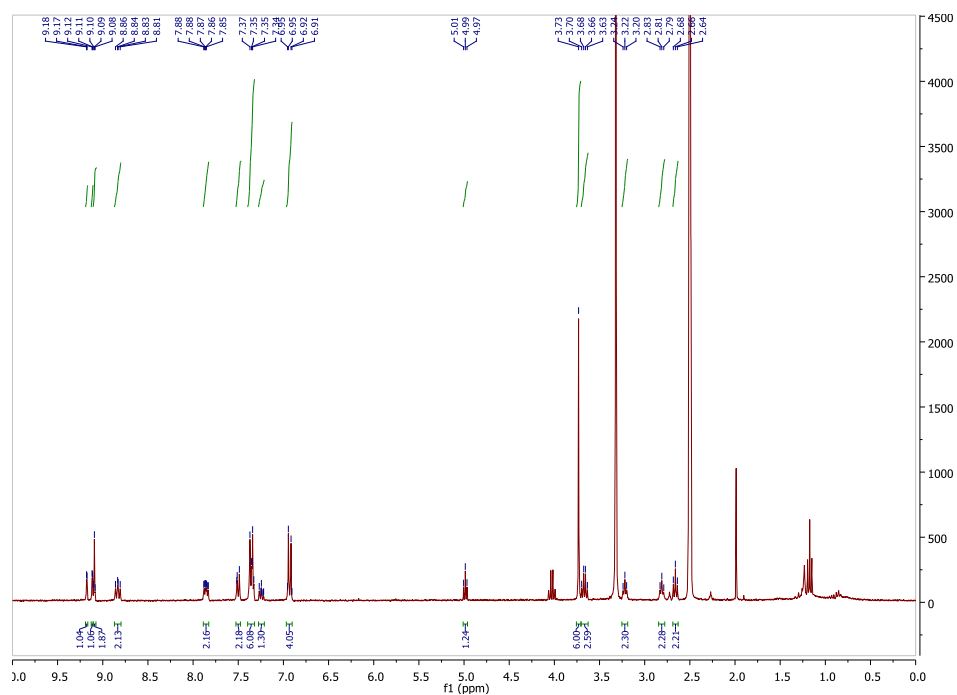
Figure 173: ¹H NMR of compound **4** in DMSO-d₆.

Figure 174: ¹H NMR of compound **5** in DMSO-d₆.

Figure 175: ^{1}H NMR of compound **6** in DMSO-d$_6$.

Figure 176: ^{13}C NMR of compound **7** in DMSO-d$_6$.

Figure 177: ^{1}H NMR of compound **7** in DMSO-d$_6$.
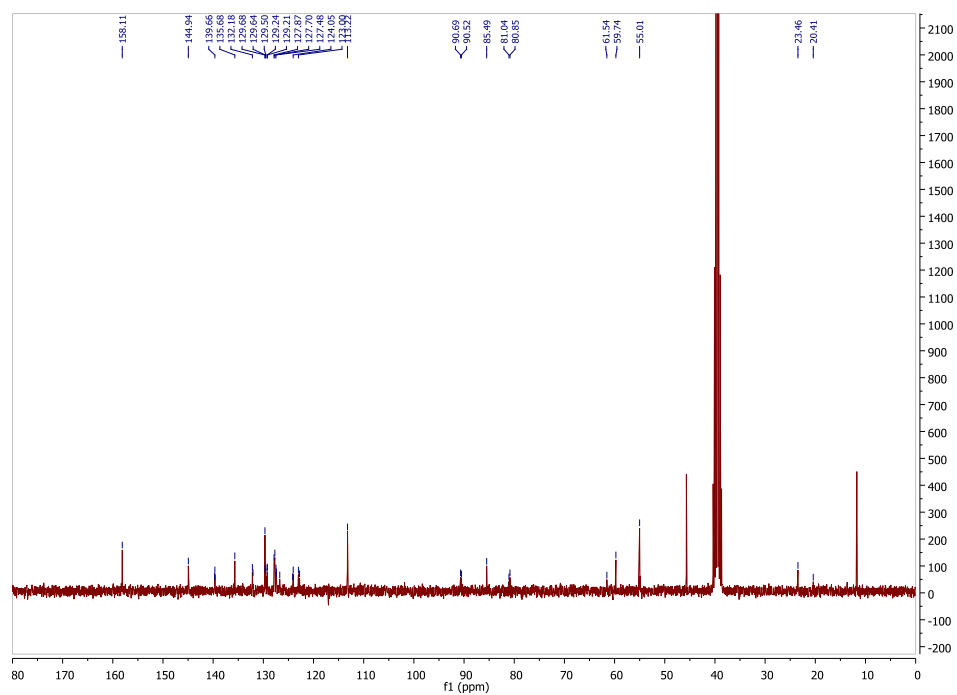
Figure 178: ^{13}C NMR of compound **7** in DMSO-d$_6$.
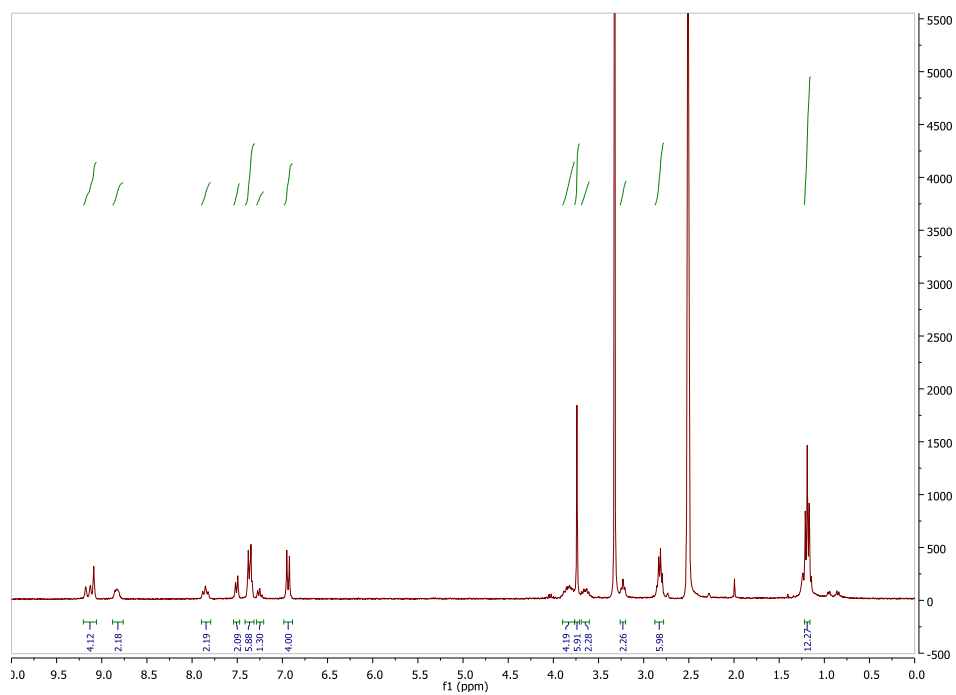
Figure 179: ^{1}H NMR of compound **8** in DMSO-d$_6$.
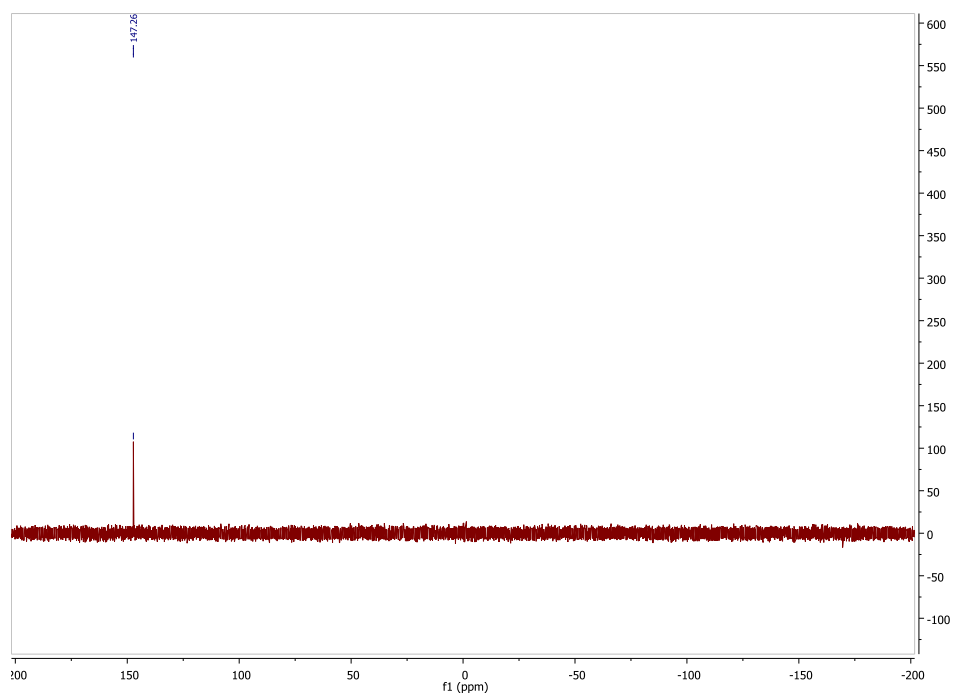
Figure 180: ^{31}P NMR of compound **8** in DMSO-d$_6$.

References

[80]   C. D. Bösch, S. M. Langenegger, R. Häner, *Angew. Chem. Int. Ed.*, 2016, **55**, 9961-9964.

[81]   (a) F. Garo, R. Häner, *Angew. Chem. Int. Ed.*, 2012, **51**, 916-919.
(b) M. Probst, S. M. Langenegger, R. Häner, *Chem. Commun.*, 2014, **50**, 159-191.
(c) C. B. Winiger, S. Li, G. R. Kumar, S. M. Langenegger, R. Häner, *Angew. Chem. Int. Ed.*, 2014, **53**, 13609-13613.

[82]   (a) T. Mirkovic, E. E. Ostroumov, J. M. Anna, R. van Grondelle, Govindjee, G. D. Scholes, *Chem. Rev.*, 2017, **117**, 249-293.
(b) G. D. Scholes, G. R. Fleming, A. Olaya-Castro, R. van Grondelle, *Nat. Chem.*, 2011, **3**, 763-774.
(c) K. Gundlach, M. Werwie, S. Wiegand, H. Paulsen, *Biochim. Biophys. Acta*, 2009, **1787**, 1499-1504.
(d) Reference Solar Spectral Irradiance: Air Mass 1.5, URL: http://rredc.nrel.gov/solar/spectra/am1.5/, accessed June 2017

[83]   W. Karcher, R. J. Fordham, J. J. Dubois, P. G. J. M. Glaude, J. A. M. Ligthart, *Spectral atlas of polycyclic aromatic compounds*, D. Reidel Publishing Company, Dordrecht, NL, 1983.

[84]   (a) G. M. Badger, *The Ultraviolet Absorption Spectra of Polycyclic Heterocyclic Aromatic Compounds*, in *Chemistry of Heterocyclic Compounds: Six Membered Heterocyclic Nitrogen Compounds with Three Condensed Rings*, Volume 12 (ed C. F. H. Allen), John Wiley & Sons, Inc., Hoboken, NJ, USA. 1958.
(b) B. Ośmiałowski, A. Zakrzewska, B. Jędrzejewska, A. Grabarz, R. Zaleśny, W. Bartkowiak, E. Kolehmainen, *J. Org. Chem.* 2015, **80**, 2072-2080.

[85]   (a) J. W. Levell, A. Ruseckas, J. B. Henry, Y. Wang, A. D. Stretton, A. R. Mount, T. H. Galow, I. D. W. Samuel, *J. Phys. Chem. A*, 2010, **114**, 13291-13295.
(b) D. Wang, J. F. Hsu, M. Bagui, V. Dusevich, Y. Wang, Y. Liu, A. J. Holder, Z. Peng, *Tetrahedron Lett.*, 2009, **50**, 2147-2149.
(c) C.-E. Chou, D. Wang, M. Bagui, J. Hsu, S. Chakraborty, Z. Peng, *J. Lumin.*, 2010, **130**, 986-994.
(d) M. Bagui, J. S. Melinger, S. Chakraborty, J. A. Keightley, Z. Peng, *Tetrahedron*, 2009, **65**, 1247-1256.
(e) H. Mao, Z. He, J. Wang, C. Zhang, P. Xie, R. Zhang, *J. Lumin.*, 2007, **122-123**, 942-945.
(f) X. Kong, Z. He, Y. Zhang, L. Mu, C. Liang, B. Chen, X. Jing, A. N. Cammidge, *Org. Lett.*, 2011, **13**, 764-767.
(g) K. Togashi, S. Nomura, N. Yokoyama, T. Yasuda, C. Adachi, *J. Mater. Chem.*, 2012, **22**, 20689-20695.

[86]   (a) T. Takahashi, K. Shizu, T. Yasuda, K. Togashi, C. Adachi, *Sci. Technol. Adv. Mater.*, 2014, **15**, 034202.
(b) Z. Khodaee, A. Yahyazadeh, N. O. Mahmoodi, M. A. Zanjanchi, V. Azimi, *J. Mol. Struct.*, 2012, **1029**, 92-97.
(c) M. Velusamy, J.-H. Huang, Y.-C. Hsu, H.-H. Chou, K.-C. Ho, P.-L. Wu, W.-H. Chang, J. T. Lin, C.-W. Chu, *Org. Lett.*, 2009, **11**, 4898-4901.

[87]   (a) E. K. Unver, S. Tarkuc, Y. A. Udum, C. Tanyeli, L. Toppare, *J. Polym. Sci. Pol. Chem.*, 2010, **48**, 1714-1720.
(b) L. A. Estrada, D. C. Neckers, *Org. Lett.*, 2011, **13**, 3304-3307.
(c) Y. Zhu, K. M. Gibbons, A. P. Kulkarni, S. A. Jenekhe, *Macromolecules*, 2007, **40**, 804-813.
(d) M.-C. Tzeng, S.-C. Liao, T.-H. Chang, S.-C. Yang, M.-W. Weng, H.-C. Yang, M. Y. Chiang, Z. Kai, J. Wu, C. W. Ong, *J. Mater. Chem.*, 2011, **21**, 1704-1712.

[88]   (a) J. Shi, J. Chen, Z. Chai, H. Wang, R. Tang, K. Fan, M. Wu, H. Han, J. Qin, T. Peng, Q. Li, Z. Li, *J. Mater. Chem.*, 2012, **22**, 18830-18838.
(b) R. He, L. Yu, P. Cai, F. Peng, J. Xu, L. Ying, J. Chen, W. Yang, Y. Cao, *Macromolecules*, 2014, **47**, 2921-2928.

[89]   (a) G. Accorsi, A. Listorti, K. Yoosaf, N. Armaroli, *Chem. Soc. Rev.*, 2009, **38**, 1690-1700.
(b) A. Bencini, V. Lippolis, *Coord. Chem. Rev.*, 2010, **254**, 2096-2180.

[90]   (a) H. S. Joshi, R. Jamshidi, Y. Tor, *Angew. Chem. Int. Ed.*, 1999, **38**, 2721-2725.
(b) D. Tzalis, Y. Tor, *J. Am. Chem. Soc.*, 1997, **119**, 852-853.
(c) D. Tzalis, Y. Tor, *Chem. Commun.*, 1996, 1043-1044.

[91]   B. Sharf, *J. Phys. Chem.*, 1971, **54**, 441-443.

[92]   E. C. Lim, Y. H. Li, *Chem. Phys. Lett.*, 1969, **4**, 68-70.

[93]   J. B. Birks, *Rep. Prog. Phys.*, 1975, **38**, 903-974.

[94]   J. W. Ciszek, J. M. Tour, *Tetrahedron Lett.* 2004, **45**, 2801-2803.

Chapter 5: Chrysene and Naphthalimide Dyes

Abstract

Oligomers consisting of chrysene and naphthalimide dyes are synthesized and their photophysical properties are investigated. Chrysene trimers form supramolecular polymers in aqueous medium. Co-assembly with a naphthalimide dye does not lead to the expected excitation energy transfer from chrysene to the acceptor. However, incorporation of those dyes into DNA duplexes leads to energy transfer. Showing that chrysene is able to transfer its excitation energy and that naphthalimide dyes can be used as acceptors in light-harvesting systems and potentially as fluorescent labels in other DNA based applications.

Introduction

Chrysene is a polycyclic aromatic hydrocarbon which has already been incorporated into DNA strands and is able to self-organize within a DNA framework.[95] Excimer formation was observed in DNA duplexes, as well as in single strands containing two chysene units next to each other; a feature which has never been observed in solution.[96] Examples of chrysene excimer formation were otherwise observed in crystals under high pressure[97] or in vinyl copolymers of chrysene.[98] Further, chrysene is another derivative of phenanthrene (1,2-benzphenanthrene) and therefore it is reasonable to investigate also its light-harvesting properties. To do so, short amphiphilic oligomers consisting of chrysene are synthesized and the formation of supramolecular polymers in aqueous medium is studied.

The other kind of chromophores which will be investigated in this chapter are 1,8-naphthalimide dyes. Derivatives of those are well studied as DNA binders, anticancer and fluorescent cellular imaging agents.[99] Other applications for naphthalimide dyes are for organic light-emitting devices (OLEDs)[100] and dyeing of polymers.[101] This chapter presents three different naphthalimide dyes which will be converted into phosphoramidites (see Table 12). Oligomers consisting of naphthalimide and chrysene are synthesized and tested for their acceptor properties in chrysene supramolecular polymers. Further, naphthalimide dyes will be incorporated into DNA strands. Duplexes containing different dyes opposite to each other will be investigated.
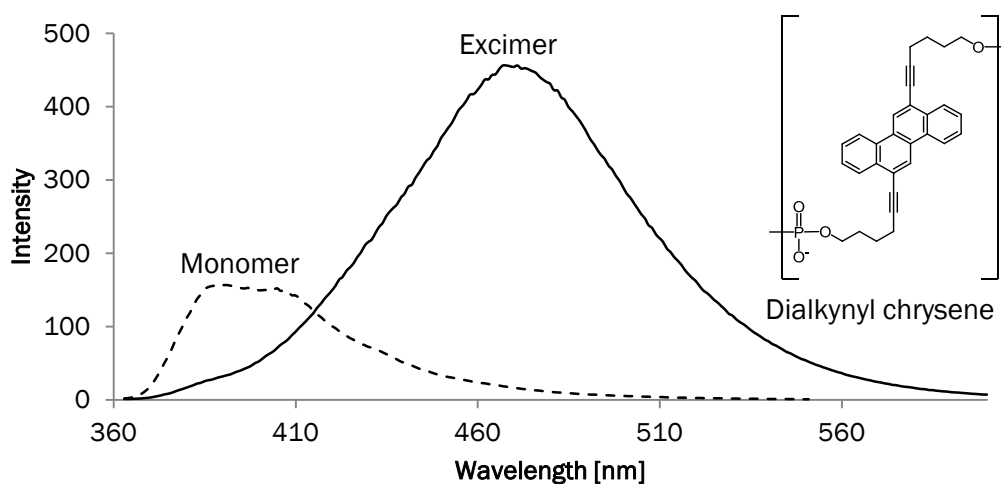
Figure 181: Fluorescence spectra of dialkynyl chrysene in a DNA single strand (monomer, dashed) and two units in a DNA duplex (excimer, solid).[95]

Table 12: Structures and spectroscopic data of naphthalimide dyes (provided by Prof. Dr. Leonid Patsenker).

Dye	Structure	Absorption maximum [nm][†]	Fluorescence maximum [nm][†]	Abs. coeff. ε [M^{-1} cm^{-1}][‡]
Naphth1		398	519	12'700
Naphth2		411	525	11'600
Naphth3		365	432	13'000

[†]measured in dichloromethane, [‡]measured in methanol

148

Results and Discussion

Overview of Oligomers

Figure 182 shows an overview of chrysene and naphthalimide oligomers presented in this chapter. Oligomers **1** and **2** consist both of three dialkynyl chrysene linked by phosphate groups. Oligomer **1** is composed of dihexynyl modified chrysene, a building block that was previously incorporated into DNA single strands.[95] To investigate the effect of the linker length on the properties of a chrysene trimer and as well for reasons of consistency, also oligomer **2** was synthesized. In this oligomer the chromophores are modified with butynyl linkers, like in all the other examples presented in previous chapters.

Oligomers **3** and **4** contain two different building blocks, namely chrysene and 4-morpholino-1,8-naphthalimide (Naphth1). Due to the chrysene unit(s), those two oligomers are expected to be incorporated into supramolecular polymers formed by either **1** or **2**. The assembled chrysene units could then absorb light and transfer it to the potential acceptor Naphth1.
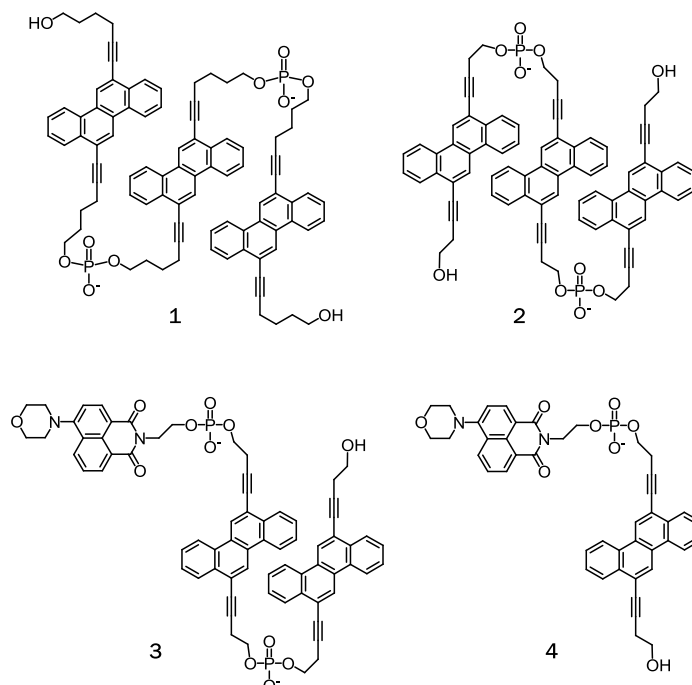
Figure 182: Overview of oligomers presented in this chapter.

Photophysical Properties of Chrysene Supramolecular Polymers

Figure 183 shows the UV-vis absorption of oligomer **1** measured in ethanol and in aqueous medium. The differences indicate a strong aggregation behavior in aqueous medium. The most significant change is the appearance of a red-shifted absorption band at 301 nm which suggests the formation of J-aggregates.[102] Such a band was also observed with supramolecular polymers composed of pyrene oligomers.[103] Further, the spectrum in ethanol shows the two first vibronic bands $S_1^{0\to0}/S_1^{0\to1}$ of 0.98. In aqueous medium this ratio decreases to 0.73, which indicates π-π stacking.[104] The absorption maximum is red-shifted by 10 nm, indicating π-conjugation between chrysenes.[105] Those aggregates in aqueous medium can be disrupted by heating the solution up to 75°C which results in a similar absorption band as the one measured in ethanol (Figure 184).
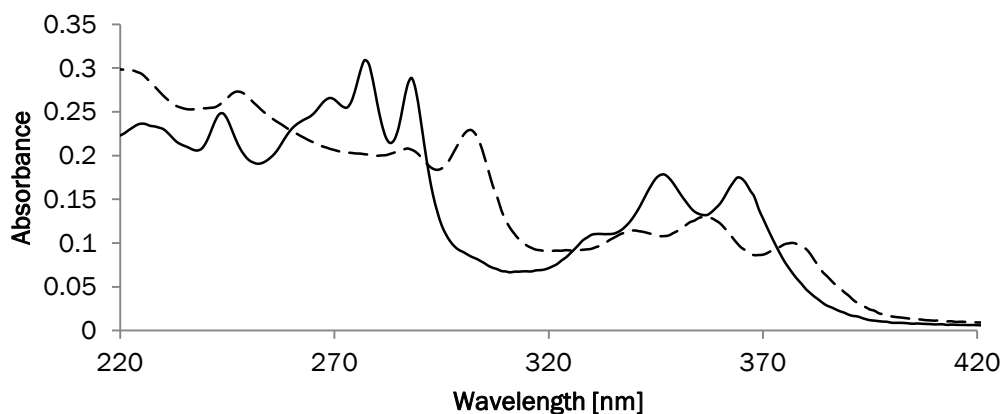
Figure 183: UV-vis spectra of oligomer **1** in ethanol (dashed) and in aqueous medium (solid, 10 mM sodium phosphate buffer pH 7.0, 10 mM NaCl, 30 vol% ethanol), 25 °C.
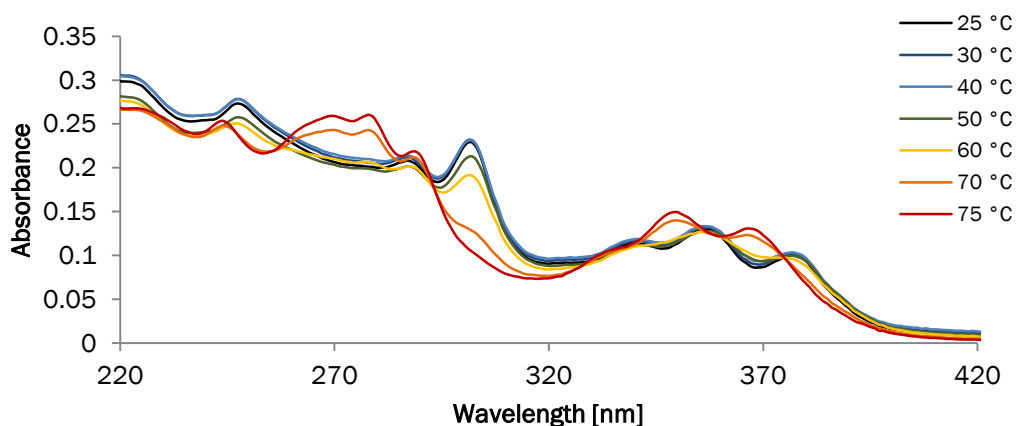
Figure 184: Temperature-dependent UV-vis spectra of oligomer **1** in aqueous medium (10 mM sodium phosphate buffer pH 7.0, 10 mM NaCl, 30 vol% ethanol).

UV-vis cooling curves were recorded to gain insight into the mechanism of the supramolecular polymerization of **1**. The absorbance was measured at three different wavelengths; 301 (J-band), 277 and 366 nm (vibronic bands of the second and first electronic transitions, respectively). The shapes of the curves indicate a cooperative supramolecular polymerization process.[106] This mechanism comprises a nucleation step followed by elongation and is characterised by a sharp bend in the cooling curves.
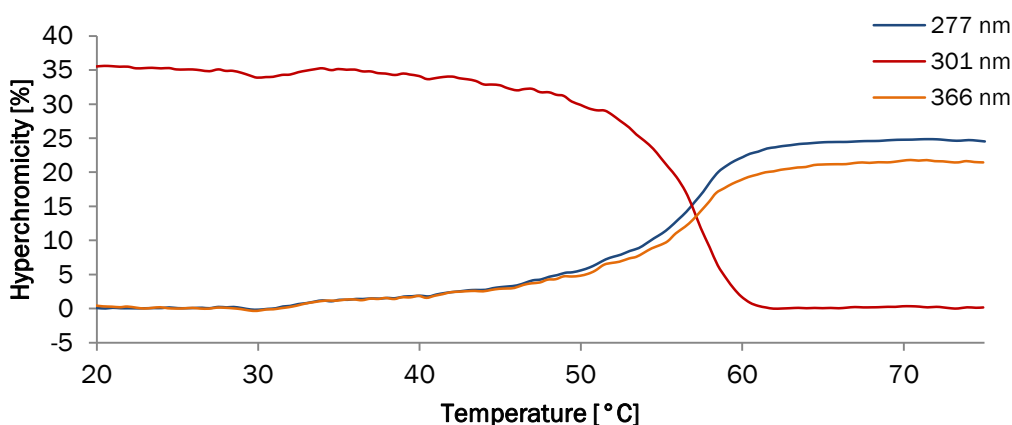

Figure 185: UV-vis cooling curves (0.5 °C/min) of oligomer **1** in aqueous medium (10 mM sodium phosphate buffer pH 7.0, 10 mM NaCl, 30 vol% ethanol), recorded for three wavelengths.

Fluorescence measurements of oligomer **1** in ethanol and in aqueous medium are shown in Figure 186. In ethanol, a strong excimer signal is observed around 450 nm. The excimer emission of two chrysene units in a DNA duplex was found to be centered at 470 nm.[95] However, intrastrand excimer emission was also observed in single strands containing two neighboring chrysenes with the maximal intensity around 450 nm. In aqueous medium the excimer emission has a much lower intensity. This quenching can be explained by the formation of aggregates which hinder the chrysenes to arrange themselves to form excimers. Also weak monomer emission can be discerned as a separate band located at 390 nm. At higher temperatures the emission increases which can be explained by disruption of the aggregates.
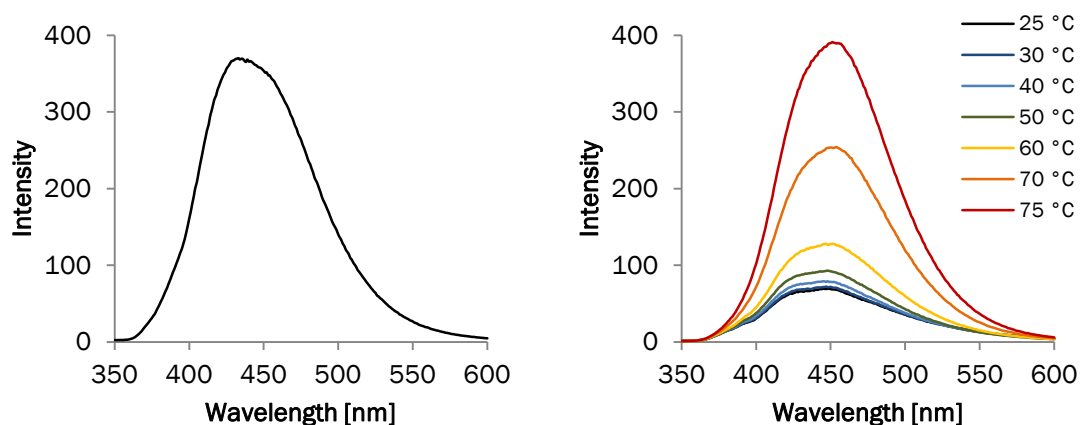
Figure 186: Left: Fluorescence spectrum of oligomer **1** in ethanol, λexc. 347 nm, 25°C. Right: Temperature-dependent fluorescence spectra of oligomer **1** in aqueous medium (10 mM sodium phosphate buffer pH 7.0, 10 mM NaCl, 30 vol% ethanol), λexc. 347 nm.

The photophysical properties of **2** are comparable to the ones of **1**, therefore the data is not shown here. Absorption and fluorescence spectra of oligomers **2**-**4** can be found in the supporting information of this chapter.

Visualization of Chrysene Supramolecular Polymers

A solution of assembled **1** in aqueous medium was deposited on APTES-modified mica. AFM revealed sheet-like structures which are mostly folded (Figure 187). The measured height of one layer is 2 nm, and consequently multiples of 2 nm are observed for the folded parts. The folded structures are usually smaller than 0.5 µm in diameter.
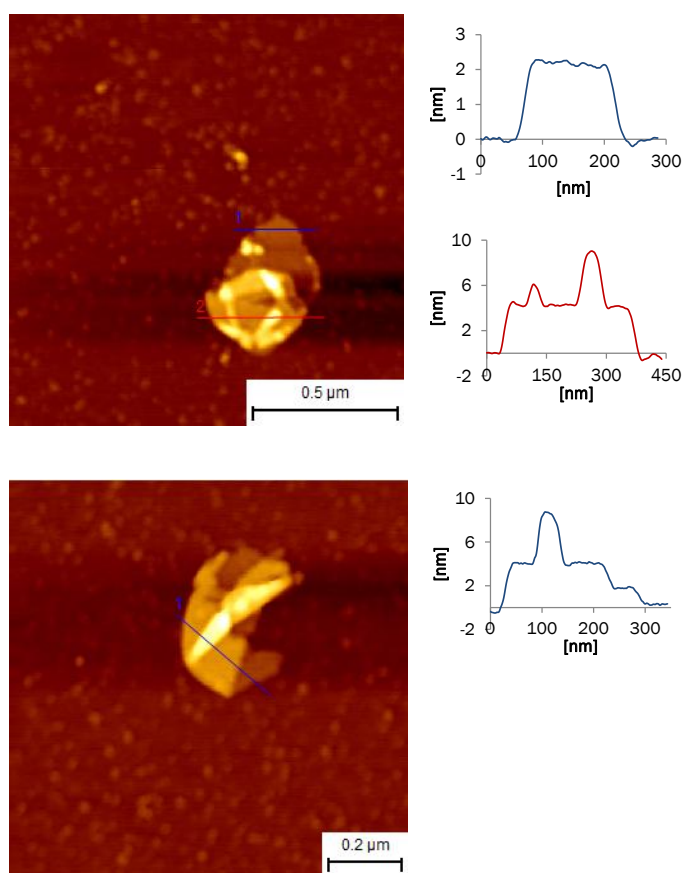
Figure 187: Tapping mode AFM images of **1** deposited on APTES-modified mica after supramolecular polymerization in aqueous medium. Conditions: 1 µM oligomer **1**, 10 mM sodium phosphate buffer pH 7.0, 10 mM NaCl, 30 vol% ethanol).

Co-Assembly of Phenanthrene Sheets with Naphthalimide Acceptors

Fluorescence measurements of oligomer **3** and **4** in ethanol show that in both cases energy is transferred from chrysene to Naphth1 (Figure 188). Samples were excited at 347 nm where solely chrysene absorbs. High emission bands at 530 nm were observed which are characteristic of Naphth1. Chrysene monomer emission (390-460 nm) is only weak; showing that most of the absorbed energy is transferred to the acceptor. In aqueous medium the energy transfer does not work so well anymore (blue and red curves). Measurements were done in the presence of 20 vol% and 2.5 vol% ethanol, showing that higher ethanol content is beneficial for energy transfer. The intensity of chrysene monomer emission is not remarkably influenced by changing the conditions.
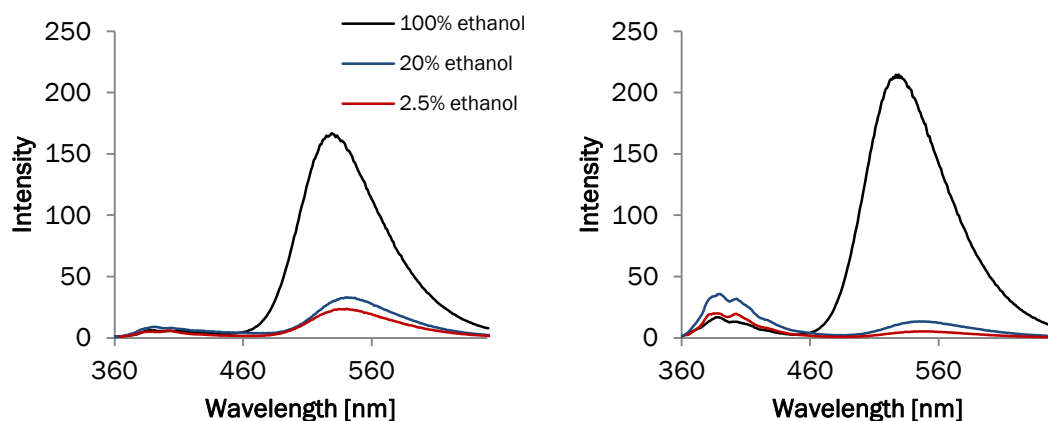
Figure 188: Fluorescence measurements of **3** (left) and **4** (right) with different ethanol contents. Black: only ethanol; blue: 10 mM sodium phosphate buffer pH 7.0, 10 mM NaCl, 20 vol% ethanol; red: 10 mM sodium phosphate buffer pH 7.0, 10 mM NaCl, 2.5 vol% ethanol. Oligomer concentrations: 1 µM; 20°C; λexc. 347 nm.

Both oligomers (**3** and **4**) were co-assembled with **2** to test the light-harvesting properties of chrysene. Naphth1 shows only weak fluorescence in aqueous medium. However, by being incorporated into a hydrophobic chrysene layer the quenching effect could fade. Unfortunately, no such energy transfer was observed in different experiments. Either chrysene supramolecular polymers cannot transfer excitation energy or the emission signal is quenched. Figure 189 shows fluorescence measurements of **3** in aqueous medium before and after the addition of equimolar **2** (sample was heated and cooled again). Both measurements show the same intensity of Naphth1 emission at 530 nm. The addition of **2** just results in an increase of chrysene emission around 400 nm, leading to the perception that there is no interaction between the two oligomers or the dyes.
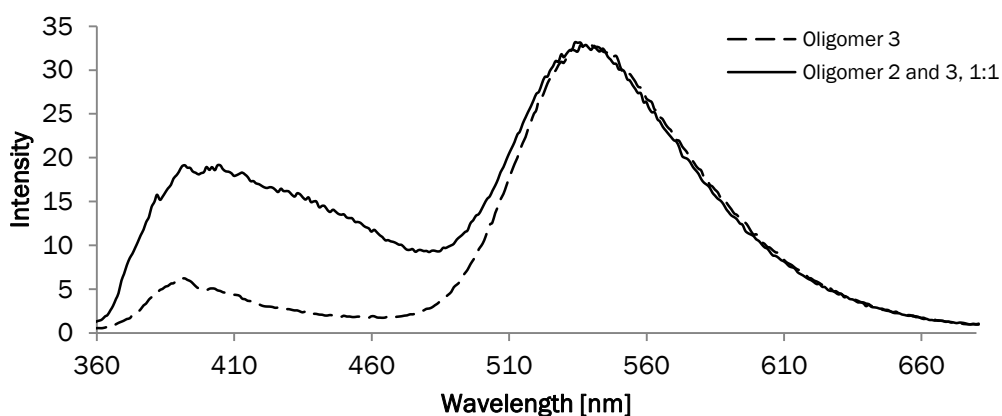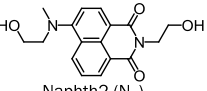
Figure 189: Fluorescence measurement of 1 µM **3** in 10 mM sodium phosphate buffer, 10 mM NaCl, 20 vol% ethanol, before (dashed) and after (solid) the addition of equimolar **2** (reassembled); λexc. 347 nm.

The same finding was observed with oligomer **4**. Figure 190 shows an experiment starting with the fluorescence measurement of assembled **2**, showing chrysene excimer at 450 nm and monomer at 390 nm. Then, oligomer **4** was added. No crucial Naphth1 emission was observed, even after heating and cooling the sample to allow efficient incorporation of the acceptor. Adding up to 1 equimolar **4** just shows the expected additional emission of the acceptor (chrysene monomer and Naphth1). Also here the conclusion is that the acceptor is either not incorporated or the fluorescence signal is mostly quenched.
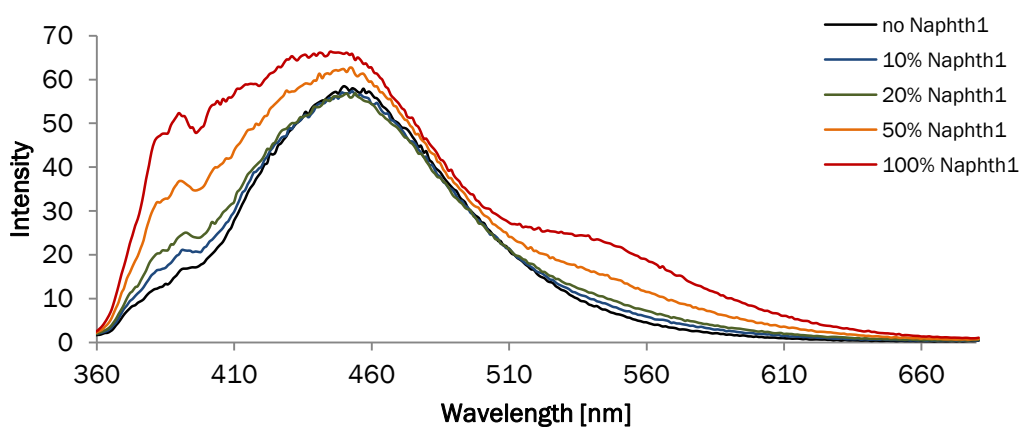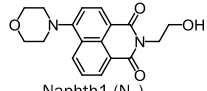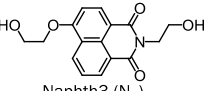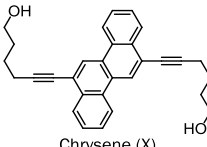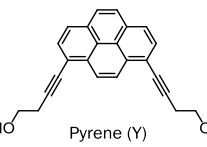
Figure 190: Fluorescence measurement of 1 µM **2** in 10 mM sodium phosphate buffer, 10 mM NaCl, 20 vol% ethanol (black). Oligomer **4** was added according to the index and the sample was reassembled, λexc. 347 nm.

155

DNA Strands Containing Naphthalimide Dyes

Three naphthalimide based dyes were converted into their corresponding phosphoramidites and incorporated into DNA strands to study their properties. Table 13 shows the synthesized DNA strands and the structures of dyes. Naphth1 has only one hydroxyl group and therefore, it can be only attached to the 5' end of a DNA strand. Oligomers **5** and **6** are ten nucleotides shorter than **7-12** but they can still be hybridized with their corresponding counterparts leading duplexes with dangling ends. Naphth2 and Naphth3 can be DMT-monoprotected and then converted into the corresponding phosphoramidites. There are two isomers possible for both dyes, but DMT-protection showed that there is always one isomer preferred, therefore only the main product was used for the phosphitylation and incorporation into DNA.

Table 13: DNA strands with naphthalimide dyes.

Strand	Sequences	Structures of incorporated dyes
5	5' N_1C GAG AGT GCA 3'	
6	3' TCG AGC CAG TN_1 5'	Naphth1 (N_1)
7	5' AGC TCG GTC AN_2C GAG AGT GCA 3'	
8	3' TCG AGC CAG TN_2G CTC TCA CGT 5'	Naphth2 (N_2)
9	5' AGC TCG GTC AN_3C GAG AGT GCA 3'	
10	3' TCG AGC CAG TN_3G CTC TCA CGT 5'	Naphth3 (N_3)

(Complementary strands for energy transfer experiments)

11	5' AGC TCG GTC A**X**C GAG AGT GCA 3' [95]	Chrysene (X)
12	5' AGC TCG GTC A**Y**C GAG AGT GCA 3' [107]	Pyrene (Y)

Photophysical Properties of Naphthalimide Dyes in DNA Strands

UV-vis absorption and fluorescence spectra of single strands **5-10** can be found in the supporting information. All three dyes show only weak emission. Quenching of naphthalimide fluorescence in polar solvents is a well-known phenomenon.[108,109] The observed lower fluorescence quantum yields in polar and H-bonding solvents was explained by specific interactions which result in non radiative decay rates. The fluorescence intensities are even lower when duplexes are formed as shown for **7** and **8** in Figure 191. Naphth2 shows a broad fluorescence with a maximum at 530 nm. The emission of single strand **8** has a lower intensity than **7** which can be accounted for the neighboring guanine base that quenches the emission.[109] The same observation was found for single strands **9** and **10** where the latter with the neighboring guanine base shows lower fluorescence as well; whereas Naphth1 shows the same fluorescence signal in both single strands as none of them has a neighboring guanine base (spectra shown in the supporting information).
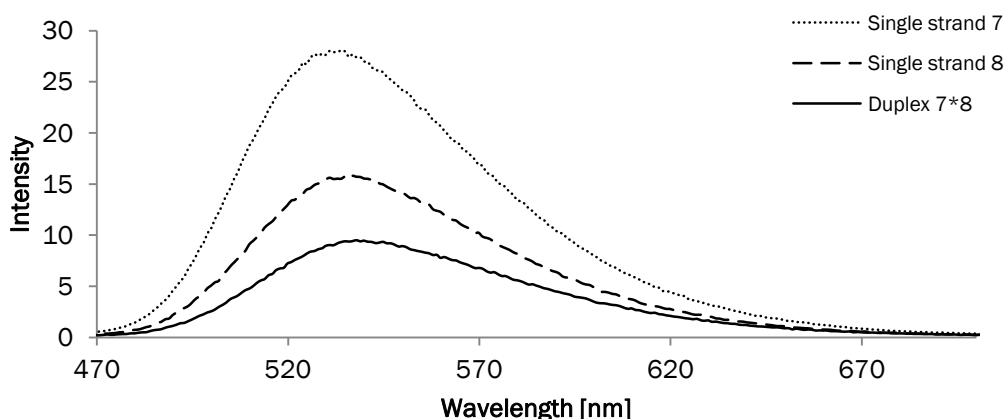
Figure 191: Fluorescence spectra of single strands **7** and **8** and duplex **7*8**. Conditions: 1 µM each strand, 10 mM sodium phosphate buffer pH 7.0, 100 mM NaCl, 20°C, λexc. 455 nm.

Combining Naphthalimide Dyes with Chrysene and Pyrene in DNA Duplexes

Single strands containing Naphth1 (**6**) or Naphth2 (**8**) were hybridized with a complementary strand containing dialkynyl chrysene (**11**) to see if there is energy transfer between those dyes when they are facing each other in a duplex. Fluorescence measurements of **6*11** and **8*11** are shown in Figure 192. Chrysene was excited at 353

nm and in both cases the corresponding naphthalimide emission is observed. Excitation spectra show clearly that the observed naphthalimide emission mainly originates from chrysene. It seems that Naphth2 is a much better acceptor, as the relative intensity is much higher than in the example with Naphth1. Of course, one has to take into account that duplex **6*11** is only "half-hybridized" as single strand **6** is shorter than **11** and therefore the dyes could be less packed together and are more exposed to the solvent. In both duplexes, the same observation is seen when the samples are heated up to dehybridize the strands: Naphthalimide fluorescence gradually decreases, whereas chrysene emission increases.
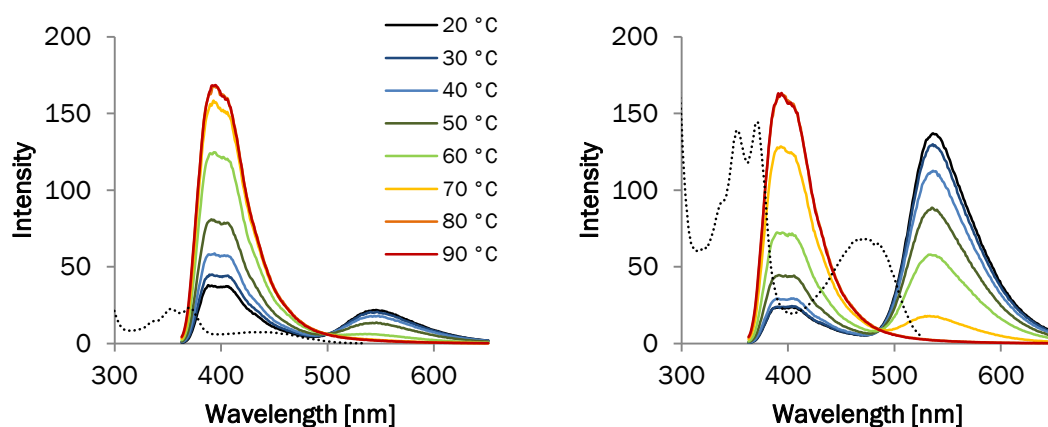
Figure 192: Emission (solid) and excitation (dotted) spectra of duplexes **6*11** (left) and **8*11** (right). Conditions: 1 µM each strand, 10 mM sodium phosphate buffer pH 7.0, 100 mM NaCl, λexc. 353 nm, λem. 545 nm (Naphth1) and 535 nm (Naphth2).

Another observation is that Naphth2 also shows a higher fluorescence signal if it is excited directly in duplex **8*11**. Figure 193 shows the fluorescence spectra of the two strands at 20°C (hybridized) and at 90°C (dehybridized) with excitation wavelength 465 nm where exclusively Naphth2 absorbs. The fluorescence signal is hardly visible at 90°C. Already in Figure 191 it was shown that single strand **8** has a low intensity. However, as soon as the strand hybridizes with **11** the emission is much higher upon excitation of Naphth2. Such a dramatic change in fluorescence intensity is not observed in a duplex with two Naphth2 opposite to each other (Figure 231). Thus, it seems that presence of a hydrophobic chrysene next to Naphth2 is enough to influence the photophysical properties and to increase the fluorescence intensity.
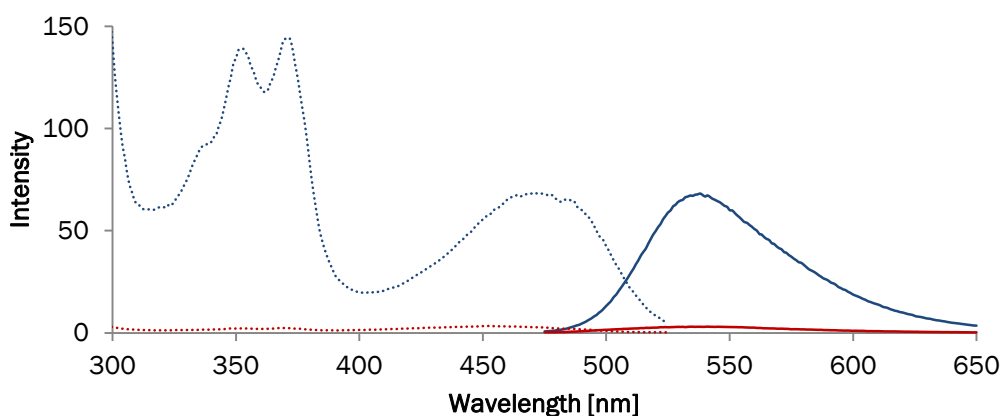
158

Figure 193: Fluorescence (with direct excitation of Naphth2, solid) and excitation (dotted) spectra at 20°C (blue) and 90°C (red) of **8*11**. Conditions: 1 µM each strand, 10 mM sodium phosphate buffer pH 7.0, 100 mM NaCl, λexc. 465 nm, λem. 535 nm.

Also dialkynyl pyrene is able to transfer its excitation energy to Naphth2, as shown in the fluorescence spectrum of duplex **8*12** (Figure 194). Upon exciting pyrene at 370 nm, emission of Naphth2 is observed at 545 nm. The intensity decreases as the sample is heated up, and at the same time the emission of pyrene at 400 nm increases. This duplex is less stable than **8*11**, as the emission of Naphth2 is zero at 70°C whereas in the other example (Figure 192, right) complete dehybridization is at 80°C.
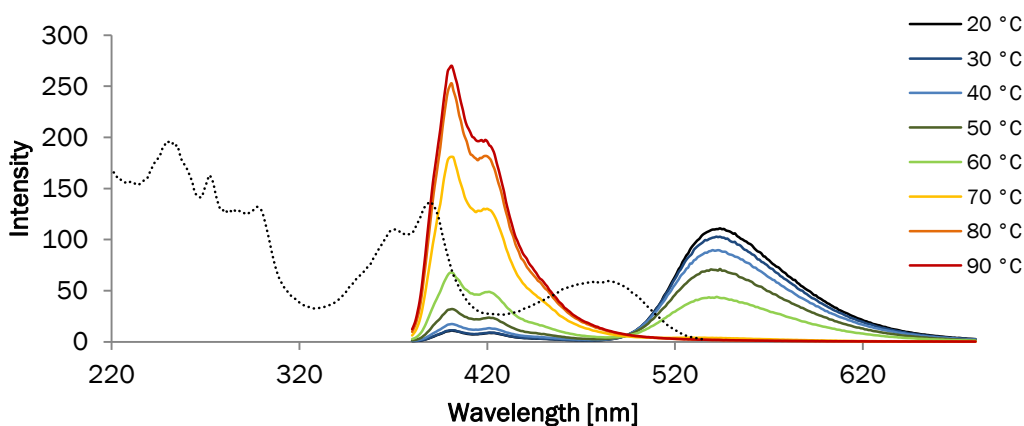
Figure 194: Emission (solid) and excitation (dotted) spectra of duplex **8*12**. Conditions: 1 µM each strand, 10 mM sodium phosphate buffer pH 7.0, 100 mM NaCl, λexc. 370 nm, λem. 545 nm.

159

Conclusion and Outlook

This chapter presented the conversion of chrysene and naphthalimide dyes into phosphoramidites which were used for oligomer synthesis. Short oligomers of chrysene self-assemble into sheet-like supramolecular polymers in aqueous medium via a cooperative nucleation-elongation mechanism. Appearance of a J-band and red-shift of the first electronic transition were observed for trimers composed of chrysenes linked by hexynyl- and by butynyl-linkers, implying that the linker-length does not influence the aggregation behavior in this example. It was tested if the assembled chrysene units can transfer the absorbed energy to a Naphth1 acceptor. Unfortunately, the naphthalimide fluorescence is highly quenched in aqueous medium and/or the acceptor oligomers are not incorporated into the chrysene sheets.

Further, three different naphthalimide dyes were incorporated into DNA strands. Single strands and duplexes containing only naphthalimide dyes showed low fluorescence intensities. Combination of naphthalimide dyes with suitable donors in a duplex can highly improve the fluorescence signal. Chrysene and pyrene show both efficient excitation energy transfer to Naphth2 (and Naphth1 in the case of chrysene) when they are excited. Dehybridization of the duplexes leads to continuous decrease of acceptor fluorescence and at the same time increase of chrysene/pyrene fluorescence.

In conclusion, naphthalimide dyes have potential to be used as acceptors in light-harvesting systems, but it has to be taken into account that the environment of the dyes seems to highly influence their photophysical properties. An interesting characteristic is that DNA strands and duplexes containing naphthalimide dyes show low fluorescence in aqueous medium. In combination with another dye in a duplex, the fluorescence intensity is much improved, regardless if the donor or the acceptor is excited. Therefore, naphthalimide dyes are interesting candidates for the use in DNA based fluorescence probes like molecular beacons where a high signal to noise ratio is to the best advantage. Also their absorption and fluorescence in the visible range would make potential applications more practicable.

Supporting Information
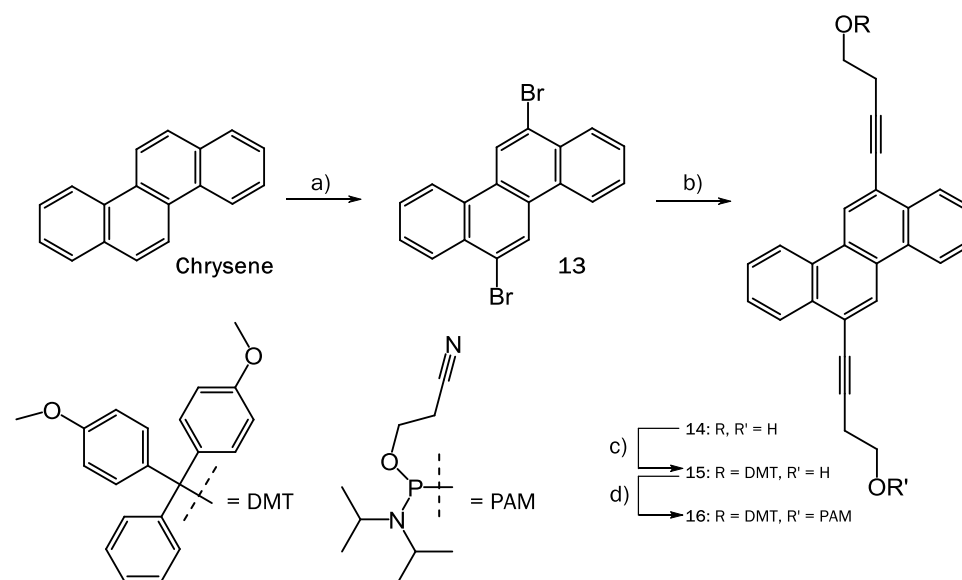
Syntheses of Phosphoramidites

Figure 195: Synthesis of dibutynyl chrysene phosphoramidite. Conditions: a) Br_2, 1,2-dichloroethane, 85°C, 18 h, 84%; b) 5-hexyn-1-ol, Pd[PPh_3]_2Cl_2, CuI, THF/Et_3N (1:1), 80°C, 24 h, 54%; c) DMT-Cl, Et_3N, THF, 24 h, r.t., 24%; d) PAM-Cl, Et_3N, DCM, 7 h, r.t., 65%.

Synthesis of 6,12-dibromochrysene (**13**) was described previously.[110]

Compound 14: Compound **13** (657.9 mg, 1.7 mmol) was dissolved in THF (10 ml) and Et_3N (5 ml). 3-Butyn-1-ol (0.4 ml, 5.28 mmol), CuI (20 mg) and Pd[PPh_3]_2Cl_2 (50 mg) were added. The reaction mixture was stirred under reflux at 80°C for 24 h. The solvent was removed in vacuo and the product was purified by silica gel chromatography (DCM/methanol 99.5:0.5→98:2) to give **14** (337.8 mg, 54%). ^{1}H NMR (300 MHz, CDCl_3): δ 8.89 (s, 2H), 8.76 (dd, J = 7.2, 2.5 Hz, 2H), 8.51-8.48 (m, 2H), 7.75-7.71(m, 4H), 4.00 (t, J = 6.3 Hz, 4H), 2.95 (t, J = 6.3 Hz, 4H).

Compound 15: Compound **14** (170 mg, 0.5 mmol) was dissolved in THF (4 ml) and Et_3N (1 ml). DMT-Cl (159.7 mg, 0.5 mmol) was added in one portion. The reaction mixture was stirred overnight, then the solvent was removed in vacuo and the product was purified by silica gel chromatography (hexane/ethyl acetate/Et_3N 6:4:0.1→5:5:0.1). Compound **15**

was isolated as a white solid (74.1 mg, 24%). ^{1}H NMR (300 MHz, CDCl$_3$): δ 8.87 (d, J = 3.4 Hz, 2H), 8.75-8.71 (m, 2H), 8.56-8.47 (m, 2H), 7.75-7.69 (m, 3H), 7.65-7.56 (m, 3H), 7.47-7.42 (m, 4H), 7.32-7.27 (m, 2H), 7.24-7.21 (m, 1H), 6.86-6.81 (m, 4H), 3.99 (q, J = 6.3 Hz, 2H), 3.76 (s, 6H), 3.45 (t, J = 6.6 Hz, 2H), 2.93 (q, J = 6.5 Hz, 4H).

Compound 16: Compound **15** (602 mg, 0.9 mmol) was dissolved in DCM (7.5 ml) and Et$_3$N (0.5 ml). PAM-Cl (213 mg, 0.9 mmol) was added and the reaction mixture was stirred at r.t. for 7 h. The solvent was removed in vacuo and the product was purified by silica gel chromatography (hexane/ethyl acetate/Et$_3$N 6:4:0.1). Phosphoramidite **16** was isolated as a white solid (506.1 mg, 65%). ^{31}P NMR (125 MHz, DMSO-d$_6$): δ 147.25.

Naphth1 phosphoramidite (17): Naphth1 (104.3 mg, 0.32 mmol) was dissolved in DCM (5 ml) and Et$_3$N (0.2 ml). PAM-Cl (82 mg, 0.35 mmol) was added in one portion. After 3 h of stirring at r.t., the solvent was removed in vacuo. The residue was purified by silica gel chromatography (hexane/ethyl acetate/Et$_3$N 6:4:0.1) to give a yellow solid (131.2 mg, 78%). ^{1}H NMR (300 MHz, DMSO-d$_6$): δ 8.52-8.48 (m, 2H), 8.43 (d, J = 8.1 Hz, 1H); 7.82 (dd, J = 8.2, 7.6 Hz, 1H), 7.37 (d, J = 8.2 Hz, 1H), 4.34-4.24 (m, 2H), 3.93-3.90 (m, 4H), 3.88-3.79 (m, 2H), 3.72-3.58 (m, 2H), 3.53-3.41 (m, 2H), 3.25-3.22 (m, 4H), 2.69 (t, J = 6.0 Hz, 2H), 1.02 (dd, J = 17.5, 6.8 Hz, 12H). ^{31}P NMR (121.5 MHz, DMSO-d$_6$): δ 147.26.

DMT-monoprotected Naphth2 (18 and 19): Naphth2 (90.2 mg, 0.29 mmol) was dissolved in DMF (5 ml) and Et$_3$N (0.2 ml) and DMT-Cl (97.4 mg, 0.29 mmol) was added in one portion. The reaction mixture was stirred at r.t. for 20 h. The solvent was removed in vacuo and the residue was purified by silica gel chromatography (hexane/ethyl acetate/Et$_3$N 45:55:1→35:65:1, stepwise gradient) to give **18** (75.8 mg, 43%) and **19** (62.4 mg, 35%) as orange solids. Analytical data for **18**: ^{1}H NMR (300 MHz, DMSO-d$_6$): δ 8.76 (d, J = 8.3 Hz, 1H), 8.51 (d, J = 7.2 Hz, 1H), 8.35 (d, J = 8.3 Hz, 1H), 7.78 (dd, J = 8.3, 7.5 Hz, 1H), 7.28-7.21 (m, 6H), 7.1 (d, J = 8.9 Hz, 4H), 6.81 (d, J = 8.9 Hz, 4H), 4.83 (t, J = 5.9 Hz, 1H), 4.17 (t, J = 6.6 Hz, 2H), 3.72 (s, 6H), 3.67-3.59 (m, 4H), 3.25 (t, J = 4.5, 2H), 2.95 (s, 3H). Analytical data for **19**: ^{1}H NMR (300 MHz, DMSO-d$_6$): δ 8.76 (dd, J = 8.5, 0.9 Hz, 1H), 8.48 (dd, J = 7.2, 0.8 Hz, 1H), 8.37 (d, J = 8.3 Hz, 1H), 7.77 (dd, J = 8.4, 7.4 Hz, 1H), 7.33-2.26 (m, 3H), 7.15-7.12 (m, 7H), 6.70 (d, J = 8.9 Hz, 4H), 4.88 (t, J = 5.4 Hz, 1H), 4.37-4.33 (m, 4H), 3.78 (q, J = 5.6 Hz, 2H), 3.67 (s, 6H), 3.22 (t, J = 5.4 Hz, 2H), 3.09 (s, 3H).

Naphth2 phosphoramidite (20): Compound **18** (75.8 mg, 0.12 mmol) was dissolved in DCM (4 ml) and Et$_3$N (0.1 ml), then PAM-Cl (35.6 mg, 0.15 mmol) was added. After stirring at r.t. for 3 h, the solvent was removed in vacuo and the product was purified by silica gel chromatography (hexane/ ethyl acetate/Et$_3$N 6:4:0.1). Phosphoramidite **20** was isolated as

a yellow solid (75.1 mg, 75%). ^{1}H NMR (300 MHz, DMSO-d$_6$): δ 8.76 (dd, J = 8.4, 0.6 Hz, 1H), 8.51 (d, J = 7.2 Hz, 1H), 8.36 (d, J = 8.3 Hz, 1H), 7.78 (dd, J = 8.3, 7.5 Hz, 1H), 7.28-7.18 (m, 6H), 7.11 (d, J = 8.8 Hz, 4H), 6.81 (d, J = 8.9 Hz, 4H), 3.91-3.74 (m, 4H), 3.72 (s, 6H), 3.69-3.57 (m, 4H), 3.55-3.42 (m, 2H), 3.26 (t, J = 4.4 Hz, 2H), 2.96 (s, 3H), 2.7 (t, J = 6.0 Hz, 2H), 1.02 (dd, J = 14.5, 6.7 Hz, 12 H). ^{31}P NMR (121.5 MHz, DMSO-d$_6$): δ 147.31.

DMT-monoprotected Naphth3 (21 and 22): Naphth3 (95.1 mg, 0.32 mmol) was dissolved in DMF (4 ml) and Et$_3$N (0.2 ml). DMT-Cl (106.7 mg, 0.31 mmol) was added in one portion and the reaction mixture was stirred at r.t. for 18 h. The solvent was removed in vacuo and the residue was purified by silica gel chromatography (hexane/ethyl acetate/Et$_3$N 45:55:1→3:7:0.1, stepwise gradient) and furnished **21** (48.2 mg, 25%) and **22** (88.5 mg, 47%) as yellowish solids. Analytical data for **21**: ^{1}H NMR (300 MHz, DMSO-d$_6$): δ 8.61-8.54 (m, 2H), 8.47 (d, J = 8.2 Hz, 1H), 7.94-7.91 (m, 1H), 7.46-7.23 (m, 10H), 6.87 (d, J = 8.9 Hz, 4H), 4.82 (t, J = 6.0 Hz, 1H), 4.60-4.56 (m, 2H), 4.16 (t, J = 6.6 Hz, 2H), 3.73 (s, 6H), 3.63 (q, J = 6.6 Hz, 2H), 3.49-3.46 (m, 2H). Analytical data for **22**: ^{1}H NMR (300 MHz, DMSO-d$_6$): δ 8.71 (dd, J = 8.4, 1.1 Hz, 1H), 8.53 (dd, J = 7.3, 1.1 Hz, 1H), 8.48 (d, J = 8.3 Hz, 1H), 7.87 (dd, J = 8.3, 7.4 Hz, 1H), 7.36 (d, J = 8.4 Hz, 1H), 7.29-7.26 (m, 2H), 7.14 – 7.12 (m, 7H), 6.70 (d, J = 8.9 Hz, 4H), 5.11 (t, J = 5.8 Hz, 1H), 4.38-4.33 (m, 4H), 3.94-3.89 (m, 2H), 3.67 (s, 6H), 3.24 (t, J = 5.9 Hz, 2H).

Naphth3 phosphoramidite (23): Compound **22** (88.5 mg, 0.15 mmol) was dissolved in DCM (4 ml) and Et$_3$N (0.2 ml). PAM-Cl (40.2 mg, 0.17 mmol) was added and the reaction mixture was stirred at r.t. for 18 h. The solvent was removed in vacuo and the product was purified by silica gel chromatography (hexane/ethyl acetate/Et$_3$N 6:4:0.1). Phosphoramidite **23** was isolated as a colorless solid (55.8 mg, 47%). ^{1}H NMR (300 MHz, DMSO-d$_6$): δ 8.62 (dd, J = 8.4, 1.0 Hz, 1H), 8.53 (dd, J = 7.3, 1.0 Hz, 1H), 8.48 (d, J = 8.3 Hz, 1H), 7.87 (dd, J = 8.3, 7.5 Hz, 1H), 7.39 (d, J = 8.4 Hz, 1H), 7.29-7.25 (m, 2H), 7.14-7.11 (m, 7H), 6.70 (d, J = 8.9 Hz, 4H), 4.35 (t, J = 5.5 Hz, 2H), 3.83-3.71 (m, 4H), 3.67 (s, 6H), 3.64-3.54 (m, 4H), 3.25 (t, J = 5.5 Hz, 2H), 2.75 (t, J = 5.9 Hz, 2H), 1.15-1.08 (m, 12H). ^{31}P NMR (121.5 MHz, DMSO-d$_6$): δ 148.26 and 147.63.

NMR Spectra
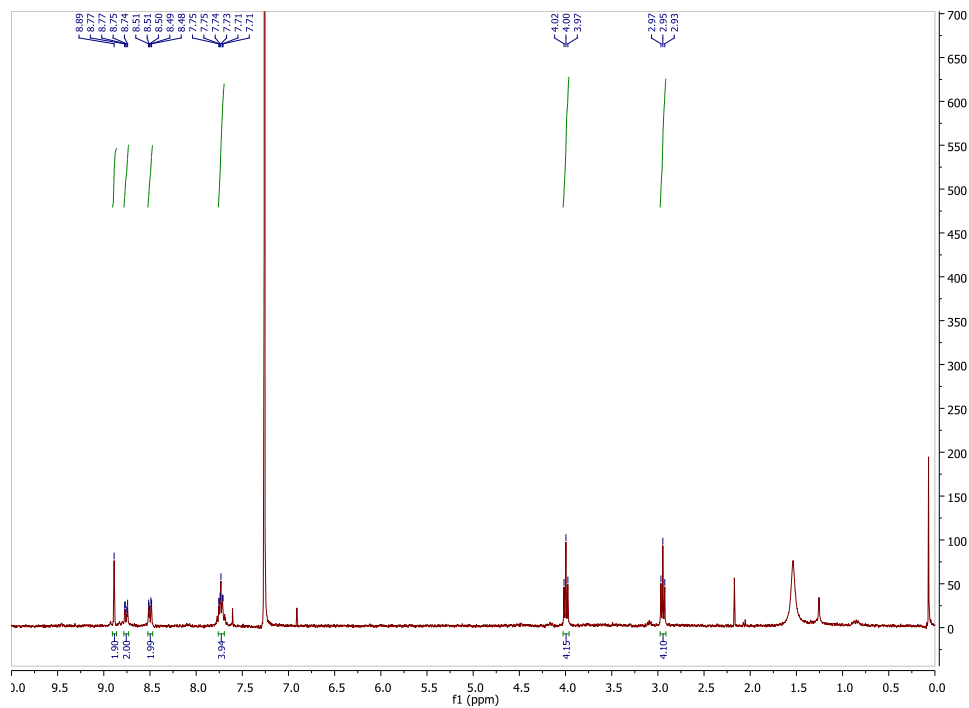
Figure 196: ^{1}H NMR of compound **14** in CDCl$_3$.
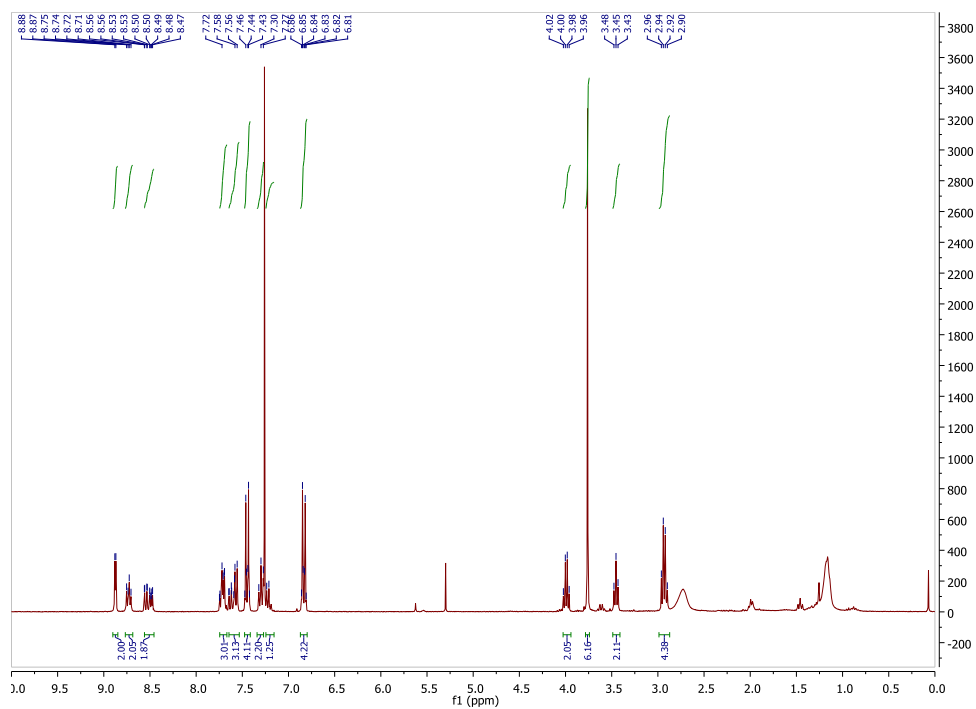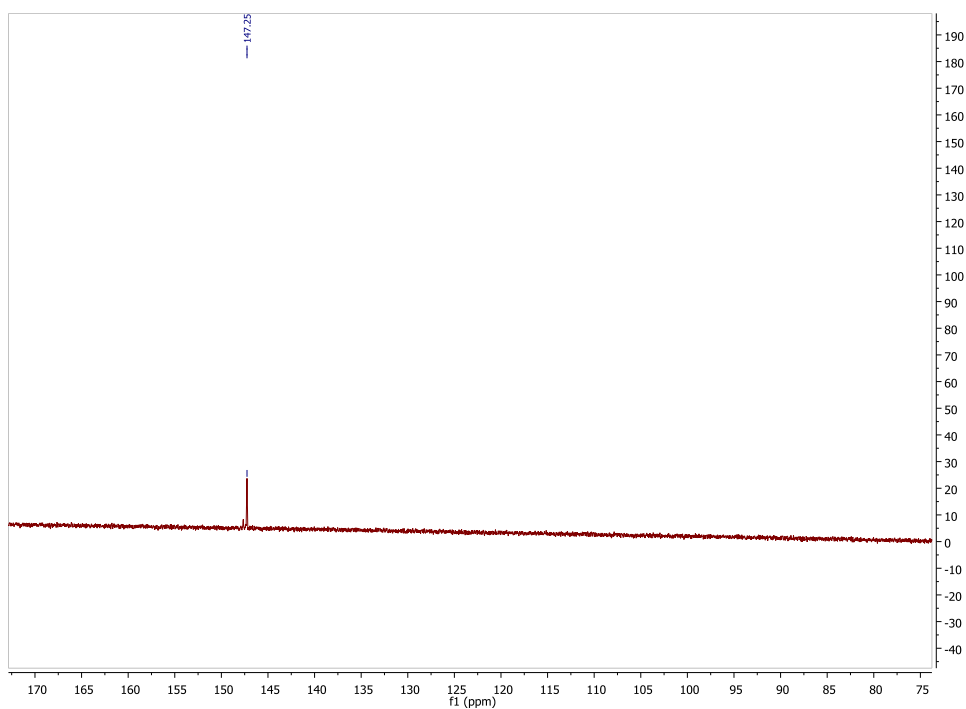

Figure 197: ^{1}H NMR of compound **15** in CDCl$_3$.
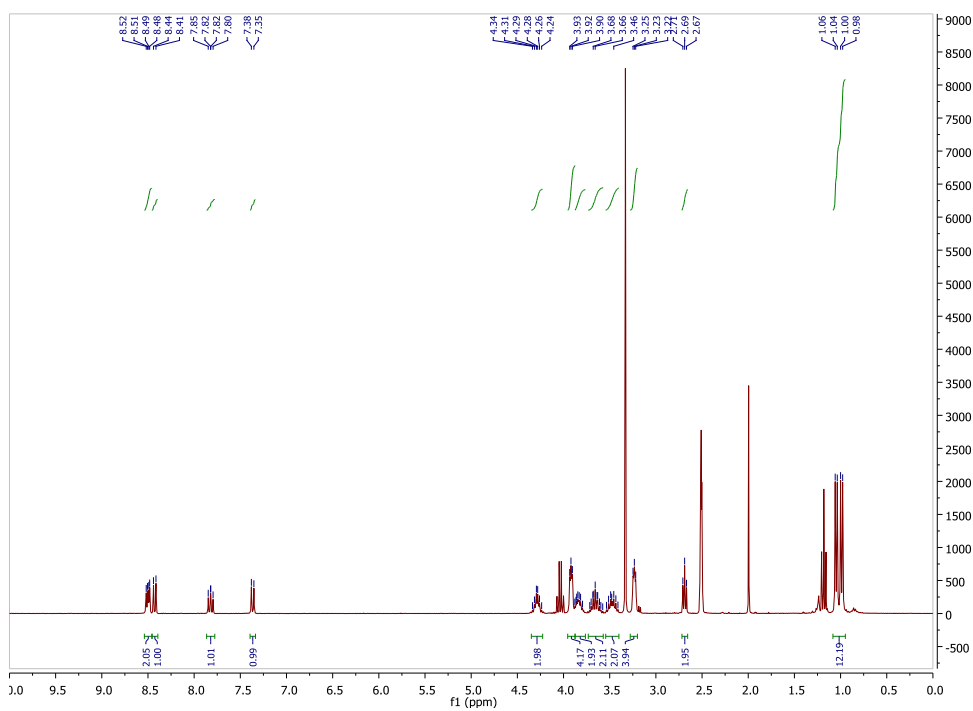
Figure 198: ^{31}P NMR of compound **16** in DMSO-d$_6$.
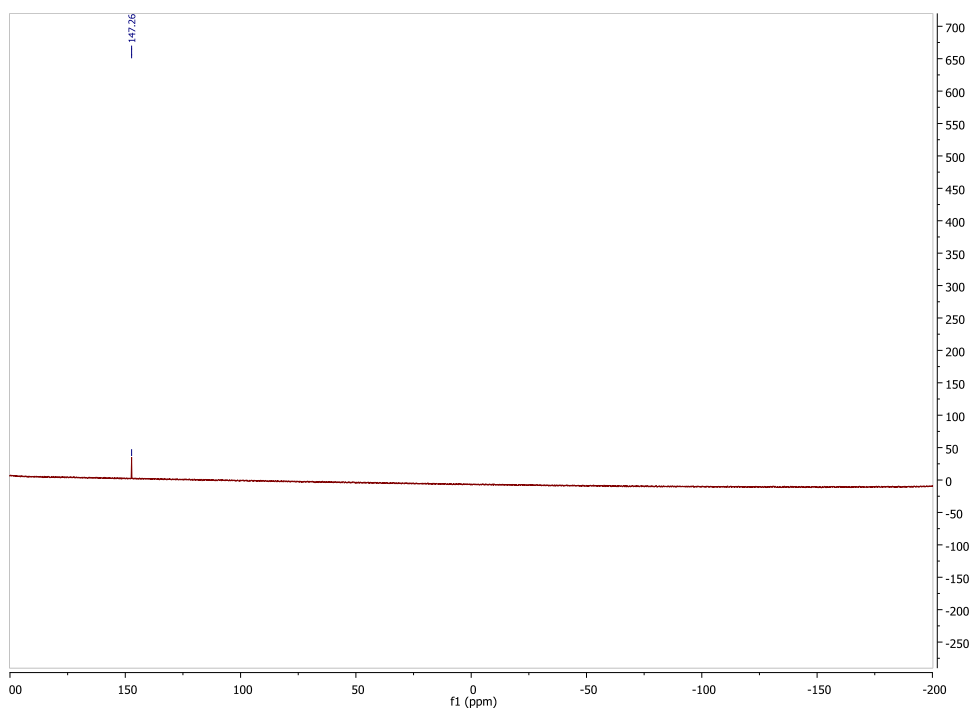

Figure 199: ^{1}H NMR of compound **17** in DMSO-d$_6$.
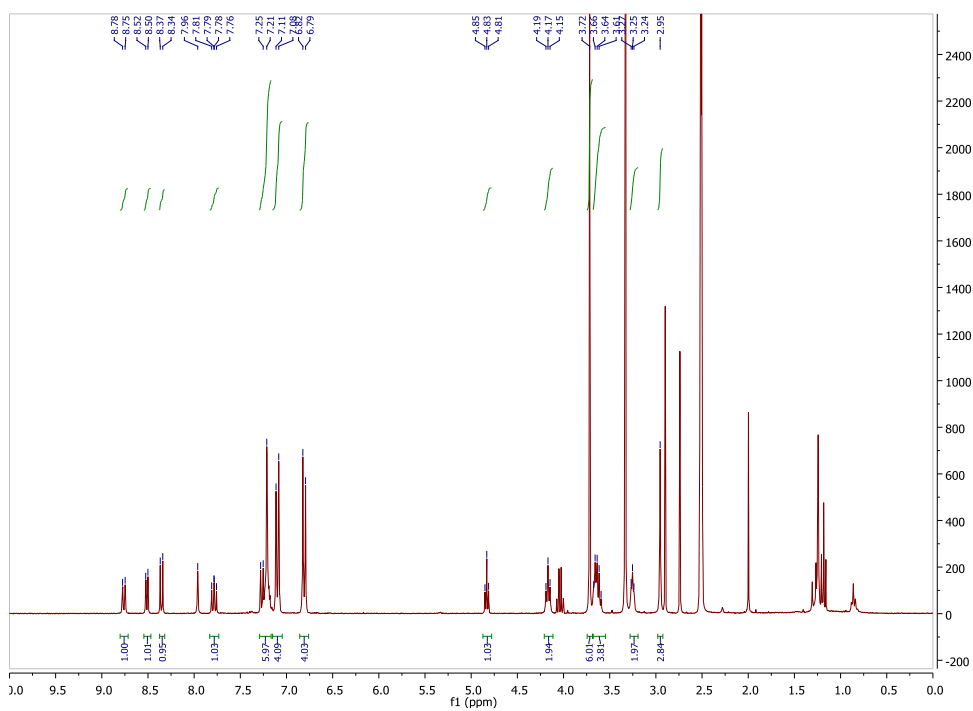
Figure 200: ^{31}P NMR of compound **17** in DMSO-d$_6$.
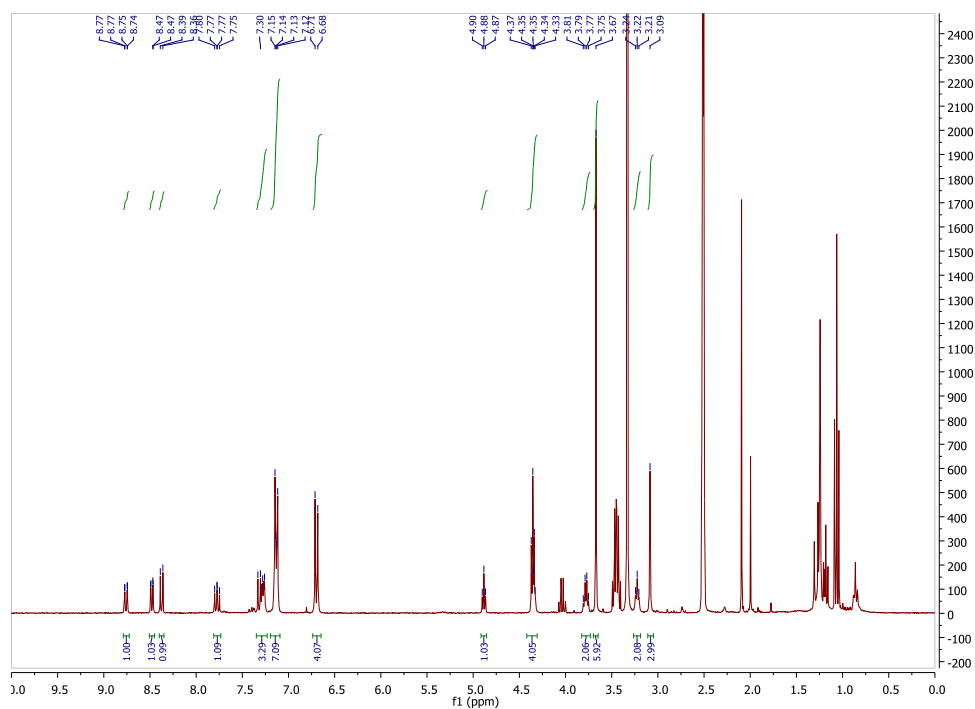

Figure 201: ^{1}H NMR of compound **18** in DMSO-d$_6$.
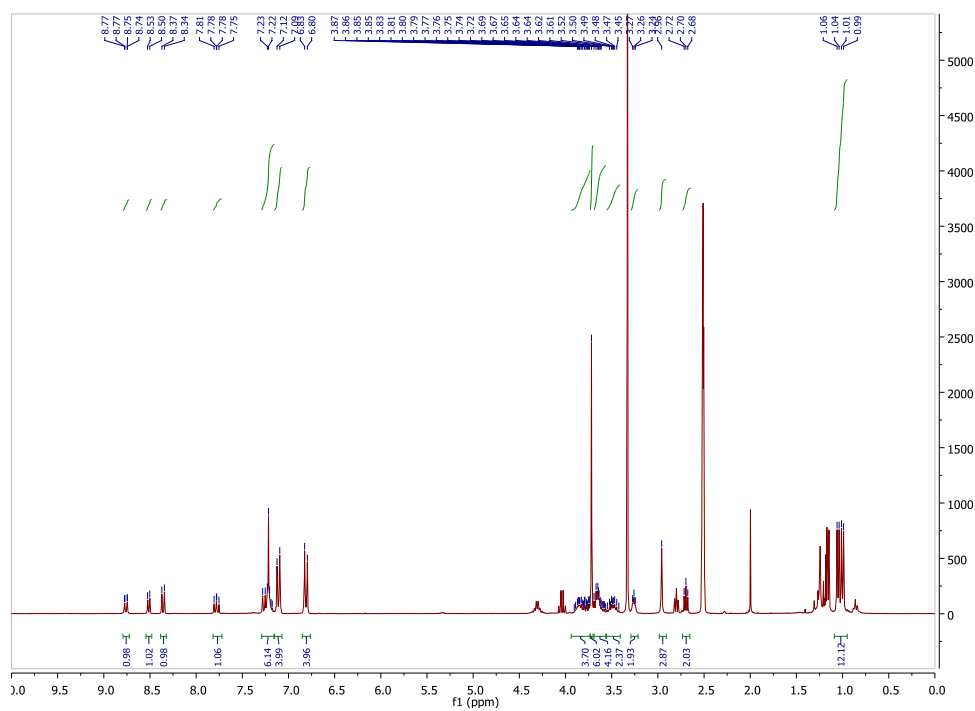
Figure 202: ^{1}H NMR of compound **19** in DMSO-d$_6$.
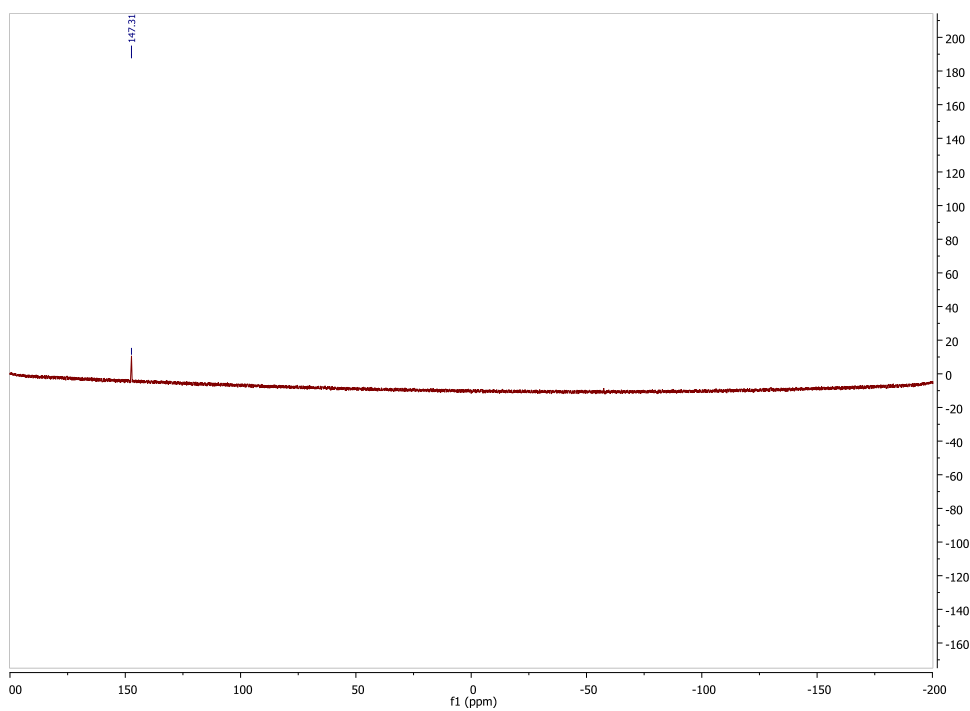

Figure 203: ^{1}H NMR of compound **20** in DMSO-d$_6$.

Figure 204: ^{31}P NMR of compound **20** in DMSO-d$_6$.
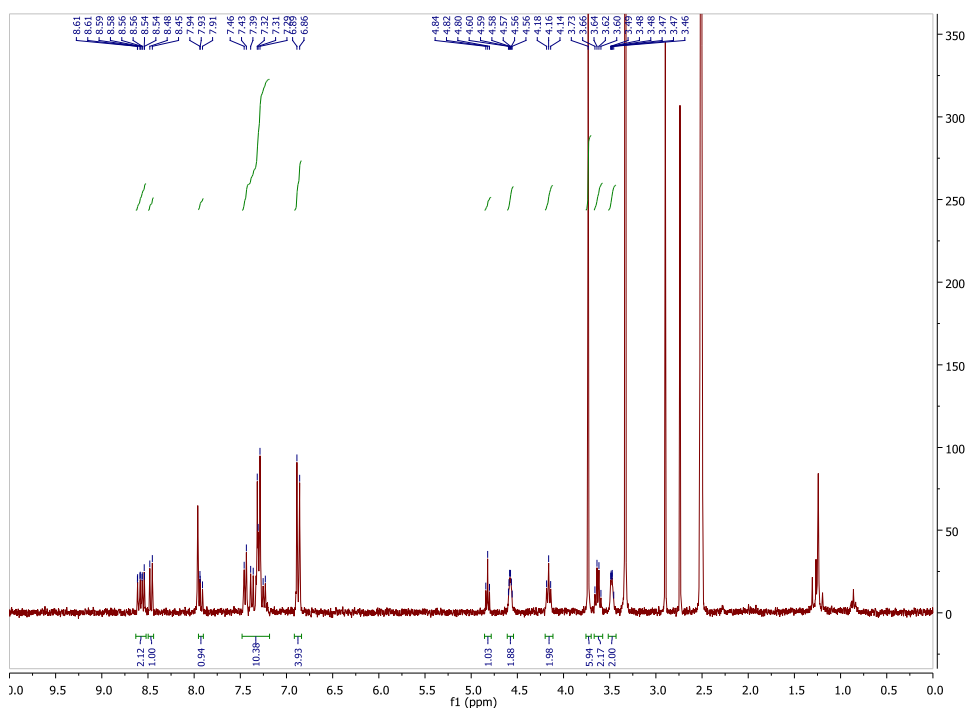
Figure 205: ^{1}H NMR of compound **21** in DMSO-d$_6$.
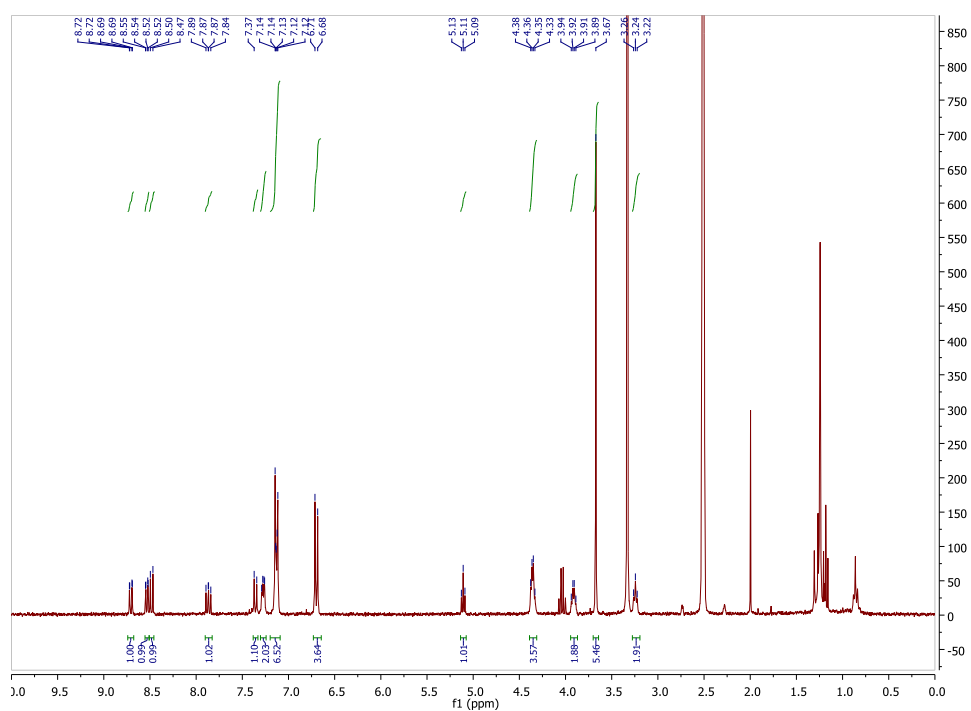
Figure 206: ¹H NMR of compound **22** in DMSO-d₆.
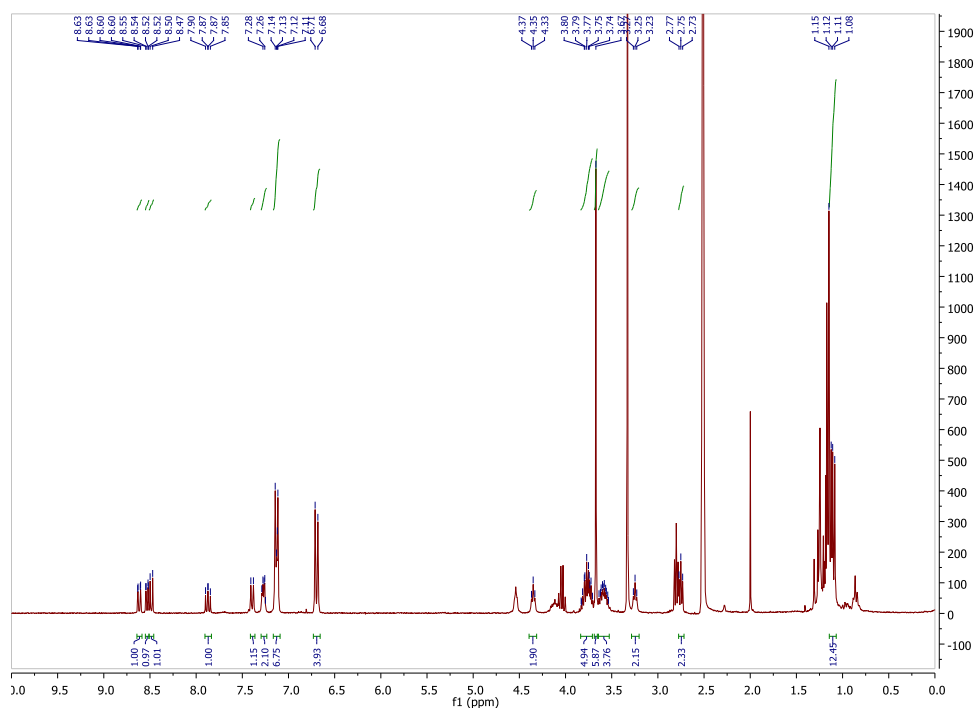
Figure 207: ¹H NMR of compound **23** in DMSO-d₆.
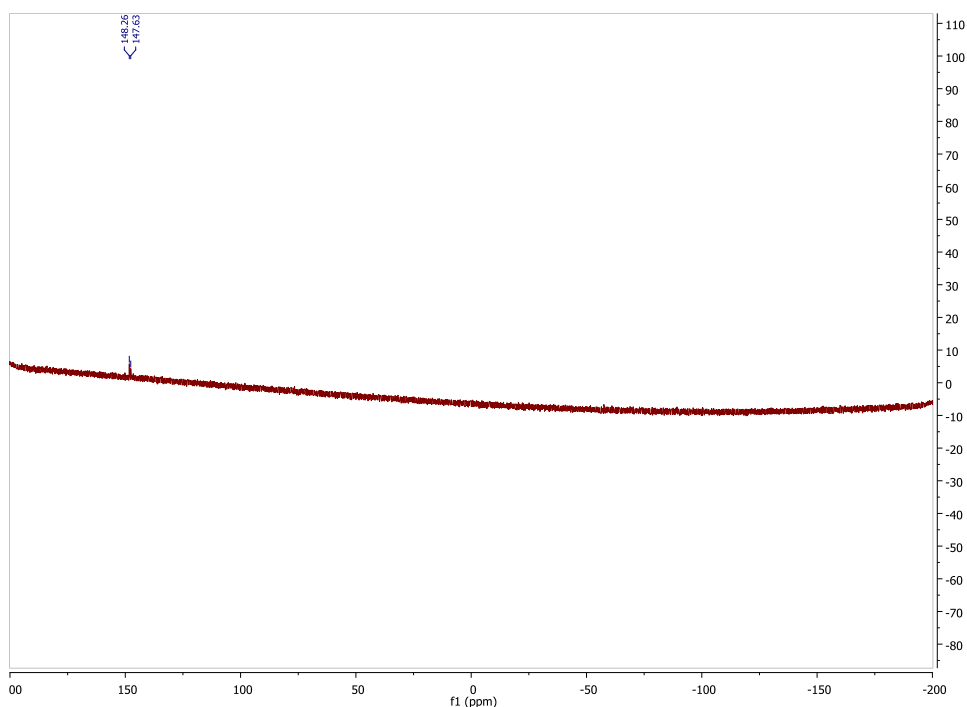
Figure 208: ^{31}P NMR of compound **23** in DMSO-d$_6$.

Oligomer Synthesis and Purification

Oligomers **1-10** were synthesized on a DNA synthesizer using Universal Support III (polystyrene) for **1-4** or nucleoside-loaded support (CPG) for **5-10**. After successful coupling, the oligomers were cleaved from the solid supports by adding 0.8 ml of 2M NH$_3$ in methanol (**1-4**) or 28-30% NH$_3$ in H$_2$O (**5-10**) in a vial, followed by incubation overnight at 55°C. The supernatants were collected and the solid supports were washed three times with ethanol/H$_2$O 1:1. The collected supernatants were lyophilized. Purification of **1-4**: The residues were redissolved in 0.1 M triethylammonium acetate/acetonitrile 1:1. The oligomers were purified by RP-HPLC (Merck LiChroCART 250-4; LiChrospher 100, RP-8, 5 µm); Solvent A: 0.1 M aqueous triethylammonium acetate; Solvent B: CH$_3$CN; 1 ml/min; T = 50°C; B[%] (tR [min]) = 50 (0); 50 (2); 80 (22). Purification of **5-10**: The residues were redissolved in 0.1 M triethylammonium acetate. The oligomers were purified by RP-HPLC (Merck LiChroCART 250-4; LiChrospher 100, RP-18, 5 µm); Solvent A: 0.1 M aqueous triethylammonium acetate; Solvent B: CH$_3$CN; 1 ml/min; T = 40°C; B[%] (tR [min]) = 0 (0); 5 (2); 50 (22). Purities were confirmed by mass spectrometry.

Table 14: Calculated and found masses (negative ion mode) of oligomers.

	Chemical Formula	Calculated mass	Found mass
1	$C_{90}H_{82}O_{10}P_2$	1384.54	691.26 (z=2)
2	$C_{78}H_{58}O_{10}P_2$	1216.35	607.17 (z=2)
3	$C_{70}H_{56}N_2O_{12}P_2$	1178.33	588.16 (z=2)
4	$C_{44}H_{37}N_2O_8P$	752.23	751.22 (z=1)
5	$C_{116}H_{139}N_{45}O_{62}P_{10}$	3465.39	1153.87 (z=3)
6	$C_{115}H_{140}N_{40}O_{64}P_{10}$	3416.35	1137.53 (z=3)
7	$C_{212}H_{261}N_{83}O_{122}P_{20}$	6543.37	653.21 (z=10)
8	$C_{210}H_{263}N_{73}O_{126}P_{20}$	6445.29	643.40 (z=10)
9	$C_{211}H_{258}N_{82}O_{123}P_{20}$	6530.32	651.90 (z=10)
10	$C_{209}H_{260}N_{72}O_{127}P_{20}$	6432.24	642.20 (z=10)

Mass Spectra of Oligomers
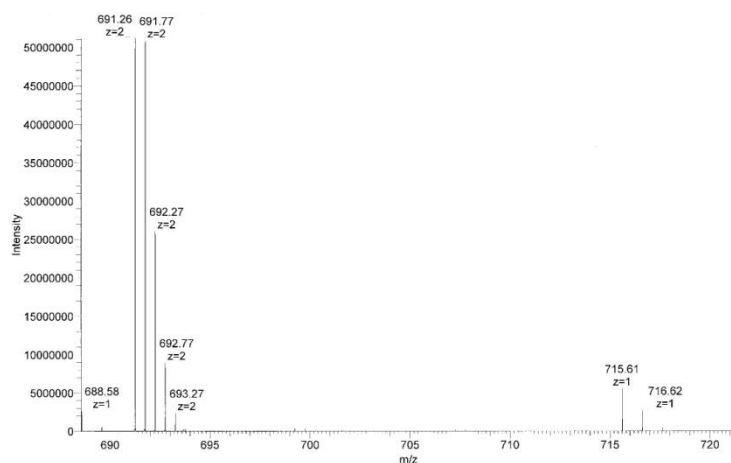
Figure 209: Mass spectrum of **1**.
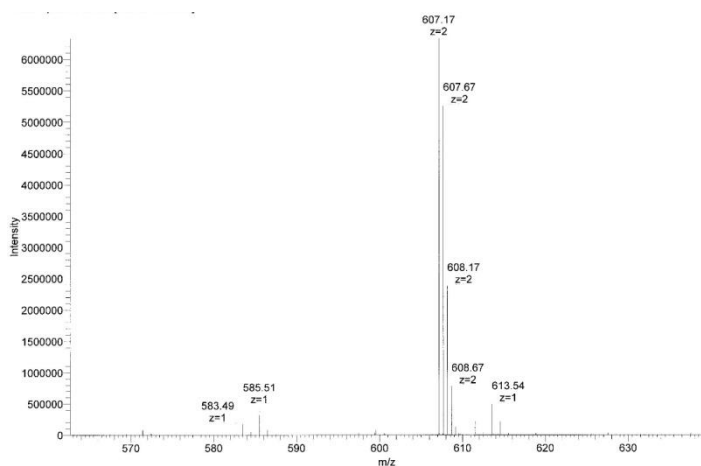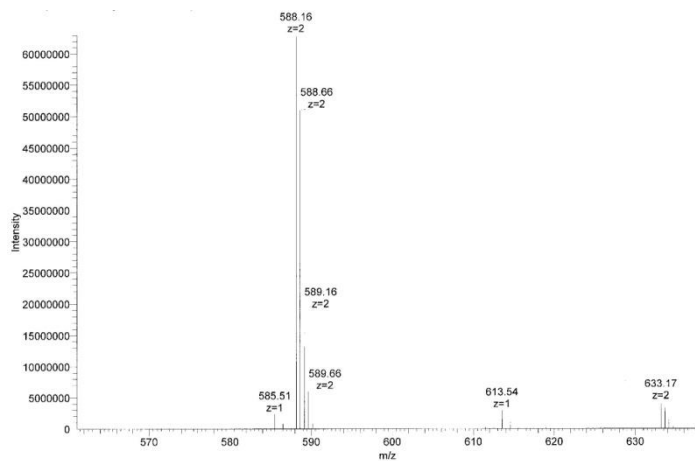
Figure 210: Mass spectrum of **2**.
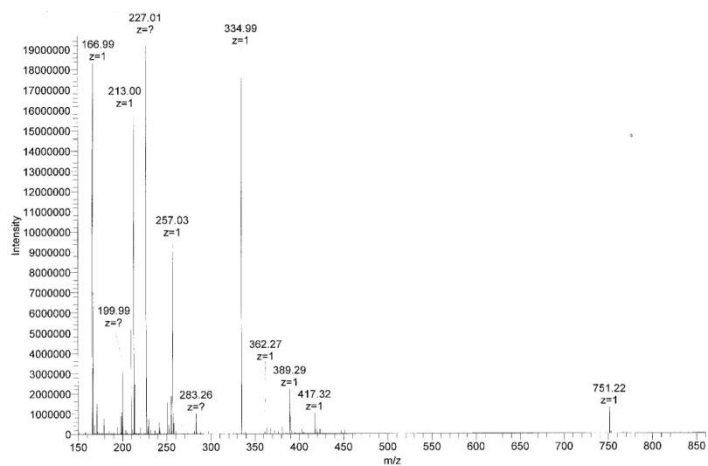

Figure 211: Mass spectrum of **3**.

Figure 212: Mass spectrum of **4**.

Figure 213: Mass spectrum of **5**.

Figure 214: Mass spectrum of **6**.

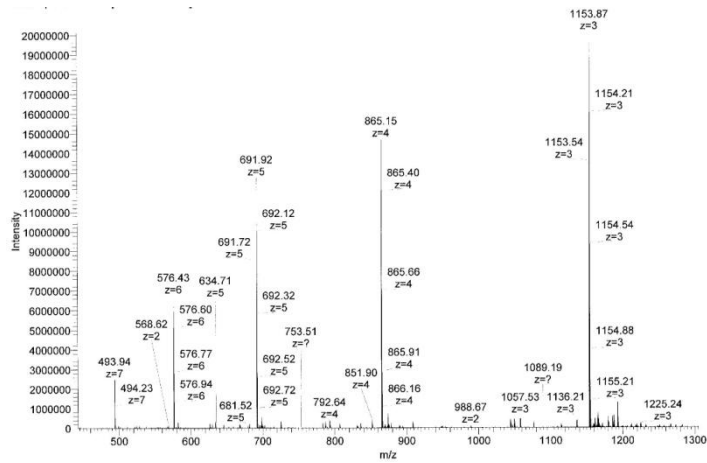Figure 215: Mass spectrum of **7**.
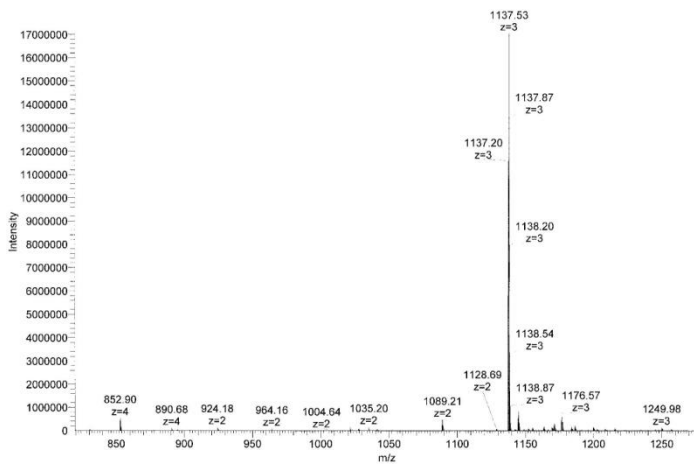
Figure 216: Mass spectrum of **8**.
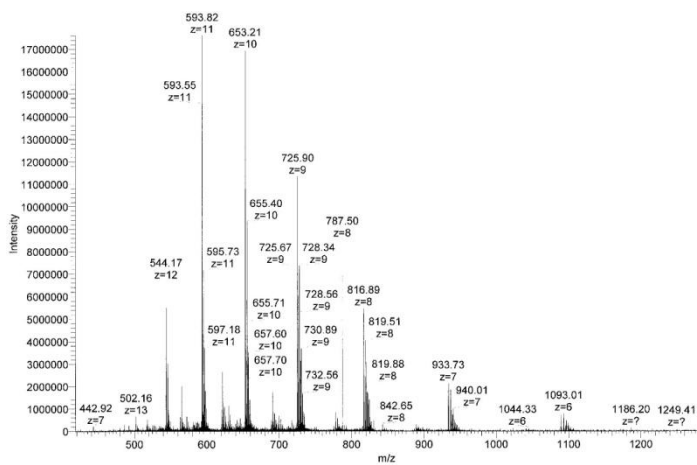

Figure 217: Mass spectrum of **9**.

Figure 218: Mass spectrum of **10**.

Photophysical Properties of Oligomer 2

The absorption spectra of **2** (Figure 219 and Figure 220) look similar to the ones of **1**. In ethanol the ratio of vibronic bands $S_1^{0 \to 1}/S_1^{0 \to 1}$ is 0.84. By changing the solvent to buffer/ethanol 8:2 this ratio decreases to 0.72 due to aggregation. Further observations are a red-shift for the S_1 transition and the appearance of a new band at 301 nm (J-band, see Figure 183). It is possible to disrupt those aggregates by heating the solution. At temperatures above 50°C the spectrum looks similar to the one measured in ethanol.
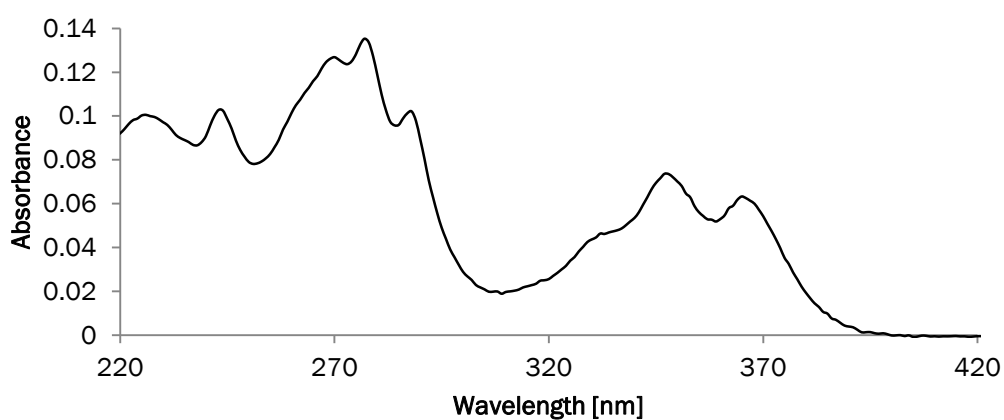

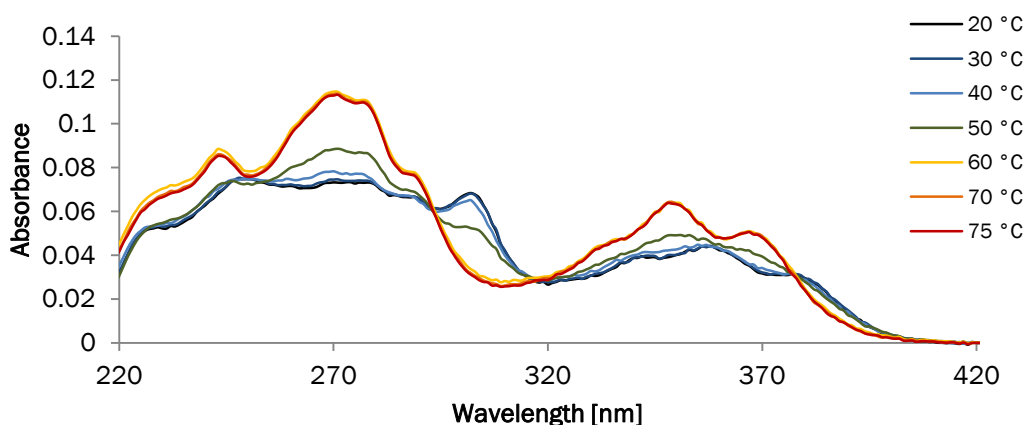Figure 219: UV-vis spectrum of **2**, 1 μM in ethanol, 20°C.

Figure 220: Temperature-dependent UV-vis spectra of **2**, 1 μM in 10 mM sodium phosphate buffer, 100 mM NaCl, 20 vol% ethanol.

175

The fluorescence spectrum of **2** in ethanol shows excimer emission around 450 nm (Figure 221). At higher temperatures the emission decreases to about 25% of the original intensity and a slight blue-shift of the emission band is observed. Also in aqueous medium an excimer emission is observed around 450 nm but with much less intensity in the assembled state (Figure 222).
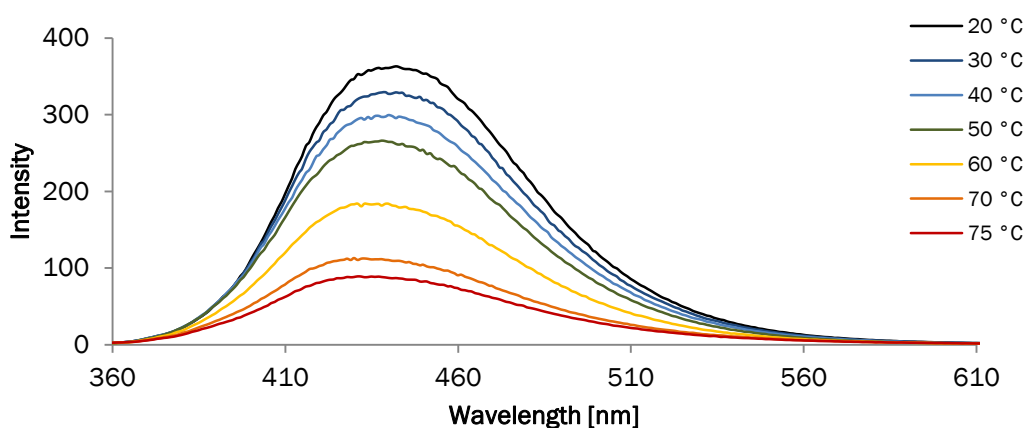

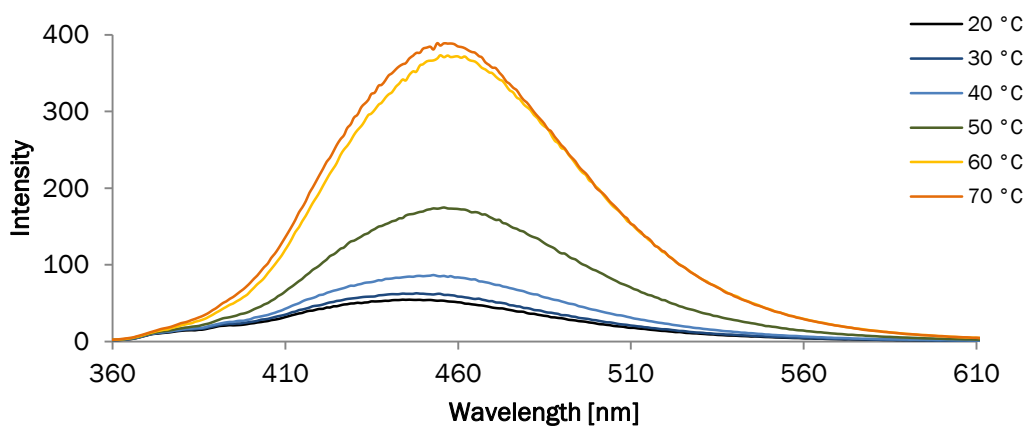Figure 221: Temperature-dependent fluorescence spectra of **2**, 1 µM in ethanol, λexc. 347 nm.

Figure 222: Temperature-dependent fluorescence spectra of **2**, 1 µM in 10 mM sodium phosphate buffer pH 7.0, 100 mM NaCl, 20 vol% ethanol, λexc. 347 nm.

AFM Measurements

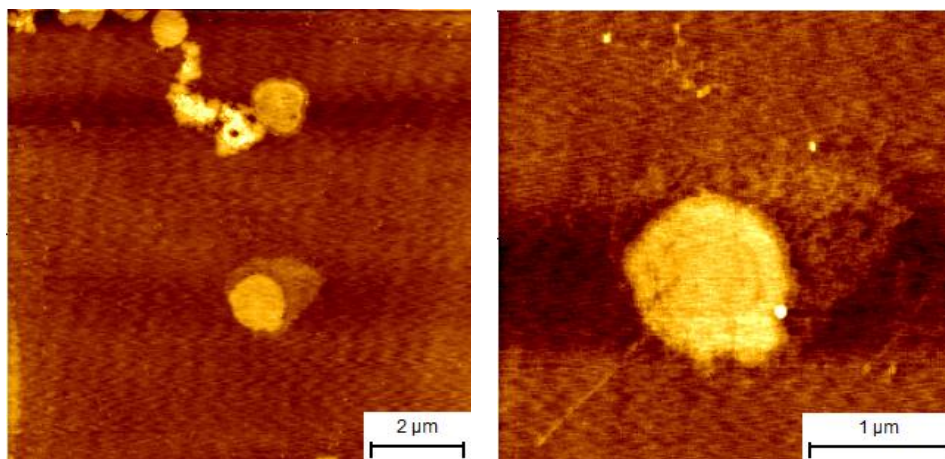Preparation of AFM samples were done as described in Chapter 1.

Figure 223: Tapping mode AFM images of oligomer **2** deposited on mica from an aqueous solution containing NiCl$_2$ as binding agent.
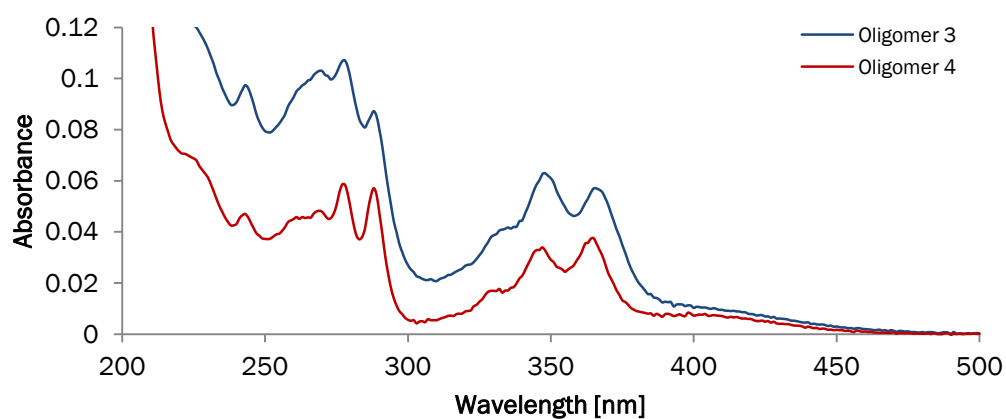
UV-vis Absorption Spectra of Oligomers 3 and 4

Figure 224: Absorption spectra of **3** and **4** in ethanol; concentrations: 1 µM.
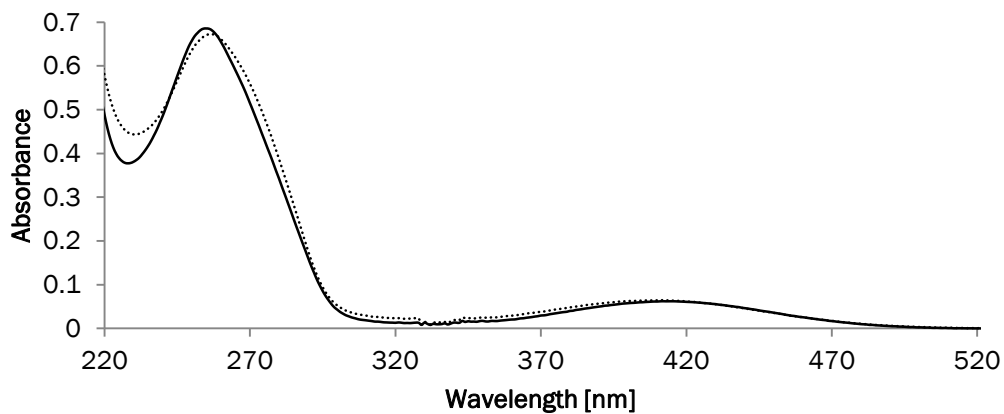
Photophysical Properties of Single Strands 5-10

Figure 225: Absorption spectra of single strands **5** (solid) and **6** (dotted), 5 µM in 10 mM sodium phosphate buffer pH 7.0, 100 mM NaCl, 20°C.

Figure 226: Fluorescence (black) and excitation (red) spectra of single strands **5** (solid) and **6** (dotted), 1 µM in 10 mM sodium phosphate buffer pH 7.0, 100 mM NaCl, 20°C, λexc. 423 nm, λem. 545 nm.

Figure 227: Absorption spectra of single strands **7** (solid) and **8** (dotted), 1 µM in 10 mM sodium phosphate buffer pH 7.0, 100 mM NaCl, 20°C.
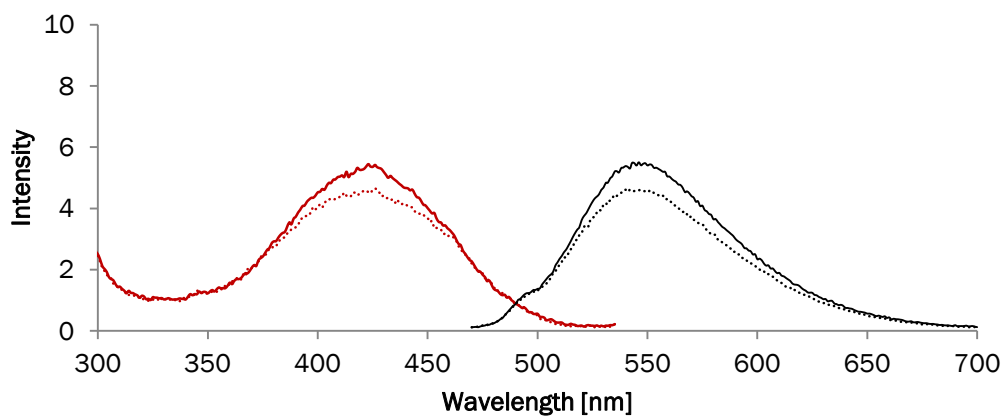

Figure 228: Fluorescence (black) and excitation (red) spectra of single strands **7** (solid) and **8** (dotted), 1 µM in 10 mM sodium phosphate buffer pH 7.0, 100 mM NaCl, 20°C, λexc. 455 nm, λem. 533 nm.
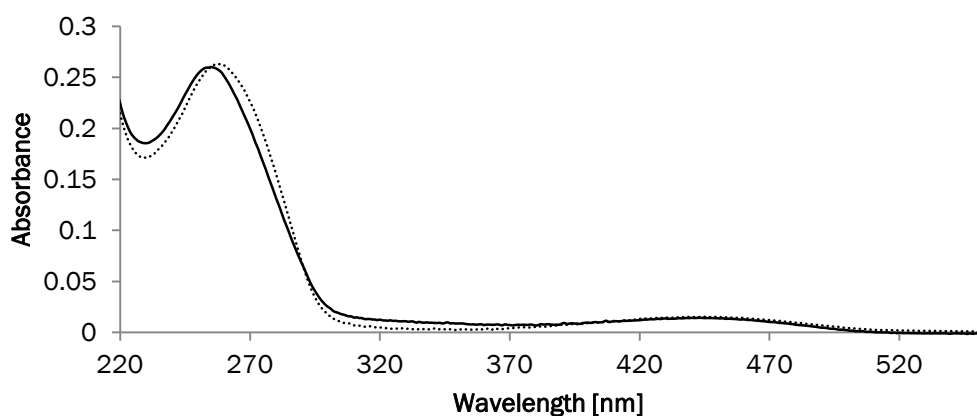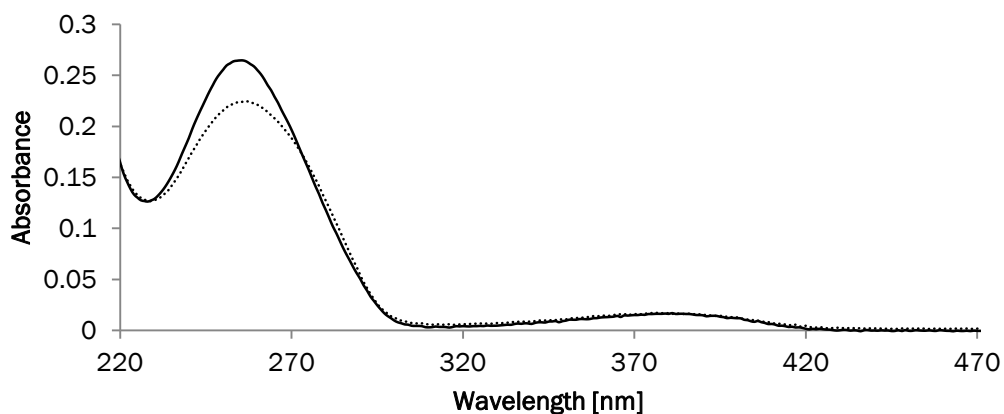
Figure 229: Absorption spectra of single strands **9** (solid) and **10** (dotted), 1 µM in 10 mM sodium phosphate buffer pH 7.0, 100 mM NaCl, 20°C.
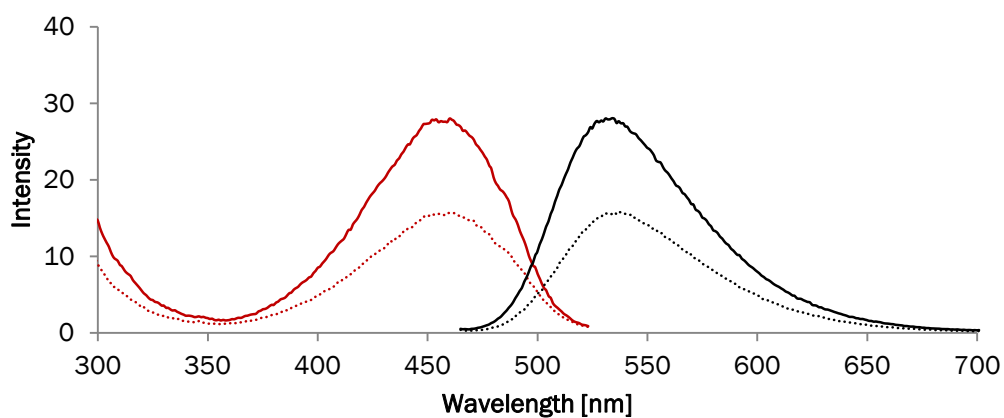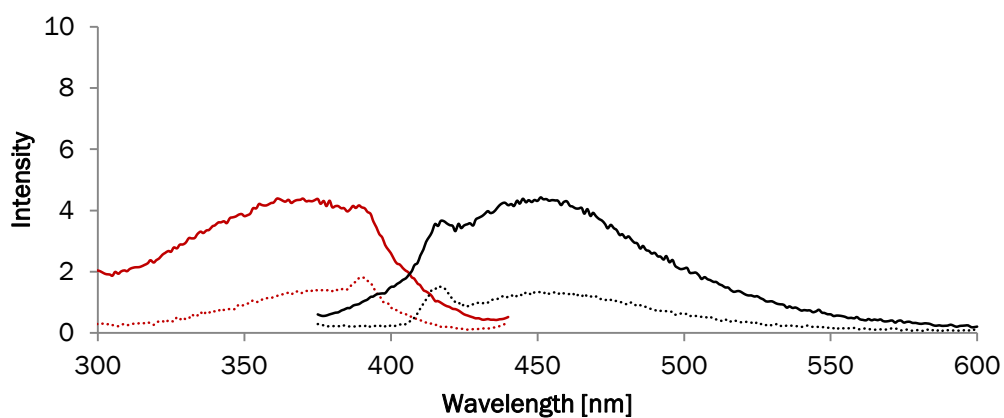

Figure 230: Fluorescence (black) and excitation (red) spectra of single strands **9** (solid) and **10** (dotted), 1 µM in 10 mM sodium phosphate buffer pH 7.0, 100 mM NaCl, 20°C, λexc. 365 nm, λem. 450 nm.

Additional Spectra of Duplexes with Single Strands 5-10
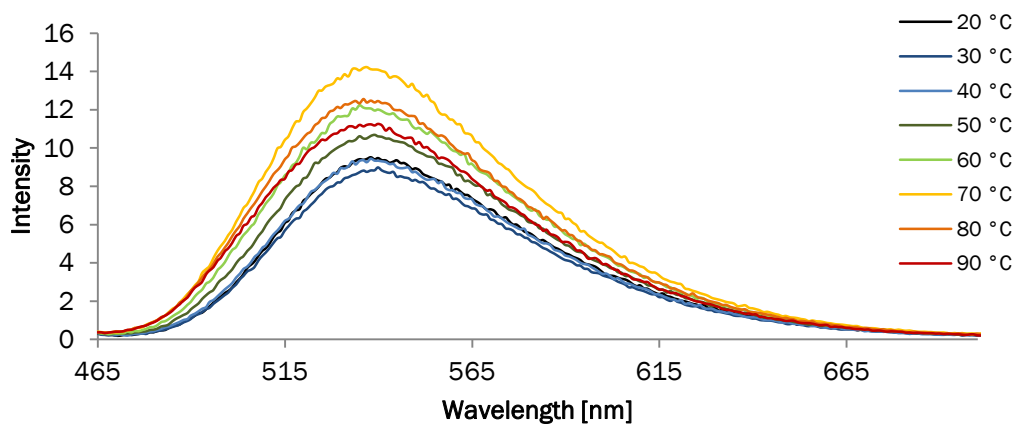
Figure 231: Temperature dependent fluorescence spectrum of **7*8**. Conditions: 1 µM each strand, 10 mM sodium phosphate buffer pH 7.0, 100 mM NaCl, 20°C, λexc. 455 nm.

Figure 232: Temperature dependent fluorescence spectrum of **9*10**. Conditions: 1 µM each strand, 10 mM sodium phosphate buffer pH 7.0, 100 mM NaCl, 20°C, λexc. 365 nm.

Figure 233: Temperature dependent fluorescence spectrum of **5*10**. Conditions: 1 µM each strand, 10 mM sodium phosphate buffer pH 7.0, 100 mM NaCl, 20°C, λexc. 365 nm.

Figure 234: Temperature dependent fluorescence spectrum of **7*10**. Conditions: 1 µM each strand, 10 mM sodium phosphate buffer pH 7.0, 100 mM NaCl, 20°C, λexc. 365 nm.
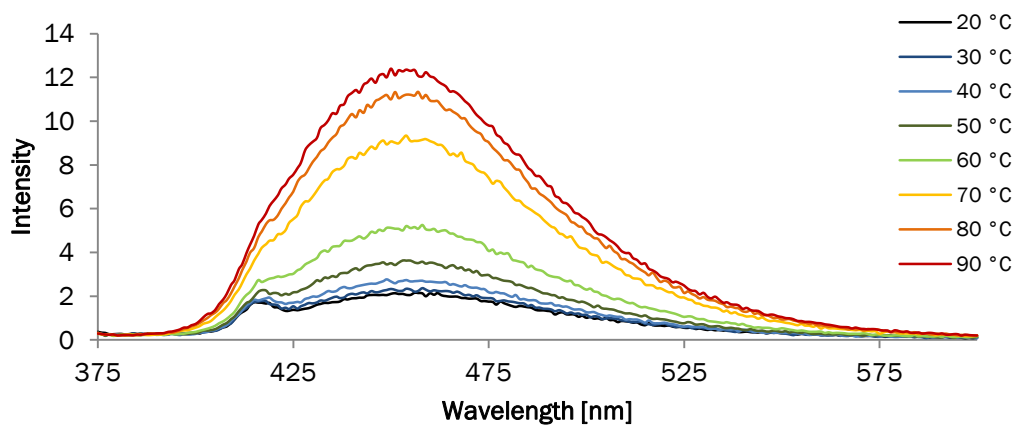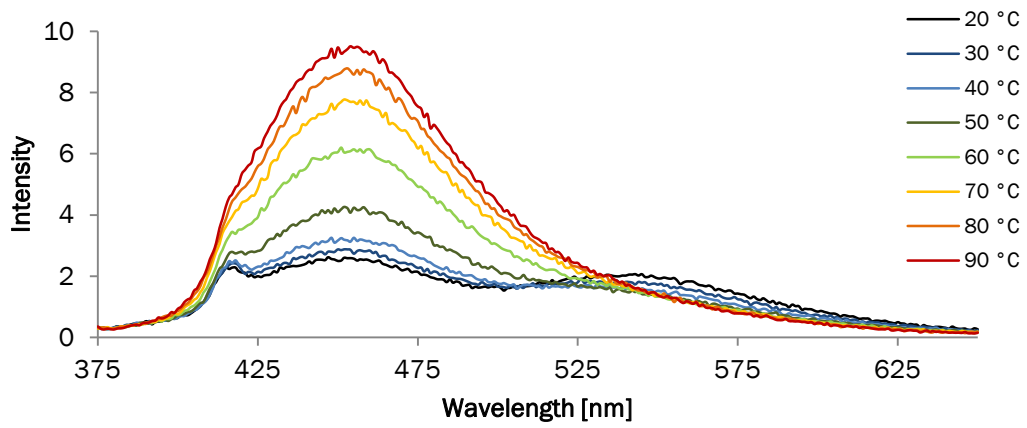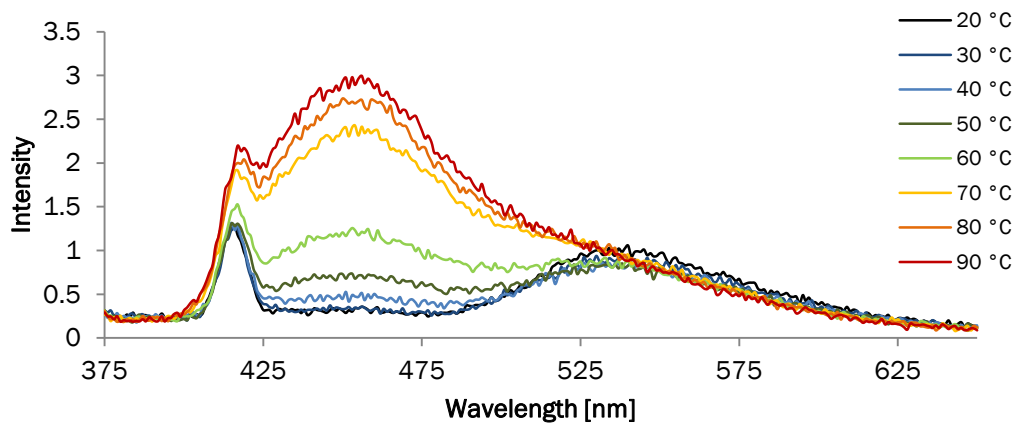
References

[95]   O. Khorev, C. D. Bösch, M. Probst, R. Häner, *Chem. Sci.*, 2014, **5**, 1506-1512.

[96]   (a) J. B. Birks, *Rep. Prog. Phys.*, 1975, **38**, 903-974.
       (b) M. A. F. Tavares, *Trans. Faraday Soc.*, 1970, **66**, 2431-2438.

[97]   (a) H. W. Offen, *J. Chem. Phys.*, 1966, **44**, 699-703.
       (b) J. Tanaka, T. Koda, S. Shionoya, S. Minomura, *Bull. Chem. Soc. Jpn.*, 1965, **38**, 1559-1560.

[98]   E. Chiellini, R. Solaro, F. Ciardelli, *Makromol. Chem.*, 2009, **13**, 1065-1084.

[99]   (a) S. Banerjee, E. B. Veale, C. M. Phelan, S. A. Murphy, G. M. Tocci, L. J. Gillespie, D. O. Frimannson, J. M. Kelly, T. Gunnlaugsson, *Chem. Soc. Rev.*, 2014, **42**, 1601-1618.
       (b) R. Tandon, V. Luxami, H. Kaur, N. Tandon, K. Paul, *Chem. Rec.*, 2017, **17**, 1-39.
       (c) M. K. Abdel-Hamid, K. A. Macgregor, L. R. Odell, N. Chau, A. Mariana, A. Whiting, P. J. Robinson, A. McCluskey, *Org. Biomol. Chem.*, 2015, **13**, 8016-8028.
       (d) Y. Sun, X. Liang, J. Fan, Q. Han, *J. Lumin.*, 2013, **141**, 93-98.
       (e) H. Xiao, M. Chen, G. Shi, L. Wang, H. Yin, C. Mei, *Res. Chem. Intermed.*, 2010, **36**, 1021-1026.

[100] (a) S. Luo, J. Lin, J. Zhou, Y. Wang, X. Liu, Y. Huang, Z. Lu, C. Hu, *J. Mater. Chem. C*, 2015, **3**, 5259-5267.
       (b) E. R. Triboni, M. R. Rernandes, J. R. Garcia, M. Costa Carreira, R. G. S. Berlinck, P. Berci Filho, L. S. Roman, I. A. Hümmelgen, R. Reyes, M. Cremona, *J. Taibah Univ. Sci.*, 2015, **9**, 579-585.
       (c) J.-A. Gan, Q. L. Song, X. Y. Hou, K. Chen, H. Tian, *J. Photochem. Photobiol. A*, 2004, **162**, 399-406.

[101] (a) T. Philipova, I. Petkov, *J. Appl. Polym. Sci.*, 2001, **80**, 1863-1869.
       (b) I. Grabchev, C. Petkov, V. Bojinov, *Macromol. Mater. Eng.*, 2002, **287**, 904-908.

[102] F. Würthner, T. E. Kaiser, C. R. Saha-Möller, *Angew. Chem.*, 2011, **123**, 3436-3473.

[103] (a) M. Vybornyi, A. V. Rudnev, S. M. Langenegger, T. Wandlowski, G. Calzaferri, R. Häner, *Angew. Chem. Int. Ed.*, 2013, **52**, 11488-11493.
       (b) Y. Vyborna, M. Vybornyi, A. V. Rudnev, R. Häner, *Angew. Chem. Int. Ed.*, 2015, **54**, 7934-7938.

[104] A. E. Clark, C. Y. Qin, A. D. Q. Li, *J. Am. Chem. Soc.*, 2007, **129**, 7586-7595.

[105] (a) Y. Morisaki, T. Ishida, Y. Chujo, *Macromolecules*, 2002, **35**, 7872-7877.
       (b) K. Ono, H. Ito, A. Nakashima, M. Uemoto, M. Tomura, K. Saito, *Tetrahedron Lett.*, 2008, **49**, 5816-5819.

[106] M. M. J. Smulders, M. M. L. Nieuwenhuizen, T. F. A. de Greef, P. van der Schoot, A. P. H. J. Schenning, E. W. Meijer, *Chem. Eur. J.*, 2010, **16**, 362-367.

[107] H. Bittermann, D. Siegemund, V. L. Malinovskii, R. Häner, *J. Am. Chem. Soc.*, 2008, **130**, 15285-15287.

[108] (a) D. Yuan, R. G. Brown, *J. Phys. Chem. A*, 1997, **101**, 3461-3461.
       (b) S. Saha, A. Samanta, *J. Phys. Chem. A*, 2002, **106**, 4763-4771.

[109] S. Banerjee, J. A. Kitchen, T. Gunnlaugsson, J. M. Kelly, *Org. Biomol. Chem.*, 2012, **10**, 3033-3043.

[110] M. Sarobe, H. C. Kwint, T. Fleer, R. W. A. Havenith, L. W. Jenneskens, E. J. Vlietstra, J. H. van Lenthe, J. Wesseling, *Eur. J. Org. Chem.*, 1999, 1191-1200.

Appendix

General Methods

All reagents and solvents were purchased from commercial suppliers and used without further purification. Reactions which are sensitive to water or air were performed under argon atmosphere; solvents for Sonogashira reaction were freshly degassed. Water was used from a Milli-Q system. NMR spectra were obtained on a Bruker AV 300 (300 MHz) spectrometer at 298 K. Mass-spectrometric data were obtained on Thermo Fisher LTQ Orbitrap XL using Nano Electrospray Ionization (NSI). UV-vis spectra were measured on a Cary 100 Bio spectrophotometer. Fluorescence and excitation spectra were measured on a Cary Eclipse spectrofluorimeter, excitation and emission slit widths were set to 5 nm if not mentioned otherwise.

Abbreviations

AFM	Atomic force microscopy
APTES	3-Aminopropyltriethoxy silane
BOP	(Benzotriazol-1-yloxy)tris(dimethylamino)phosphonium hexafluorophosphate
DCM	Dichloromethane
DIPEA	*N,N*-Diisopropylethylamine
DMAP	*N,N*-Dimethylpyridin-4-amine
DMF	*N,N*-Dimethylformamide
DMT-Cl	4,4′-Dimethoxytriphenylmethyl chloride
EET	Excitation energy transfer
ESA	Excited state absorption
FRET	Förster resonance energy transfer
GSB	Ground state bleaching
LCAA-CPG	Long chain alkylamine controlled pore glass
LHC	Light-harvesting complex
PAH	Polycyclic aromatic hydrocarbon
PAM-Cl	2-Cyanoethyl *N,N*-diisopropylchlorophosphoramidite
r.t.	Room temperature
TA	Transient absorption
TEM	Transmission electron microscopy
THF	Tetrahydrofuran
TLC	Thin layer chromatography

Erklärung

Erklärung

gemäss Art. 28 Abs. 2 RSL 05

Name/Vorname: Bösch Caroline Désirée

Matrikelnummer: 09-100-611

Studiengang: Chemie und Molekulare Wissenschaften

Bachelor ☐   Master ☐   Dissertation ☒

Titel der Arbeit: Assembly of DNA-Inspired Aromatic Oligophosphates into Light-Harvesting Supramolecular Polymers

LeiterIn der Arbeit: Prof. Dr. Robert Häner

Ich erkläre hiermit, dass ich diese Arbeit selbständig verfasst und keine anderen als die angegebenen Quellen benutzt habe. Alle Stellen, die wörtlich oder sinngemäss aus Quellen entnommen wurden, habe ich als solche gekennzeichnet. Mir ist bekannt, dass andernfalls der Senat gemäss Artikel 36 Absatz 1 Buchstabe r des Gesetzes vom 5. September 1996 über die Universität zum Entzug des auf Grund dieser Arbeit verliehenen Titels berechtigt ist. Ich gewähre hiermit Einsicht in diese Arbeit.

Ort/Datum

Unterschrift

Curriculum Vitae

Persönliche Daten

Name	Caroline Désirée Bösch
Geburtstag	24.10.1989
Heimatort	Grossaffoltern BE
Adresse	Wankdorffeldstrasse 95, 3014 Bern
E-Mail	caroline.d.boesch@gmail.com
Telefon	+41 79 649 88 33

Ausbildung

2014-2017	Doktorat in Chemie und Molekulare Wissenschaften, Universität Bern
2012-2013	Master in Chemie und Molekulare Wissenschaften, Universität Bern
2009-2012	Bachelor in Chemie und Molekulare Wissenschaften, Universität Bern
2005-2009	Eidgenössische Maturität, Kollegium Heilig-Kreuz, Fribourg

Publikationen

Caroline D. Bösch, Simon M. Langenegger, Robert Häner, *Light-Harvesting Nanotubes Formed by Supramolecular Assembly of Aromatic Oligophosphates, Angew. Chem. Int. Ed.*, 2016, **55**, 9961-9964.

Oleg Khorev, Caroline D. Bösch, Markus Probst, Robert Häner, *Observation of the rare chrysene excimer, Chem. Sci.*, 2014, **5**, 1506-1512.

Andere Aktivitäten

Beiträge zu *Swiss Science Concentrates, CHIMIA*, 2015 – 2017.